UNIVERSITY OF SOUTHAMPTON

FACULTY OF PHYSICAL SCIENCE AND ENGINEERING

School of Electronics and Computer Science

Surface Fluorinated Epoxy Resin for High Voltage DC Application

by

Azwadi Mohamad

Supervisor: Prof. George Chen

Final Thesis

October 2015

ABSTRACT

UNIVERSITY OF SOUTHAMPTON

FACULTY OF PHYSICAL SCIENCES AND ENGINEERING

Electronics and Computer Science

Doctor of Philosophy

Surface Fluorinated Epoxy Resin for High Voltage DC Applications

by Azwadi Mohamad

Charge build up under high voltage DC is a significant concern in the transmission system as its presence may distort the local electric field. By chemically treat polymeric insulation via direct-fluorination, and plasma enhanced fluorination process, the charge transport characteristics of the material can be modified. In doing so, excellent surface properties similar to those of fluoropolymers can be attained without compromising the bulk properties of the original polymeric insulation. The change in chemical components at the surface of polymeric insulation should lead to a corresponding change in dielectric properties at the surface and consequently may suppress the occurrences of charge build up. In this research, epoxy resin samples with various surface fluorinating conditions were formulated and treated. The samples then were characterised by SEM and EDX analysis, Raman spectroscopy, and DC surface conductivity measurements. To further explain the effects of fluorination treatment, modelling of the electric field and current density distribution had been carried out. Surface potential decay tests from corona discharge, as well as PEA measurements, show that there is a significant change in decay characteristics with the introduction of surface fluorinated layer. The decay mechanisms responsible for the observed phenomena were thoroughly discussed. The effect of moisture absorption on the treated surface was studied and proved to be the limiting factor in the improvement of dielectric properties of fluorination treatment. Finally, surface DC flashover test using a pair of finger electrodes were performed. This research proved that the introduction of the fluorinated surface layer on epoxy resins does play a major role in improving the surface dielectric properties for the use as insulation spacer in high voltage DC GIS systems.

CONTENTS

LIST OF FIGURES

LIST OF TABLES

DECLARATION OF AUTHORSHIP

I, Azwadi Mohamad, declare that, this thesis entitled:

"Surface Fluorinated Epoxy Resin for High Voltage DC Application"

and the work presented in the thesis is both my own, and has been generated by me as the result of my own original research. I confirm that:

- this work was done wholly or mainly while in candidature for a research degree at this University;
- where any part of this thesis has previously been submitted for a degree or any other qualification at this University or any other institution, this has been clearly stated;
- where I have consulted the published work of others, this is always clearly attributed;
- where I have quoted from the work of others, the source is always given. With the exception of such quotations, this thesis is entirely my own work;
- I have acknowledged all main sources of help;
- where the thesis is based on work done by myself jointly with others, I have made clear exactly what was done by others and what I have contributed myself;
-

ACKNOWLEDGEMENT

First of all, I would like to express my sincere and deepest thanks to my supervisor, Professor George Chen for his expert guidance, encouragement, insightful advice, understanding and patience in helping me throughout the completion of this thesis. Without his help, finishing this thesis would not have been possible.

Special thanks are dedicated to Dr. Qi Wang for sharing the knowledge on material processing and experimental techniques, and Dr. Kwan Yiew Lau, Dr. Yuan Zhuang, Dr. Van Truc Nguyen, Dr. Ian Hosier, Dr. Celia Yeung, Dr. Matt Praeger, Mr. Bin Qi and many of the Tony Davies High Voltage Laboratory members, including the Laboratory Operations Director, Professor Paul Lewin for providing their opinion, discussion and technical support. Not forgotten, my internal examiner, Professor Alun Vaughan, the invaluable comments given during the viva was kindly appreciated.

Finally, to my family including my mothers, father, and especially to my dearest wife, Tengku Liyana Tengku Ibrahim, I will forever be in your debt. Thank you so much for being there with me throughout the good and hard times. Without your love, support and encouragement, I could not have finished this thesis.

Dear God Almighty, my PhD journey was an uphill climb, but I put my faith in you. At times when I was flooded with endless problems, you give me the strength to endure and show me the way out. Thank you for all the blessings in my life.

ABBREVIATIONS AND SYMBOLS

AC	-	Alternating current
AIS	-	Air insulated switchgears
ASTM	-	American Society for Testing and Materials
B	-	Boron element
C	-	Capacitance
C	-	Carbon element
c	-	Speed of light in vacuum
d	-	Thickness of sample
DBD	-	Dielectric barrier discharges
DC	-	Direct current
DGEBA	-	Diglycidyl ether of Bisphenol-A
e	-	Electron charge of 1.602×10^{-19} C
ε	-	Permittivity
ε	-	Dielectric constant

EDX	-	Energy dispersive X-ray
eV	-	Electron volt
F	-	Fluorine element
F(x)	-	Weibull probability density function
F_2	-	Fluorine gas
Fe	-	Iron element
GIS	-	Gas insulated switchgears
H	-	Hydrogen element
h	-	Planck constant
HF	-	Hydrogen fluoride
LIPP	-	Laser-induced pressure pulse
LLDPE	-	Linear low density polyethylene
LSE	-	Least Squares estimation
MHz	-	Mega Hertz
MLE	-	Maximum likelihood estimation
Mo/Al_2O_3	-	Molybdenum/Alumina

NaF	-	Sodium fluoride
$NaHF_2$	-	Sodium bifluoride
O	-	Oxygen element
O_2	-	Oxygen gas
PEA	-	Pulsed electroacoustic
PWP	-	Pressure wave propagation
R	-	Resistance
R	-	Radius of sample
RF	-	Radio frequency
S	-	Conductance
SCCM	-	Standard cubic centimetres per minute
SEM	-	Scanning-electron microscopy
SF_6	-	Sulphur hexafluoride
Si	-	Silicon element
T_g	-	Glass transition temperature
TSM	-	Thermal step method

T_t	-	Transmission time
U	-	Uranium element
UV	-	Ultra violet
XeF_2	-	Xenon difluoride
α	-	Weibull scale parameter
β	-	Weibull shape parameter
λ	-	Wavelength of an electron
ρ	-	Volume resistivity
σ_s	-	Surface conductivity
σ_v	-	Bulk conductivity
τ	-	Decay time constant
Ψ	-	Water contact angle

CHAPTER ONE: INTRODUCTION

1.1 BACKGROUND PROBLEMS

Electrification started in the middle of the 19th century where the power generation and consumers are placed near to one another. At that time, generators were powered by water wheel from the river with voltages about 100 V transmitted using DC mode [1]. In these early times, arguments of DC against AC transmission started to take place which led to two main front-runners; Tesla and Edison. Tesla favoured AC transmission as it is easy for switching purposes, plus, the ease of converting to another voltage level while Edison favoured DC transmission because of its high efficiency and low transmission losses. We know today that Tesla position won the argument that led to the wide usage of AC transmission nowadays.

With the advancements in new AC technology, higher operating voltages were achieved as well as improvement in reliability of circuit breakers and switches. The discovery of an artificial gas of sulphur hexafluoride (SF_6) that has excellent insulating properties paved the way for the first generation of gas insulated switchgears (GIS) which was initially designed in the early 1920s [1, 2]. A typical GIS consists of high voltage components such as conductors, circuit-breakers, and disconnectors inside a compact metal encapsulation. Insulating spacers, usually made from cast epoxy are used to hold these components in place due to its strong mechanical strength and good dielectric properties. The intersection of the metal conductor, insulating spacer and insulating gas is called the 'triple junction' and is of a high interest in this research due to its role in charge injection. In the 1960s, experimental works were done using SF_6 in enclosed aluminium compartment under high voltage AC or DC, and, since then, it was regarded as the best arc quenching solution for high voltage power transmission. In comparison with GIS, its predecessor, the air insulated switchgears (AIS) which is bigger in size due to poor the dielectric strength of air, suffers inconsistency in the dielectric capability of air to withstand ever changing ambient surroundings and deterioration of exposed components due to oxidisation and the corrosive

nature of the environment [2]. Hence, switchgears that are kept inside a metal enclosure, as illustrated in Figure 1-1, as in the case of GIS. This is indeed a simple yet effective solution to the inconsistency problems of the AIS. With further development in this area, the world of electric power transmission has seen a great service from GIS, particularly in the AC transmission mode.

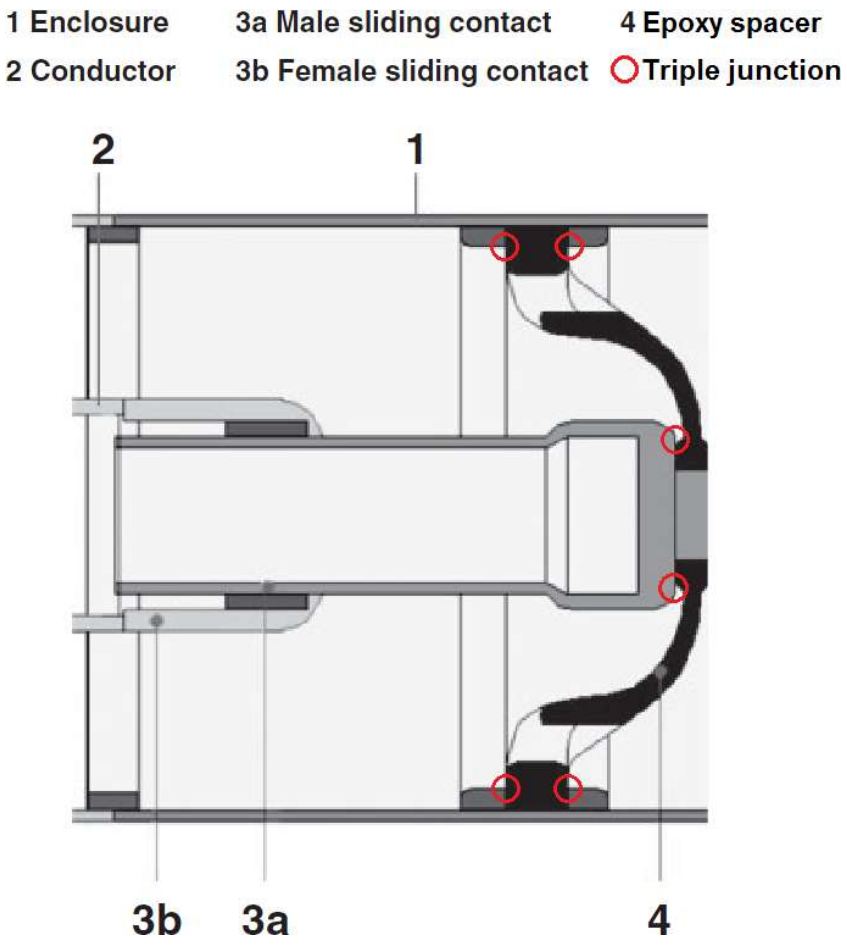

Figure 1-1: Components inside GIS and locations of triple junctions as shown by the red circles [1]

The DC transmission, on the other hand, has had many difficulties in the dielectric stability of the insulating system due to its invariant direction as opposed to AC system [1, 3, 4]. Some physical phenomena like space charge in the bulk and on the surface of the insulator were not fully understood then. Space charges are the trapped charge carriers in the

insulator from electrons and/or ions that have been associated with many undesired consequences such as electrical ageing or degradation. Nevertheless, due to the nature of DC transmission, which possesses high efficiency and low transmission losses, there has been a resurgence of interests in high voltage DC transmission. Studies in this area have revealed an unforeseen behaviour concerning the electric stresses at the triple junction of conductor-spacer-gas interface (as illustrated in Figure 1-1) during prolonged DC stress [5, 6]. The static surface charge caused by prolonged DC stress is believed to cause a significant drop in spacer DC flashover voltage, a phenomenon not seen in AC or short-term stress. A large amount of space charge started to accumulate along the surface of cast epoxy spacers with prolonged DC stress, which may distort the local electric field. A study done by Fujinami et al. listed three possible factors for this phenomenon [7]; (i) micro discharge or field emission from surface projections, (ii) motion of dust particles, and (iii) natural ionisation of SF_6 gas in a prolonged time range. To overcome the charging problem, they proposed the design of anti-charging spacer profile which has no normal field component on the surface. In a similar study done by Hama et al. [8], they implied that the accumulation of surface charges on solid insulators inside of a GIS may come from the residual DC voltages on high-voltage conductors, localised field concentration, and field emissions. They further stressed that there are two theories that govern the mechanism of charging. The first theory suggests that the charge may be caused by inhomogeneous surface conductions of the insulating spacer as its conductivity is highly dependent on the electric field value along the surface. Positive and negative charges can move in the opposite directions subject to the electric field distribution under the DC voltage. The second theory being that charge carriers are produced by field emissions or micro discharges at highly stressed parts of the spacer surface and the electrode. The charge carriers can move along the electric lines of force and accumulate at the end of the lines if they are on an insulating spacer. They also concluded that the instant the DC voltage is applied to GIS, the electric field distribution of the electrode system is dominated by a capacitive field, which then will become a resistive field after a certain operating transmission time T_t given by the following equation:

$$T_t = C.R = \varepsilon \frac{S}{t} . \rho \frac{t}{S} = \varepsilon_\circ . \varepsilon_s . \rho \quad (1\text{-}1)$$

where $\varepsilon_\circ$, ε_s , and ρ are the permittivity of a vacuum, the relative permittivity of the insulator, and the volume resistivity of insulator respectively. Typically, the value for transmission time T_t is of several hours and, for this reason, the insulation system should be designed for a resistive electric field.

In another study conducted by Nakanishi et al. [9], they stated that heterocharges that accumulate on the spacer surface at the time of abrupt polarity reversal reduce the flashover voltage along the spacer surface. On top of that, Okabe et al. [10] reported that charges on the spacer model may have opposite or same polarity depending on the ratio of the insulating gas resistance and spacer resistance. They further concluded three kinds of surface charging mechanisms; (i) volume conduction, (ii) surface conduction, and (iii) electric field emission that were characterised in term of a time constant, applied voltage and charge distribution. In short, the occurrence of surface charging on an insulating spacer is among the critical parameters that define the electrical strength of high voltage DC GIS. Charges deposited on the surface of cast epoxy spacer may eventually distort the local field, especially during DC polarity reversal and in the worst case can lead to premature failure of the insulating spacer inside GIS.

1.2 MOTIVATION

Looking inside the metal enclosure of GIS as illustrated in Figure 1-1, it can be seen that a structurally strong cast epoxy resin is used as insulating spacers that firmly holds the central conductor in place. In fact, epoxy resin is one of the most widely used groups of epoxide polymer and has been extensively used for decades as insulation in high voltage transmission system due to its excellent mechanical and dielectric properties. As excellent as it may be, this insulation material does suffer from bulk and surface charging when used as an insulating spacer in GIS, particularly in DC applications. To date, a large number of

papers have been published to get a better understanding and control of surface charging under high voltage stress [11, 12]. These studies involve various modifications and treatments of epoxy resin, which may lead to the suppression of space charge accumulation. For example, a recent research has found that the functionally graded material reduces the electric field up to 11 % on the electrode and spacer interface under AC applications [13]. Another example was the work done by Li et al. [14], in which, inorganic A-B-A insulator system of Mo/Al_2O_3 cermet - Al_2O_3 ceramic – Mo/Al_2O_3 cermet was adopted. This system can improve the DC and impulse surface flashover voltage by 52 % and 86 % respectively in a vacuum environment.

As mentioned earlier, because the conductor-spacer-gas triple junction interface in high voltage DC GIS is most susceptible to flashover as it is the headstream of charge injection [15], its significance has been highlighted in controlling charge accumulation along the surface of cast epoxy spacers under prolonged AC or DC stress. A key aspect of surface charge accumulation is thought to involve the interface of the conductor, spacer surface and insulating gas. Therefore, a suitable modification in one of these three areas is believed to have significant effects on suppressing charge accumulation on the spacer surface, and so limiting the flashover occurrences inside GIS. More recently, a semi-conductive coating for the solid insulator has been proposed as an alternative method to prevent the occurrences of charge accumulation [8, 16]. Despite having a mix outcomes in the validity of using the semi-conductive coating in numerical calculation results [3, 16], experimental work has shown that such semi-conductive coatings may reduce charge accumulation on the insulators and enhance the flashover performances [8, 17, 18]. On top of that, laboratory work done by Jia et al. [19] on the insulation made from different insulating materials of higher surface conductivity shows that such insulation has an improved surface flashover voltage.

Extensive works from fundamental researches to industrial applications have been done to minimise and suppress surface charge accumulation. The work involves optimisation of the design of insulating spacer profile, reduction of the micro-protrusions on the electrode

surface and the electric field at the conductor-spacer-gas triple junction, as well as by cleaning up the environment inside GIS. Still it is inevitable to prevent the space charges from reaching the insulating spacer. Alternatively, a designed increase in surface conductivity of the insulating spacer, without compromising the bulk insulation properties, would allow the charge arriving on the insulating surface to be dispersed along the surface, and, consequently, results in the suppression of the surface charge accumulation. Therefore, surface treatment of insulating spacers by a semi-conducting coating is often considered as a smart solution to prevent the surface charging problem in GIS.

The studies to date tend to focus on the modifications of bulk polymeric insulation, which lead to changes in the whole properties of the bulk including the surface layer and its interface properties with the electrode. However, far too little attention has been given to modifications limited to surface properties alone by directly treating the surface layer of polymeric insulation. The main idea of this research is to chemically treat the surface of polymeric insulation, and, consequently, modify the charge transport characteristics of the subjected material via fluorination process, i.e. treatment of polymeric materials with fluorine or fluorine-inert gas (nitrogen, helium, etc.) mixtures. This chemical treatment process has been well developed from fundamental concepts to industrial work, and is amongst the most effective approaches to improving materials in term of barrier properties, separation properties, thermal and chemical stability, as well as biocompatibility [20-22].

It is interesting to note that, through surface-fluorination treatment, excellent surface properties similar to those of fluoropolymers can be achieved without compromising the bulk characteristics of the pristine polymeric insulation. The practical use of fluoropolymer material, however, is restricted due to their high cost and complexity of synthesis. The studies and applications of surface-fluorination process so far are mostly concentrated on improving properties with regards to wettability, adhesion, chemical stability, barrier properties, biocompatibility, and grafting [23]. There has been far too little attention given to the development of dielectric properties. In truth, the modifications in the chemical

components of polymeric insulation should also lead to corresponding modifications in dielectric properties as well [24].

1.3 OBJECTIVE AND SCOPES

The subject of epoxy resin undergoing surface modification through surface-fluorination process has become increasingly important as this chemical treatment should have shown improvement in chemical and dielectric properties in polymeric insulation. Therefore, the main objectives and scopes of this research are;

1. To prepare and characterise fluorinated epoxy samples for high voltage application. The samples prepared and used throughout this project will be formulated from Diglycidyl ether of Bisphenol-A (DGEBA) epoxy resin (Araldite LY556) which is used for high-performance composite parts. The epoxy resin samples will be prepared in Chemical Preparation Room of Tony Davies High Voltage Laboratory and will be sent away to undergo direct-fluorination treatment in Tongji University, China. Another set of cast epoxy resin will be sent to Laboratory of Plasma Physics and Materials, Beijing for undergoing plasma-enhanced fluorination treatment. The samples then will be subjected to a series of characterisation tests, including scanning electron microscopy (SEM), energy dispersive X-ray (EDX) and Raman spectroscopy.

2. Simulation work on the electric potential and current density distribution will be carried out to help in the design of an insulating spacer in high voltage DC GIS systems. The simulation will denote the influence of various degrees of fluorination treatment in the outcome of the electric field and current density distribution.

3. The dielectric performance of various degrees of direct-fluorination and plasma-enhanced-fluorination condition will then be explored. Previous experimental work on fluorinated polymeric insulation shows favourable improvements in dielectric performance. Such improvement is to be anticipated in the case of the surface-

fluorinated epoxy resin samples. The samples will be subjected to a series of test including surface potential decay measurement, as well as space charge analysis using the PEA method to explain the dynamics of charge movement. The treated samples will also undergo DC surface flashover test using finger electrode system to see the anticipated improvement in surface flashover strength.

1.4 THESIS OUTLINE

Chapter 1

This chapter provides a basic introduction to HV GIS including the basic components inside GIS, as well as the background problems concerning DC GIS.

Chapter 2

This chapter tells the information regarding epoxy resin, the chemical composition, the curing process, as well as the direct-fluorination and plasma-enhanced-fluorination treatment. It also contains the theories behind all the experimental techniques used in this research.

Chapter 3

This chapter covers the details on the epoxy used throughout this project, as well as the detailed steps to formulate the fluorinated epoxy samples.

Chapter 4

This chapter describes the characterisation tests used, including SEM, EDX, Raman spectroscopy and surface DC conductivity test.

Chapter 5

This chapter investigates the charge transport theory by surface potential decay measurement and space charge analysis using the PEA method to explain the dynamics of space charge inside the fluorinated samples.

Chapter 6

The influence of surface moisture towards the dielectric performances of surface-fluorinated epoxy resins is investigated by drying the epoxy samples in vacuum-oven and nitrogen chamber.

Chapter 7

DC surface flashover test using a pair of finger electrodes is performed and discussed in this chapter. The model of the electrode system was also developed using COMSOL Multiphysics software for potential distribution and current simulation.

Chapter 8

This chapter investigates the alternative surface treatment, the plasma-enhanced-fluorination treatment on epoxy resin samples by repeating the key experimental procedures.

Chapter 9

This last chapter summarises the entire findings from this research and draws conclusions and suggestions for future works.

CHAPTER TWO: MATERIALS AND EXPERIMENTAL TECHNIQUES

This chapter intends to outline the basic concepts of the material properties, and the experimental techniques involved in this research.

2.1 THE CONCEPT OF EPOXY RESIN

Epoxy resins are classified under epoxy oligomer group. They can react with curing agent or hardener to form a three-dimensional net structure of the thermosetting plastic. The epoxy resin has excellent adhesiveness, low contraction percentage, easy to shape, good chemical/heat resistance, as well as outstanding mechanical and dielectric properties [25]. Most importantly, all of these features come at a very low cost. Interestingly, there are many combinations of epoxy with curing agent/hardener that can be selected to yield different properties.

Because of its properties, epoxy resin based materials are used extensively in the industries from basic structural adhesives to structural matrix material in aerospace applications. Epoxy resins also possess excellent dielectric properties that are crucial in preventing the occurrences of short circuit and, therefore, they have become one of the most popular thermosetting resins in high voltage applications. For example, cast epoxy resins are successfully used in motors, transformers, switchgear, bushings and insulators.

2.2 DEFINITIONS AND CLASSIFICATION OF EPOXY RESIN

Epoxy resins are network-structured thermosets that evolve through crosslinking reactions. It is formed by a ring that consists of two carbon atoms and one oxygen atom. A compound

that has such ring structure is called epoxide. The simplest structure of epoxide compound is called ethylene epoxide as illustrated in Figure 2-1. Ethylene epoxide can be transformed into polyethylene oxide through the ionic polymerisation process [26]. Epoxy resin contains two or more epoxy groups in its molecular structure and may form a solid three-dimensional net structure under suitable chemical reaction. The chemical reactions that occur during the polymerisation process are associated with phenomenological changes, such as macroscopic gelation and vitrification.

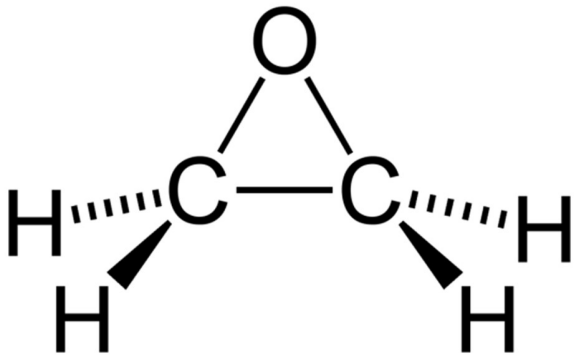

Figure 2-1: A representation of molecular structure of ethylene epoxide, the simplest structure of epoxide compound

Basically, there are two types of epoxy resins based on the synthesis method; (i) glycidyl epoxy resin and (ii) non-glycidyl epoxy resin [27]. The former is produced by a condensation reaction of dihydroxy compound, dibasic/diamine acid and epichlorohydrin while the latter is produced by peroxidation of the olefinic double bond. Glycidyl ester resin, glycidyl ether resin, and glycidyl amine resin are classified under glycidyl resins. Meanwhile, alicyclic epoxy resin and alipthatic epoxy resin are classified under non-glycidyl epoxy resins.

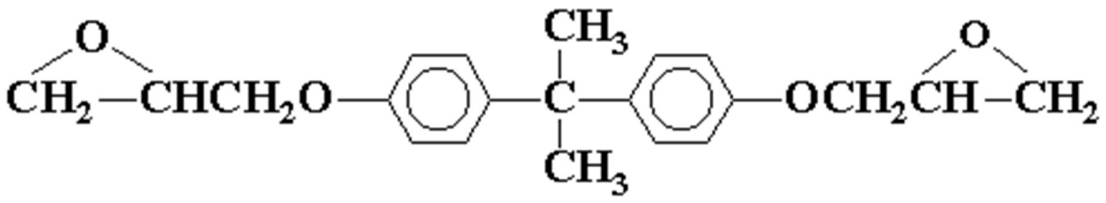

Figure 2-2: A representation of molecular structure of DGEBA. It contains active epoxy groups in its molecular structure.

Furthermore, under glycidyl ether epoxy resin, there are two groups namely (i) Diglycidyl ether of Bisphenol-A (DGEBA) and (ii) novalac epoxy resin [28]. DGEBA epoxy resin is formed from the reaction between epichlorohydrin and Bisphenol-A. It contains active epoxy groups in its molecular structure (as illustrated in Figure 2-2) and, therefore, can perform crosslinking reactions with hardeners to form a three-dimensional cross-linked net of polymer. As for novalac epoxy resin, it is formed from the reaction between phenolic novolac resin and epichlorohydrin. Novolac epoxy resin contains more than two epoxy groups in its molecular structure as illustrated in Figure 2-3. The cured systems have larger cross-linking density, better thermal stability, mechanical and dielectric properties, as well as water and corrosion resistance.

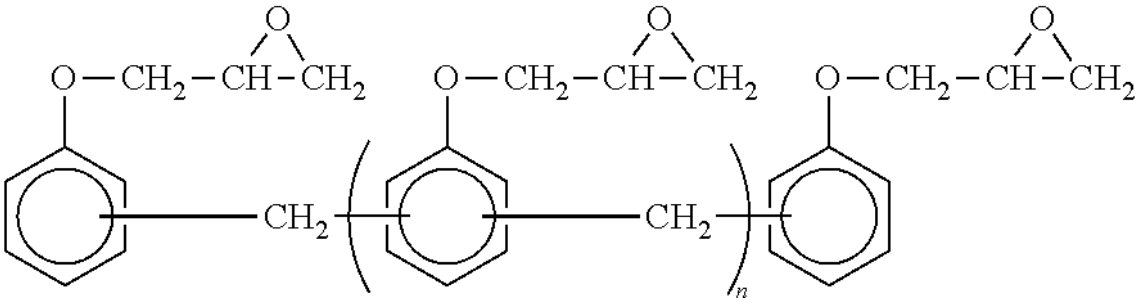

Figure 2-3: A representation of molecular structure of novalac epoxy resin. It contains more than two epoxy groups in its molecular structure

2.3 CURING OF EPOXY RESIN

Epoxy resin in its original form is just a high viscosity clear liquid of very little use. It needs to go through a curing process to form a three-dimensional crosslinking network. This curing process is a reaction between the epoxy groups with the curing agent/hardener to produce a solid material, which has high mechanical strength, as well as chemical and thermal stability. The Bisphenol-A type epoxy resin, for instance, is thermally stable even at a temperature as high as 200 ºC.

Curing of epoxy resin involves the conversion of a low-molecular-weight liquid to an amorphous network of macroscopic molecules. The outcome of the curing process is determined by the chemical change and the curing temperature. The curing process is associated with exothermic chemical reactions and consequent chemo-rheological conversions. With thermal activation, the viscosity of the mixture drops at first, and the monomers are ready to react with one another to produce oligomers. As the curing process resume, the length of molecular chains and the degree of crosslinking and branching increases. This chemical process leads to a surge in the molecular weight as well as in viscosity value. The produced microgel particles are distributed in the low-molecular-weight phase, also known as the ‘continuous phase’. More molecular chains will link together until the microgels are fully established in the continuous phase. The original phase of low-molecular-weight particles is trapped in the matrix of this new phase. At this instance, a continuous 3D network is produced and is called ‘gelation’ [29, 30]. It is a change from a highly viscous liquid to an elastic gel or rubber that is no longer reversible. The gelation point is defined as the point at which the viscosity approaches infinity, and a mechanical modulus is produced as illustrated in Figure 2-4 [31].

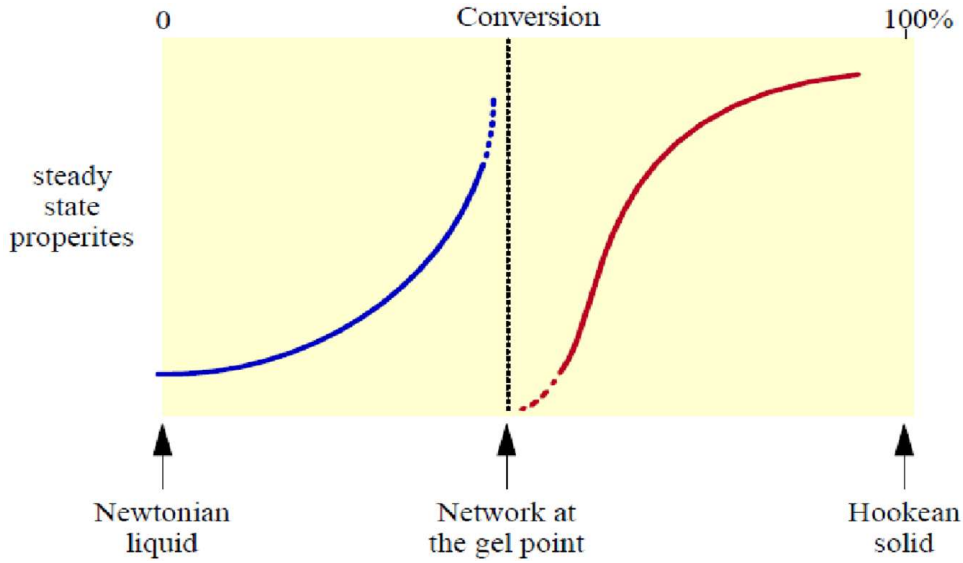

Figure 2-4: A plot of macroscopic development of network formation. The gelation point is defined as the point at which the viscosity approaches infinity, and a mechanical modulus is produced.

Gelation point is a significant parameter of epoxy in regards of processability. It is the starting point for the formation of a cross-linked network. Before gelation point, the system is mobile, however, beyond this point, the material loses its ability to flow due to the surge in viscosity. At the same time, its microstructure becomes permanent, and its self-diffusion is radically limited. A study done by O'Brien et al. [32] stated that small changes in the curing process can cause significant effects on relaxation, especially near the gelation point. As the material approached gelation point, the relaxation is considerably slowed down. As the curing process goes beyond the gelation point, the mixture reaction continues to form a fully cured 3D network with high cross-linking density and high glass transition temperature T_g. The glass transition temperature T_g occurs during the transformation in which an amorphous thermoset is changed from the glassy state to a rubbery state with the characteristics of rubber or a highly viscous liquid. Figure 2-5 shows the curing process of a thermoset from an uncured phase to a fully cured phase.

In theory, during the curing process, the glass transition temperature T_g of the reacting system increases from the initial value T_{g_0} of the uncured monomer mixture to the fully

cured value $T_{g\infty}$. Vitrification is the transition from a liquid/rubbery state into a glassy state when T_g increases from under the curing temperature (T_{cure}) to T_{cure}, i.e. $T_g = T_{cure}$ [33-35]. At this point, the mobility of the reactive groups is restricted due to the drop in free volume and, therefore, the rate of reaction decreases drastically. Chemical reactions in the region near vitrification become diffusion and/or mobility controlled [34, 36]. Because of the restriction of diffusion, the final conversion is usually lower than unity. Even without any diffusion restrictions, topological limitations can reduce the eventual conversion since the remaining reactive groups cannot meet and react with one another [37]. The vitrification phase is reversible by heating to devitrify the partially cured resin. Then, chemical control of the curing process can be re-enacted. Hence, it is usually necessary to increase the temperature after vitrification to complete the curing process, i.e. a post-cure at an elevated temperature is usually required.

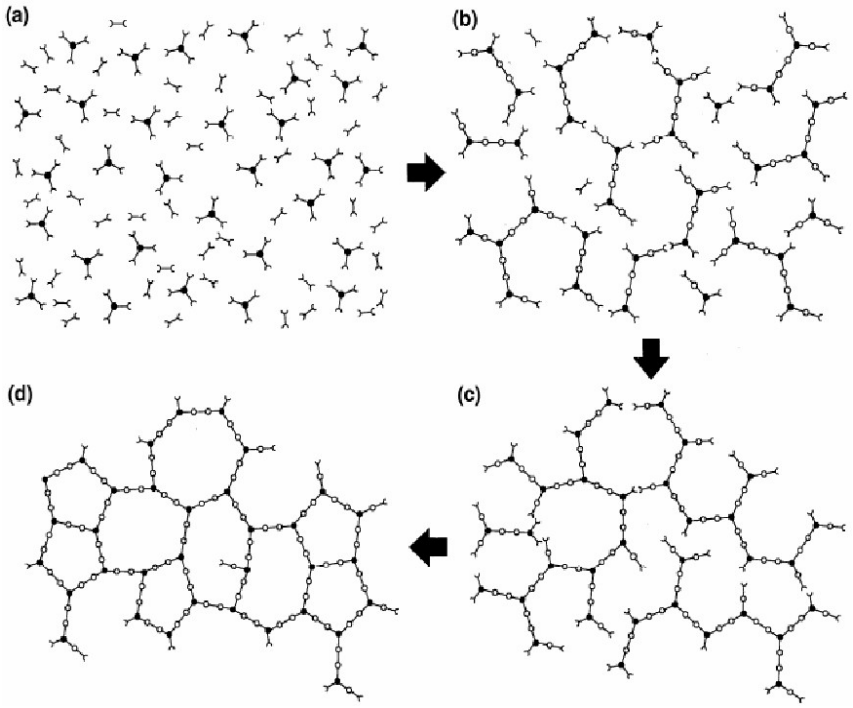

Figure 2-5: The curing process of a thermoset. (a) Uncured state (b) Gelation point (c) Vitrification (d) Fully cured state [38].

Typically, epoxy resins are known to have high reactivity and due to this fact, they are able to be cured with curing agent/hardener under suitable conditions. However, different epoxy resins may have different curing conditions. Some are cured at low or room temperature, and some need to be cured under high temperature. The properties of cured products are, to a certain degree, influenced by the curing agent/hardener used. Because of this, it is equally important to choose a suitable curing agent/hardener for each application. Alternatively, the curing temperature and time can be reduced by adding an accelerator into the mixture.

It is worth to note that there are two types of hardener; (i) addition polymerisation type and (ii) catalytic type [39]. As the name suggests, the former can produce addition polymerisation reaction with epoxy groups within the mixture, and it is used in large quantity. Mixing the right amount of hardener is important as its volume will react with epoxy groups during the curing process to form three-dimensional cross-linking network structures. If the quantity is inadequate, there is a possibility of non-cured epoxy groups left in the mixture, which may result in a system of inferior properties. On the contrary, the catalytic type hardener only offers ions of positive or negative charge during the curing process. Therefore, the amount used only influences the reaction speed and had no impact on the outcome of the properties of the cured product.

Another equally important factor that plays a major role in hardener selection is the curing temperature. The increase in curing temperature will also increase the reaction speed as typically happened in all chemical reaction process. It is important to note that if the curing temperature is too high, the epoxy resin may as well be unevenly heated and possibly yields asymmetric cross-linking density inside the mixture [40], which again may result in a system of inferior properties. It is clear, therefore, to consider the top limit of curing temperature and optimise curing time to get epoxy matrix system with improved overall properties.

2.4 DIRECT-FLUORINATION PROCESS

A considerable amount of literature has been published on surface-fluorination process starting from fundamental researches to practical industrial applications [41, 42]. These studies confirm that the introduction of fluorinated substituents onto polymeric structure is a smart approach to improving properties regarding wettability, adhesion, chemical stability, barrier properties, biocompatibility, and grafting. Hence, it is considered as one of the most effective approaches for chemical modification of polymers. So far, however, there has been little discussion regarding the improvement in term of dielectric properties. In fact, modifications in chemical components at the surface of polymeric insulation should also lead to corresponding modifications in dielectric properties at the surface [43]. Therefore, theoretically, such modification can alter the accumulation of space charge along the surface of the polymeric materials when they are used as insulating material under high voltage DC stress.

There are a couple of approaches to perform this chemical treatment. One of the popular surface treatment techniques, which is being used in this research, is the elemental fluorine treatment, or better known as direct-fluorination [44]. The main advantage of this approach is the high exothermicity of the main elementary stages. Due to this fact, fluorination process can proceed spontaneously in a vacuum chamber or a flow reactor even at low or room temperature and do not require initiation, heating or catalysts. The volume of functional groups, such as COOH, can be adjusted according to the polymer surface when F_2/O_2 mixtures are used. It is a dry process since starting reagents, and the end products are gasses and solids only. There are proven safe ways to neutralise unused F_2 and the by-product HF by converting them into a solid phase.

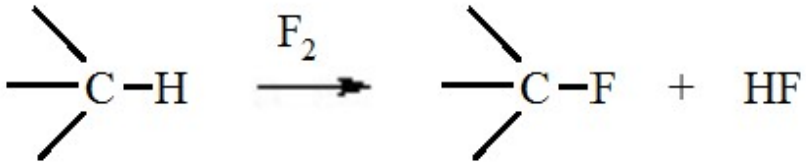

Figure 2-6: A schematic of direct-fluorination treatment; hydrogen atom is substituted by fluorine atom and producing by-product HF.

Furthermore, Kharitonov [45] suggested that there are three different techniques to perform direct-fluorination treatment. The first of those techniques is (i) normal direct-fluorination where hydrogen atoms are substituted by fluorine as illustrated in Figure 2-6, while double and conjugated bonds are saturated with fluorine. Cross-linking and destruction of C-C bonds take place. The thickness of fluorinated surface layer depends on the fluorine partial pressure and treatment duration. Another technique for direct-fluorination is (ii) oxyfluorination that subjects treated polymeric materials with fluorine–oxygen gas mixtures. Additional >C=O, –C(O)F and –C(O)OH groups are incorporated into the polymer structure. The last technique is (iii) an extension of oxyfluorination with the graft polymerisation of some monomers with double bonds, e.g. tetrafluoroethylene, acrylonitrile, acrylic acid and methyl methacrylate. The surface properties of the modified polymer are controlled by the grafted polymer, and there are more chances to change surface properties, e.g. from hydrophobic to hydrophilic.

The direct-fluorination process is a heterogeneous reaction between fluorine gas and its mixtures with the surface of a polymer. Polymeric objects of any shape can be treated, and only the upper surface layer is modified (~0.01–10 μm in thickness), while the bulk properties remain unchanged [46]. In doing so, exceptional surface properties similar to fluoropolymers can be achieved without compromising the bulk characteristics of the pristine polymeric insulation. It is much easier, cheaper and more convenient to apply fluorination treatment on polymers rather than manufacturing fluoropolymers.

The introduction of fluorinated groups through the fluorination treatment reduces the dielectric constant of epoxy resin because of their small dipole and the low polarisation ability of the C-F bond as well as the existence of large free volume [47]. This treatment can also improve the resin's durability in a moist environment and in some cases, reduce moisture absorption due to the nonpolar character of fluorocarbon groups, which further reduces the dielectric constant.

2.5 PLASMA-ENHANCED TREATMENT

As an alternative to direct-type fluorination, plasma techniques have been widely used in industrial applications for treating or pre-treating surfaces of various materials before any coating, printing or adhesion is applied. In most industrial applications, plasma treatment is used to remove any foreign contaminants from the surface of a material, thus making it more suitable for further treatment [48]. Suitable plasma techniques are used to alter material's surface characteristics such as friction, printability, wettability, adhesion, penetrability, biocompatibility, or dye-ability, to adjust them for particular applications [49, 50]. Based on the plasma setup, fast, clean, environmentally friendly plasma-based treatment can introduce surface modifications physically and chemically through numerous parallel processes e.g. cross-linking, grafting, etching, and polymerisation. The physical and chemical modifications on the surface in most cases happened without any changes to the original bulk characteristics [51, 52].

In pre-treatment applications, plasma techniques are used on surfaces before any gluing, printing or lacquering could take place. Likewise, materials like glass and ceramics may also undergo plasma treatment. Glossy materials tend to lose any coating or printing done on their surfaces unless plasma-treated. Typically, industrial oxygen is used in plasma treatment as a process gas, thus getting the label 'Oxygen Plasma' [53, 54]. On the other hand, ambient air from the atmosphere is also used in plasma surface treatments, thus known as 'Atmospheric Plasma'. Subject to the material that is being treated, plasma effects for pre-treatment can last from just a few minutes to even months.

In order to start a plasma, the breakdown voltage, V_b, for the gas must be reached. V_b follows the equation [55, 56];

$$V_b = \frac{B\ (p.d)}{\ln[A(p.d) - \ln[\ln\left(1 + \frac{1}{\gamma_{se}}\right)]} \quad (2\text{-}1)$$

where d is the electrode spacing, p is the pressure, A and B are constants found experimentally, and γ_{se} is the secondary electron emission coefficient of the cathode. According to [57, 58], a small gap is needed to achieve a reasonable V_b at atmospheric pressure. For instance, the V_b for argon at 1 bar and 5 mm gap is estimated to be 2500 V.

Plasma treatment is performed by channelling compressed gas through two concentric electrodes and is subjected to a strong electric field that ionises most of its atoms, as illustrated in Figure 2-7. By applying RF power to the inner electrode between 40 – 500 W, the gas discharge is ignited [59]. From the small electrode gap, the plasma torches are produced from deep within, discharging between the electrodes. The process gas moves from the nozzle to stabilise the plasma torch, and a sharp plasma passage is formed downstream to interact with the treated material a few millimetres away. In a typical operating conditions, the gas velocity is about 12 m s^{-1} with discharge temperature of 150 ˚C [60]. The produced super-ionised-air (i.e. atmospheric plasma) is emitted from the nozzle tip and can be used for surface modification or surface cleaning. The charged particles from the plasma are responsible for its high electrical conductivity [61, 62]. Because plasma consists of electrons, positive ions, UV light along with excited gas molecules and atoms, as well as molecules or neutral gas atoms, it provides a high amount of internal energy. So when all these ions, atoms and molecules mix and interact with a specific surface, plasma treatment is initiated. Therefore, by choosing a set of a gas mixture, power, pressure, etc., the effects of plasma treatment on any surface can also be specified and precisely tuned.

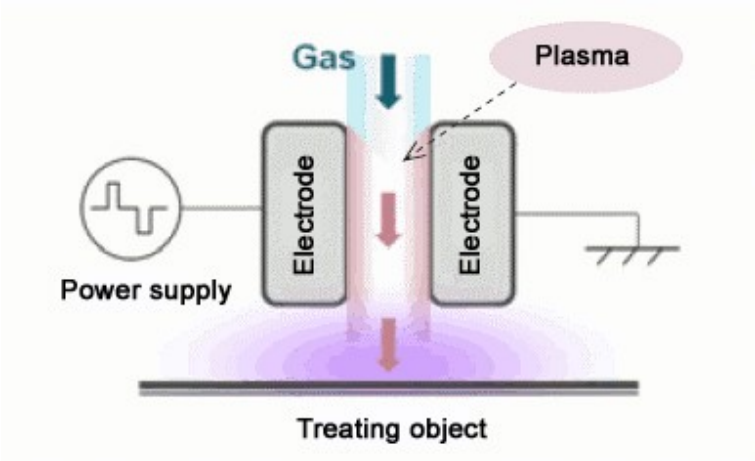

Figure 2-7: A schematic of basic plasma treatment process [63]. A sharp plasma passage is formed downstream to interact with the treated material

2.6 SURFACE FLASHOVER MECHANISM

The occurrences of surface charging inside and on the insulator clearly disturb the local field. Therefore, various studies have been carried out to verify the elements on the dielectric strength of gas insulated systems that include insulating spacers [64, 65]. The insulator material, size, surface condition, contact angle at the triple-junctions, particle contamination, surface charging, and various parameters are known to impact the surface flashover parameters. Most studies are designed to investigate the importance of some parameters for flashover or establish a link between the flashover voltage and the parameter under consideration. These studies showed that the flashover is hugely influenced by components from the fundamental properties of the dielectric material such as surface conductivity and permittivity, as well as non-fundamental components such as metal particle contamination, surface defects, and defects at the triple junction interface [66].

It is widely believed that the surface flashover on epoxy spacer inside a GIS is triggered either (i) by a micro-discharge at an imperfect contact at the triple junction interface, (ii) by a micro-discharge at a defect in the spacer surface, or (iii) by the particle in proximity to the

spacer surface [67]. These discharges produce vapours that may have ionisation energies below that of the system insulation gas, and they may, as well, inject metastable excited species of the insulation gas into the gap region that can affect ionisation growth. These discharges also act as a high-field spot and cause intense electron emission and ionisation. The resulting charges are trapped in the gas-spacer interface and further distort the local field as well as the ionisation process. The flashover path then develops in a way comparable to an electrical tree. In a similar study done by Hama et al. [8], they stressed that the local field concentration at the interface of the cathode and the spacer within the triple junction can generate electrons that will be accelerated by electric field and collide with the insulating spacer to produce secondary electrons. These secondary electrons may accumulate on the insulator surface which further accelerates additional electron emissions that may lead to field distortion and ultimately result in surface flashovers. De Lorenzi et al. [68, 69] stated that the charge injection onto the surface may come from the current driven by the normal component of electric field, and/or from the gradient of the flowing current along the spacer surface, driven by the tangential component of the field. Dynamic unbalance between these two components may result in surface charge accumulation on insulator surface that ultimately may lead to surface flashover phenomena.

Interestingly, under AC or impulse voltages, permittivity is another parameter that determines the surface flashover strength. An increase in this parameter may upset the localised field at the particle on the spacer surface [19]. It will also decrease the applied field and, hence, results in the formation of micro-discharges as described earlier. An increase in permittivity will also increase the energy in the micro-discharges.

2.7 STATISTICAL ANALYSIS OF DATA

Electrical surface flashover is an insulation system failure that occurs when a weak link on the surface of a polymeric insulation fails. The distributions of surface defects on the insulating surface are random, and so do the occurrences of micro-discharges. Therefore, each sample may undergo surface flashover at different voltage even though in theory, the samples are of the same material undergoing the same treatment. Accordingly, in

measuring such random variances, it is necessary to analyse the flashover data using a statistical analysis tool. Although some statistical distribution functions can be applied to electrical breakdown (e.g. Gumbel and Lognormal distribution [70]), the Weibull distribution is the most popular tool used for the analysis of time-to-breakdown from the constant-stress voltage tests or breakdown voltage from ramp-stress voltage tests.

In general, the flashover performance of solid insulation system can be described using two-parameter Weibull distribution. Assuming that the random breakdown process follows the Weibull distribution, the Weibull probability density function *F(x)* indicates the probability of the breakdown phenomenon at an applied field *x*. The overall probability of electrical breakdown of a sample under an applied field less than or equal to *x* can be expressed by the cumulative distribution function:

$$F(x) = \int_0^x f(u)du = 1 - \exp\left(-\frac{x}{\alpha}\right)^{\beta} \qquad (2\text{-}2)$$

where the scale parameter, α, represents the breakdown strength at the cumulative failure probability of 63.2 %. The shape parameter, β, in a simple term, represents a measure of the spread of the breakdown data. The smaller value of β, the larger is the scatter of the breakdown data. The value of β also has an influence on the skewness of the distribution. When a minimum voltage is anticipated in the breakdown data, below which breakdown is not expected to occur, the Weibull distribution can be described by a three-parameter estimate. In this case, the probability of electrical breakdown can be expressed by the cumulative distribution function [71]:

$$F(x) = \int_0^x f(u)du = 1 - \exp\left(-\frac{x-\gamma}{\alpha}\right)^{\beta} \qquad (2\text{-}3)$$

where the values of x are offset by the value γ, the shift parameter. For comparison, a two-parameter Weibull distribution applied to electrical breakdown assumes that breakdown is possible, though perhaps unlikely, at any value of voltage no matter how low. On the other hand, a three-parameter Weibull distribution assumes that there is a minimum voltage γ below which breakdown cannot occur. The third parameter of the Weibull distribution, γ, is utilised when the data points do not fall on a straight line, but on a concave up or down curve. A general indication that a three-parameter Weibull plot should be used is that if on a two-parameter Weibull plot, the points at low failure probabilities fall consistently above or below the linear behaviour associated with the points at higher failure probabilities, giving the Weibull plot a curved appearance rather than a straight line.

In the plot of failure probability as a function of the breakdown strength, Benard's approximation of median rank [72] is normally used to evaluate the unreliability of each failure and provide a 50% confidence interval of the true i th failure among n samples. One axis of the graph should be in a non-linear probability of failure scale while the other axis should indicate the breakdown strength. The axes are scaled in such way that plotted data follows a straight line in the Weibull distribution. When the data are plotted, the data are ordered from the smallest to the largest, and a cumulative probability of failure, $F(x)$ has to be assigned to each point. One best straight line is drawn through the points using the Maximum Likelihood Estimation (MLE) method that gives a better estimation of α and β. The cumulative probability of failure, $F(x)$ is estimated using the median rank method given by:

$$F(x) = \frac{i - 0.3}{m + 0.4} \qquad (2\text{-}4)$$

where i is the progressive order of failed tests and m is the total number of tests. This technique has been recognized to be a good estimation of cumulative failure probability and is even more consistent with the acknowledged computational use of the MLE technique [73]. An example of a Weibull plot is shown in Figure 2-8.

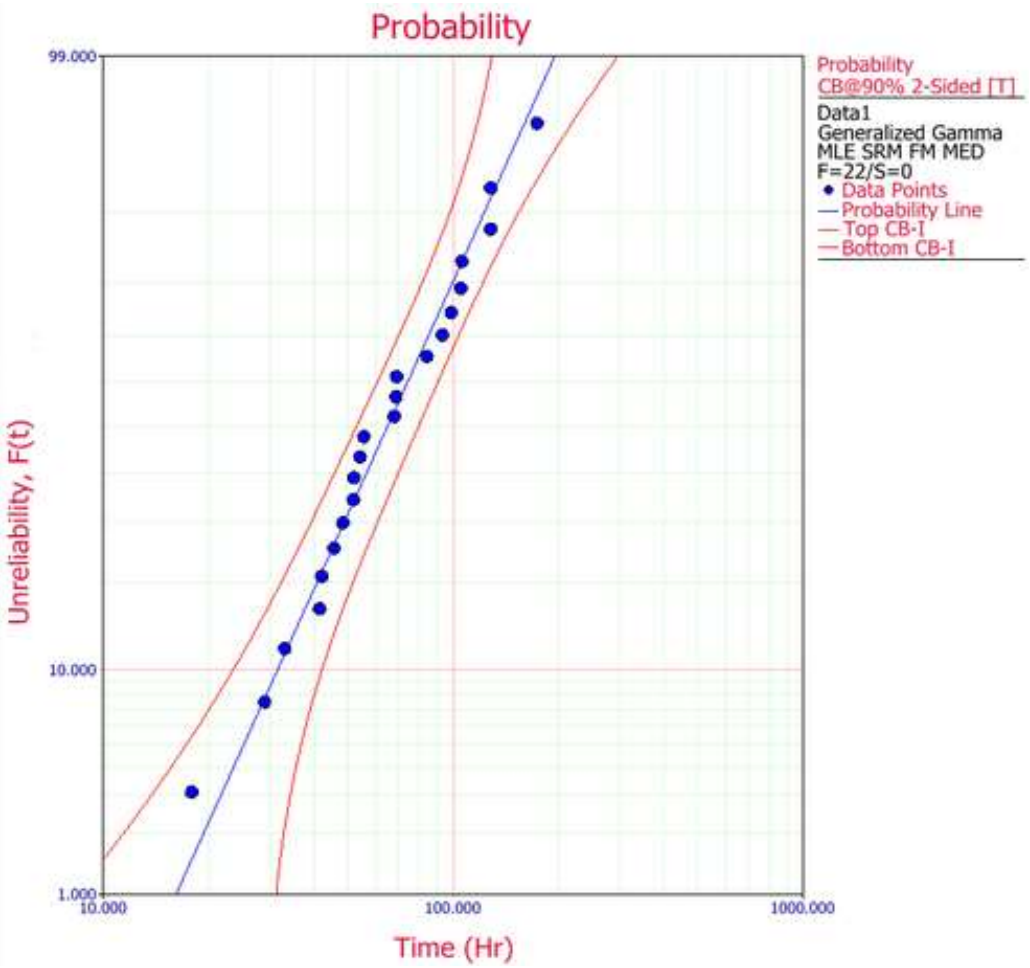

Figure 2-8: Example of Weibull plot using MLE fitted line with 90 % confidence bounds [74]

When applicable, MLE is probably the better choice of methods, because it is presumably more efficient. But MLE does not work in all cases, and other estimation methods, such as the Least Squares estimation (LSE), are required. This alternative method can be useful in cases when maximum likelihood fails, for instance, data that include a threshold parameter. In LSE, it is assumed that there is a linear relationship between two variables. Therefore, a dataset that constitute a pair (x_i, y_i) = (x_1, y_1), (x_2, y_2),..., (x_n, y_n) were obtained and plotted. The least squares principle minimises the vertical distance between the data points and the straight line fitted to the data. To fit a Weibull distribution to the flashover data, notice that the CDF for the Weibull can be transformed to log-log representation to give [75]:

$$\log(\alpha) + \log(-\log(1 - F(x))) * \left(\frac{1}{\beta}\right) = \log(x - \gamma) \qquad (2\text{-}5)$$

This log-log representation gives a linear relationship between log [-log (1 - *F(x)*)] and log (x - γ). Least squares can be used to fit a straight line on the transformed scale using *F(x)* and (x - γ) from the empirical CDF. The slope and intercept of that line lead to estimates of α and β.

2.8 THE PULSED ELECTROACOUSTIC TECHNIQUE

Space charge dynamics plays a key role in the performance of insulating materials and, therefore, it is crucial to develop a suitable experiment technique to measure the accumulated space charge inside the bulk of the dielectric materials [76]. For this reason, there are generally two types of measurement technique being developed. The first of those two techniques is destructive techniques, which were first developed in the early 20th century, involving the use of powders, a field mill, or an electrostatic probe. As the name suggests, using this technique, the dielectric had to be cut into small slices, which may disturb the charge distribution. This apparent drawback paved the way for the development of the second measurement technique, the non-destructive technique.

The thermal shock method or thermal step method (TSM) was the first non-destructive measurement technique in which a flat sample is placed in between two thin electrodes [77]. The sample is subjected to a thermal pulse, which will travel as a thermal wave through the sample and, therefore, may slightly shift the space charge. At the same time, charges on electrodes are also shifted, which in turn produce small voltage and current. The movement of the thermal wave can be measured and, therefore, by solving convolution formula, the original space charge profile can be determined. This method, however, requires costly instrumentations and complex mathematical formula, hence limiting its

usage. The pressure wave propagation (PWP) is another non-destructive measurement technique that has been widely used [78]. Instead of using the thermal pulses as in TSM, this method uses a pressure pulse of very short duration generated from a piezoelectric foil. There is no need for solving complex convolution since the pulse is short and, thus, makes it easier to use in comparison to TSM method. The laser-induced pressure pulse (LIPP) method, on the other hand, uses short laser pulse (<< 1 ns) at one side of the sample that causes energy shock on the surface [79]. This shock generates a pulsed acoustic wave that travels through the volume of the sample. The theory is similar to PWP, but with a faster rise time.

The non-destructive space charge measurement technique used in this study is the PEA method. The basic principle of PEA technique is shown schematically in Figure 2-9. This technique is based on the principle that, when an electrical pulse is applied to a dielectric with stored charges, acoustic pulses are generated by the displacement of each locally charged region and propagates through the material. The acoustic wave is sensed by a piezoelectric transducer and is translated into a meaningful electrical signal. The use of a polymeric piezoelectric transducer is based on its properties, including high levels of piezo activity, wide frequency range and dynamic response, low acoustic impedance, etc. [80].

The PEA system used in this study includes the top and bottom electrodes, a dielectric sample, a transducer and an acoustic absorber. A pulse source and a DC voltage source are connected in parallel to the electrodes. On the application of DC voltage, charges are injected into the sample when the field is high enough. The charge distribution in the bulk induces surface sheet charges on both electrodes, as a function of distance from the electrode. With the application of short electrical pulses across the sample, the charges are stimulated by the pulse field to create the pulsed electrostatic forces. These forces generate pressure waves that travel as acoustic waves through the sample in both directions. The wave travelling downwards will be transmitted to the bottom electrode and then to the transducer. Surface charge is induced at the transducer surface from the piezoelectric effect [80]. The transducer will translate the surface charge into a meaningful electrical signal.

The amplitude obtained is determined by the waveform profile in the time domain as it is proportional to the local charge density. The acoustic absorber is needed to absorb the acoustic wave, so that the reflection of the acoustic wave is filtered, which otherwise would cause interference and distortion to the signal. The signal is then amplified and is fed to an oscilloscope for further analysis.

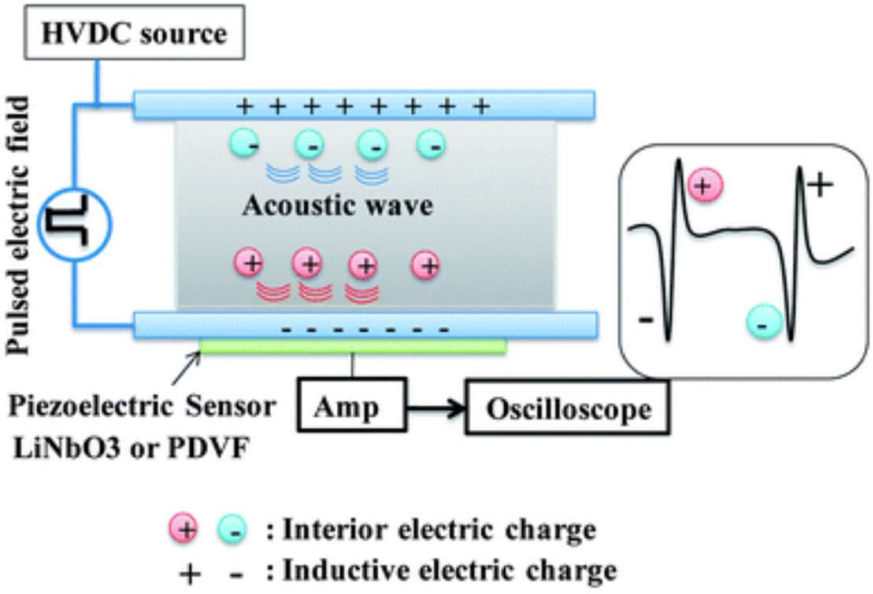

Figure 2-9: A schematic of basic principle of PEA method [81]. Surface charge is induced at the transducer surface from the piezoelectric effect. The transducer will translate the surface charge into a meaningful electrical signal

Meanwhile, the wave that travels upwards will be transmitted to the top electrode and then to the interface, where it will be reflected down and back into the system. This wave will reach the transducer at a later time without overlapping with the other wave [81]. Due to the simple design, ease of usage and low cost, the PEA method has been widely used in the study of space charge dynamics in dielectric materials.

2.9 RAMAN MICROPROBE SPECTROSCOPY

The foundation of Raman spectroscopy started in the early 20th century when the scattering of monochromatic radiation with a change of frequency was anticipated in theory by A.

Smekal [82]. The scattering of light by different means had long been investigated by Rayleigh in 1871, Einstein in 1910 and others. However, no major variation of wavelength had been detected. With this in mind, many researchers were looking into the idea of inelastic scattering, which was first reported by Raman in 1928 [83], a discovery that led him to the Nobel Prize in Physics. This discovery used monochromatised sunlight as a light source and the human eye as a detector. Raman instrumentation was further developed (based around arc lamps and photographic plates) and soon became very popular in 1950's and onwards. From then on, Raman instrumentation has transformed to a great height and modern instrumentation typically consists of a laser source, a detector, objective lens, Rayleigh filter, and a spectrograph.

In principle, Raman spectroscopy involves using a monochromatic light source (e.g. laser) to excite molecules in a material into vibration. These vibrations are associated with a specific molecule, and although most of the light is scattered back elastically, some of it is scattered back inelastically. This change in energy is unique for each molecule and, hence, provides a unique trait of the molecular composition of the material [84]. During this process, energy is exchanged between the photon and the molecule in a way that the scattered photon is of higher or lower energy than the incident photon. The difference in energy is made up by a change in the vibrational and rotational energy of the molecule and provides information on its energy levels. Stokes radiation happened at lower energy, i.e. longer wavelength when compared to Rayleigh radiation. On the other hand, anti-Stokes radiation possesses higher energy. The energy decrease or increase is associated with the vibrational energy levels in the ground electronic state of the molecule. In other words, the observed Raman shift of the Stokes and anti-Stokes radiation are a direct measure of the vibrational energies of the molecule. A schematic of Raman spectrum may appear as shown in Figure 2-10. As the energy level of the photons are connected to their original state of the material, this results in spectral peaks with higher intensity. For this reason, it is the Stokes region of the spectrum that is usually applied in Raman spectroscopy.

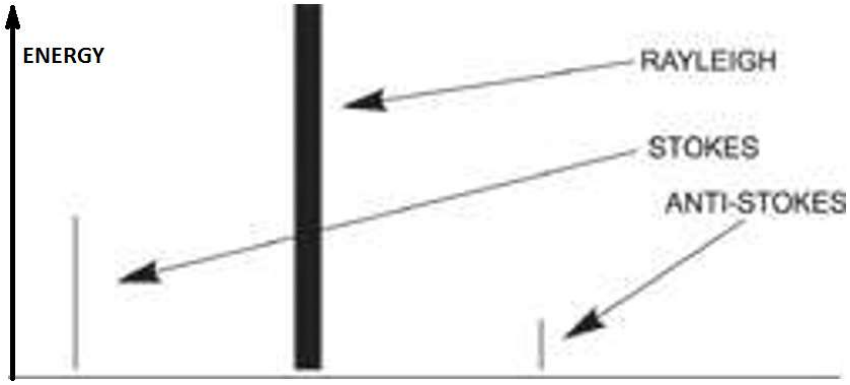

Figure 2-10: A schematic of the energy level of Raman spectrum; Rayleigh, Stokes and anti-Stokes [85]. Stokes region of the spectrum that is usually applied in Raman spectroscopy.

From the beginning, much of the theoretical and experimental work in Raman spectroscopy focused on the fundamentals of inelastic scattering and its application to understanding molecular structure. However, as the time passed, Raman spectroscopy became ever more significant for the advancement in chemical measurements. Undoubtedly, Raman spectroscopy has a big contribution to the field of analytical chemistry as a whole, not only because of the impact of the technique itself, but also because its development anticipated a revolution in the way analytical measurements were to be made. The revolution was the insertion of powerful physical methods into a discipline that had been primarily pure chemistry.

Among Raman instrumentations, a research grade optical microscope is used together with the excitation laser and the spectrometer, in order to obtain both conventional images and to generate Raman spectrum from the sample areas approaching the diffraction limit (~1 μm). One advance feature of Raman microprobe spectroscopy is the confocal mode. Confocal mode involves placing a pinhole at the back focal plane of the objective lens. In doing so, photons coming from areas of the sample that are remote from the focal plane are strongly rejected, as illustrated in Figure 2-11. Therefore, analysis of specific layers within a material and depth profiling through a sample can be accomplished [86].

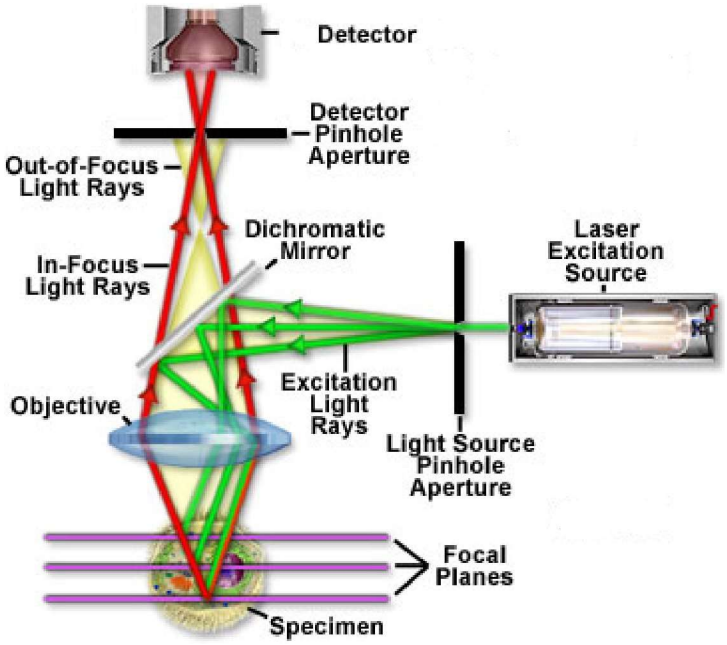

Figure 2-11: A schematic showing the optical arrangement in the confocal microscope. Only in-focus light rays pass through a confocal pinhole [87]

2.10 SCANNING ELECTRON MICROSCOPY

One big concern with a conventional optical microscope is the poor image resolution due to the limited wavelengths of light (~500 nm). With the advancement in scope technology, Max Knoll [88] was able to observe the surface of a sample at nano-scale using scanning electron microscopy (SEM) in 1935. Since then, SEM has been used extensively to investigate the morphology of the material under study. In theory, the wavelength of electrons in SEM is shorter than that of visible light, leading to much-improved resolution as compared to the conventional microscope. The equation of wavelength λ of an electron with the accelerating voltage, V, is given by;

$$\lambda = \frac{h}{\sqrt{2meV}} \qquad (2\text{-}6)$$

where h is the Planck constant, m is the mass of an electron (9.109×10^{-31} kg), and e is the electron charge (1.602×10^{-19} C).

The SEM main components are kept in a vacuum chamber to avoid collisions with gas particles during operation as illustrated in Figure 2-12. An electron beam from a tungsten-filament electron gun is accelerated through a potential difference of 5-30 kV. The beam passes through an optical system containing a condenser lens and an objective lens, as well as an adjustable aperture, through which the high-angle electrons of the beam are eradicated. The condenser lens is used to produce a thin coherent beam while objective lens is used to focus the beam onto the sample. The electron beam is projected onto the surface, and the resulted electrons are captured by the two detectors. The signal from the detector is then electronically amplified and sent to a viewing monitor [89].

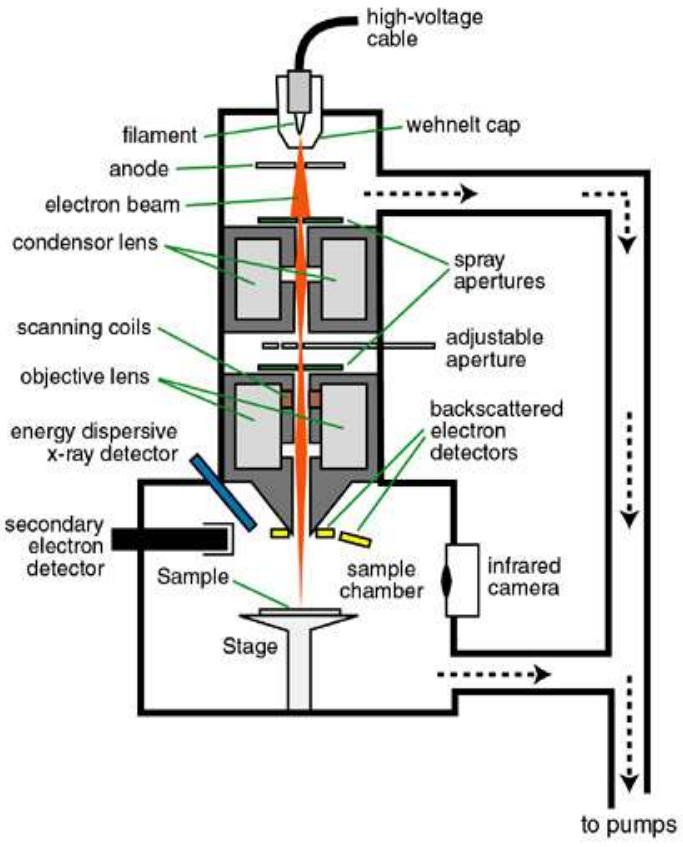

Figure 2-12: A schematic of Scanning Electron Microscope [90]. The electron beam is projected onto the surface, and the resulted electrons are captured by the detectors.

The type of signals produced by SEM includes secondary electrons and back-scattered electron. The secondary electron is formed by inelastic collisions, resulting in the emission of low energy secondary electrons in the range of 10-50 eV [91]. These low energy electrons can only escape from areas near the surface of the sample. On the other hand, back-scattered electrons possess higher energy level, which is released from the deep layer within the sample, as well as from the surface due to elastic back-scattering.

2.11 ENERGY-DISPERSIVE X-RAY SPECTROSCOPY

In SEM, once a projected beam of electrons hits atoms on the top of a tested material, secondary and backscattered electrons are released from the surface of the material. Upon the release of secondary electrons, the collision leaves thousands of the sample's atoms with holes in the electron shells where the secondary electrons used to be. If the 'holes' are in inner shells, the atoms are not in a stable state. To stabilise the system, electrons from outer shells will drop into the inner shells. Since the outer shells are at a higher energy level, for this to happen, the atom must lose some energy. It does so by releasing X-rays energy.

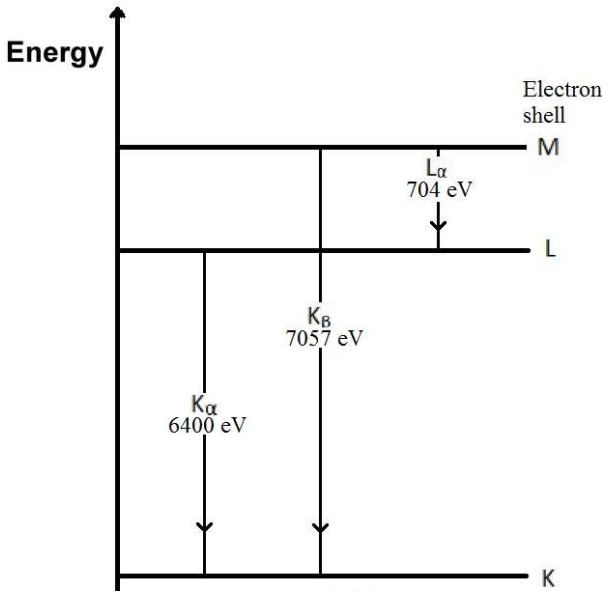

Figure 2-13: Examples of X-rays energy being released from electron shells. When an electron from the inner shell is substituted by an electron from the outer shell, X-ray energy is released from the material.

The X-rays produced from the sample atoms are unique in energy and wavelength to the element of the parent atom, as well as the exact shells that lost those electrons and the exact shells that replaced them. For example in Figure 2-13 for iron (Fe) atom, when the electron in the inner-K shell is substituted by an electron from the middle-L shell, a 6400 eV K_α X-ray is released from the material. When the electron from the inner-K shell is substituted by an electron from the outer-M shell, a 7057 eV K_β X-ray is released from the material. So when an electron from the middle-L shell is substituted by an electron from the outer-M shell, a 704 eV L_α X-ray is released from the material.

So, an EDX spectrum of iron (Fe) would have three peaks; the first peak of an L_α at 704 eV, the second peak with largest X-ray energy of a K_α at 6400 eV, and the third peak of a K_β at 7057 eV, as in Figure 2-14.

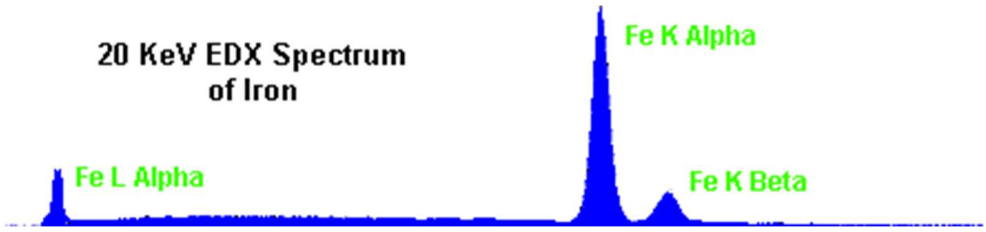

Figure 2-14: Example of EDX spectrum for iron (Fe) [92] with 3 peaks; L_α at 704 eV, K_α at 6400 eV, and K_β at 7057 eV

The fact that lower atomic number elements have fewer filled shells, they have a lower number of X-ray peaks. For example, carbon only has one peak, a K_α X-ray at 282 eV. Meanwhile, the higher atomic numbered elements have a higher number of X-ray peaks. Though some of the high atomic numbered X-rays can be over 50 keV, a typical spectrum range of 0-20 keV can qualitatively identify all the elements from element number 5 boron (B) to element number 92 uranium (U).

In essence, each element has unique X-ray lines that permit a sample's elemental composition to be recognized by a non-destructive technique. Since the X-rays involve the electron beam interaction with the sample surface, only the area of the sample being focused is studied. This feature enables the SEM to execute elemental study in designated areas as small as 0.5 μm in size. The X-rays are produced from a depth comparable to the depth of the secondary electrons being emitted. Based on the material's density and accelerating voltage of the incident beam, this is typically from 0.5 to 2 μm in size. Detectability limitation can be as small as 0.2 % for the higher atomic number elements.

EDX analysis can also quantify the elements being detected. A quantitative analysis can be performed either by a standard-less or a standard analysis. A standard-less analysis involves quantifying the elements by measuring the area under the peak of every identified element [93, 94]. Based on the accelerating voltage of the beam-producing-spectrum, a calculation is performed to create sensitivity factors that will translate the area under the peak into the weight or atomic percentage. Computer software is utilised to filter out the background noise in the EDX spectrometer. The software then does a Gaussian fit on the elemental peaks involved. Then it performs the calculations for the area under the peaks. Among the most used algorithms is ZAF [95] where Z represents the elemental atomic number, A represents the absorbance while F represents the fluorescence values to compensate for the X-ray peak interaction. From this information, the atomic and weight percentage are computed.

Another quantitative analysis, the standard quantification [96, 97], is carried out in a similar way. Instead of executing ZAF algorithms on the areas under the elemental peaks, the areas are compared to standard files that are spectra of the elements to be quantified acquired under the exact conditions of the unknown spectrum. Because this analysis requires the additional comparing spectrum, this analysis is lengthy and usually is of the same accuracy

with a standard-less analysis, excluding the case when the X-ray peaks overlap one another or when the elements are in a very small quantity.

2.12 SURFACE POTENTIAL DECAY

The study of surface potential decay of insulating materials has become an area of interest since the discovery of cross-over phenomenon in surface potential decay in 1967 by Ieda [98], as shown in Figure 2-15. This discovery reveals that dielectric material with a high initial-surface-potential, decays faster in comparison to the dielectric material of low initial-surface-potential. In order to understand the mechanism that governs this phenomenon, many assumptions and theories have been made to describe this discovery. The concept of the deep traps on the surface and shallow traps in the material were used to qualitatively describe the cross-over phenomenon. As corona source deposited charges onto the insulating material, the potential at the surface of the material increases to a high value, thus allowing electrons to move easily across the deep trap due to their high energy state. Therefore, charges on the high surface-potential decay faster. Equally, if the surface of the insulating material is charged to a lower value by corona discharge (i.e. the surface potential is low), the electrons do not have enough energy to move across the deep trap. Therefore, charges on the low surface-potential decay slower [99]

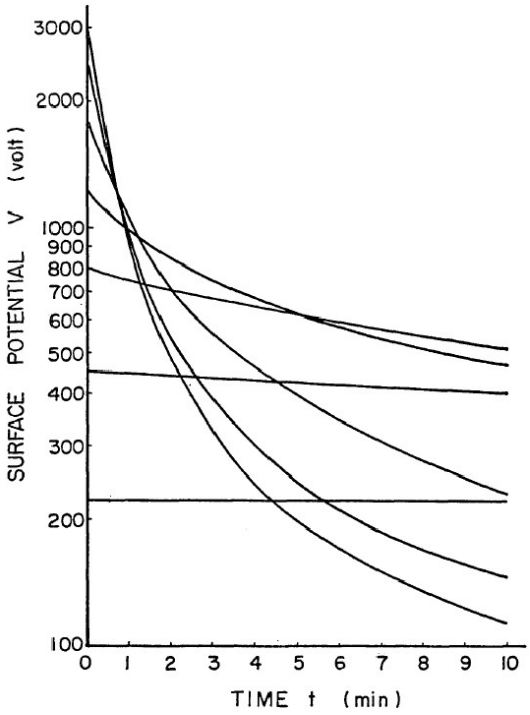

Figure 2-15: Example of cross-over phenomenon as discovered by Ieda [98]. It proves that dielectric material with a high initial-surface-potential, decays faster in comparison to the dielectric material with low initial-surface-potential.

There are several techniques to quantify surface potential without making contact with the surface of the insulating material. Among the techniques, Kelvin probe method utilises a non-contact, non-destructive vibrating capacitor device, which is used to measure the potential of the surface of insulating material [100]. The probe vibrates perpendicularly to the surface in test and the current flowing to and from the probe changes proportionately to the amplitude and frequency of the vibration. The tip of the probe is positioned around 0.2 – 2.0 mm away from the surface of the sample. It is important to note that Kelvin probe is an extremely sensitive instrument. Therefore, the results can be affected by electromagnetic noise and mechanical disturbance from the cables, external electric field source, piezoelectric effects and mechanical parts of the instrument. Therefore, this technique needs a stable ambient condition for it to work accurately and the price of this instrument is relatively expensive, which makes it a less favourable technique to adopt.

Another surface potential measuring technique, the electrostatic probe method, involves a control loop and an integrated high voltage source driving the probe potential for cancelling out the electric field between the surface and the measuring probe [101]. Thus, this instrument can measure the potential of the insulating surface directly. This method is also known as 'feedback-null surface potential monitors' or 'non-contact voltmeters'. While electrostatic probe can directly measure the potential of the insulating surface, the measuring range is less than 5 kV, which is rather small.

The measuring technique used in this research is based on the field mill method [102]. Field mill method utilises the principle of electrostatic induction. Field mill comprises of one or more electrodes and a rotating shutter that is earthed. Because the rate of decay is constantly changing, there is a need to measure the strength of the electric field continuously which explains the need to measure the charged state of the sensor plate, discharge it, and measure again in sequence. This is done by repeatedly exposing the sensor plate to the external electric field to charge it, then shielding the plate to allow it to discharge. A charge amplifier measures the amount of charge on the charge plate and translates this value to an analogue voltage. The result obtained using this method varies with the distance between the instrument and the measured surface. Hence, this instrument needs to be properly calibrated. Figure 2-16 shows the schematic diagram of the field mill operation. This technique has the advantage of being low cost and has a wide measuring range.

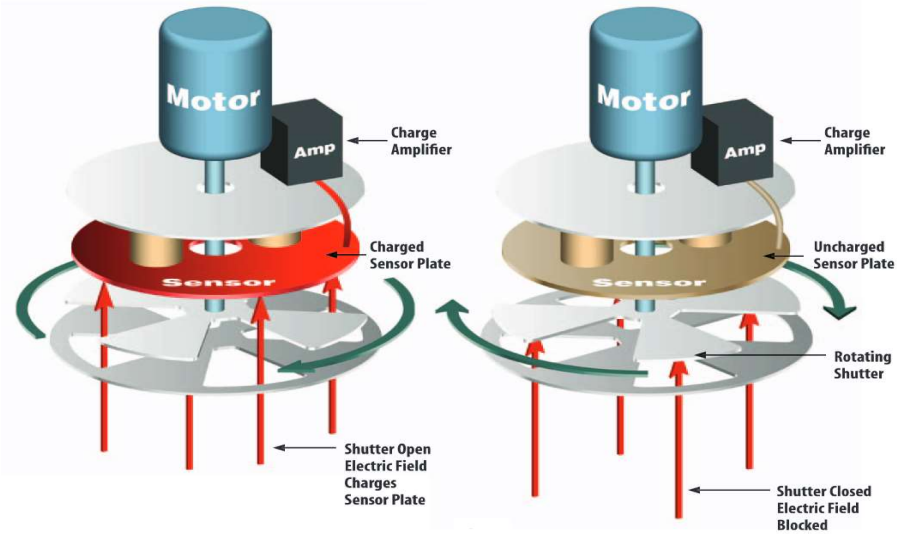

Figure 2-16: A schematic diagram of the field mill operation [103]. The electric field is continuously being quantified by measuring the charged state of the sensor plate, discharge it, and measure again in sequence.

CHAPTER THREE: SAMPLE PREPARATION

3.1 MATERIALS

Bisphenol-A type epoxy resin (Araldite LY556) together with anhydride hardener (Aradur 917) and imidazole accelerator (DY070) from Huntsman Advanced Materials were used to make hot curing epoxy samples throughout this research. This matrix of epoxy resin has outstanding mechanical, dynamic and thermal properties, as well as low room temperature viscosity [104]. It also possesses long pot life (>1 week at room temperature) and excellent chemical stability, especially to acids at a temperature up to 80 ºC. Because of these outstanding attributes, this epoxy resin mixture is widely used for high-performance composite parts. On top of that, it has good fibre impregnation properties, and it is easy to produce. Figure 3-1 shows a representation of repeat unit of Araldite LY556 resin, Aradur 917 hardener, accelerator DY070 and the formed three-dimensional network structures of the system [105]. During the curing process, the epoxide ring at the end of the resin chain reacts with the anhydride in the hardener to form a link between the two molecules and, thus, allowing a chain to be formed.

a

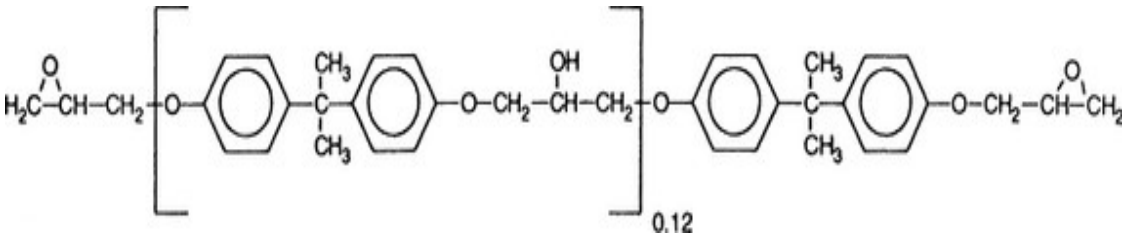

b

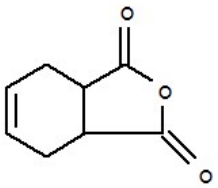

c

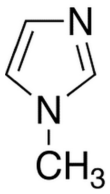

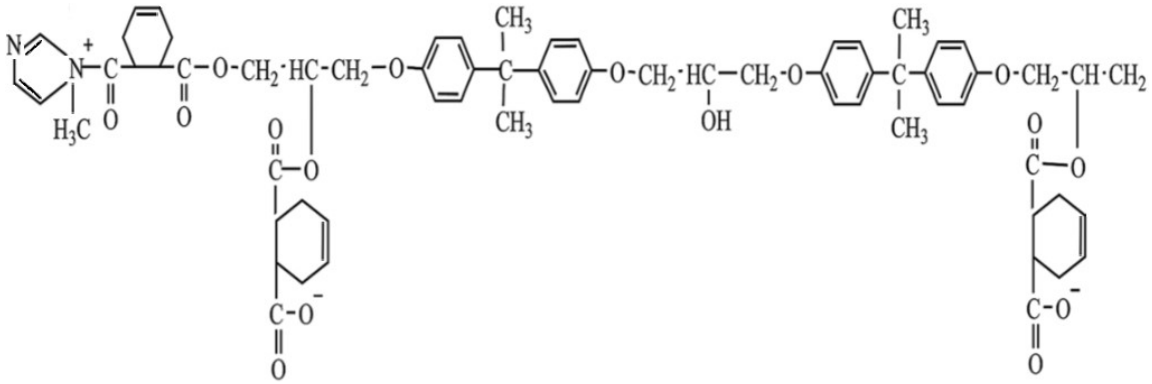

d

Figure 3-1: Representation of chemical structure of (a) Araldite LY556 resin (b) Aradur 917 hardener (c) Accelerator DY070 and (d) the formed three-dimensional network structures of the system

The key data for Araldite LY556, Aradur 917 and Accelerator DY070 are shown in the datasheet as in Table 3-1 below:

	Araldite LY556	**Aradur 917**	**Accelerator DY070**
Aspect (visual)	Clear, pale yellow liquid	Clear liquid	Clear liquid
Colour (Gardner)	< 2	< 2	< 9
Viscosity at 25 ºC	10000 – 12000 mPa s	50 – 100 mPa s	$\leq$ 50 mPa s
Density at 25 ºC	1.15 – 1.20 g cm^{-3}	1.20 – 1.25 g cm^{-3}	0.95 – 1.05 g cm^{-3}
Epoxy content	5.30 – 5.45 eq kg^{-1}	-	-
Flash point	>200 ºC	195 ºC	92 ºC

Table 3-1: Key data for Araldite LY556, Aradur HY917 and Accelerator DY070 by Huntsman Advanced Materials [104]

3.2 EPOXY SAMPLE PREPARATION

The product mixture of epoxy resin Araldite LY556 and hardener Aradur 917 with accelerator DY070 is a low viscosity, solvent-free system based on the attributes of Bisphenol-A epoxy resin with anhydride hardener. The ratio of this epoxy matrix system is shown in Table 3-2 below. A stoichiometry investigation done by Nguyen [106] revealed that the ratio from the manufacturer gives the optimum dielectric performance for unfilled epoxy resin samples.

	Parts by weight	**Parts by volume**
Araldite LY556	100	100
Aradur 917	90	86
Accelerator DY070	0.5 – 2	0.6 – 2.4

Table 3-2: Ratio for epoxy resin mixture provided by Huntsman Advanced Materials [104] for optimum dielectric performance for unfilled epoxy resin samples

The mould used for preparing epoxy resin samples is made up of two stainless steel plates with the dimension of 120 mm x 150 mm as pictured in Figure 3-2. There are two slots on both sides of the upper plates. These slots are used to fill in viscous epoxy resin mixture. A plastic film spacer, which defines the thickness of the sample is prepared by cutting out the middle part and is placed in between the two steel plates. During curing, the mould is placed in the oven at an angle so that the mixture can flow into the mould using gravity feed. A release agent QZ13 is then applied to the surface of the mould to help release the cured sample from the mould when curing is done. The detailed steps in epoxy resin preparation are listed in Table 3-3 below:

1	The epoxy resin is preheated to 40 ºC to reduce its viscosity
2	The right ratio of epoxy resin and hardener is degassed separately inside vacuum-oven (10^3 Pa at 40 ºC) for 30 min
3	The mixture is mixed together using magnetic stirring (600 rpm at 40 ºC) for 60 min

4	The mixture is again degassed inside vacuum-oven (10^3 Pa at 40 ºC) for 10 min
5	The prepared plastic film spacer is positioned in between the two stainless steel plates and are fastened together with screws
6	The mixture is filled into the slot of the mould
7	The mould is then placed in the oven at 80 ºC for 4 hours for curing process
8	The mould is again heated at 120 ºC for another 8 hours for post-cured process
9	The sample is released from the mould and is cut into the desired shape

Table 3-3: Detailed steps for epoxy resin preparation. During curing, the mould is placed at an angle so that the mixture can flow into the mould using gravity feed.

The epoxy resin samples prepared this way are only as thick as the plastic film spacer being used. The typical sample thickness prepared using this method is between 50 – 700 µm. The thickness of the sample is determined by the middle spacer. So, to get different sample thickness, a different set of middle spacer is used.

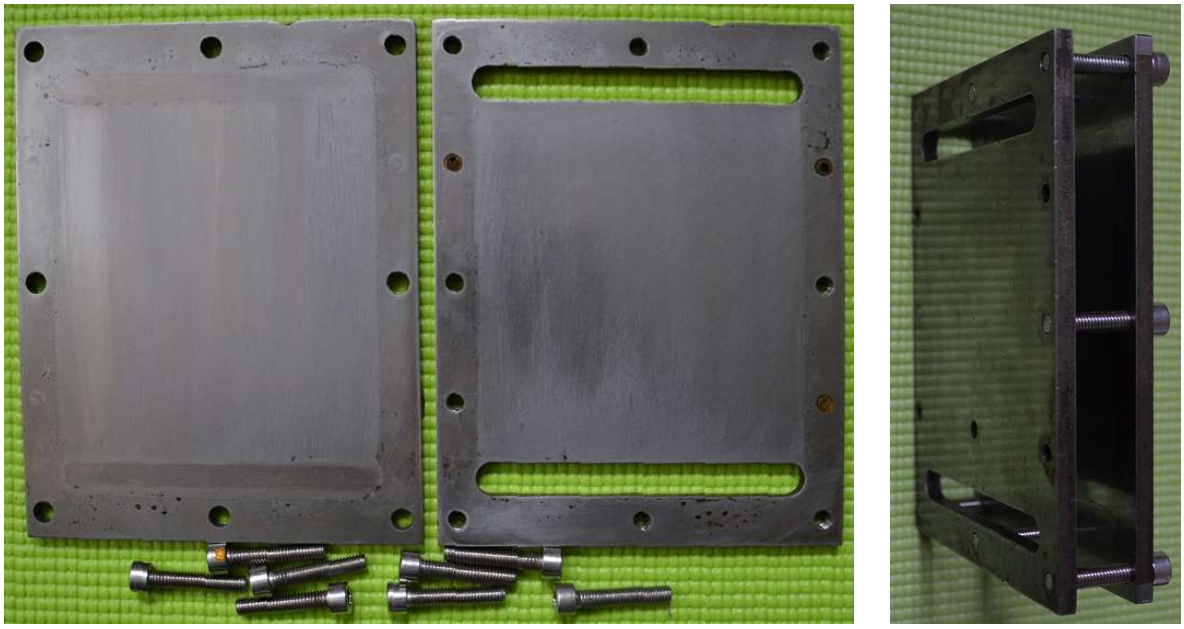

Figure 3-2: Mould used for making epoxy resin samples. A release agent QZ13 is used to help release the cured sample from the mould when curing is done.

For this research, three different thickness set of epoxy resin samples were prepared in the chemical prep room; 250 µm, 300 µm, and 10 mm as shown in Figure 3-3. The 250 µm and 300 µm thick samples are cut into a square shape of 4 cm x 4 cm size while the 10 mm samples are already moulded into a cylinder of diameter 3 cm. The properties of the cured formulation of the samples (cured for 4 hours at 80 ºC and post-cured for 8 hours at 120 ºC) are given in Table 3-4.

Properties	Value
Glass transition temperature (TG DSC)	144 - 148 ºC
Glass transition temperature (TG TMA)	125 - 128 ºC
Tensile strength	83 - 93 MPa
Elongation at tensile strength	4.2 - 5.6 %
Ultimate strength	80 - 90 MPa
Ultimate elongation	5.0 - 7.0 %
Tensile modulus	3100 - 3300 MPa
Flexural strength	125 - 135 MPa
Deflection at maximum load	10 - 18 mm
Fracture toughness K1C	0.56 - 0.6 MPa m^{-1}
Fracture energy G1C	88 - 96 J m^{-2}
Water absorption (1 day, 23 ºC)	0.10 - 0.15 %
Coefficient of linear thermal expansion (20 - 100 ºC)	55 - 57 x 10^{-6} K^{-1}
Coefficient of linear thermal expansion (100 - 130 ºC)	67 - 70 x 10^{-6} K^{-1}
Poisson's ratio, µ	0.35

Table 3-4: Properties of cured formulation of epoxy resin; Araldite LY556, Aradur HY917 and Accelerator DY070 [104]

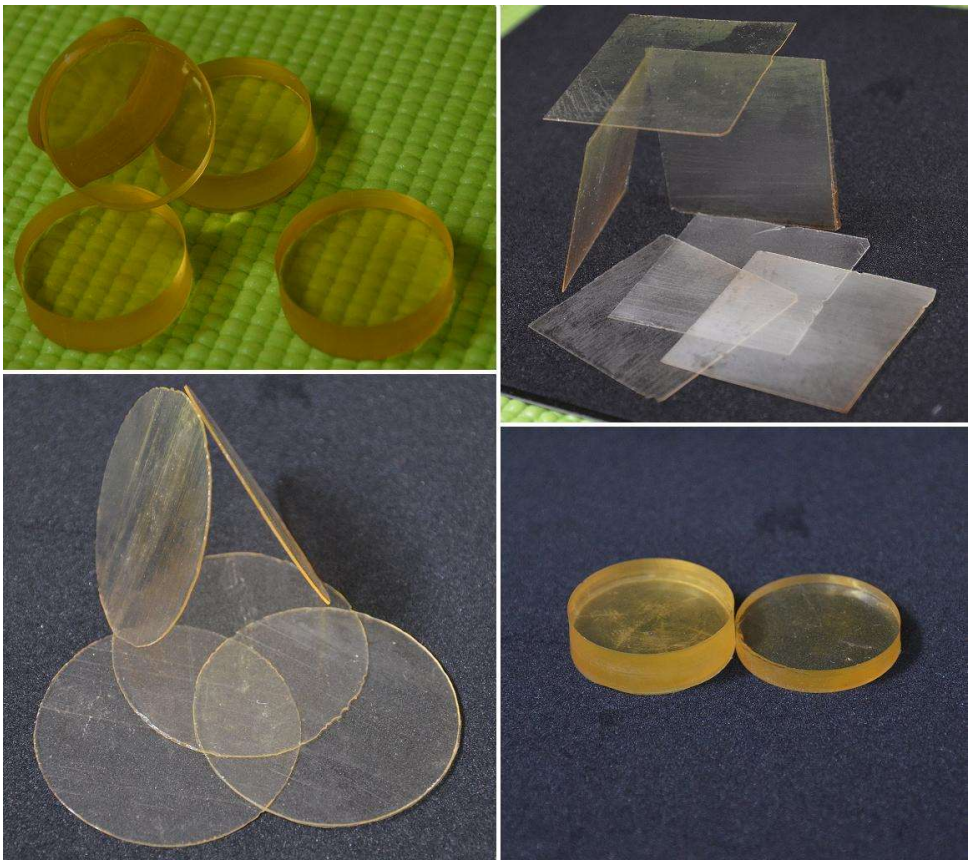

Figure 3-3: Epoxy resin samples of different thickness prepared in the lab. The epoxy is cured for 4 hours at 80 ºC and post-cured for 8 hours at 120 ºC

3.3 FLUORINATION PROCESS

Once the epoxy resin was cured, it was sent to undergo direct-fluorination treatment in Tongji University, China. The fluorination process was carried out in a closed stainless steel vessel. After evacuation, the fluorine and nitrogen mixture of 12.5 % F_2 was pumped into the vessel, and the samples were fluorinated on both sides. The gas mixture pressure in the vessel at 55 °C was maintained at 0.1 MPa. Five different fluorination times were done onto each epoxy resin sample set; 30 min, 60 min, 120 min, 180 min, and 240 min. For simplification, the fluorinated samples will be referred to as F30, F60 and so on, while the non-fluorinated sample will be referred to as F00. After the reaction, the reactive gases were purged from the vessel with nitrogen. In order to remove the emitted by-product

hydrogen fluoride (HF) gas from the reaction, sodium fluoride (NaF) pellets were placed inside the vessel to produce neutralised solid form of sodium bifluoride ($NaHF_2$) [107].

Through direct-fluorination treatment, the 'light' hydrogen atoms are replaced with 'heavier' fluorine atoms, so the density of the treated surface-fluorinated epoxy resins should be greater as compared with the density of the original materials [108]. In order to reduce the possibility of defect formations in the polymer during the fluorination treatment, namely the chain scissions, macro- and micro-defects, as well as caverns, a "mild" treatment condition is adopted at the industrial level, as well as in this research. For example, the fluorine gas is diluted with nitrogen gas, helium gas, argon gas, carbon dioxide, etc. and the composition of fluorine gas is typically around 1–20 vol%. Even when fluorine composition is at 1 vol%, the surface-fluorination thickness dependence on fluorination time is still valid. It has been found that the influence of diluents such as nitrogen gas, helium gas, argon gas, and carbon dioxide on the fluorination rate is significant but not very high [21].

Another set of epoxy resin samples was sent to Laboratory of Plasma Physics and Materials, Beijing to undergo plasma-enhanced fluorination (PEF) treatment. The reaction gas was ignited by an RF source at 30 kHz. The reactor contained two aluminium barrel electrodes that were coated with alumina. The inner electrode on which the sample was placed was connected to the RF source while the outer one was grounded. The main vacuum pump was used with a liquid nitrogen condenser that trapped any residual gases. The chamber was thermostatically controlled and maintained either at room temperature or about 90 °C during the process. Several parameters could be tuned, in particular, inlet precursor composition, e.g. the possible presence of a second gas with the fluorinated reagent. Detailed plasma treatment parameters are available in Chapter 8.

3.4 CHAPTER SUMMARY

This chapter gives a brief explanation of the component materials and the selection rationale adopted for this research. It also gives information regarding fluorination treatment carried out on the prepared epoxy resin samples. Stoichiometrically balanced reactions of Bisphenol-A type epoxy resin (Araldite LY556) together with anhydride hardener (Aradur 917) and imidazole accelerator (DY070) from Huntsman Advanced Materials (with weight ratio 100:90:2) offer a pathway to a host of high-molecular-weight polymers that have robust mechanical behaviour, adhesion to a variety of active surfaces, attractive optical characteristics and an exceptional barrier to oxygen and other atmospheric gases. On top of that, the followed-through fluorination treatment gives the polymer a high surface energy, high thermal stability, enhanced chemical resistance, and immiscibility with most other hydrocarbon-based polymers. These features are a direct result of the low polarisability of the fluorine atom, the exceptionally strong nature of the C–F bonds, and the relatively small size of fluorine [109].

CHAPTER FOUR: SAMPLE CHARACTERISATION

4.1 SCANNING ELECTRON MICROSCOPY

By only looking at the direct-fluorinated and non-fluorinated epoxy resin samples, one can tell no difference in term of appearance, colour, transparency, elasticity, etc. between these samples. A special tool is needed to see and characterise the change in surface morphology that the fluorination treatment had done on the epoxy samples. Among the available tools, a microscope is used to study the microscopic morphology of the surface-fluorinated samples. However, conventional optical microscope only gives a standard magnification, which is not good enough to view the fluorinated layer. Hence, SEM is used for this purpose. In fact, SEM has been widely used in the morphological study of insulating materials. The ease of sample preparation is a significant advantage over other microscope types, namely the transmission electron microscopy (TEM), and this has led to its widespread usage. For SEM, the structure of bulk specimens of the order of nanometres in size, or larger, can be revealed by only using the cryofracture technique. On the other hand, the sample preparation for TEM usually involves complex ultra-microtomy techniques.

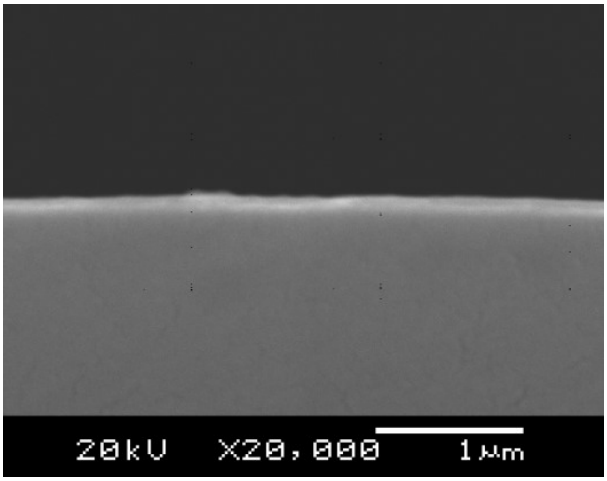

Figure 4-1: The cross-section SEM image of original epoxy sample. The sample was cryofractured and gold-coated at 25 mA for 6 min. A voltage of 10 kV and a working distance of 10 mm were applied throughout the SEM analysis.

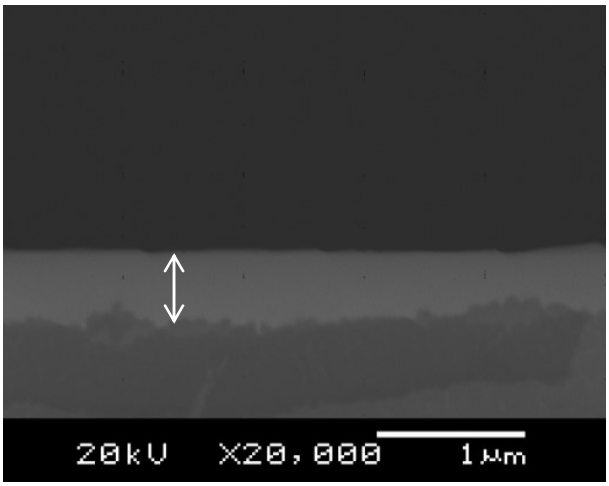

Figure 4-2: The cross-section SEM image of 30-min-fluorinated sample. The sample was cryofractured and gold-coated at 25 mA for 6 min. A voltage of 10 kV and a working distance of 10 mm were applied throughout the SEM analysis.

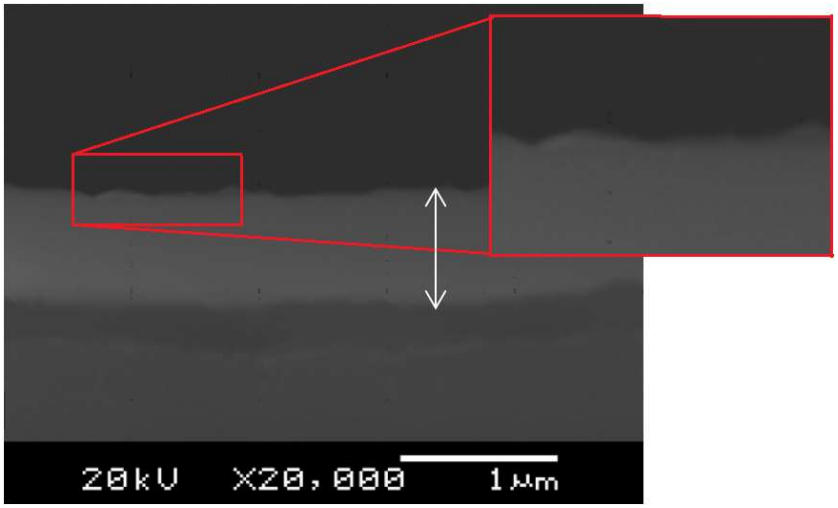

Figure 4-3: The cross-section SEM image of 60-min-fluorinated sample. The sample was cryofractured and gold-coated at 25 mA for 6 min. A voltage of 10 kV and a working distance of 10 mm were applied throughout the SEM analysis. Inset shows the surface roughening process.

Before the work can be carried out, the fluorinated samples, as well as non-fluorinated samples were cut into 15 mm x 15 mm size. The samples were mounted onto standard aluminium SEM stubs and were gold-coated using Emitech K550X coating unit with Edwards E2M2 high-vacuum pump. The coating was carried out at 25 mA for 6 min to create the necessary grounding path for the electron beam during the operation of SEM. A

JEOL Model JSM-5910 was used for this SEM analysis. A voltage of 10 kV and a working distance of 10 mm were applied throughout the analysis.

Figure 4-1 to Figure 4-3 show the cross section SEM images of the 30-min and the 60-min-surface-fluorinated samples, as well as the original sample for reference. The newly formed layer is marked with the white line. From the cross-section images, the top surface of the original sample is clear without any additional layer formation, unlike the fluorinated samples. In the 30-min-surface-fluorinated image, there is a thin layer with a sharp boundary forming on top of the surface with a thickness of a ~0.4 μm, showing an obvious increase with the treatment time as expected. For the 60-min-surface-fluorinated image, the layer is more obvious with a thickness of ~0.6 μm. Since this thin layer does not exist on the untreated sample, and becomes thicker with prolonged fluorination time, we can logically assume that this layer is the product of the fluorination treatment. Obviously, the thickness of this new layer is limited by fluorination treatment duration, with longer treatment time yields thicker new surface layer. Other authors have suggested that the newly-formed-layer's thickness is governed by the rate of penetration of fluorine molecule through the surface and into the bulk [45, 47, 110]. An in-depth study by Kharitonov [20] suggested that the thickness of fluorinated layer, δ_F, is proportional to the square root of fluorination time, *t*:

$$\delta_F = B(p_F)^k \, t^{0.5} \qquad (4\text{-}1)$$

where the *B* value depends on partial pressures of diluents gas, p_F is the permeability of fluorine gas through fluorinated layer, and *k* is a constant. In the case of epoxy resin treated at room temperature, the value of *B* and *k* are 0.070 μm $s^{-0.5}$ and 0.52 respectively. It is important to note that this equation is derived from the direct-fluorination treatment prepared using pure fluorine gas at room temperature, slightly different from the treatment conditions being applied in this research. Nevertheless, it is appropriate to say that the thickness of the newly-formed-layer increases with fluorination time. The same author also proposed that the level of fluorination increases with applied temperature. However, from

the obtained SEM images, the obvious sharp boundaries of the newly-formed-layer in F30 and F60 contradicts the diffusion model suggested by Kharitonov. Fluorinated layer formed by diffusion of fluorine through the surface should not possess an abrupt boundaries as in Figure 4-2 and Figure 4-3. Different level of brightness between the new layer (bright) and the unaffected epoxy (dark) may suggest a different yield of secondary electron during SEM operation. According to Seiler [111], the difference in secondary electron yield may arise from material contrast or from electron channelling contrast (among other factors) due to contamination on the surface. However, comparable bright sharp layer was also seen by other authors [46, 112] as a result of fluorination treatment on polymeric materials. Further characterisation tests are needed to further analyse the composition of this newly-formed-layer. For ease of identification in this thesis, it is fitting to call this layer as 'fluorinated layer' since it is the product of the surface fluorination treatment.

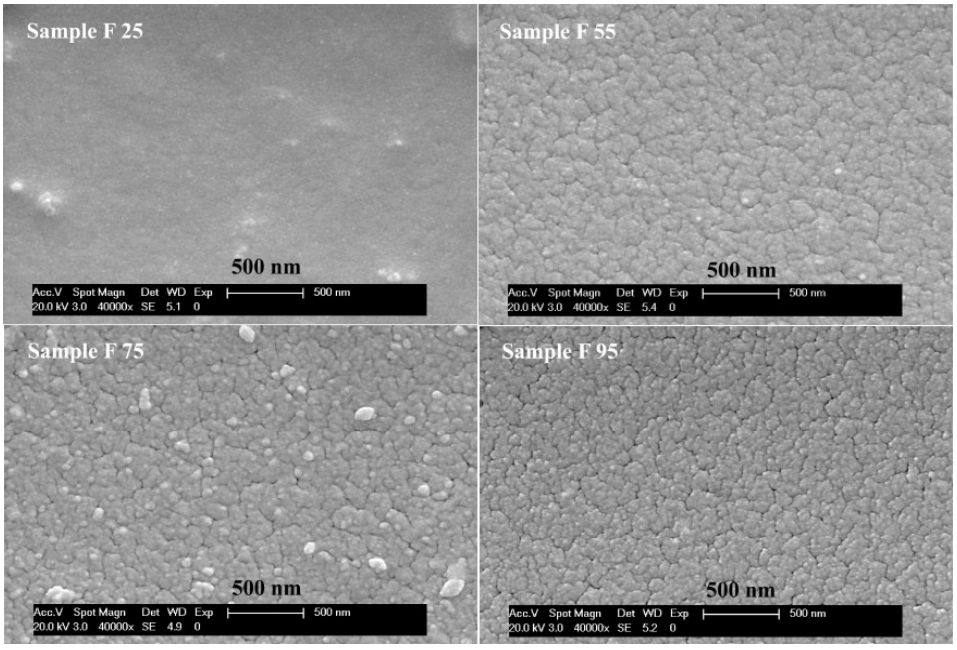

Figure 4-4: Images on surface roughening effect from surface-fluorination treatment on epoxy resin taken from [113]. The appearance of surface cracking appears at higher fluorination temperatures can be due to a rapid increase in molecular volume.

From the cross-section image in Figure 4-3, as well as the top-view images from [113] in Figure 4-4 (the same direct-fluorination treatment from Tongji University were performed

on these samples), structural changes in the form of small cracks and bumps can obviously be seen on the surface as the direct-fluorination level increases, as an outcome from the surface roughening process. Surface roughening appears and intensifies with the increase in fluorination level. It is believed that the surface roughening process of the epoxy samples at extended fluorination time is due to a rapid increase in molecular volume by the substitution and addition of 'heavy' and bigger fluorine atoms, and, also due to the on-going chain-scission process occurring on the surface of the treated epoxies [114]. In an 'ideal scenario' when there is no structural modification after the fluorine atoms are integrated into the polymeric surface, the surface conductivity should, in fact, be reduced by the formation of deep traps since fluorine has the highest electronegativity among the elements from the periodic table. However, the integration of fluorine atoms in the direct-fluorination treatment of polymeric materials is typically followed by physical and structural changes on the surface. The chain scission process, in particular, should produce substantial physical and structural modifications, as well as disorder at the molecular level. Moreover, the introduction of structural changes on the surface of the treated material should incorporate physical defects on the surface layer, which are known to have trap depth shallower than the trap produced by chemical defects [115]. Therefore, dielectric properties on the surface of the fluorinated epoxy samples are governed by the contest in the number of compositional changes and the structural changes i.e. the chemical defects and the physical defects in the fluorinated surface layer [116].

An increase in surface roughness may reduce the contact angle of a water droplet for a hydrophilic surface, while increase the water contact angle for a hydrophobic surface. As evident from the SEM images, the surface-fluorination treatment does increase the surface roughness of the treated samples and, therefore, reduced the water contact angle on the surface. The small water contact angle for fluorinated epoxy samples is attributed to the introduction of polar groups of -CHF-, as well as the chain scission process that introduces a highly polar group inside the fluorinated layer [114]. The contact angle of a water droplet on the surface of a solid indicates the degree of wetting of the solid. If the contact angle, $\Psi > 90°$, the solid is non-hydrophilic, while if $\Psi < 90°$, the solid is easily wetted i.e. the attraction of the water molecule by the solid surface is very strong. In short, the wettability

of a material is determined by the chemical structure on the surface, as well as the surface roughness [117].

4.2 ENERGY-DISPERSIVE X-RAY SPECTROSCOPY

Energy dispersive X-ray (EDX) analysis uses the X-ray spectrum produced by a material bombarded with a focused beam of electrons to achieve a localised chemical spectroscopy. All elements from atomic number 4 (beryllium) to 92 (uranium) can be identified [118]. On top of that, EDX analysis can determine both qualitative and quantitative value of the element under the scope. Qualitative analysis is relatively straightforward due to the simplicity of X-ray spectra and is used for the classification of the peaks in the spectroscopy. The determination of the concentrations of the elements present in the quantitative analysis involves evaluating peak's amplitude for each component in the material.

The samples were cryofractured into 10 mm x 10 mm pieces and were gold-coated. For this analysis, the energy dispersive X-ray microanalysis of Oxford Inca 300 was used together with the SEM instrumentations. As discussed in Chapter 2, once the electron beam hits the atoms on the top of the sample, secondary and backscattered electrons were released from the surface of the test subject. Unique x-rays energies which corresponds to each element on the surface were released in order to replace the electrons and, thus, stabilise the system. Figure 4-5 to Figure 4-7 show the top view EDX spectroscopy of non-fluorinated, 30-min-surface-fluorinated and 60-min-surface-fluorinated epoxy samples. Peaks of carbon (C) and oxygen (O) are clearly visible from the spectrum in Figure 4-5, which are the main elements for epoxy. However, another primary component for epoxy, which is hydrogen (H), is not visible due to the limitation of EDX in spotting elements of a small atomic number. Small peaks of gold (Au) can also be seen from the spectroscopy due to the existence of small gold element from the gold-coating layer. In Figure 4-6, the peak for fluorine (F) can be seen from the spectroscopy due to the presence of the fluorinated layer from the fluorination treatment. The fluorine peak is greater in intensity in Figure 4-7, indicating a greater number of fluorin in the electron interaction spot i.e. thicker fluorine

layer in the 60-min-surface-fluorinated epoxy. This observation is consistent with the cross-section SEM images in Figure 4-2 and Figure 4-3 which show obvious increases in fluorination layer thickness with respect to treatment time. No other element is detected from this analysis indicating only the fluorine element is integrated into the surface layer.

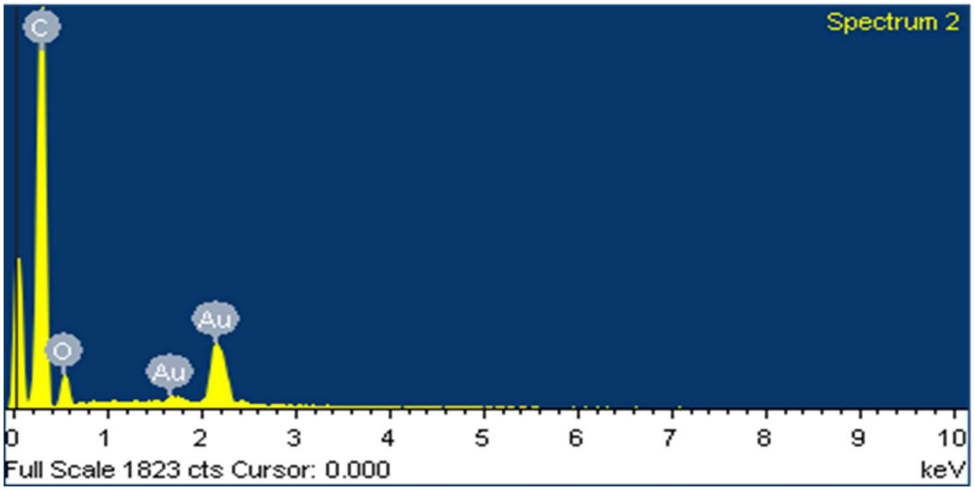

Figure 4-5: Top-view EDX spectrum for non-fluorinated epoxy. No other element is detected besides aurum (Au) which is a result of gold-coating.

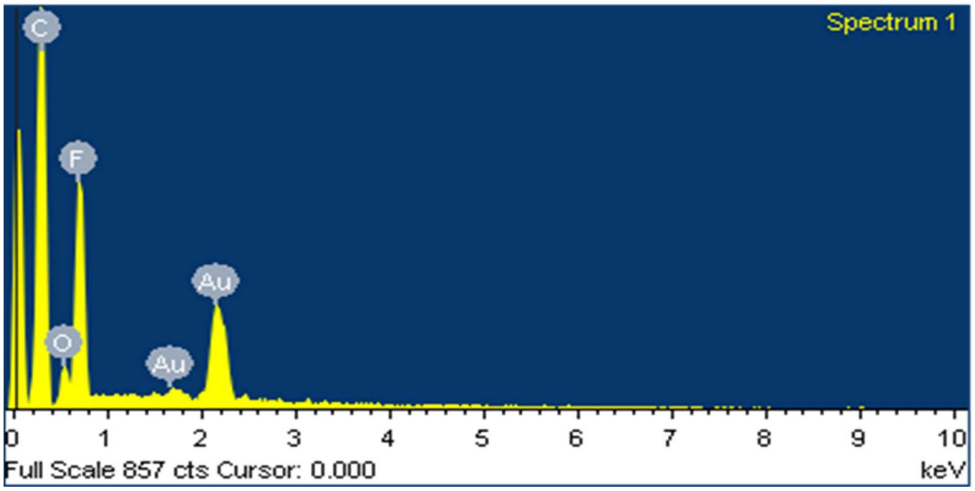

Figure 4-6: Top-view EDX spectrum for 30-min-fluorinated epoxy. Fluorine is detected together with the original epoxy element of carbon and oxygen. No other element is detected.

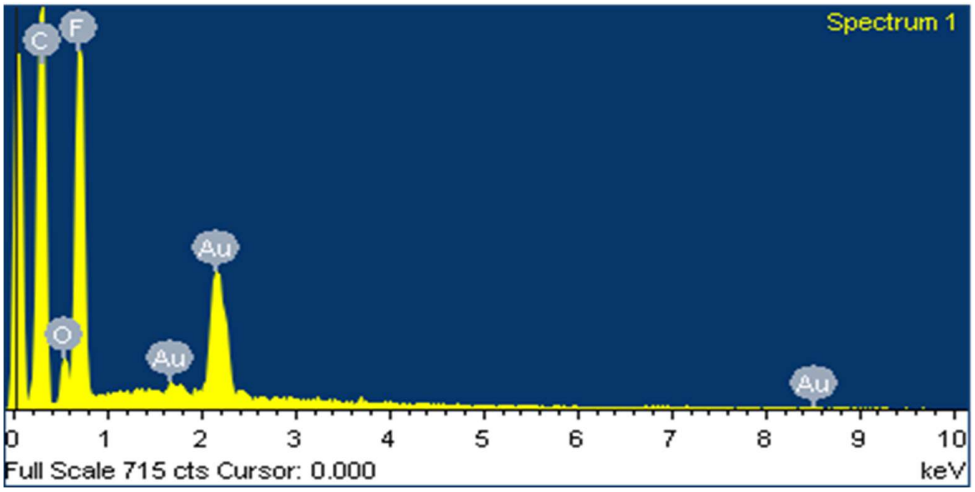

Figure 4-7: Top-view EDX spectrum for 60-min-fluorinated epoxy. Higher peak for fluorine is observed with longer fluorination time. No other element is detected.

The epoxy samples then were placed vertically inside the microscope chamber to view the cross-section image of the treated material. Figure 4-8 and Figure 4-9 show the scanning electron microscope (SEM) images and EDX spectrum of the cross-section of a 60-min-surface-fluorinated epoxy sample. From the SEM images, the fluorinated layer can clearly be seen on the top of the epoxy samples with a thickness of 0.6 μm. The thickness of the fluorinated layer from the treatment is determined by a few factors; namely the treatment time, the pressure and composition of the reactive mixture, and fluorine partial pressure [119]. The chamber's temperature and nature of the treated material may also influence the degree of fluorination. From the Raman spectroscopy analysis in next sub-chapter, the spectrum shows that chemical reactions between the fluorine gas and the surface of epoxy did take place during the fluorination treatment [120].

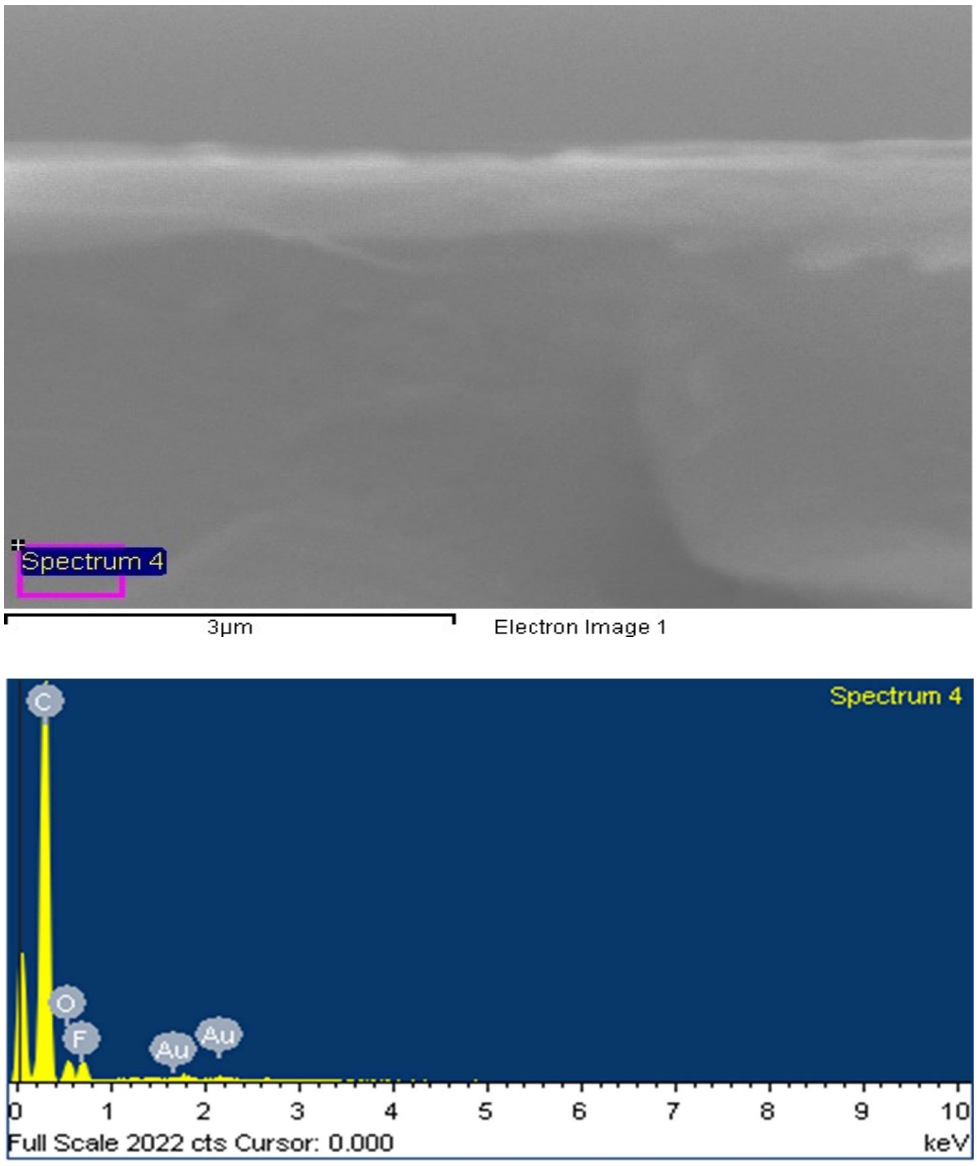

Figure 4-8: The cross-section SEM image and EDX spectrum of the epoxy layer. No other element is detected besides aurum (Au) which is a result of gold-coating.

The EDX spectrum in Figure 4-8 shows peaks of carbon (C) and oxygen (O) taken from the spot 3 µm deep into the sample. A small trace of fluorine (F) can be seen as well due to the existence of fluorine element near the vicinity of the EDX focus spot. The fluorine peak is greater in intensity in Figure 4-9, indicating a higher concentration of the fluorine element on the top layer as a consequence of the direct-fluorination treatment.

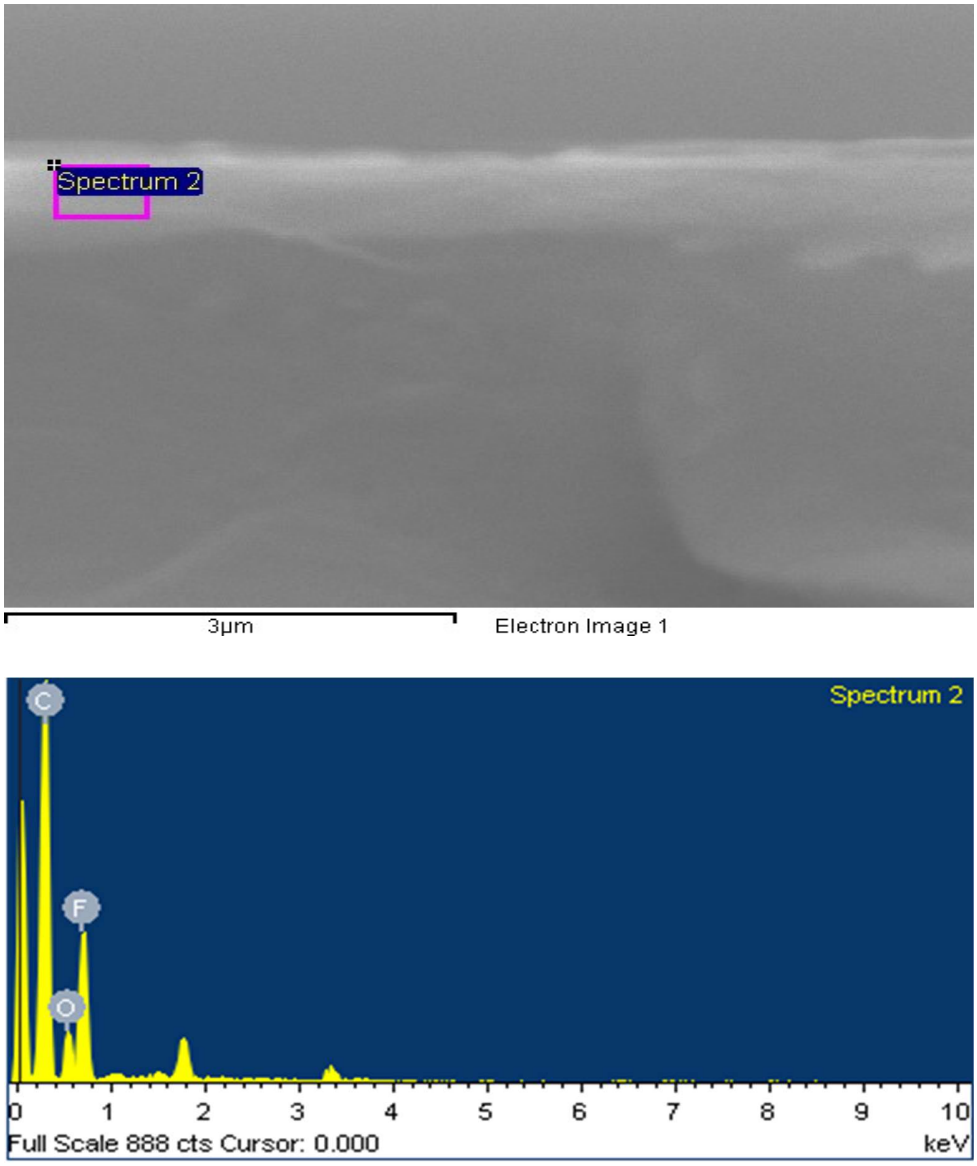

Figure 4-9: The cross-section SEM image and EDX spectrum of the 60-min-fluorinated layer. Fluorine is detected besides the original epoxy element of carbon and oxygen. No other element is detected.

The presence of fluorine element from the EDX spectrum comes from the formation of fluoride groups that are bound to happen because bond energy of C–F bonds is much higher than the bond of C–H and C–OH of pristine epoxies [121]. During a direct-fluorination treatment on hydrogen-carbon based polymeric materials, C–H and C–OH

bonds are disrupted while the conjugated double bonds are saturated and followed by the formation of C–F, C–F_2 and C–F_3 groups [122, 123]. At industrial level, where fluorination duration does not exceed 1–2 hours, the reacting temperature is between 20–60 °C and fluorine pressure does not exceed 0.1 bars, the transformation of hydrogen-carbon-based polymers into a perfect fluoropolymer does not usually happen. Nevertheless, the degree of fluorination inside the top fluorinated layer is rather high and sometimes it is close to 90–100 %. Most of the C–H bonds are transformed into C–F bonds.

4.3 RAMAN SPECTROSCOPY ANALYSIS

SEM analysis gives information on the morphological structure of the so-assumed fluorination layer. Still, the information does not reveal any chemical evidence to support the claim. Hence, another characterisation technique using Raman spectroscopy was performed. This technique provides information about functional groups or chemical bonds within the molecules. In a Raman spectrum, each line has a characteristic polarisation and, therefore, polarisation data provide information about the molecular structure. This spectroscopic technique utilises the inelastic scattering of monochromatic light to interact with the molecular vibrations, phonons and other excitation in the matrix, resulting in the energy of the laser photons being shifted up and down.

This experiment was conducted using Leica microscope and Renishaw Raman RM1000 system with a 785 nm CW diode laser of 25 mW. The system uses Peltier cooled charged coupled device (CCD) detector. There is a holographic grating of 1800 grooves mm^{-1} to disperse the scattered radiation by wavelength and a holographic (notch) filter that prevents back-scattered radiation from entering the detector. The device was set up in confocal mode, with a slit width of 15 μm and a CCD area of 4 pixels (image height) x 574 pixels (spectrometer range) which, together with the mechanical slit, acts as a virtual confocal pinhole. These settings are consistent with Renishaw's recommendations for confocal mode. For a start, the lens was focused on top of the sample surface, which is the fluorinated layer and the spectrum was captured. Then the focal point was adjusted to go 1

μm deeper into the bulk where the epoxy region was, and the spectrum was again captured. These steps were repeated until the depth is 5 μm deep. Since the Raman is in confocal mode, traces of epoxy resin key peaks can be seen on the fluorinated layer and vice versa.

Figure 4-10 shows the Raman spectrums of the surface fluorinated layer and epoxy resin region for depth 3 μm and 5 μm with some of the key peaks indicated. Table 4-1 identifies all of the key peaks in these spectra and the bonds within the samples from which they originate. It is important to note that the spectrum at 3 and 5 μm are well below the 0.6 μm penetration of the fluorinated layer, as seen from the SEM image of F60 and, thus, the spectra are identical. Since C–F bond possesses higher energy bond compared to C–H bond, surface-fluorination of the epoxy resin can instantly take place and results in the disruption of C–H bond, followed by the formations of C–F, $C–F_2$ and $C–F_3$ groups [124, 125]. The level of fluorination and thickness of the fluorinated layer depends upon the treatment parameters of the composition and pressure of the reactive mixture, fluorine partial pressure, treatment time and temperature, and polymer nature [119]. The fluorination level increases with the treatment time.

Clearly, the direct-fluorination treatment triggers significant changes in the chemical composition of the epoxy surface layer. Fluorine atoms are introduced into the polymer surface layer typically by the substitution of hydrogen and addition to carbon-carbon double bonds. An obvious C–F band appears in the range 900–1400 cm^{-1} in the fluorinated surface spectrum [46]. At the same time, in the tail section, the C–H peaks at 2850 and 2915 cm^{-1} are significantly reduced in intensity or even disappear from the top layer. In other words, for anhydride-cured DGEBA epoxy resins, direct-fluorination would lead to an increase in C–H formation and a decrease in C–F formation in Raman spectrum, as the focus goes from the surface to bulk. Peaks at 1221 cm^{-1} and 1180 cm^{-1} which are attributed to C–F covalent bonds and $C–F_2$ bonds respectively, are seen on the spectrum of fluorinated surface. For comparison, from the Raman spectrum of the non-fluorinated surface layer of epoxy resin in Figure 4-11, the carbon-fluoride groups' band in the broad

region of 900–1400 cm^{-1} is not visible, unlike the fluorinated surface spectrum, indicating no fluorination process has taken place.

As stated before, it is known that direct-fluorination treatment of epoxy resins is usually followed by the occurrences of chain-scission process due to the high reactivity and oxidizing factor of fluorine gas. The chain-scission process and the presence of fluorine molecules are the reasons for the significant reduction and/or disappearance of the bands for the aromatic and aliphatic ether groups (at 1259, 1095, and 1032 cm^{-1}) and the ester groups (at 1734 cm^{-1}) in Figure 4-10 [116]. With the presence of oxygen in the molecular chain of the epoxy resin, the chain-scission process during fluorination treatment resulted in the formation –C(O)F groups that have a strong absorption band around 1856 cm^{-1} [20]. The –C(O)F groups would then be hydrolysed into –C(O)OH groups when the fluorinated polymer is exposed to atmospheric air due to the moisture absorption. In fact, a small peak of the –C(O)F groups can still be seen at 1856 cm^{-1} in the Raman spectrum because of the sample's exposure to air before the Raman analysis was performed.

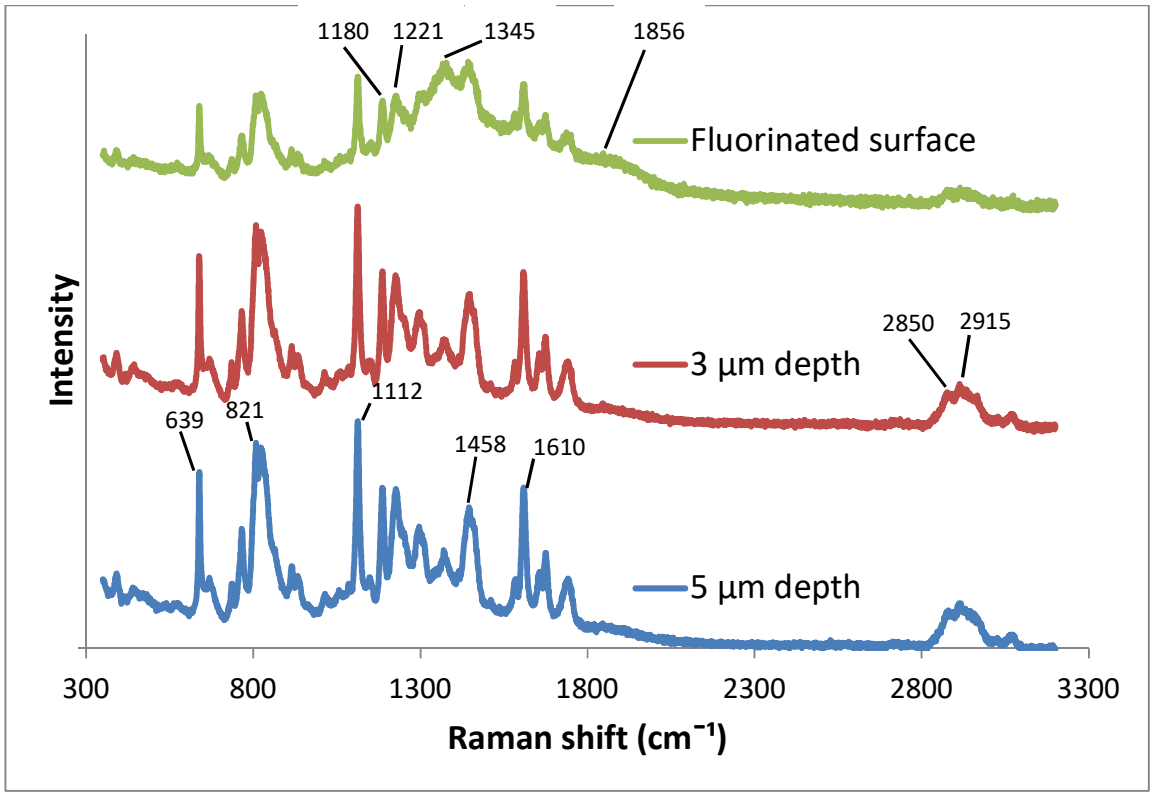

Figure 4-10: Raman spectrum of surface-fluorinated layer, 3 µm depth and 5 µm depth epoxy layer. The formation of C-H peaks (2850 and 2915 cm^{-1}) can clearly be seen in the tail-section as the focus goes deeper into the bulk.

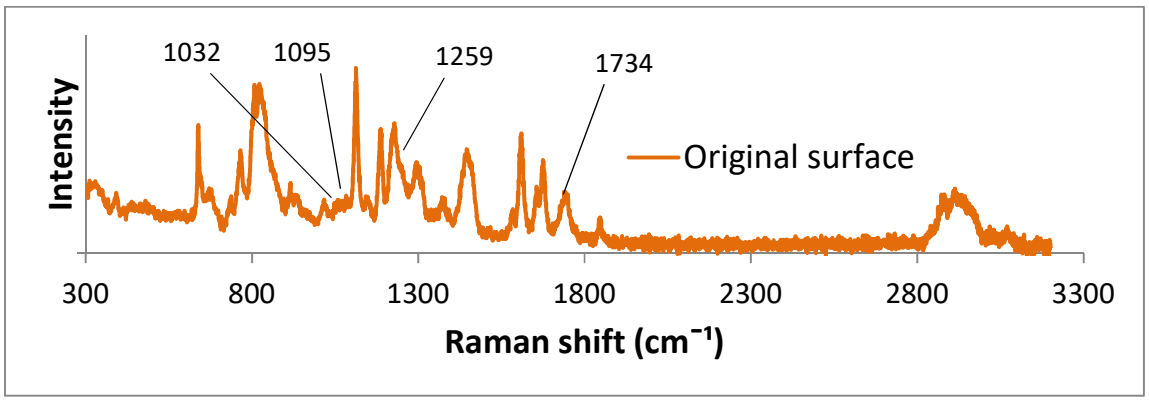

Figure 4-11: Raman spectrum of non-fluorinated F00 surface layer for comparison. There is no broad-band associated to fluorine in the middle-section.

Layer	Peak (cm^{-1})	Vibrational mode	Reference
Fluorinated layer	730	$C–F_2$, $C–F_3$	[46]
	1180	$C–F_2$,	
	1221	C-F	
	1345	$C–F_2$, $C–F_3$	
Epoxy layer	639	γ Epoxy	[126]
	736	α Epoxy	
	821	W C-H	
	916	γ Epoxy	
	936	W C-H	
	1012	v aromatic ring	
	1031	v C-O	
	1112	α Epoxy	
	1186	W C-H	
	1252	Epoxy ring breathing	
	1458	δ $C-H_2$	
	1580	v aromatic ring	
	1610	v aromatic ring	
	2850	C-H	[46]
	2915	C-H	

Table 4-1: Key Raman spectral peaks identified in fluorinated and epoxy layer. * v - stretch, β - in plane bend, α - in plane ring def, γ - out of plane bend, δ - deformation, W - wagging

To further analyse the data, spectral subtraction was performed to see the spectrum of the fluorinated surface layer alone without the influence from the bulk spectrum. To perform this operation, the Raman spectrum of the non-fluorinated surface layer (F00) was subtracted from the Raman spectrum of the fluorinated surface (F60). The spectrum of the non-fluorinated surface is selected instead of the spectrum of fluorinated layer at 3 µm depth or 5 µm depth is because the fluorinated layer at such depth still contain peaks attributed to fluorine components. As a result, such subtraction may produce a spectrum without key fluorine peaks. Comparable Raman subtraction method was applied by other

authors in the characterisation of epoxy resin [127-129]. A weighting factor of 0.7 is used on the Raman spectrum of the original surface (F00) in order to eliminate the peaks of epoxy resin in the interested central region. In doing so, the tail section which shows peaks for C-H bonds are compromised (appears dented). A weighting factor lower than 0.7 does not totally eliminate the peaks attributed to epoxy in the central region while factor higher than 0.7 will result in more dents in the central region. The Raman spectrums of F60 and the subtraction result are shifted vertically in order to see the outcome more clearly. It is important to note that as the Raman is in confocal mode, the spectrum of the top fluorinated surface will contain peaks of fluorine components, as well as peaks of epoxy from the layer beneath. For that reason, peaks of C-H bonds are still visible in the tail section of the spectrum of the top fluorinated layer because of the confocal mode. Figure 4-12 shows the outcome of the spectrum subtraction operation. After the subtraction, the carbon-fluoride groups' band in the broad region of 900–1400 cm^{-1} is clearly visible with a peak at 1345 cm^{-1} ($C–F_2$ and $C–F_3$) indicating fluorination process has indeed taken place on the surface layer. Due to the broad band in the central section, other peaks associated with fluorine are not clearly visible. The formation of broad region in the subtraction spectrum, which is not visible in the original epoxy, could be due to overlap of fluorinated peaks with epoxy peaks. However, as the broad region covers a long range of frequency, it is more likely that it reflects the amorphous character of the fluorination layer [130]. A comparable broad Raman peak can also be seen in [131] in which the author attributed the broad Raman peak seen in fluorinated carbon nano-tubes to a greater amount of decomposition occuring at higher reaction temperature. In another study [132] on fluorinated system, they attributed the broadening Raman peak with the enhanced disorder in the lattice induced by fluorination. Similarly, Im et al. [133] attributed the broad Raman peak of fluorinated carbon nano-tube to the destruction of the graphite structure. Based on these findings, it is appropriate to say that the broad Raman peak seen on the subtraction result can be attributed to the destruction and disorder in the epoxy structure due to the fluorination treatment, especially at high temperature.

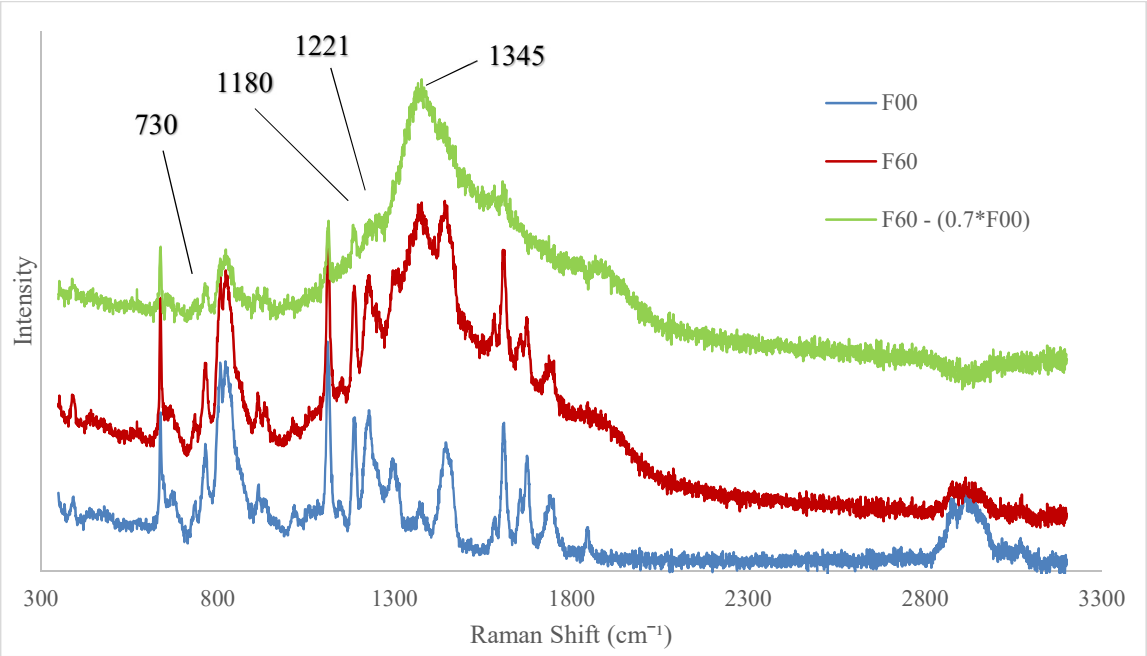

Figure 4-12: The spectrum of subtraction result of non-fluorinated layer from the fluorinated layer using a factor of 0.7. Broad Raman peak can be seen on the subtraction result and can be attributed to the destruction and disorder in the epoxy structure due to the fluorination treatment.

4.4 PRELIMINARY SURFACE CURRENT MEASUREMENT

Having performed the characterisation analysis using SEM and Raman spectroscopy, a test for another fundamental property of an insulator, the electrical conductivity test, is needed. The conductivity or resistivity measurement can be used to determine the dissipation factor, moisture content, and other important properties of a material. A small increase in surface conductivity value may increase the dielectric breakdown voltage because the electric field intensity is reduced. One test method that is usually adopted for measuring resistivity or conductivity of dielectrics is 'DC Resistance or Conductance of Insulating Materials' from ASTM D-257. In this method, Keithley 6517A electrometer is used for measuring purposes since it can measure a small value of currents (1 fA – 20 mA) [134].

In theory, the resistivity of an insulator is measured by applying a known voltage, measuring the resulting current, and calculating the resistance using Ohm's Law, V = IR.

From there, the resistivity is determined based on the geometry of the specimen. The resistivity may vary for several reasons. As it is a function of the applied voltage, at times, the voltage may be varied to determine an insulator's voltage dependence. Environmental conditions may also play a significant part on insulator's resistivity. As the humidity goes up, the resistivity goes down. For a better accuracy, environmental conditions, the applied voltage and electrification time should be kept constant from one test to another.

The area of interest in this study is the top surface of the epoxy resin sample and, therefore, the surface current is measured, as well as the bulk. Surface resistivity is defined as the electrical resistance along the surface of an insulating material. It is measured from one electrode to the other electrode along the sample surface. For simplicity, the current measurement is deemed independent of the physical dimensions (e.g. thickness) of the insulating sample because the measured surface length is permanent. Surface resistivity is quantified by applying a voltage across the surface of the dielectric sample and measuring the resultant current, as illustrated in Figure 4-13. The electrode design for surface current measurement was taken from the surface breakdown system (in Chapter 7) which consists of a pair of finger-shape stainless steel electrodes attached the top of the sample. The justification of this electrode arrangement is discussed further in Chapter 7. It is important to note that, repeated experimental runs showed that data variations within a factor of 3 are typical, which causes the quantitative analysis of such behaviour to become questionable. The poor reproducibility of test data is, however, a common issue with current measurements [135].

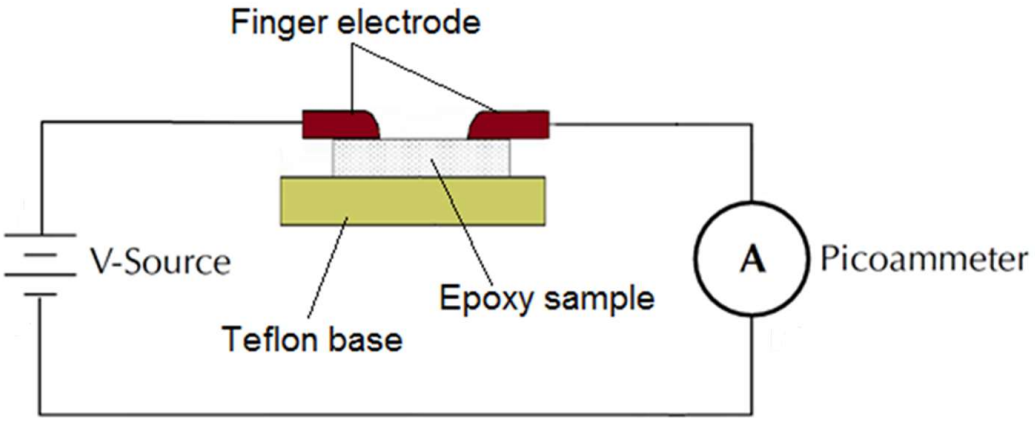

Figure 4-13: A schematic diagram of DC surface current measurement using a pair of finger electrode. The sample is placed in between the Teflon base and the finger electrodes.

Resistivity or conductivity on the surface cannot be measured accurately, only approximated, because some degree of volume resistance or conductance is always involved in the measurement. The measured value is also affected by the surface contamination, including moisture absorption. As this analysis is only used for comparison purpose, the role of a grounding electrode is neglected. The conducting current from the applied voltage is assumed to flow along the surface only, and not through the bulk. Figure 4-14 shows plots of the time dependence of measured current for 250 μm non-fluorinated sample (F00), 30-min-surface-fluorinated sample (F30), and 60-min-surface-fluorinated sample (F60) at a constant applied DC voltage of 5 kV across the 8 mm gap over a duration of 60 min at room temperature. It is noted that for all the samples, the value of the measured current drops significantly in the first few minutes, and only settles down after about five minutes. This is due to the different low frequency polarisation mechanisms decaying with increasing measuring time, and from depletion of free charge carriers [136, 137]. After 60 min, the current measurement of F00, F30 and F60 are 5.66 x 10^{-13} A, 2.16 x 10^{-12} A and 5.03 x 10^{-12} A respectively, showing a clear increase in surface current with the direct-fluorination treatment time.

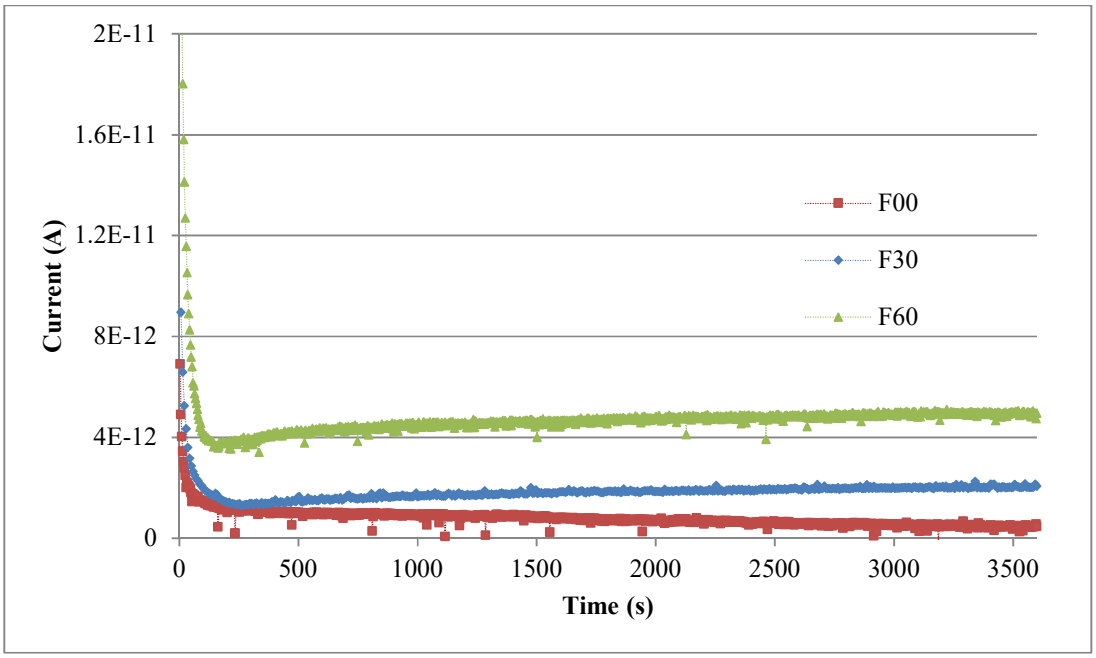

Figure 4-14: Plot of current against time for 250 µm samples of F00, F30 and F60 at a constant applied DC of 5 kV across the 8 mm gap over 60 min at room temperature. After 5 min, the current for F30 and F60 show small increment with time due to the moisture effect.

The observed increase in surface current value of the treated epoxy samples can be attributed to the increase in the level of fluorination. The changes in the physicochemical characteristics of the fluorinated surface may lead to an increase in surface conductivity [116]. This structural change does not only come from the substitution of fluorine atoms, but also from the occurrences of chain-scission process that would lead to the formation of highly polar groups (e.g. –CHF groups and oxygen-containing groups) and, thus, influences the surface polarity of the treated epoxy sample. On top of that, due to the surrounding moisture and the high surface energy of the treated epoxy resin, the water absorption effect also plays a major role in influencing the conducting surface current [138]. Theoretically, in a controlled environment, where the moisture level on the sample's surface is kept constant all the time, a transient behaviour is expected in the first few minutes with the current falling due to bulk and surface polarisation followed by a steady state current once the field distribution across the sample has become constant. In this experiment, however, after five minutes, the current measurement for F30 and F60 show small increment with time, presumably, due to the moisture effect. For F30 sample, there is an increase of 0.86 x

10^{-12} A in surface current from the lowest value of 1.30 x 10^{-12} A at 200 s to 2.16 x 10^{-12} A after 60 min, while, the F60 sample recorded an increase of 1.39 x 10^{-12} A from its lowest reading. Direct-fluorination treatment on polymeric materials is known to turn the treated surface into hydrophilic with small water contact angle [110, 114]. Experimental evidences on moisture effect are available in Chapter 6, in which shows that direct-fluorination treatment on the surface (for F60 sample) did influence the amount of moisture being absorbed. It is believed that the increase in the degree of direct-fluorination would also lead to an increase in the amount of absorbed surface moisture. The same observation can also be seen in the moisture study done on the plasma-fluorinated samples in Chapter 8, where a decrease in surface current measurement was recorded as the PEF sample loose absorbed surface moisture. The increase in absorbed moisture, on top of the changes in physicochemical structure of the surface, leads to the increase in surface current, as evidenced from the surface current measurement.

It is important to note that these samples were just taken out from a sealed bag for this measurement. Previously, once the fluorinated treatment was performed onto the samples in Tongji University, China, the samples were placed in a sealed plastic bag for transportation. The transportation bag is not vacuumed, nor filled with dry gas, so a limited amount of ambient moisture is expected within the sealed plastic bag. Therefore, when the samples were taken out for measurements, the samples' surfaces were still not in equilibrium with ambient moisture; i.e. the surface would still be absorbing surrounding moisture. The increase in water absorption level on the surface with prolonged fluorination time introduces more hydrogen and hydroxyl ions onto the surface and, thus, yields higher surface conductivity value due to moisture-assisted charge movement. The significance of moisture effect is highly critical on the dielectric performances of epoxy samples which requires another chapter on its own. More detailed explanation on moisture effect on the surface-fluorinated epoxy resin samples is given in Chapter 6.

4.5 BULK DC CURRENT USING PARALLEL ELECTRODE GEOMETRY

To further examine the effect of direct-fluorination treatment, the bulk DC current measurement was performed in order to observe the absorption current inside the non-fluorinated and surface-fluorinated epoxy resin samples. The schematic diagram of DC current measurement is shown in Figure 4-15.

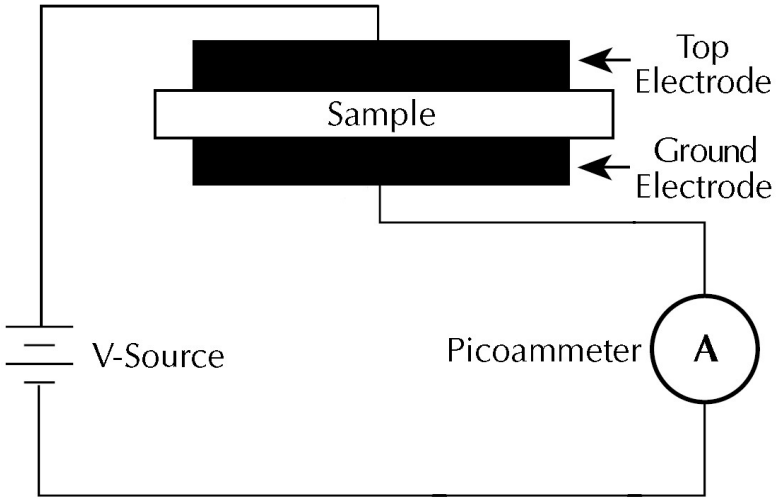

Figure 4-15: A schematic diagram of DC bulk current measurement using parallel electrode geometry

The top and ground electrodes are made of copper and both are 30 mm in diameter, sandwiching the epoxy sample of 250 µm in thickness. A constant DC voltage of 5 kV was applied for a duration of 50 min at room temperature. As the surface current is presumably dominant for the fluorinated samples, the grounding ring electrode is omitted. This is because the guard ring would eliminate the current that flows on the surface, which is presumed to be the main route of current flow of the fluorinated samples. These treated samples have higher surface conductivity due to the presence of fluorine layer on the surface. The dominance of conduction path through the surface layer over the bulk had been observed by other author [139].

The same experimental procedures as before were repeated for all the samples. Figure 4-16 shows plots of the time dependence of absorption current for non-fluorinated sample (F00), 30-min-surface-fluorinated sample (F30) and 60-min-surface-fluorinated sample (F60) while Figure 4-17 shows the plot of log current against log time of the same data set for the first 300 s , during the transient current phase, well before the samples reach steady state. It is noted again that, for all the samples, the value of the absorption current drops significantly in the first few minutes of the measurement, similar to previous surface current measurement.

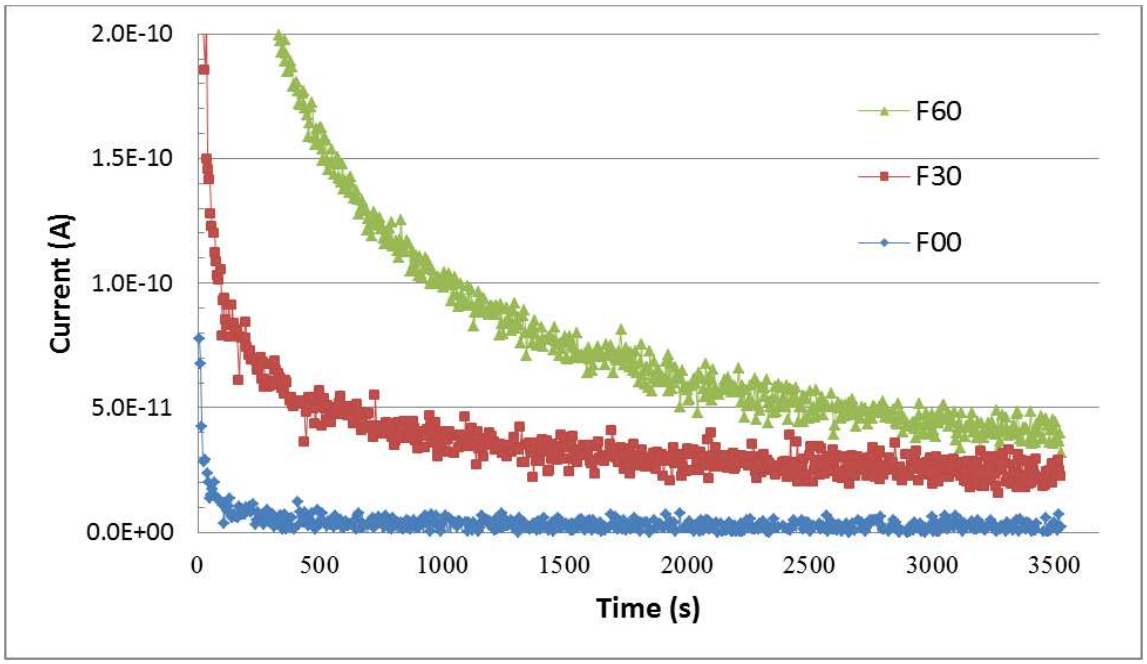

Figure 4-16: DC current measurement for 250 μm epoxy resin samples of different fluorination time. The highest DC current reading is seen in F60, followed by F30 and finally F00 throughout the measurement period.

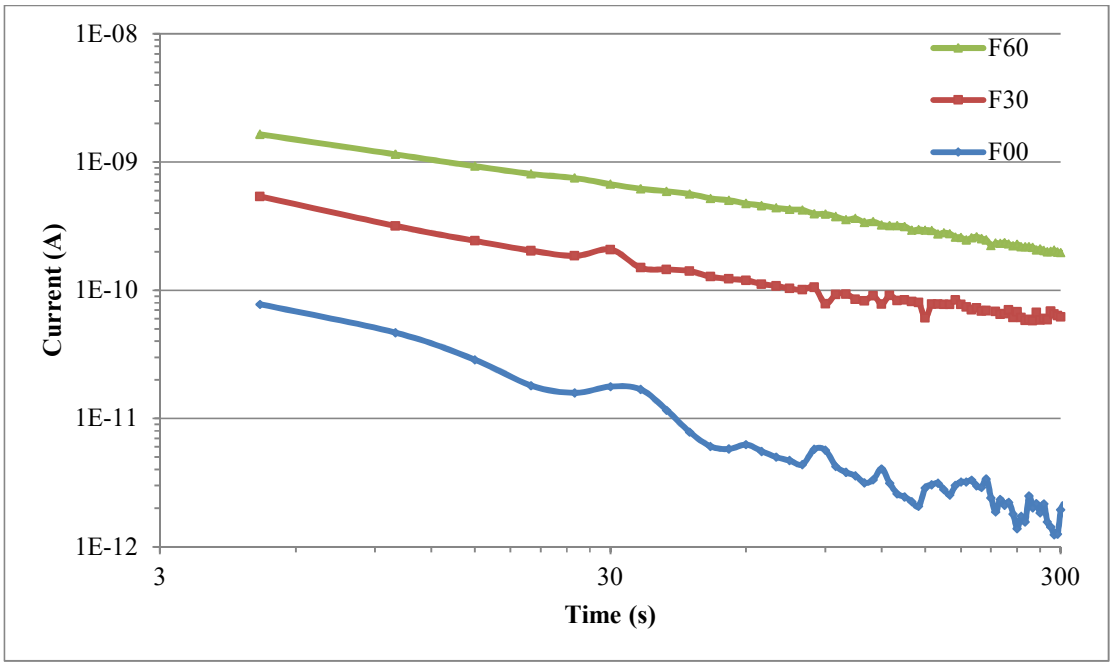

Figure 4-17: Log-log representation of DC current measurement on first 300 s of data for 250 µm epoxy resin sample of different fluorination time. The value of the absorption current drops significantly in the first few minutes of the measurement.

In the non-fluorinated epoxy sample, as illustrated in Figure 4-18, the absorption current that flows through the bulk of the sample is minimal and after 50 min, the measured current is 1.19 x 10^{-12} A. Whereas, in the surface-fluorinated epoxy sample, as illustrated in Figure 4-19, there exists a new pathway for the current to flow in the form of the fluorinated layer, which have less resistance than the bulk. The fluorinated layer covered the whole surface of the epoxy sample with a thickness of ~0.4 µm for 30-min-surface-fluorinated sample and ~0.6 µm for 60-min-surface-fluorinated sample, as evident from SEM analysis. The current measurements increase to 2.40 x 10^{-11} A and 4.12 x 10^{-11} A respectively after 50 min. This observation implies that, with the introduction of a surface-fluorinated layer, a huge portion of the current flows through this new channel instead of the bulk with a current ratio of 20:1 for 30-min-surface-fluorinated sample and 35:1 for 60-min-surface-fluorinated sample. Alternatively, this observation can also be described by the fact that the fluorinated layer in each case is less than 1 µm thick while the sample thickness is 250 µm. Therefore, the change in electric field across the bulk of the non-fluorinated bulk section of the sample

as the result of the more conductive fluorinated layers in contact with the electrodes would be small, and, therefore, the corresponding current change would also be small.

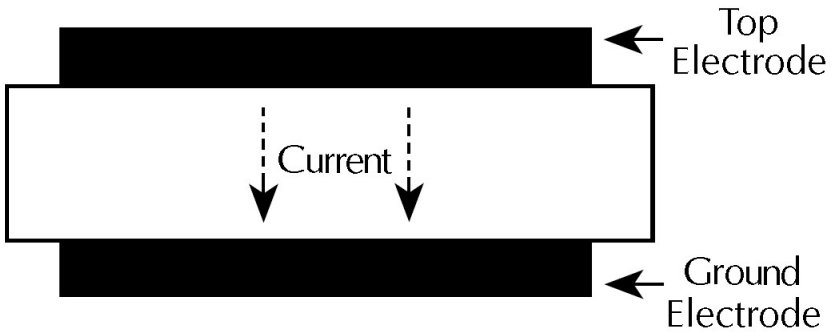

Figure 4-18: Minimal current flow through the bulk of non-fluorinated epoxy sample in the absence of surface fluorinated layer

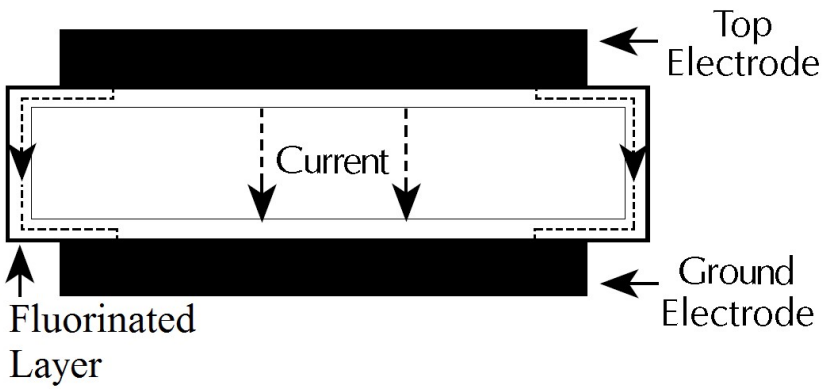

Figure 4-19: Extra current can flow through the fluorinated layer in the direct-fluorinated epoxy sample

In relation to the surface potential decay measurement (in Chapter 5), the author suggests that the main mechanism that governs the surface potential decay is the conduction along the fluorinated surface layer, as illustrated by the current flow from this test. Only a small portion of the conducting current flows through the bulk. This result is consistent with the space charge analysis in Chapter 5 that suggests the surface-fluorination treatment suppresses the charge injection into the bulk [140]. A similar observation was made by An

et al. [43] on charge injection into surface-fluorinated linear low density polyethylene (LLDPE).

The measured absorption current in time domain characteristic is often found to follow the power law relationship [141]:

$$I = At^{-b} \tag{4-2}$$

where I is the current, t is the time, A is a temperature dependent factor and b is a constant representing the slope of the current-time plot. Since the observed transient currents are based on polarisation, therefore a DC component of current would be expected in the equation. So, the current would follow:

$$I = At^{-b} + C \tag{4-3}$$

where C is the DC current component that is assumed to be the final current value at the end of the measurement.

Sample	A	b	C
F00	$3.72 \times 10^{-10} \pm 0.36 \times 10^{-10}$	0.733 ± 0.042	$1.19 \times 10^{-12} \pm 0.16 \times 10^{-12}$
F30	$1.43 \times 10^{-9} \pm 0.24 \times 10^{-9}$	0.581 ± 0.049	$2.40 \times 10^{-11} \pm 0.21 \times 10^{-11}$
F60	$3.73 \times 10^{-9} \pm 0.22 \times 10^{-9}$	0.573 ± 0.047	$4.12 \times 10^{-11} \pm 0.33 \times 10^{-11}$

Table 4-2: Values of parameter A, b and C of the power law line fitting on first 300 s data for bulk DC current of F00, F30, and F60 at 95 % confidence bounds

Table 4-2 shows the values for parameter A, b and C of the curve-fitting result for bulk DC current measurement of F00, F30, and F60 samples. Generally, the fluorinated epoxies possess a lower value of exponential b when compared to the non-fluorinated epoxy. Also, F30 and F60 samples show roughly the same value of parameter b. This implies that the factors that contribute to the value of exponential b e.g. dipole orientation, carrier, carrier hopping as well as charge injection forming trapped space charge [142], are mainly bulk phenomena and only play a minor role on the surface. Unlike F00, for F30 and F60, more current can flow on the less resistive fluorinated surface as discussed earlier, hence higher value of parameter A.

In order to enhance the understanding in surface conductivity behaviour, Meunier et al. [115] had done a molecular modelling work to calculate the trap energies of the chemical and physical defects in a polymeric insulator. They concluded that the chemical defects represent the formation of deep traps in the model while physical defects represent the formation of shallow traps. On top of that, the influence of neighbouring molecules on the trap energies of the shallow and deep traps, as well as the interaction among the traps, should be taken into account. The extra current flows through the surface of the fluorinated sample, as a result of the high surface conductivities from fluorination treatment, suggests that the depth of charges being trapped in the surface layers is considerably reduced by the fluorination treatment. Ironically, the introduction of fluoride molecules into the epoxy surface layer should lead to the formation of deep traps (chemical defect) and consequently reduce the surface conductivity because fluorine atom has the highest electronegativity value in the periodic table. However, in a practical situation, the compositional changes are followed by the corresponding structural changes, namely the occurrences of chain scission (physical defect) from the breaking of molecular bond and shortening of the chain on the top surface. This structural changes increase the average number of shallow traps on the surface, and, consequently enhance the surface conductivity.

The presence of oxygen in the reaction mixture or the polymer chemical composition, such as epoxy resin, may speed up the occurrences of chain scission. Therefore, high surface

conductivity of the fluorinated epoxy samples should mainly come from the structural changes, that introduce a large amount of the physical defects and shallow traps. A larger occurrence of chain scission can be expected on the fluorinated surface layers as the fluorination time increases, as evident from the DC current test result. The increase in surface current with fluorination time is a product of the competition between the chemical traps and the physical traps. On top of this physicochemical changes, the increase in the surface current may also be described by the ability of fluorinated layer to absorb surface moisture and, hence, increases the surface conductivity due to the moisture assisted charge movement. Further explanation on surface moisture effect are done in Chapter 6.

4.6 CHAPTER SUMMARY

This chapter gives an in-depth explanation on the characterisation test being carried out on the direct-fluorination of the epoxy sample as well as the non-fluorinated epoxy sample. Morphological analysis was performed through the use of SEM. The microscopy images show a clear formation of the fluorinated layer, getting thicker as the fluorination treatment time increases. The rate of formation of a fluorinated layer is limited by the rate of penetration of fluorine gas through the fluorinated layer, and into the untreated bulk. To further characterise the samples, Raman spectroscopy analysis was carried out to provide information about functional groups or chemical bonds in molecules through the inelastic scattering of monochromatic light. By using the confocal mode, it is clear that the spectrum shows a decrease in C–F absorption and increase in C–H absorption as the focus goes from the surface fluorinated layer and into the bulk of epoxy resin. From Raman subtraction, a broad Raman peak can be seen in the central section of the subtraction spectrum, and can be attributed to the destruction and disorder in the epoxy structure due to the fluorination treatment.

DC surface current measurement was also carried out in order to determine the extent of dielectric improvement as a result from the fluorination treatment. From the DC current measurement result, it is established that a big portion of current flows along the surface of

the fluorinated sample, with only a fraction of the current flows through the bulk. This is because, the direct-fluorination treatment introduces a new surface layer that possesses higher surface current reading as compared to original epoxy, which offers a less resistive path for the charges to decay away from the surface. The increase in surface current value of the treated epoxy samples can be attributed to the increase in the degree of fluorination with fluorination time. The changes in the physicochemical characteristics of the fluorinated layer, as well as absorbed moisture on the surface may, lead to an increase in surface conductivity. This structural changes do not only come from the substitution of fluorine atoms, but also from the occurrences of chain-scission process that would lead to the formation of highly polar groups (e.g. –CHF groups and oxygen-containing groups) and, thus, influences the surface polarity of the treated epoxy sample.

CHAPTER FIVE: SURFACE CHARGE DYNAMICS

The non-fluorinated and direct-fluorinated samples were characterised in the previous chapter. The effect of direct-fluorination treatment can clearly be distinguished from the characterisation tests. In this chapter, the surface charge dynamics is investigated using surface potential decay test and PEA measurement.

5.1 CORONA DISCHARGE MECHANISM

The study in surface potential decay of dielectric materials has become an increasingly popular topic after the discovery of cross-over phenomenon by Ieda in 1967 [98] and it is closely related to the wide usage of corona charged dielectrics. There are several methods available to deposit charges on the insulator's surface. In this research, a corona discharge from a needle electrode was used throughout the surface potential decay study. Corona discharge is a sustainable, non-thermal plasma, which takes place in the proximity of a sharp high voltage discharge electrode e.g. a needle. Resulting coronas are either positive or negative, depending on the polarity of the supply connected to the discharge electrode. Both positive and negative corona may lead to an avalanche of electrons. This avalanche happens when free electrons in the air are subjected to strong acceleration by an electric field. The electric field accelerates these electrons until they acquire enough kinetic energy to create ionisation when they hit neutral gas molecules in their path. As a result, more electrons are liberated and upon being accelerated by the field, they can cause further ionisation. As the cycle goes on, more and more electrons are emitted, and avalanche is bound to happen. In short, a small number of electrons may cause ionisation of an entire gas and turn them into plasma. For a positive corona, the avalanche of electrons is accelerated towards the electrode while the resulting positive ions are repelled. Likewise, for a negative corona, the avalanche is in the opposite direction, with the electrons moving away and the positive ions are drawn towards the electrode [143].

5.2 SURFACE POTENTIAL DECAY MEASUREMENT

When the corona charges are being deposited onto the insulator's surface, the charge will immediately start to decay away from the surface through various mechanisms. A measurement technique called surface potential decay measurement is adopted in this research to measure this particular dielectric property. This technique enables a simple quantification of decay rate for each fluorination conditions upon corona charging the surface to a set voltage. From another study [143], it is known that bipolar charge injection is the main mechanism for the decay of corona charged sample. A schematic diagram for typical needle-grid-ground corona charging setup and the surface potential decay kits used in this study are shown in Figure 5-1 and Figure 5-2.

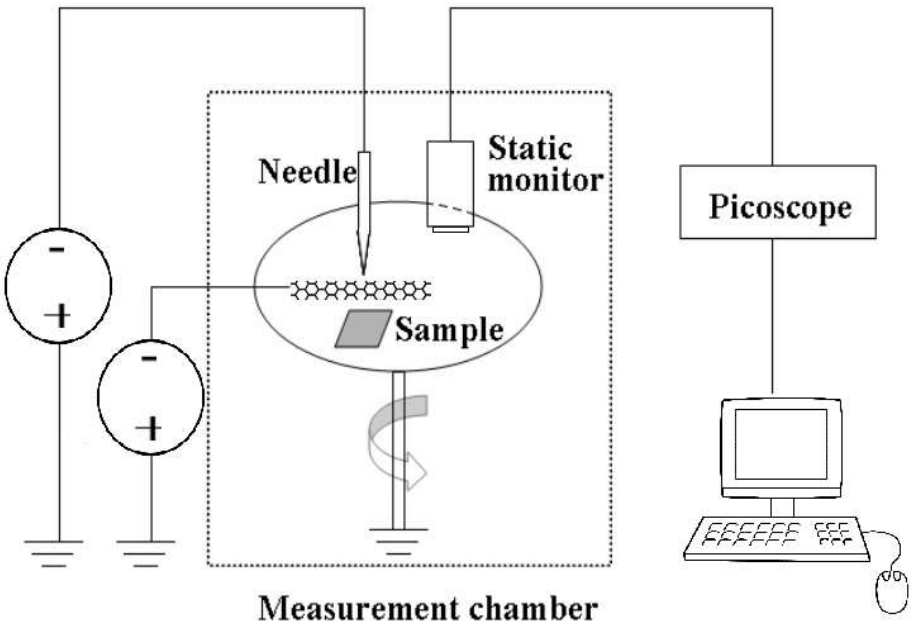

Figure 5-1: A surface potential decay schematic diagram [144]. DC voltage sources were connected to the needle and the grid. Once the sample's surface is charged by corona effect, the sample is moved towards the static monitor for decay measurement.

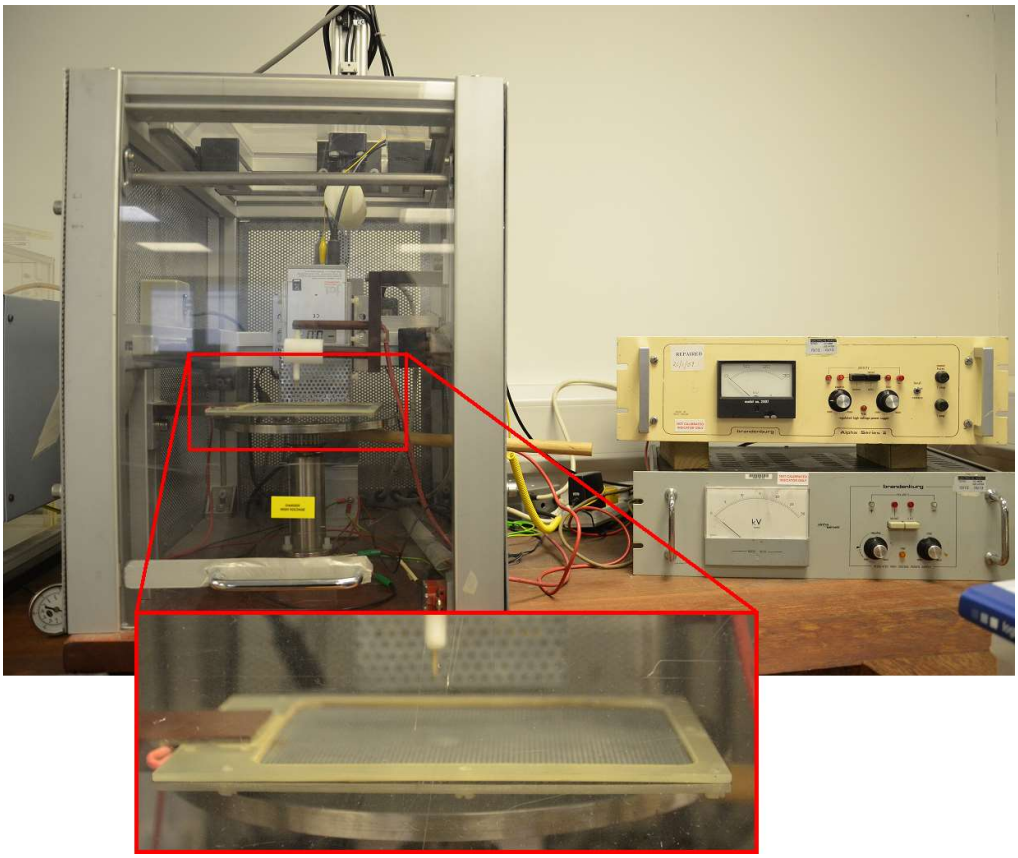

Figure 5-2: The surface potential decay kits used in this experiment. The inset picture shows the tip of the corona charging needle, the grid, and the sample holder.

300 µm thick epoxy resin samples were used for this experiment. The samples were placed on top of a rotatable earthed electrode plate, just underneath the high-voltage needle electrode and the wire mesh grid electrode. The grid acts as an interpose between the surface and the needle, and it needs to be as close as possible to the surface. The supply for grid voltage had the same polarity as the needle, but with a lower magnitude. In this experimental setup, the distance between the needle and the grid was 4.5 cm while the distance between the grid and the ground plate was 1.5 cm. The grid has a surface area of 150 cm², wide enough to provide uniform distribution of corona charge on the sample surface of 16 cm² (4 cm x 4 cm). The epoxy samples were negatively charged by corona effect on their free surface for 1 min. The needle and grid voltage were -16 kV and -5 kV respectively. Immediately after charging, the sample was quickly moved using the rotating system towards a compact JCI 140 static monitor to measure the surface potential decay,

and the decay versus time characteristic was plotted. It is important to note that, as this experiment was conducted in open air, the obtained results were highly influenced by the atmospheric condition.

5.2.1 RESULTS AND DISCUSSIONS

From Figure 5-3, the initial-surface-potential for all three samples are ~ -2.8 kV. Different rates of surface potential decay for epoxy resin samples of different fluorination time can clearly be seen from the decay curves. For non-fluorinated epoxy resin sample, F00, the surface potential is stable throughout the measurement period, signifying that the charges remain deeply trapped on the surface layer. At the end of the 40 min decay time, the surface potential value is -2.6 kV, a reduction of just 0.2 kV from initial charging. Several decay mechanisms in the form of surface conduction, bulk conduction (i.e. charge injection), bulk polarisation, and neutralisation by ions in the air can be held responsible for the surface potential decay of insulating materials with a grounded electrode on one side immediately after corona charging. From the study done by Molinie et al. [145] on the surface potential decay of epoxy resin insulators, they discovered that the charge injection into the bulk was not dominant. The main process responsible for potential decay was a slow bulk polarisation, which occurred under the influence of the deposited charges.

For the 30-min-surface-fluorinated sample, F30, the decay rate is faster as the surface potential drops to -1.3 kV after 40 min. The fastest decay rate can be seen for the 60-min-surface-fluorinated sample, F60, indicating faster movement of charges away from the surface as the fluorination time increases. A significant drop to -0.5 kV can clearly be seen at the end of the measurement. The faster decay trend occurs because surface fluorination treatment may have improved the surface conductivity of epoxy samples (due to shallow traps and water absorption). The increase in conductivity is even more significant with prolonged time of fluorination treatment. It is important to note that the increase in surface conductivity may enable trapped charges on the surface to move away faster as reflected from the resulting decay rate. From the same decay data in Figure 5-3, small oscillations can be observed in the decay plots, which are more noticeable in the fluorinated samples.

One possible reason for such observation can be explained in the way the charge moves through the surface. During the surface decay, the charges seems to decay in series of small pulses, and not through a steady-state decay [146, 147]. However, this observation is not seen in the work done by Liu et al. [113] for the surface potential decay on the surface-fluorinated epoxy resin. This is possibly due to the high sampling rate (every five seconds) used in this experimental setup. Alternatively, the fact that the steps in surface potential match each other closely in F30 and F60 plots, albeit on different timescales due to the surface conductivity differences, suggests a measurement artefact [148, 149] possibly due to the placement of field mill. The probe head was placed and calibrated just 3 cm on top of the measured surface for increased sensitivity [144]. This action might have introduced measurement artefacts in the plots. However, not all decay measurements are affected by these small oscillations.

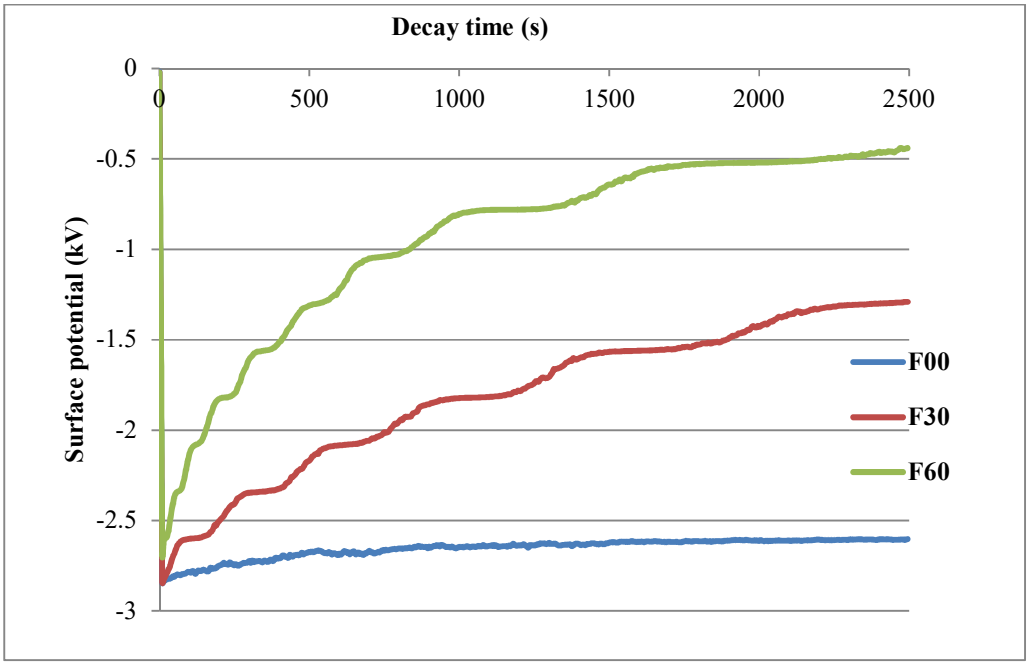

Figure 5-3: Surface potential decay for non-fluorinated and surface-fluorinated epoxy resin samples using negative corona. The fastest decay is observed by F60, followed by F30 and F00.

It is known that the surface potential of a homogeneous insulator decays exponentially with a time constant, τ, given by:

$$\tau = \frac{\varepsilon}{\sigma_v} \qquad (5\text{-}1)$$

where ε is the dielectric constant, and σ_v is the bulk conductivity. This equation applies when the potential decay is caused purely by the bulk conduction/polarisation. Meanwhile, for the potential decay of a homogeneous insulator surface due to the surface conductions, as in the case of surface-fluorinated epoxy resin samples, Crisci et al. [139] proposed another model where the time constant is given by:

$$\tau = \left(\frac{R}{2.41}\right)^2 . \frac{\varepsilon}{d} . \frac{1}{\sigma_s} \qquad (5\text{-}2)$$

where R stands for radius of the sample, d stands for thickness of the sample, and σ_s stands for surface conductivity of the insulator. However, it is worth to note that the proposed model by Crisci et al. cannot be used to numerically evaluate the relationship between the decay time constant and the surface conductivity of the surface-fluorinated samples because the surface layer and the bulk consist of different materials with different conductivity values and different dielectric constants. Nevertheless, from the proposed model, it is known that the decay time constant and the surface conductivity value have an inverse relationship i.e. decay time is faster when the conductivity is higher. The proposed model is in agreement with the obtained results.

5.3 DOUBLE EXPONENTIAL DECAY FIT

Baum et al. [150] had reported that the single exponential decay equation can be used to fit the decay curves for a shorter time and that there is a divergence at a longer period. The surface potential decay equation is given by

$$V(t) = A_0 exp\left(-\frac{\mathrm{t}}{B_0}\right) \quad (5\text{-}3)$$

where V(t) is the surface potential at any point of time after a certain decay period, parameter A_0 is the initial surface potential at any point of time after charging and parameter B_0 is the decay time constant. However, after applying equation 5-3 into the surface potential decay experimental results, it was observed that this equation is not suitable to represent the decay curves. In another similar work done by Zhuang [144], he adopted the double exponential decay analysis, representing the two type of charges inside the corona charged material; mobile and trapped.

$$V(t) = A_m exp\left(-\frac{\mathrm{t}}{B_m}\right) + A_t exp(-\frac{\mathrm{t}}{B_t}) \quad (5\text{-}4)$$

where A_m and A_t represent the amount of mobile charges and trapped charges after the removal of the applied voltage, while B_m and B_t show the decay time constant of mobile charges and trapped charges. He assumed that these two types of charges decay simultaneously; mobile charges can easily travel across the sample, and the trapped charges stay inside the material for a longer time. Equation 5-4 can be applied for the decay of the fluorinated samples as mobile charges can easily move through the more-conductive-fluorinated layer and should give a faster surface potential decay rate.

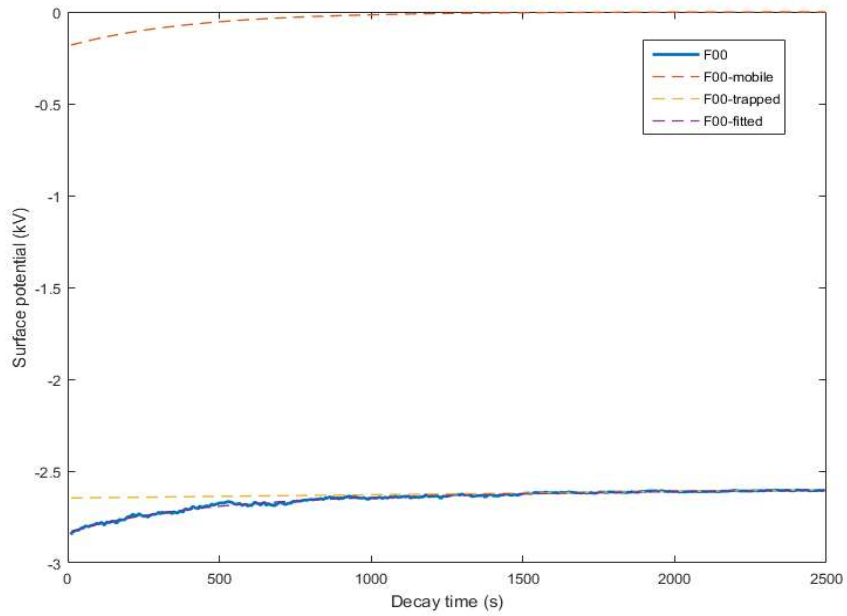

Figure 5-4: Double exponential decay fitting for F00. The fitted line is the summation of the mobile charge exponential component and trapped charge exponential component.

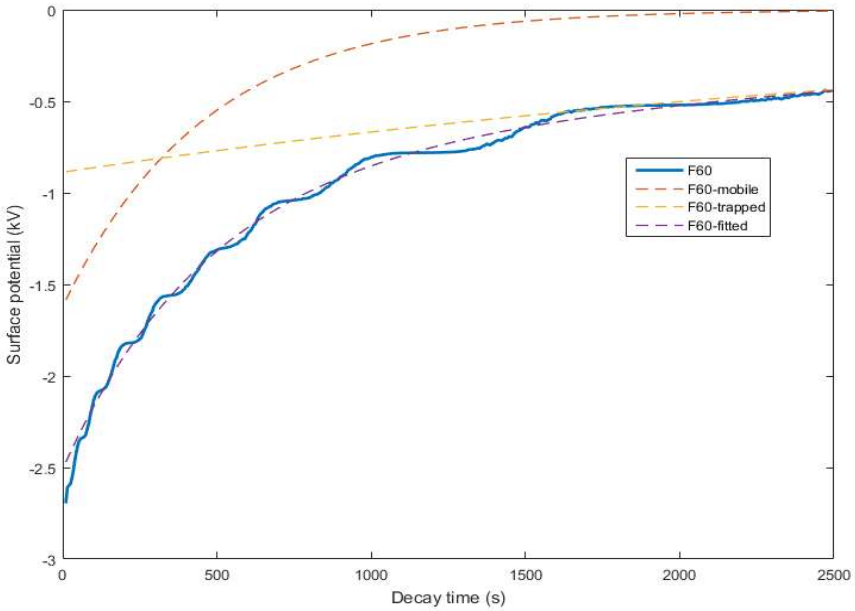

Figure 5-5: Double exponential decay fitting for F60. The fitted line is the summation of the mobile charge exponential component and trapped charge exponential component.

Parameters from equation 5-4 were calculated by the curve fitting application in MATLAB. All the parameters were focused to be positive and the best-fitted result was selected. The fitted results and parameters can be found in Table 5-1. Figure 5-4 and Figure 5-5 clearly show that equation 5-4 can fit the experimental results very well for both original and fluorinated samples, and it can also reveal the detailed change in mobile charges and trapped charges with time. The decay process of surface potential is determined by the decay of both mobile and trapped charges. The decay of the mobile charges dominates during the first 5 to 10 min. After this interval, the surface potential decay is totally governed by the trapped charges. Figure 5-6 shows that the number of mobile charges, represented by A_m, is increasing with prolonged fluorination time. As the sum of A_m and A_t is broadly the same for all the samples, the number of deep charges, represented by parameter A_t, shows a decreasing trend as the fluorination time increases. Figure 5-7 represents the decay speed for both type of charges. It is found that mobile charges always decay faster than the trapped charges. By using the fzero function in MATLAB to solve the equation, the relaxation time, T_r (time to reach 1/e of initial potential) for sample F00, F30 and F60 are 9.79 x 10^4 s (27.2 h), 4.23 x 10^3 s (1.18 h) and 1380 s (0.246 h) respectively.

Sample	A_m	$A_m/(A_m + A_t)$	A_t	$A_t/(A_m + A_t)$	B_m	B_t
F00	- 0.126 ± 0.012	0.05 ± 0.01	- 2.66 ± 0.09	0.95 ± 0.06	357 ± 57	105000 ± 3000
F30	- 0.868 ± 0.080	0.30 ± 0.04	- 2.01 ± 0.06	0.70 ± 0.05	277 ± 50	6450 ± 160
F60	- 0.969 ± 0.088	0.36 ± 0.05	- 1.74 ± 0.06	0.64 ± 0.06	187 ± 34	1550 ± 40

Table 5-1: Parameter A_m, A_t, ratios, B_m, and B_t for curve-fitting result of F00, F30 and F60 at 95 % confidence bounds. The relaxation time, T_r (time to reach 1/e of initial potential) for sample F00, F30 and F60 are 9.79 x 10^4 s (27.2 h), 4.23 x 10^3 s (1.18 h) and 1380 s (0.246 h) respectively.

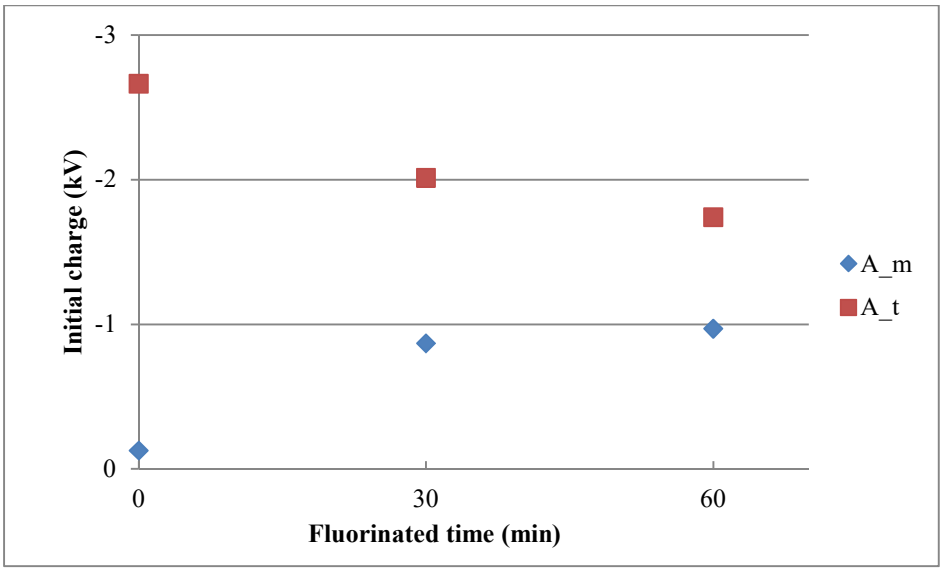

Figure 5-6: Plots of parameters $\boldsymbol{A_m}$ and $\boldsymbol{A_t}$ for curve-fitting result of F00, F30 and F60. The values of $\boldsymbol{A_m}$ is increasing while $\boldsymbol{A_t}$ is decreasing as the fluorination level increases.

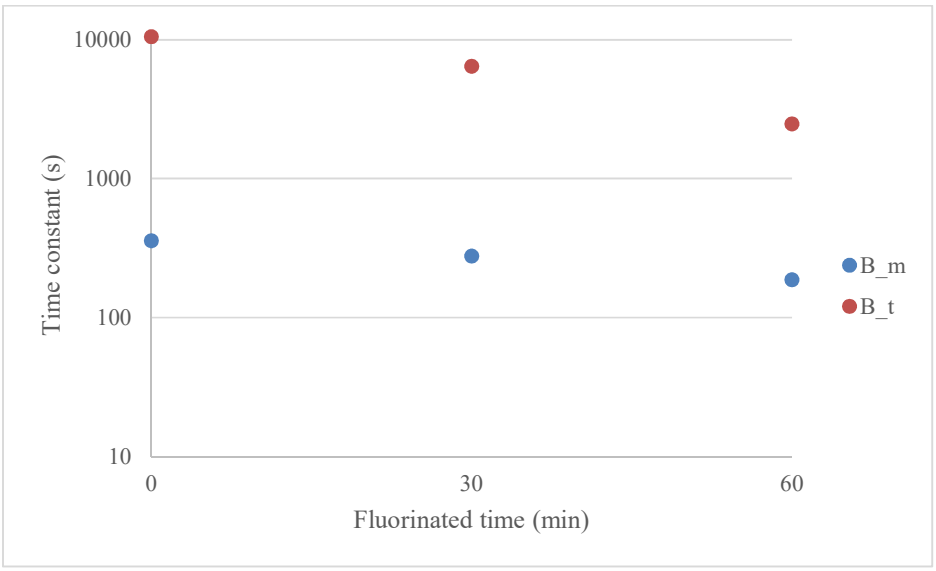

Figure 5-7: Plots of parameter $\boldsymbol{B_m}$ and $\boldsymbol{B_t}$ for curve-fitting result of F00, F30 and F60. Both parameters decrease as the fluorination level increases.

As explained earlier in Chapter 4, the fluorination treatment on the surface introduced a contest in the number of compositional and structural changes i.e. the chemical defects and

the physical defects in the fluorinated surface layer. The chemical defects from the surface treatment process introduce deep traps that is associated to the number of trapped charges on the surface of the fluorinated sample. The physical defects, on the other hand, introduce shallow traps that is associated to the number of mobile charges on the surface. From Figure 5-6, it can be seen that the number of mobile charges (shallow traps) is increasing with fluorination time while the number of trapped charges in deep traps is decreasing, indicating the conductivity is increasing with the treatment time. Likewise from Figure 5-7, the decrease in time constant $\boldsymbol{B_m}$ value as the fluorination degree increases, implies that the average trapping level is becoming shallower. The value for time constant $\boldsymbol{B_t}$ shows a significant decrease from over 10000 s before the fluorination treatment to 6450 s and 2480 s for F30 and F60 respectively, suggesting an introduction of entirely new level of traps in between the shallow and deep traps. However, there is no experimental evidence yet to support this claim. When the surface conductivity is high, the decay mechanism through field-dependent surface conduction is dominant, hence the fast decay at the start of the measurement and slowed down towards the end of the measurement i.e. exponential decay. This observation is in line with the work done by Alam et al. [151] in which they reported that the enhanced surface conduction intensifies charge spreading along the surface and yields a faster potential decay. As for the non-fluorinated epoxy sample which doesn't possess the conductive fluorinated layer, the decay mechanism comes mainly from bulk injection and gas neutralisation [152], which are slow processes as compared to surface conduction decay through fluorinated layer, hence slow decay.

5.4 DECAY FOR GROOVED SAMPLE

The surface current measurement and surface potential decay study have shown that the newly formed fluorinated layer did play an important role in dispersing the charges away due to the increased in conductivity of the surface layer. The surface potential decay measurement was again repeated, this time using 'grooved' samples. The samples were prepared by cutting a chunk off the top surface layer (as illustrated in Figure 5-8) in order to cut off the conductive path of the fluorinated layer. In doing so, this test should confirm

the decay path taken (either through the bulk or on the surface) by the corona-deposited charges on the fluorinated surface of the epoxy resin.

It is proven from DC current measurement that the difference in conductivity value between the fluorinated layer and epoxy layer will dictate the movement of charge either along the surface or through the bulk. The fluorinated samples should allow more charges to be channelled away via the more-conductive-fluorinated layer to the ground. By simply using a razor, four fine lines were cut 3 mm away from each four edges of the surface-fluorinated epoxy samples. The lines were made deep enough to penetrate into the bulk and, thus, cutting off the fluorinated path, leaving an isolated fluorinated layer on top of the epoxy sample. As the decay path along the fluorinated layer is compromised, the grooved samples should show a slower surface potential decay characteristic because the remaining decay route is through the bulk and bulk conduction is comparably a slow process. The same steps as previous surface potential decay measurements were repeated. The results were compared with the potential decay of the original samples. Similar to previous experimental setup, the needle and grid voltage were set to -16 kV and -5 kV respectively. For ease of presentation from now onwards, the absolute value of the surface potential is used in the decay plot.

Figure 5-8: Cross-section view of a grooved sample. Red marks are the place where chunks of fluorinated layer were cut off in order to isolate the trapped charge on the surface

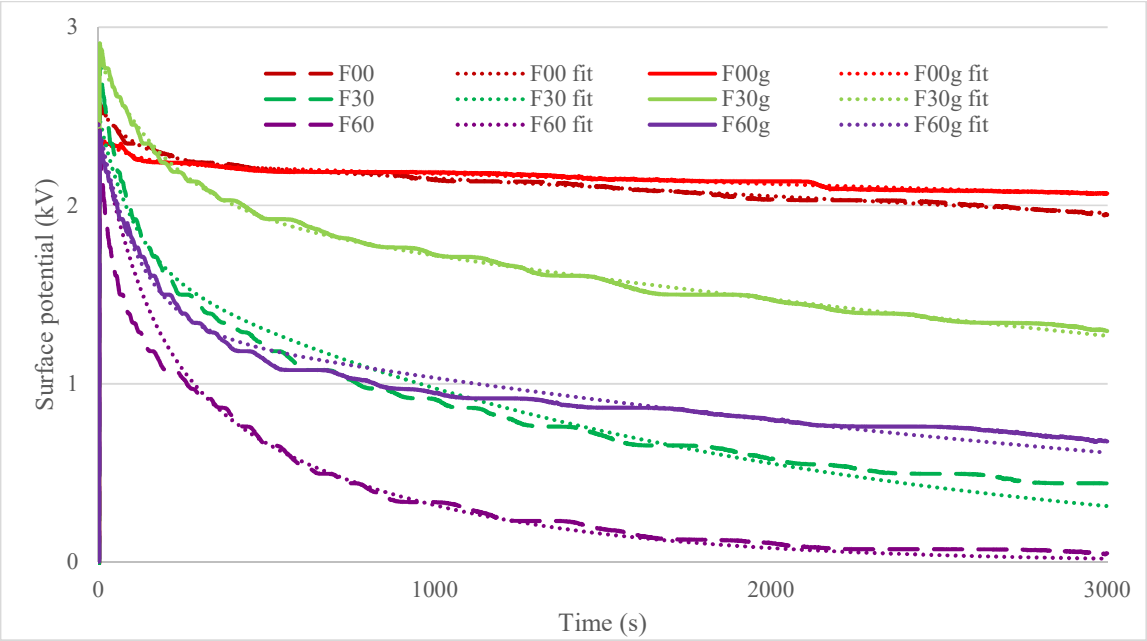

Figure 5-9: Surface potential decay for original, fluorinated, grooved samples and the fitted lines. The grooved sample exhibit slower decay with respect to the corresponding fluorinated sample, but not as slow as F00 sample.

In order to established the relationship between the samples here with the samples for preliminary measurement, the parameters in Table 5-2 are compared with the parameters in Table 5-1. The ratios of pre-exponential $\boldsymbol{A_m}$ and $\boldsymbol{A_t}$ for F00 and F30 samples are largely similar. However, the ratios of $\boldsymbol{A_m}$ and $\boldsymbol{A_t}$ for the F60 samples are slightly different, presumably due to F60 sample in this experiment absorbed more surface moisture, thus higher number of mobile charges. Such observation is not seen in the case of F00 and F30. The values of parameter $\boldsymbol{B_m}$ are broadly the same between the two tables for each samples. As for parameter $\boldsymbol{B_t}$, there is a clear difference in the time constant associated with the two F00 samples, as well as F30 samples. The two F60 samples have broadly the same value of time constant $\boldsymbol{B_t}$. In theory, the values of parameter $\boldsymbol{B_t}$ should be broadly the same between each samples since the physicochemical state between these pairs should be the same. The difference in the time constant values can be attributed to the inconsistency in the measurement technique, or alternatively, because of environmental influences. As mentioned earlier, the surface decay performance is highly influenced by environmental factors.

The result from Figure 5-9, in general, shows a slower decay rate for the grooved samples as well as the decay of non-grooved samples. For simplification, the absolute value for surface potential is used to represent the result. Supposedly, the decay rate for the grooved sample should be as slow as the original F00 sample because the fluorinated layer that supposed to channel the deposited charges to the ground was cut off, thus, limit the charge decay through the surface. This action should result in the deposited charges being trapped on the isolated surface, unable to move towards ground. However, the decay for both grooved-fluorinated samples are not at the same rate as the original F00 sample, because (i) there still exist a small area of the fluorinated surface (3 mm from the edges) that was connected the ground electrode through the fluorinated channel, and (ii) the groove did not totally block the current flowing through the surface, instead, it just adds resistance on the surface. The groove still permits some deposited charges to go through towards ground and, therefore, alter the surface decay rate.

Sample	A_m	$A_m/(A_m + A_t)$	A_t	$A_t/(A_m + A_t)$	B_m	B_t
F00	0.108 ± 0.010	0.05 ± 0.01	2.14 ± 0.07	0.95 ± 0.07	375 ± 68	85500 ± 2000
F00g	0.098 ± 0.009	0.04 ± 0.01	2.17 ± 0.07	0.96 ± 0.06	400 ± 64	101000 ± 2000
F30	0.896 ± 0.081	0.32 ± 0.04	1.92 ± 0.05	0.68 ± 0.05	192 ± 35	1490 ± 31
F30g	0.828 ± 0.076	0.30 ± 0.04	1.95 ± 0.07	0.70 ± 0.06	256 ± 41	7040 ± 171
F60	1.17 ± 0.11	0.48 ± 0.07	1.29 ± 0.04	0.52 ± 0.05	178 ± 32	1180 ± 30
F60g	1.11 ± 0.10	0.45 ± 0.07	1.34 ± 0.04	0.55 ± 0.05	200 ± 32	3750 ± 92

Table 5-2: Parameter A_m, A_t, ratios, B_m, B_t and T_r for curve-fitting result of F00, F30, F60 and the corresponding grooved samples at 95 % confidence bounds. The grooved sample exhibit slower decay constants with respect to the corresponding fluorinated sample, but not to the value of F00 sample.

From Table 5-2, the pre-exponential value of A_m for the grooved samples is slightly reduced as compared to the un-grooved samples in each fluorination level indicating a reduction in charge mobility as the groove is introduced onto the samples. The changes in time constants value of both B_m and B_t, in theory, would suggest changes in the average trapping level. However, this is not the case for these grooved samples as the introduction of groove on the surface of the sample would not alter the physicochemical structure of the material and, thus, would not change the time constants associated with the shallow and deep trapping level. The introduction of grooves simply adds extra resistance to the charge movement on the sample surface.

5.5 PEA METHOD

From the surface potential decay measurements, a big question arises on the dominant decay mechanisms of the deposited charges. It is well documented that there are three mechanisms that govern surface charge decay, which are (i) bulk conduction/polarisation, (ii) diffusion along the surface and (iii) neutralisation by ion present in the gas volume above the sample surface [153]. Zehira et al. [154] reported that atmospheric neutralisation plays a negligible role in the surface potential decay process on insulation surface. The neutralisation by surrounding ion may not be significant as all tests are conducted at the same atmospheric condition in a controlled environment, leaving the possibility of surface charge decay mechanisms to be through bulk conduction or along the surface. Hence another measurement tool, the pulsed electroacoustic (PEA) method, was carried out to see the movement of space charges, which will help to determine the exact nature of the decay mechanism.

PEA method was utilised to observe the space charge behaviour inside the surface-fluorinated epoxy sample, as well as the non-fluorinated epoxy sample. The Pulsed Electroacoustic Non-destructive Test System (PEANUTS) instrument was used for the space charge measurement. A voltage of 7 kV was applied to samples of approximately 300 μm thickness (23.34 V mm^{-1}) at room temperature for 120 min. At each time interval,

a pulse (width 5 ns, voltage 600 V, and frequency 400 Hz) was applied to generate acoustic pulses from the stored charges within the dielectrics for measurement purposes. After 120 min, the voltage supply was turned off, and the decay measurement was taken at each time interval to see the decay characteristics. Calibration was made using LabVIEW to filter out the background noise.

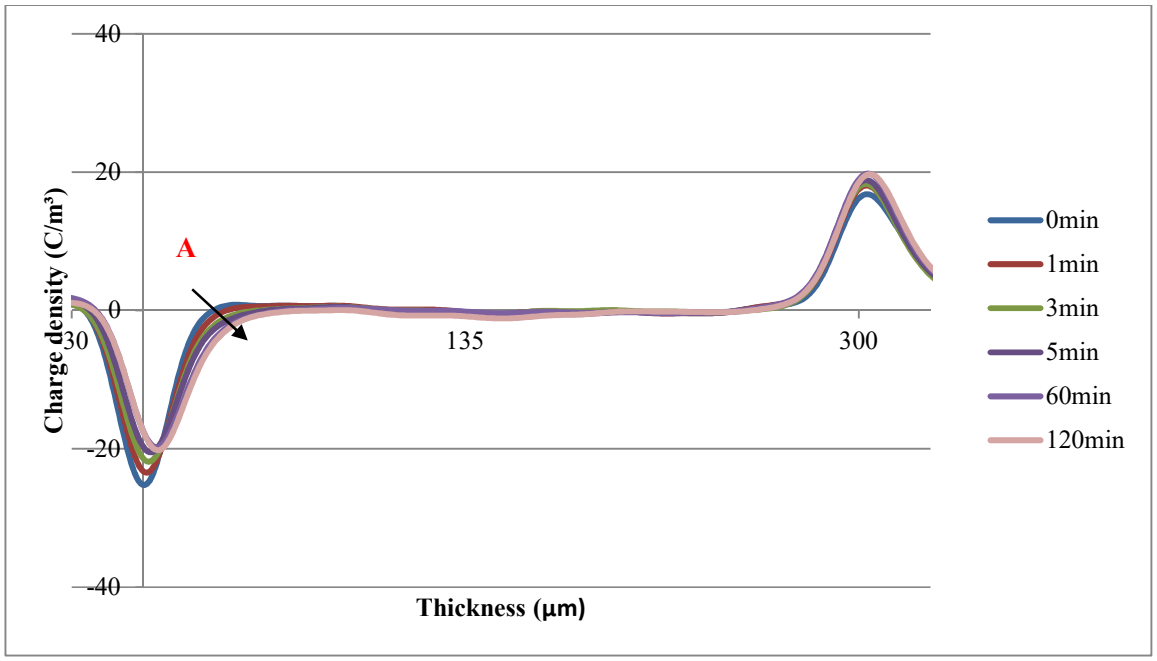

Figure 5-10: Charge build-up in non-fluorinated epoxy resin sample at 7 kV (23.34 V mm^{-1}) for 120 min. Homocharge build-up can be seen near cathode at position A

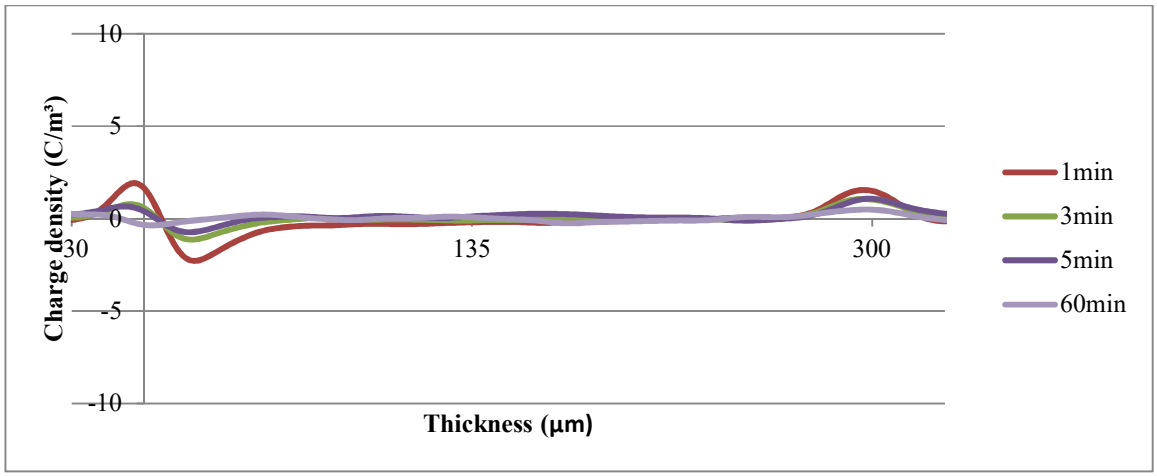

Figure 5-11: Charge decay in non-fluorinated epoxy resin sample for 60 min when the voltage source is removed. Fast dissipation of injected charges implies that there is a fast de-trapping process going on.

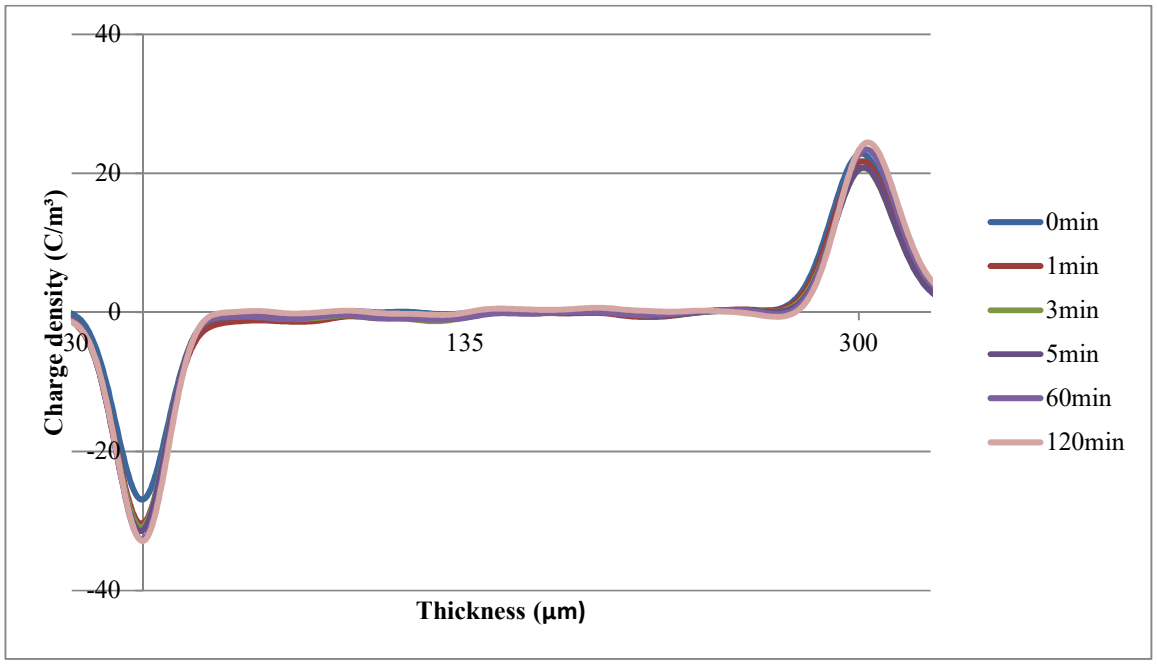

Figure 5-12: Charge build-up in 60-min-surface-fluorinated epoxy resin sample at 7 kV (23.34 V mm^{-1}) for 120 min. No apparent charge build-up can be seen at anode nor cathode.

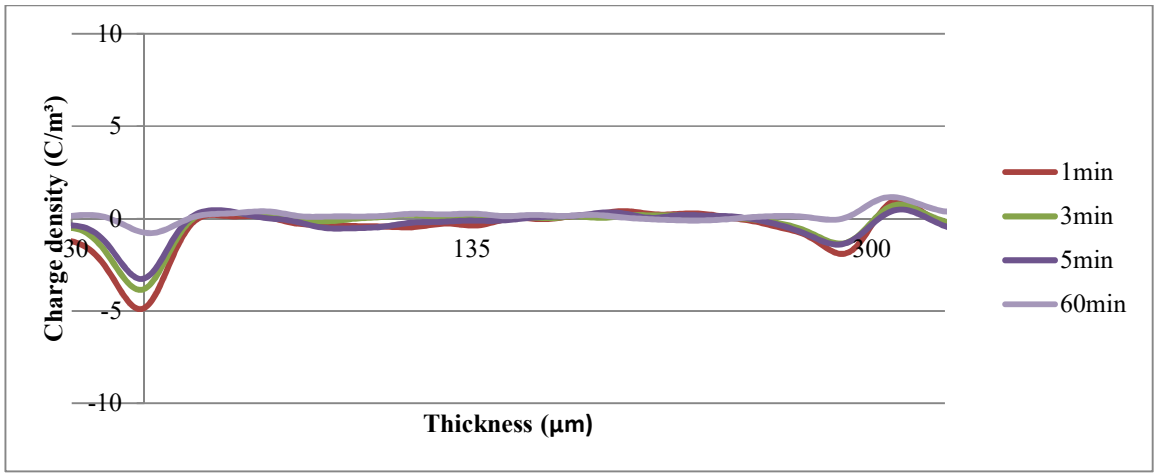

Figure 5-13: Charge decay in 60-min-surface-fluorinated epoxy resin sample for 60 min when the voltage source is removed. Fast dissipation of injected charges implies that there is a fast de-trapping process going on.

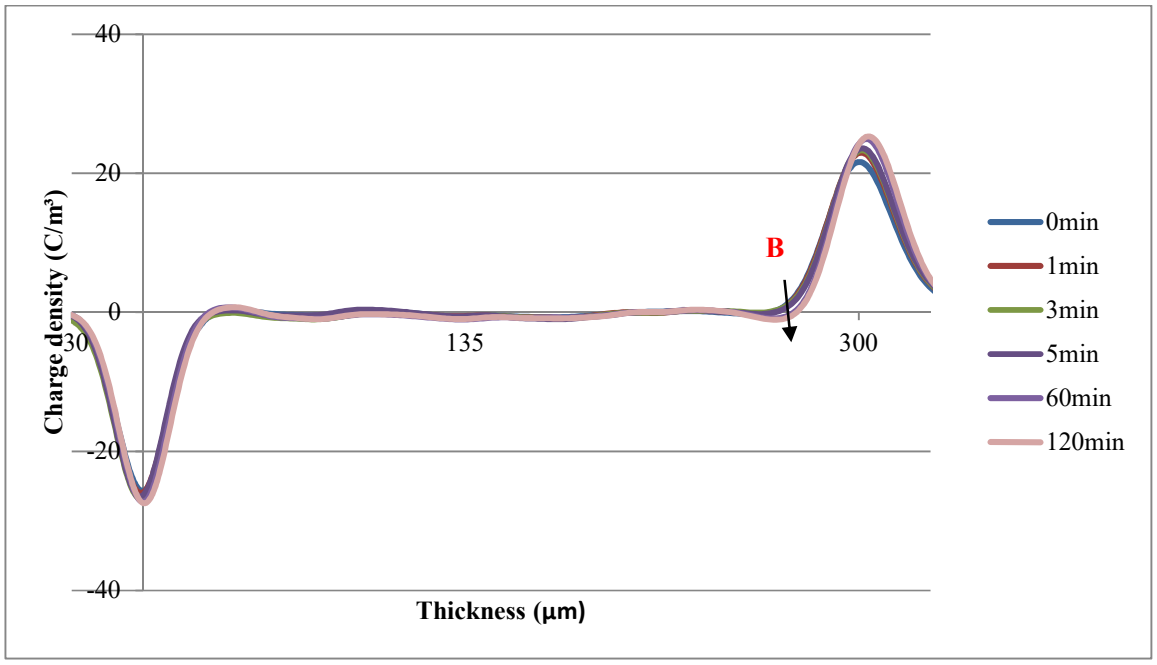

Figure 5-14: Charge build-up in 120-min-surface-fluorinated epoxy resin sample at 7 kV (23.34 V mm^{-1}) for 120 min. Small heterocharge build-up can be seen near anode at position B.

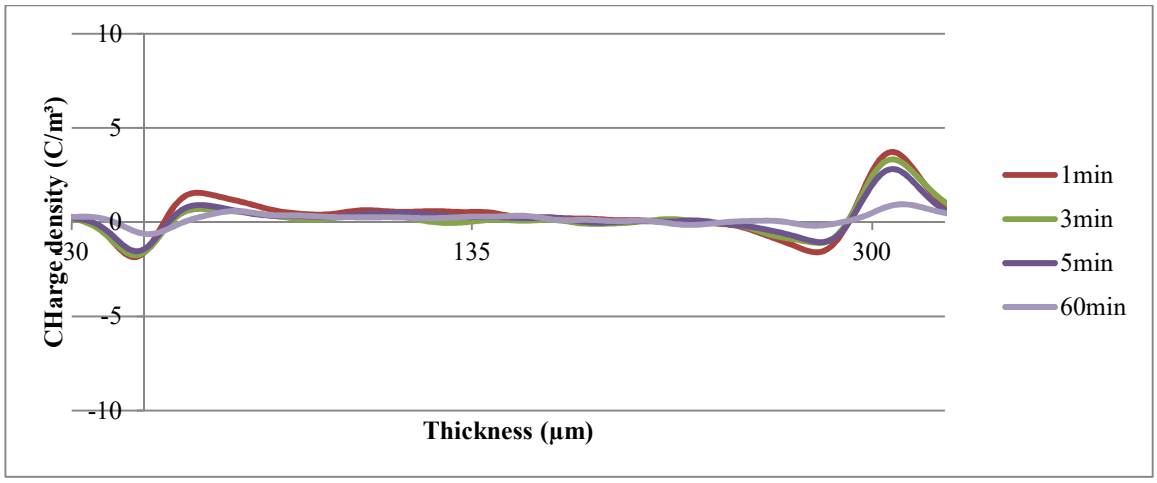

Figure 5-15: Charge decay in 120-min-surface-fluorinated epoxy resin sample for 60 min when the voltage source is removed. Fast dissipation of injected charges implies that there is a fast de-trapping process going on.

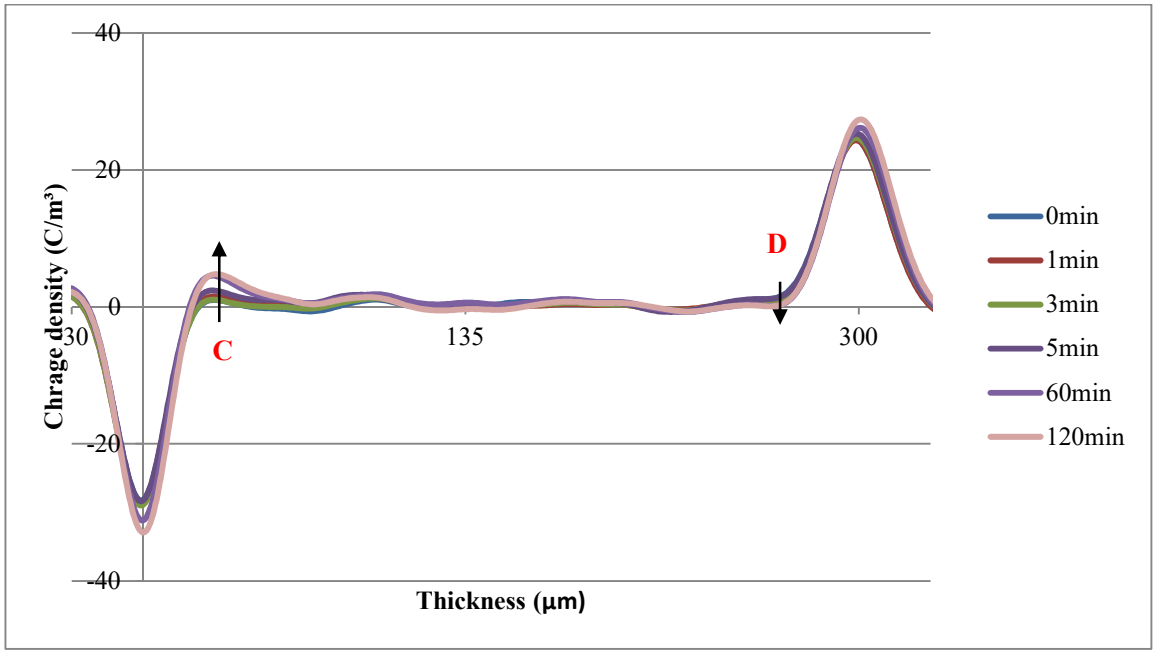

Figure 5-16: Charge build-up in 180-min-surface-fluorinated epoxy resin sample at 7 kV (23.34 V mm^{-1}) for 120 min. Heterocharge build-up can be seen near anode (D) and cathode (C).

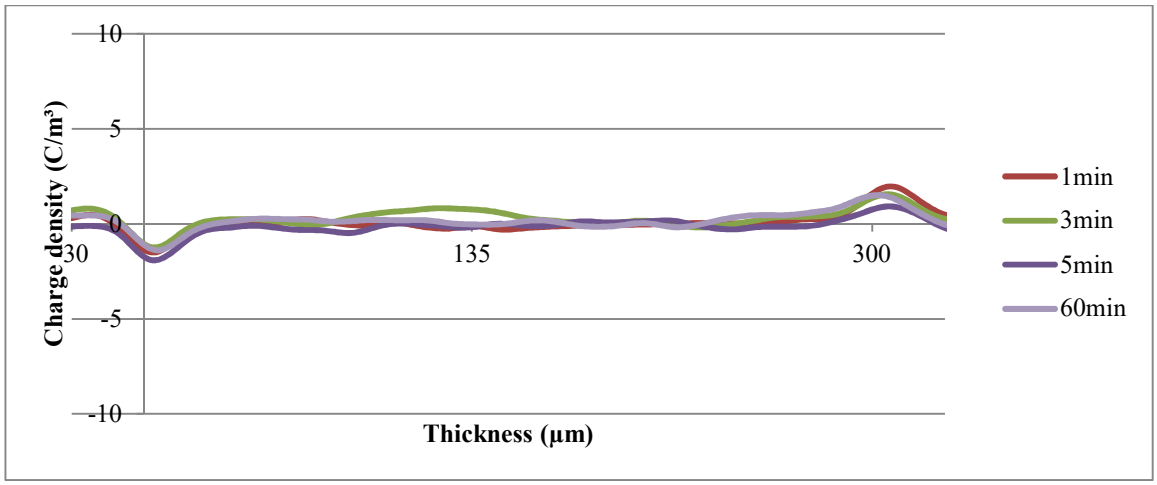

Figure 5-17: Charge decay in 180-min-surface-fluorinated epoxy resin sample for 60 min when the voltage source is removed. Fast dissipation of injected charges implies that there is a fast de-trapping process going on.

5.5.1 DISCUSSIONS

From the obtained PEA data for non-fluorinated epoxy resin sample (F00) in Figure 5-10, it is evident that there is a small amount of homocharges (negative charges) injected from the cathode during the 120 min of charging period (position A). The injected charges are trapped and remained in the vicinity of the cathode electrode, as depicted in Figure 5-18. There is no internal space charge accumulation detected by the PEA within the bulk of the epoxy samples. The presence of homocharges at the cathode reduces the local electric field and, therefore, suppresses further charge injections. Similar observations about the space charge behaviour on epoxy resin have been reported elsewhere. Iizuka et al. [155] had reported that there was no internal space charge in pristine epoxy resin and that the charges appeared close to the vicinity of the electrodes. Another report by Fukunaga et al. [156] suggested that homocharges accumulated near the electrodes and that no internal space charge was observed at other locations within the bulk of the epoxy resin. The accumulation of homocharges in the vicinity of electrodes was also observed in the work of Dissado et al. [157]. From the decay data in Figure 5-11, the fast dissipation of injected charges after voltage removal implies that there is a fast de-trapping process going on and the charges are extracted at the neighbouring electrode. Dissado et al. also stated that the space charge decay is dominantly governed by the de-trapping mechanism from traps with

a depth range from 0.94 to 1.15 eV and to be extracted at the neighbouring electrode during the decay process. It is important to note that all the samples under investigation possess high glass transition temperature T_g (128 °C from DSC measurement) while the PEA measurements were performed at room temperature. Under this experimental condition, the epoxy samples were deep in their glassy state and, therefore, the polarisation and movement of charges from impurities present in the material will be restricted.

From the PEA data of the 60-min-surface-fluorinated epoxy resin sample in Figure 5-12, there is no clear evidence of formation of either heterocharge or homocharge near the surface of the epoxy resin sample as in the previous case of F00. This observation can be explained by the cancellation of net charge density from the injection of opposite charges into the surface. As opposed to the non-fluorinated sample, the thin surface-fluorinated layer on the 60-min-surface-fluorinated sample presumably suppresses the injection of homocharges from anode and cathode, as illustrated in Figure 5-19. Due to the limitation of the PEA measurement system that can only measure the net charge density, the reduced injection of homocharges cancels out the presence of induced heterocharge that accumulates near the vicinity of both anode and cathode. The formation of heterocharges inside epoxy resin sample may come from the usage of additives during the curing process and from the impurities within the sample itself. The net cancellation of charges may explain the non-formation of charges near the vicinity of anode and cathode during the voltage-on measurement. Similar to the non-fluorinated sample, there is no internal space charge observed at other locations within the bulk of the sample, which implies that the injected charges cannot gain enough energy to transit to the opposite electrode in the glassy state, in which the molecular mobility was severely restricted. When the voltage is removed after the 120 min of charging time, the fast dissipation of the injected homocharges (as seen in Figure 5-13) implies that, there is a fast de-trapping process going on from the distribution of shallow traps near the surface of the samples, only to be extracted at the neighbouring electrode [158]. Direct-fluorination treatment remarkably introduces traps in the surface layer, as discussed in detail in the characterisation tests. When the charges are effectively trapped, they may block and suppress further charge injection from the electrodes into the surface layer. Similar observation regarding the blocking of charge

injection is observed in the work of An et al. [43] on linear low density polyethylene (LLDPE).

As the fluorination duration increases, and the fluorination layer gets thicker, the blocking of charge injection becomes more dominant since there would be more filled traps to suppress further injection, as illustrated in Figure 5-20. For the 120-min-surface-fluorinated epoxy sample, F120 (as in Figure 5-14), a small amount of induced heterocharges is seen in the vicinity of the anode as more charge injections are blocked into the surface layer (position B). Meanwhile, from the PEA waveform in Figure 5-16 for the 180-min-surface-fluorinated epoxy resin sample, F180, there is a small amount of induced heterocharges near the surface of both electrodes (position C and D), mainly at cathode, as most of the injected charges are blocked from entering the surface layer. The accumulation of heterocharges increases with the time of the applied voltage. This is because the treated layer from direct-fluorination treatment is believed to have a suppression effect, which limits charge injection from the electrodes and into the epoxy resin samples. As in previous cases, no internal space charge is observed at other locations within the bulk of the thick-surface-fluorinated epoxy. Furthermore, any ionic conduction is extremely slow due to a limited fluctuation of chain segments at this temperature. Therefore, the contribution of space charge transit across the bulk cannot be observed [159].

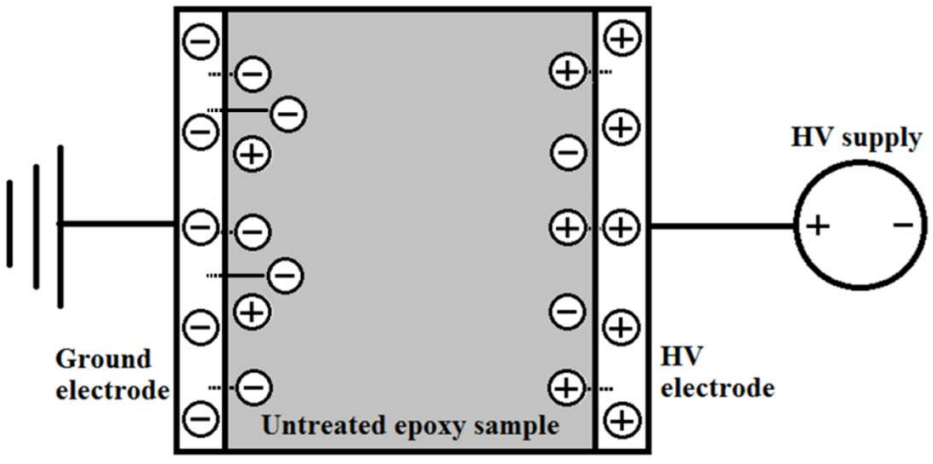

Figure 5-18: A schematic of non-fluorinated epoxy sample in PEA measurement. Charges can easily move into the untreated epoxy from the electrodes.

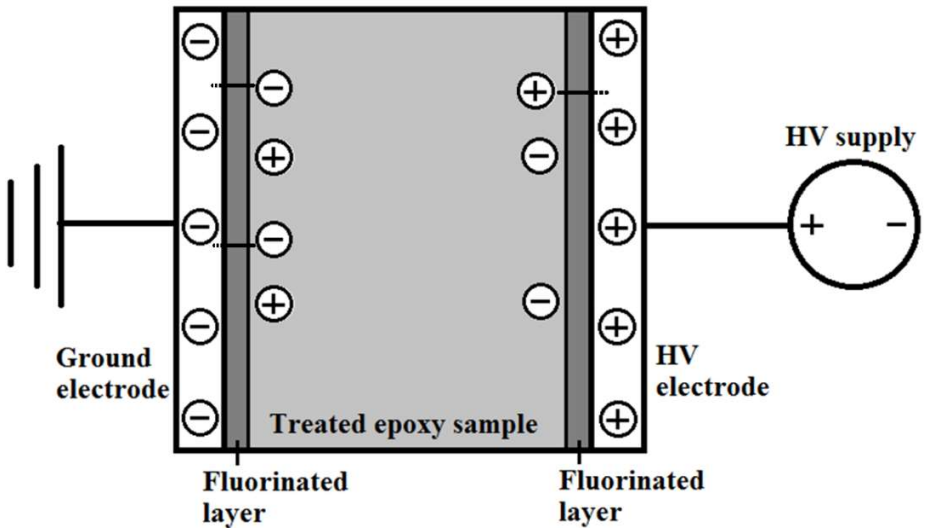

Figure 5-19: Schematic of treated epoxy sample with fluorinated layer in PEA measurement. The number of injected charges is reduced due to the suppresion-effect of the fluorinated layer.

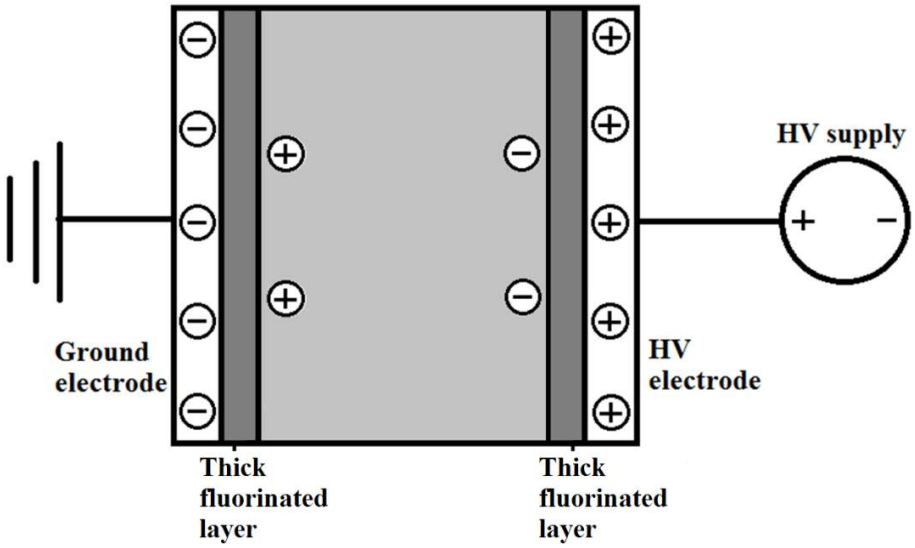

Figure 5-20: Schematic of treated epoxy sample with thick fluorinated layer in PEA measurement. Charges are blocked from being injected into the sample due to the thick fluorinated layer.

In relation to the surface potential decay measurement, the dominant decay mechanism is believed to be conduction along the surface of the epoxy resin sample. This is because the

surface fluorination layer acts as a shield and blocks charge injection into the bulk, as explained earlier from the PEA data, i.e. it is not possible for the decay to be through the bulk. Furthermore, as the epoxy is in a glassy state, the charge movement is severely restricted and, therefore, the only logical path for the decay mechanism is through the surface conduction. It is important to note that for the non-fluorinated epoxy resin sample, the decay rate from the PEA measurement (fast) is totally different from the decay rate of surface potential decay test (very slow). This is because, in PEA measurement, the neighbouring electrode was attached to the surface of the sample all the time throughout the decay measurement. The de-trapped charges from the surface can easily be extracted via the neighbouring electrodes [157]. Meanwhile in the surface potential decay test, there is no neighbouring electrode in the experimental set-up, and the nearest neutralisation/extraction point for the de-trapped charges is through the slow bulk conduction, hence the slow decay rate.

5.6 CHAPTER SUMMARY

The direct-fluorinated epoxy resins were subjected to surface potential decay test with negative corona discharge in order to investigate the dielectric performances of the insulation material. With the increase in fluorination time, substantial increase in the decay rate of the surface potential is observed due to the increase in the surface current when compared to non-fluorinated epoxy. From the surface potential decay measurement, a big question arises on the dominant decay mechanisms of the deposited charges. It is well documented that there are three mechanisms that govern surface charge decay; (i) bulk conduction/polarisation, (ii) diffusion along the surface and (iii) neutralisation by ion present in the gas volume above the sample surface. The experiment with the grooved sample proved that the decay path is highly dependent on the fluorinated surface layer. From the PEA data of the surface-fluorinated epoxy sample, a large amount of heterocharges is observed near the vicinity of both electrodes, which is not seen in the PEA data of non-fluorinated sample. This is because the introduction of the direct-fluorinated surface layer is believed to have suppression effect, which restricts charge injection into the epoxy resin sample. Therefore, it is fitting to believe that the dominant mechanism that governs the decay process in fluorinated sample is through conduction along the surface.

CHAPTER SIX: MOISTURE ABSORPTION STUDY

Surface fluorination treatment has proven to be an effective tool in enhancing the dielectric properties of insulating materials. This surface treatment improves the surface conductivity value and enhances the surface potential decay rate, which in turn help to prevent the accumulation of surface charge and consequently improve the surface breakdown strength of epoxy resin. However, the author suspected the introduction of the fluorinated layer on top of epoxy samples may have the capacity to absorb moisture from the environment. The dielectric improvements by the fluorination treatment may not only come from the fluorine layer itself, but also from the absorbed moisture in the surface layer. Although fluoropolymer surfaces are known to exhibit repellency towards both polar and apolar liquids (e.g. water and oil) [160, 161], there are instances when fluorination treatment turns treated surfaces into hydrophilic [162, 163].

In practical applications, the presence of absorbed water in insulation materials is unavoidable and could have a negative impact on dielectric properties. In truth, moisture absorption has been reported in the literature to be linked with epoxy resin and its composites [164-166]. Popineau et al. [167] stated that molecular water with strong interactions diffuses into the epoxy resin and after some time, the interaction sites for molecular water become saturated i.e. absorption reaches quasi-equilibrium. The absorption process resumes until the water molecules filled all the micro-voids, i.e. real equilibrium. In general, there are two types of moisture absorption; physically-bound, and chemically-bound water. Physically-bound water involves molecules occupying free volume in the network or is weakly attached to the polymeric chains. For this type of bound, molecular water can be removed from the samples by applying heat for a certain period. On the other hand, chemically-bound water molecules may attach firmly to an epoxy network due to their strong interaction with particular moieties. Although some studies on surface

treatment have been proven to limit moisture absorption [168, 169], the presence of molecular water in epoxy resins is inevitable.

From the DC current measurement in the previous chapter, an increase in surface current is observed as the fluorination time increases. In addition to the increase in number of shallow traps on the surface, the absorbed moisture on the surface may also contribute towards the increase in the surface current reading. The same observation can be seen in surface potential decay measurement in which the surface-fluorinated samples of extended time decay faster. In order to test the role of the absorbed-physically-bound surface moisture towards the surface conductivity, an experimental procedure was designed which involves the investigation of the surface current measurement and decay rate with and without the absorbed surface moisture. For that reason, a set of fluorinated samples were left at ambient surrounding until the weight of each sample is stable i.e. the samples is in real equilibrium and do not absorb anymore surrounding moisture. Subsequently, the surface moisture was forcefully dried using vacuum-oven at high temperature. Measurements for weight, surface current and surface potential decay were taken before and after the drying process for both original and fluorinated samples. It is important to note that, while the absolute surface current values differ for each sample, these variations fall within experimental uncertainties. The poor reproducibility of test data is, however, a common issue with current measurements [135]. Due to the variations in each measurement, the average data over two samples were plotted in the graph for a more accurate representation of the data. An example is shown in Figure 6-1 for the F00 data before the drying treatment, that was an average value of F00 sample 1 and F00 sample 2. For simplification, only the average measurement values are used to represent the data in this study.

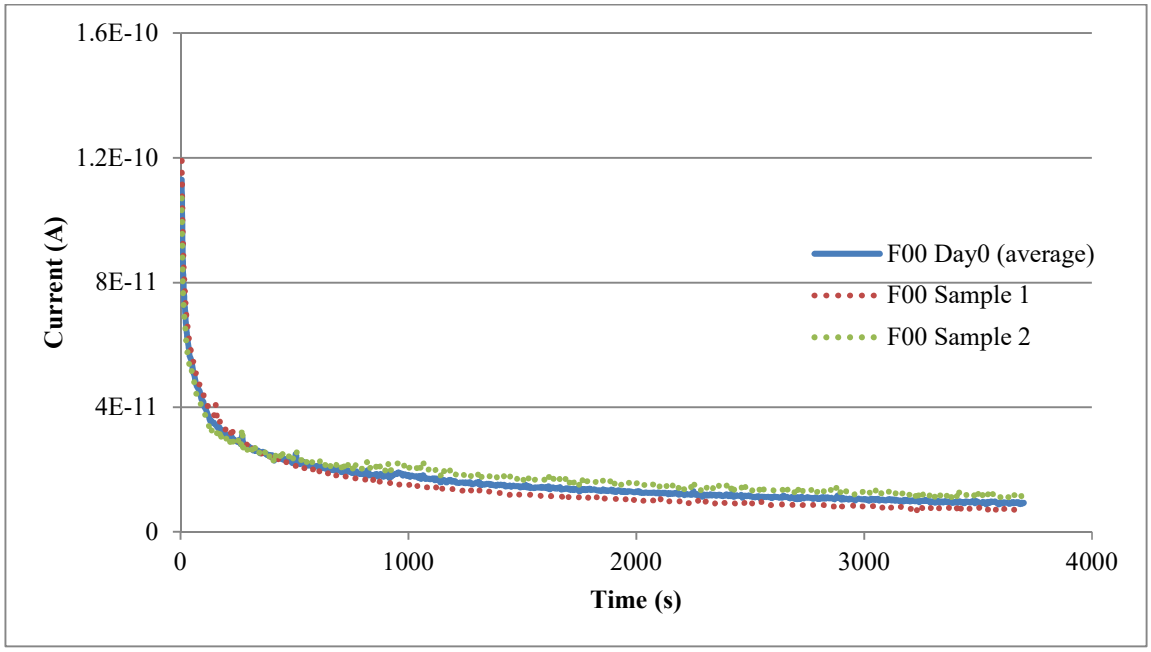

Figure 6-1: Plot of the average of two samples for a more accurate representation of the surface current measurement data. In this example, the average value of F00 Sample 1 and 2 is used for F00 Day 0.

6.1 SURFACE DC CURRENT TEST

One sure way to forcefully remove the physically-bound moisture from the surface is to vacuum-dry the sample at high temperature. For this reason, the samples were put in a vacuum-oven at 105 °C for a duration of 24 hours. The samples were weighed, and readings for the surface DC current were taken before and after the drying process. To measure the weight, Sartorius Microbalance MC210P was used throughout this experiment that has a readability value of 0.01 mg. Table 6-1 shows the weight of the samples before and after drying.

	Weight before drying	Weight after drying	Percentage weight loss
F00	0.4551 ± 0.0016 g	0.4529 ± 0.0009 g	0.48 %
F60	0.4563 ± 0.0021 g	0.4531 ± 0.0011 g	0.71 %

Table 6-1: Samples weight before and after oven-drying for DC current test. The weight lost after drying in F60 is bigger than F00 because there is more moisture being absorbed in fluorinated surface

Figure 6-2 shows plots of the time dependence of resulting current for the non-fluorinated sample (F00) and the 60-min-surface-fluorinated sample (F60). The experimental setup was done at a constant applied DC voltage of 5 kV across the 8 mm gap over 60 min at room temperature. The value of the measured current drops significantly in the transient phase and settles down after ~300 s in the steady state phase.

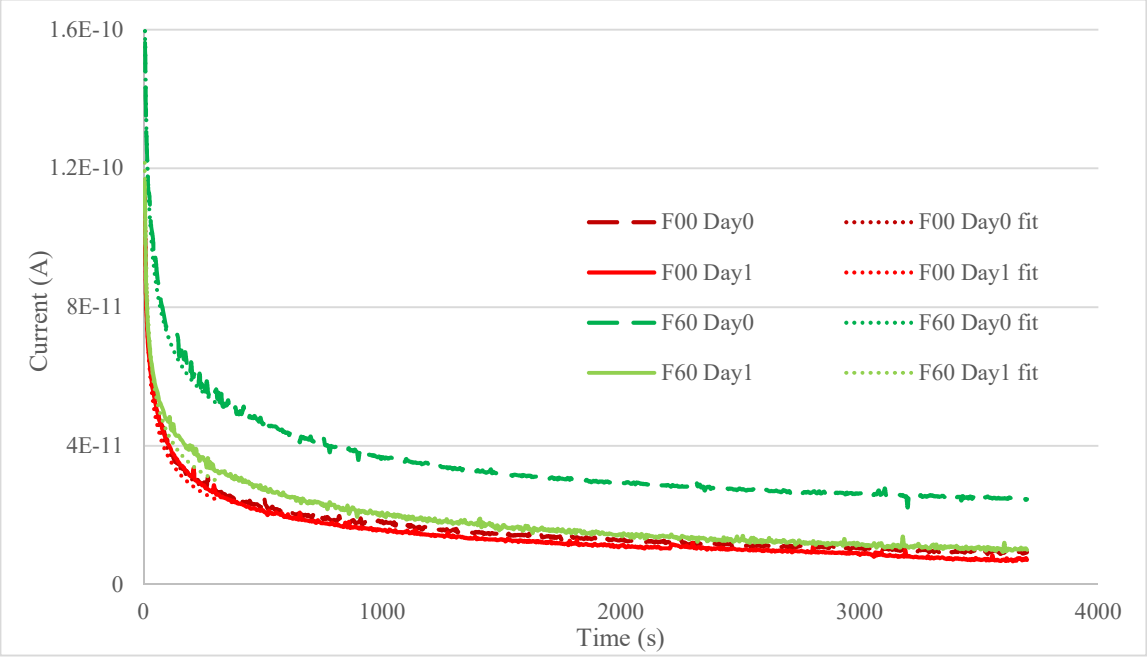

Figure 6-2: Plot of current against time for vacuum-oven-dried non-fluorinated (F00) and 60-min-surface-fluorinated (F60) epoxy sample. After 1 day of drying, F60 shows current measurement almost similar to F00

For the non-fluorinated sample (F00), the weight loss due to the drying process is 0.48 % and is reflected in the surface current measurement. There is a slight reduction in the surface current reading after the 24-hours-drying-process with the final current value at 7.03 x 10^{-12} A, down from 9.43 x 10^{-12} A the day 0. For the 60-min-surface-fluorinated sample (F60), the weight loss was higher at 0.71 % due to larger moisture content on the surface. The oven-dried fluorinated sample shows a significant reduction in surface current reading after the drying treatment. The final current reading before drying is 2.47 x 10^{-11} A and the current drops to 1.02 x 10^{-11} A after. Although the reduction in current magnitude at the end of 60 min does not fully reflect the percentage weight loss of moisture for the two samples, such observation is not without precedent. It is believed that the moisture loss in F00 mainly comes from the bulk, therefore, has a minimum influence on surface current. Consequently, the reduction in current after drying is small as shown in Figure 6-2. This is because, when the non-fluorinated sample F00 initially became saturated with ambient moisture, water would uniformly occupy the free-space within the volume/bulk of the sample. When F00 sample was dried, the water would uniformly escape from the sample. As the bulk has far bigger volume than the surface, therefore, most of the moisture lost in F00 comes from within the bulk. As for the fluorinated sample F60, since this sample possesses extra fluorinated layer that has good wettability value and small water contact angle, more moisture was trapped within the surface layer. When F60 was dried, most of the moisture lost would come from the surface. However, there is no experimental evidence to support this claim. On the other hand, at least 0.23 % of moisture loss in F60 comes from the surface that may have a major impact on surface conductivity of the sample. Consequently, a large drop in current at the end of 60 min is expected because of the large reduction in surface moisture. Judging from this result, the surface current for the dried fluorinated sample is very close to that of an untreated sample for times greater than 1000 s. This observation suggests that the role of absorbed moisture has far outweigh the role of physicochemical change as a direct result from the fluorination treatment. The presence of absorbed water is essential in the improvement of the dielectric properties in the treated material. However, in this project, no experimental work has been done to independently

measure the number of water molecules in order to estimate the water concentration, which need to be investigated in the future work.

Looking at Figure 6-2, the surface current plot for day 0 and day 1 samples are observed to be in quasi-equilibrium with ambient humidity after 1000 s. Real equilibrium with surrounding moisture would take much longer than the duration of measured data. By determining the ratio of additional surface current at day 1 to day 0 for both treated and un-treated samples at a time after quasi-equilibrium is reached, the proportion of current due to presence of absorbed water can be determined, as well as the proportion of current due to dry fluorinated layer. At quasi-equilibrium point of 2000 s, the proportion of current due to the dry fluorinated layer is:

$$\frac{'F60\ Day\ 1' - 'F00\ Day\ 1'}{'F00\ Day\ 1'} = 0.28$$

Likewise, the proportion of current due to presence of absorbed water for F00 sample at 2000 s is:

$$\frac{'F00\ Day\ 0' - 'F00\ Day\ 1'}{'F00\ Day\ 1'} = 0.15$$

The proportion of current due to presence of absorbed water for F60 sample at 2000 s is:

$$\frac{'F60\ Day\ 0' - 'F60\ Day\ 1'}{'F00\ Day\ 1'} = 1.34$$

From this simple calculation, it can be deduced that the proportion of current due to the presence of absorbed water in the case of F60, far outweigh the proportion of current due to dry fluorinated layer by 1.34 to 0.28. However, this is not true for the case of the original F00 sample, which only have a proportion of 0.15, due to the lack of moisture assisted charge movement. Similarly, by using the same approach at the beginning of the plot, before the system reach quasi-equilibrium, for example at 400 s, the proportion of current due to dry fluorinated layer is calculated to be 0.28, the same value as after quasi-equilibrium is reached, implying that the conduction of current due to fluorine layer per se

is not effected by absorb moisture. The proportion of current due to presence of absorbed water for F00 and F60 at 400 s are 0.06 and 0.82 respectively. Again, a similar pattern can be seen here with the current due to the presence of absorbed water in F60 far outweigh the current due to dry fluorinated layer, albeit at a smaller degree.

To represent the current-time characteristic of the measured surface current, the same power law fitting is used as previously used in the bulk current measurement (Equation 4-3). For consistency, only the first 300 s of the data is fitted and the parameters are shown in Table 6-2. From the fitting parameters, for both samples, the fitted values for exponential $\boldsymbol{b_s}$ can be regarded as common before and after the drying process, while the value for parameter A_s decreases at day 1. The common value of exponential $\boldsymbol{b_s}$ implies that the polarisation mechanism during transient current phase remain the same before and after the drying process. As listed in [170], these mechanisms include dipole orientation and charge injection forming trapped space charge. The removal of absorbed moisture through drying would not change the polarisation of bonds in the system, nor would it change the distribution of traps in the material, hence the common value of exponential $\boldsymbol{b_s}$. Nonetheless, the removal of absorbed moisture from the surface would certainly reduce the moisture-assisted charge injection and, therefore, the reduced values for parameter A_s after the drying process for both F00 and F60 samples.

Sample	$\boldsymbol{A_s}$	$\boldsymbol{b_s}$	$\boldsymbol{C_s}$
F00 Day0	$1.96 \times 10^{-10} \pm 0.36 \times 10^{-10}$	0.363 ± 0.044	$9.32 \times 10^{-12} \pm 2.38 \times 10^{-12}$
F00 Day1	$1.89 \times 10^{-10} \pm 0.27 \times 10^{-10}$	0.356 ± 0.035	$7.23 \times 10^{-12} \pm 1.84 \times 10^{-12}$
F60 Day0	$2.61 \times 10^{-10} \pm 0.79 \times 10^{-10}$	0.371 ± 0.070	$2.48 \times 10^{-11} \pm 0.09 \times 10^{-11}$
F60 Day1	$1.9 \times 10^{-10} \pm 0.36 \times 10^{-10}$	0.362 ± 0.045	$1.03 \times 10^{-11} \pm 0.04 \times 10^{-11}$

Table 6-2: Parameter $\boldsymbol{A_s}$, $\boldsymbol{b_s}$ and $\boldsymbol{C_s}$ of curve-fitting on first 300 s data for F00 and F60 epoxy samples dried in vacuum-oven for 24 h at 95 % confidence bounds

To established relationship between the saturated samples and the samples in preliminary surface current measurement, Figure 6-2 is compared against the preliminary measurement in Figure 4-14. The preliminary result shows a lower surface current value for both F00 and F60 (5.66×10^{-13} A and 5.03×10^{-12} A respectively). The increase in surface current measurement in this moisture test is a direct result from water absorption as the samples were left at ambient surrounding until the water content on the surface is in equilibrium with atmosphere. Even after the drying process, the surface current for F00 and F60 went down significantly, but not to the level of preliminary surface current measurement. The higher surface current measurement, even after the drying process could be attributed to the nature of surface current measurement itself. During the surface current measurement, although it is assumed that all current flows on the surface, there exist a fraction of current that flows through the un-dried bulk. Since the drying treatment may have dried the surface only and not the bulk, therefore, this surface current measurements yield a comparably higher measurement values than preliminary measurement. Alternatively, such observation could be attributed to the existence of chemically-bound water molecules that attached firmly to the hydrophilic groups in epoxy network and cannot be removed by heat application [106, 171]. The drying process can only remove the physically-bound water that diffuses into microvoids or free volume near the surface of the epoxy. It is also worth to point out that, from Figure 4-14, there is an increase in surface current value for F60 sample that is attributed to absorbed moisture. However, such observation is not seen in the plot of F60 day 1 sample in Figure 6-2. The dried F60 samples is expected to exhibit an increase in surface current value due to moisture absorption, similar to the F60 plot in Figure 4-14. As both measurements were done at ambient condition, one logical explanation for this observation can be attributed to the relative humidity level during the measurement. Although the value of relative humidity is not recorded, it is fitting to assume that the measurement for Figure 6-2 was done in a relatively low humidity condition, hence, the slow rate for surface water absorption. The work done by Zou et al. [172] confirmed that the rate for water absorption in epoxy samples increased with the increase in relative humidity.

6.2 SURFACE POTENTIAL DECAY

A similar set of procedures was performed for surface potential decay test using negative corona discharge. The samples were put in a vacuum-oven at 105 °C for 24 hours. The samples were weighed, and readings for surface potential decay were taken before and after the drying process. During the drying process, the epoxy samples were wrapped in conducting aluminium sheet to short-circuit/neutralise any accumulating charges between the top and bottom surfaces. Table 6-3 shows the weight of the samples before and after treatment for surface potential decay test.

	Weight before drying	**Weight after drying**	**Percentage weight loss**
F00	0.4245 $\pm$ 0.0012 g	0.4227 $\pm$ 0.0023 g	0.42 %
F60	0.4485 $\pm$ 0.0038 g	0.4455 $\pm$ 0.0027 g	0.66 %

Table 6-3: Samples weight before and after oven-drying for potential decay test. The weight lost after drying in F60 is more than F00 because there is more absorbed moisture in the fluorinated surface.

Figure 6-3 shows the surface potential decay rate for the non-fluorinated sample (F00), and the 60-min-surface-fluorinated sample (F60). For the non-fluorinated sample (F00), the weight loss due to the drying process is 0.42 %. The vacuum-oven-dried non-fluorinated sample shows a slight reduction in surface potential decay rate with the final potential reading at 2.61 kV, up from 2.45 kV before the drying process. In the case of 60-min-surface-fluorinated sample (F60), the weight loss for the oven-dried epoxy sample was higher at 0.66 % due to the larger surface moisture loss. The dried F60 sample experienced a massive reduction in surface potential decay rate. The final surface potential value before drying is 0.65 kV, and the potential rises to 2.45 kV after, similar to the value of the non-fluorinated sample. Again, a similar pattern can be seen here with the decay rate of F60 sample and simply proves that the presence of absorbed moisture on the surface is

considered to be the limiting factor in the improvement of decay performance of dielectric materials.

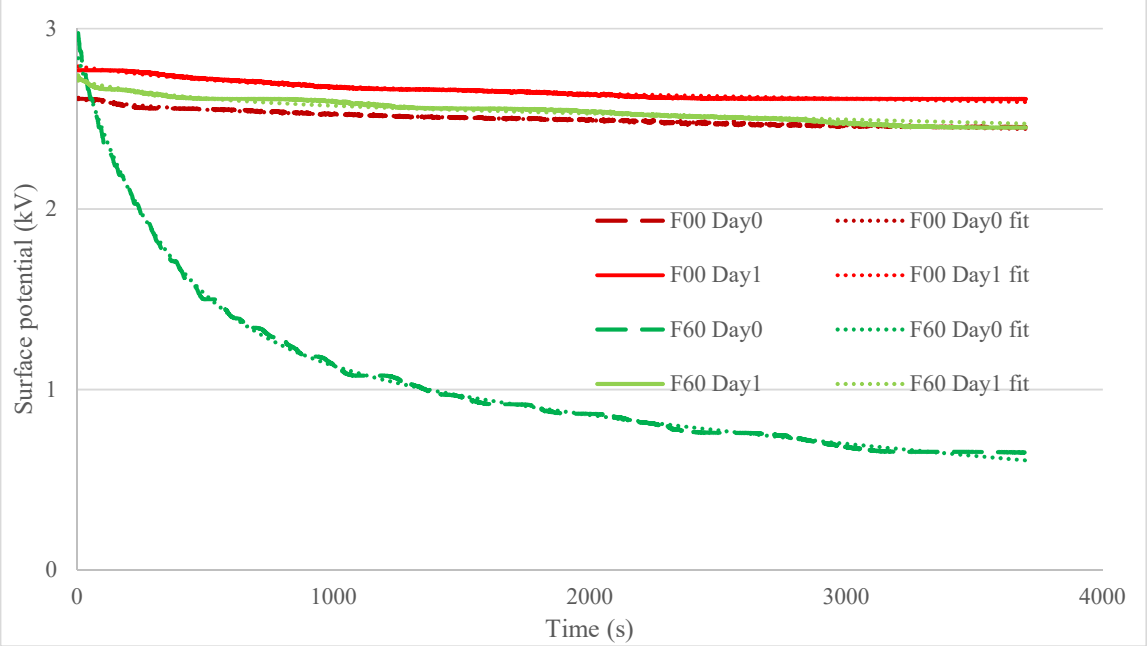

Figure 6-3: Potential decay rate for oven-dried non-fluorinated (F00) and 60-min-surface-fluorinated (F60) epoxy sample. After 1 day of drying, F60 shows decay performance almost similar to F00

To represent the surface potential decay data, the double exponential equation from Equation 5-4 is used. The fitting parameters $\boldsymbol{A_m}$, $\boldsymbol{A_t}$, ratios, $\boldsymbol{B_m}$, and $\boldsymbol{B_t}$ as well as the relaxation time, $\boldsymbol{T_r}$ (time to reach 1/*e* of initial potential) are shown in Table 6-4. From the curve-fitting result, the un-dried sample of F60 only need 0.370 h (22.2 min) to reach 1/*e* of its initial value, while the dried sample of F60 need more than 20 h.

From the ratios of pre-exponential parameters $\boldsymbol{A_m}$ and $\boldsymbol{A_t}$ in Table 6-4, for F60 sample, it can be seen that the ratio of mobile charges decreases from 0.39 to 0.04 after drying, while the number of trapped charges increased from 0.61 to 0.96. This behaviour is not seen in the F00 sample in which the ratios of parameters $\boldsymbol{A_m}$ and $\boldsymbol{A_t}$ remain broadly the same

before and after drying. As for the decay parameters of $\boldsymbol{B_m}$ and $\boldsymbol{B_t}$, there seems to be an overall increase of these time constants after drying, indicating slower decays for both F00 and F60 samples due to lack of moisture assisted movement. The increase in decay time constants in F60 are significant, but not to the level of values seen in F00. The increase of time constant value at day 1, unlike the explanation given in Chapter 5, does not mean that the average trapping level is becoming deeper. Removal of physically-bound absorbed moisture from the surface does not change the physicochemical state of the samples. It does, however, reduce the mobility of water molecules and, hence, longer decay constants.

Sample	A_m	$\frac{A_m}{(A_m + A_t)}$	A_t	$\frac{A_t}{(A_m + A_t)}$	B_m	B_t	T_r
F00 Day0	0.0980 ± 0.009	0.04 ± 0.01	2.54 ± 0.06	0.96 ± 0.009	529 ± 85	99000 ± 2000	26.7 h
F00 Day1	0.101 ± 0.009	0.04 ± 0.01	2.69 ± 0.07	0.96 ± 0.009	538 ± 97	101000 ± 2000	27.2 h
F60 Day0	1.14 ± 0.15	0.39 ± 0.08	1.77 ± 0.05	0.61 ± 0.009	190 ± 30	2640 ± 100	0.370 h
F60 Day1	0.116 ± 0.010	0.04 ± 0.01	2.60 ± 0.06	0.96 ± 0.009	410 ± 74	76300 ± 2000	20.1 h

Table 6-4: Parameter $\boldsymbol{A_m}$, $\boldsymbol{A_t}$, ratios, $\boldsymbol{B_m}$, $\boldsymbol{B_t}$ and $\boldsymbol{T_r}$ of curve-fitting result for F00 and F60 epoxy samples dried in vacuum-oven for 24 h at 95 % confidence bounds

To established relationship between the saturated samples and the samples in preliminary decay measurement, the parameters in Table 6-4 are compared with the parameters in Table 5-1. The ratios of pre-exponential $\boldsymbol{A_m}$ and $\boldsymbol{A_t}$ for F00 samples are largely similar. However, the ratios of $\boldsymbol{A_m}$ and $\boldsymbol{A_t}$ for the F60 samples are slightly different, presumably due to F60 sample in this experiment being in equilibrium with surrounding moisture at day 0. As for parameter $\boldsymbol{B_m}$, there is a clear difference in the time constant associated with the two F00 samples; the time constant for the F00 Day0 sample is larger (529 and 357 respectively). However, parameter $\boldsymbol{B_m}$ is not significant in the decay of F00 samples as the ratio for

mobile charges is only 0.04. The decay of F00 samples largely depend on the value of parameter $\boldsymbol{B_t}$, which are broadly the same in both tables. The values for the time constant $\boldsymbol{B_t}$ for the F60 and F60 Day0 shows a slight difference (1550 and 2640 respectively), while the values of time constant $\boldsymbol{B_m}$ are largely similar. In theory, the values of parameter $\boldsymbol{B_m}$ and $\boldsymbol{B_t}$ should be broadly the same between F00 and F00 Day 0, also between F60 and F60 Day 0 since the physicochemical state between these pairs should be the same. The difference in the time constant values can be attributed to the inconsistency in measurement technique, or alternatively because of environmental influences. As mentioned earlier, the surface decay performance is highly influenced by environmental factors.

Nevertheless, from the surface current measurement and potential decay results, it is obvious that the absorbed moisture in fluorinated samples has significant influences on both current value and decay rate. One underlying explanation for this observation is in the differences in the mobility of water molecules attached to each surface. From a similar study by Law et al. [173], they stated that the presence of water molecules by themselves is not enough to produce a change in surface conductance, but there had to be sufficient water for the molecules to be mobile and, hence increase the conductivity value from translational motion. In the case of the non-fluorinated surface layer, the slow decay process only happened dominantly due to ions present on the surface. Although there is a small amount of absorbed water on the surface, it is not enough for the water molecules to be mobile. Unless the surface is completely covered with water molecules, the molecules are rather strongly bound to the surface by interaction with the solid. Meanwhile, as the surface is sufficiently covered with water molecules, (as believed to be the case in the fluorinated samples) the water molecules may become mobile. Therefore, not only the number of ions, but also their average mobility will increase with the amount of absorbed water. Hence, the fast decay rate for surface-fluorinated epoxy sample before the drying process due to moisture assisted charge movement. After the drying process, it is believed that the surface is no longer sufficiently covered with water molecules, and, therefore, the mobility of the charges is severely restricted. Hence the slow decay rate similar to non-fluorinated sample.

6.3 NITROGEN-DRIED TEST

Drying the sample in a vacuum-oven at a temperature of 105 °C for 24 hours is an extreme measure to remove the moisture from the surface. A significant weight loss up to 0.71 % was recorded within 24 hours of drying. Surface moisture loss of this extent is unlikely to happen in normal operating GIS. The water content in a GIS system, according to BS 60376, should be less than 200 ppm by volume, which is about 0.02 %. For comparison, the average atmospheric water content is about 5000 ppm (0.5 %), subject to changes from one place to another and from one season to the next [174]. So, to emulate the real GIS, the samples were dried in insulating gas instead of vacuum-oven. The insulation gas that was used for this test was dry nitrogen gas. To test the moisture effect for samples dried in nitrogen gas, the same set of procedures was repeated as before. Instead of using vacuum-oven at 105 °C, this time, the samples were dried in a nitrogen gas chamber at room temperature for 24 hours. However, the equilibrium concentration of water in the epoxy samples in contact with dry nitrogen gas was not recorded in this experiment. The compressed nitrogen tank used in this experiment has moisture content of less than 5 ppm. The nitrogen-dried samples were weighed, and measurements of DC current as well as surface decay rate were taken before and after the drying process.

	Weight before drying	**Weight after drying**	**Percentage weight loss**
F00	0.4224 ± 0.0026 g	0.4220 ± 0.0019 g	0.12 %
F60	0.4355 ± 0.0004 g	0.4346 ± 0.0015 g	0.21 %

Table 6-5: Samples weight before and after nitrogen-drying for DC current test. The moisture weight loss from nitrogen-drying is less the weight loss from vacuum-oven-drying

The weight of the epoxy samples before and after the drying process inside the nitrogen gas chamber is shown in Table 6-5. Additional weight loss would have been expected if the samples were dried for a longer period. In this measurement, the drying was stop after 24

hours. Figure 6-4 shows the plots of surface DC current measurements for the corresponding epoxy resin samples.

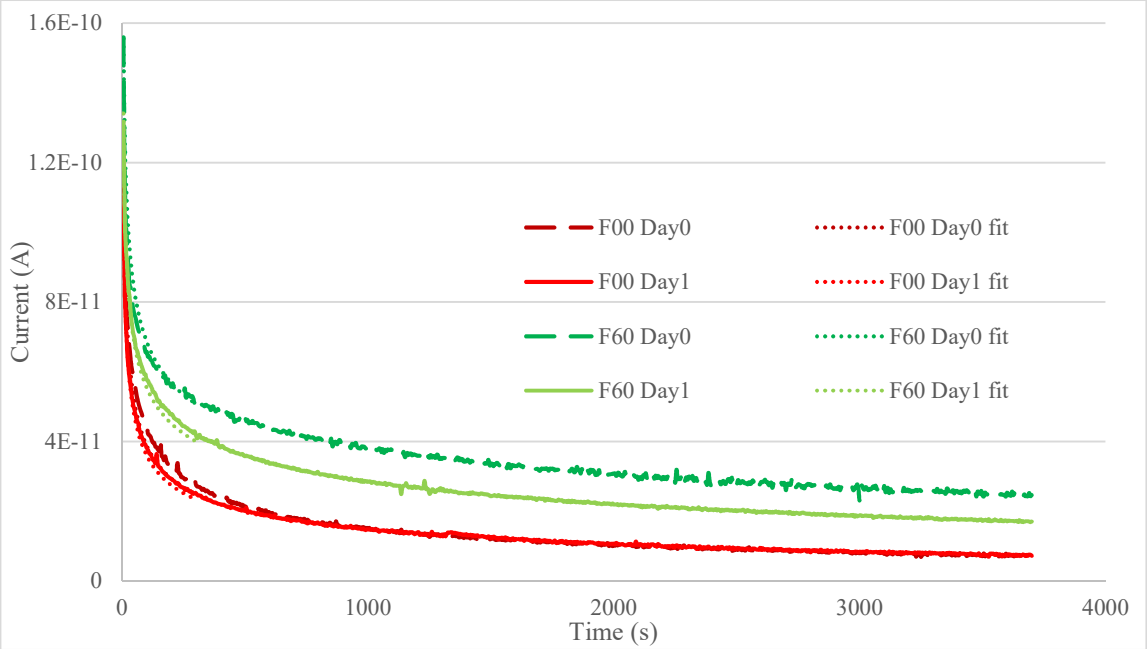

Figure 6-4: Plot of current against time for nitrogen-dried non-fluorinated (F00) and 60-min-surface-fluorinated (F60) epoxy sample. After 1 day of drying, F60 shows reduced current reading.

By comparing Table 6-1 and Table 6-5, the moisture lost for F60 sample is 0.71 % after vacuum-oven drying, while the moisture lost after nitrogen-drying is only 0.21 %. The amount of moisture lost through vaporisation in vacuum-oven drying is far greater than the moisture lost through diffusion in dry nitrogen gas tank. The huge difference in surface moisture lost correlates to the difference in current reading for F60 day 1 of vacuum-oven-dried sample and nitrogen-dried sample. The higher surface current reading at day 1 of nitrogen-dried F60 sample, is not the result of fluorination layer alone, but, to a large extent, from the remaining surface moisture. The remaining physically-bound absorbed moisture on the surface does increase the mobility of water molecules and, hence, higher surface current reading for nitrogen-dried sample.

For the non-fluorinated sample (F00), the weight loss due to the drying process is 0.12 %. This small weight loss is reflected in the surface current measurement. The nitrogen-dried non-fluorinated sample has a slightly lower current value initially and after 3600 seconds, both samples have the same current reading of 9.23 x 10^{-12} A due to water being absorbed onto the surface during the course of the measurement, which inevitably increased the current reading on the surface. Such observation was not noticeable in the vacuum-oven-dried samples, nor for the nitrogen-dried F60 sample. Comparable result was also obtained by Ollier-Durbault et al. [175] on the surface conductivity measurement done on epoxy resin due to moisture effect at different relative humidity. For the 60-min-fluorinated sample (F60), the weight loss is relatively higher at 0.21 % and shows a significant reduction in surface current reading after the nitrogen-drying process. The final current measurement before drying is 2.44 x 10^{-11} A and the current drops to 1.71 x 10^{-11} A after. Again, it is believed that most of the moisture loss in nitrogen-dried F00 comes from the bulk and has a minimum influence on surface current. As explained earlier, when F00 sample was in equilibrium with ambient moisture, water would uniformly occupy the bulk. As the bulk has far bigger volume than the surface, therefore, most of the moisture lost during drying comes from within the bulk.

Sample	A_s	b_s	C_s
F00 Day0	$2.05 \times 10^{-10} \pm 0.27 \times 10^{-10}$	0.362 ± 0.032	$9.23 \times 10^{-12} \pm 1.84 \times 10^{-12}$
F00 Day1	$1.99 \times 10^{-10} \pm 0.30 \times 10^{-10}$	0.351 ± 0.037	$9.23 \times 10^{-12} \pm 1.88 \times 10^{-12}$
F60 Day0	$2.54 \times 10^{-10} \pm 0.86 \times 10^{-10}$	0.370 ± 0.079	$2.47 \times 10^{-11} \pm 0.09 \times 10^{-11}$
F60 Day1	$2.06 \times 10^{-10} \pm 0.55 \times 10^{-10}$	0.357 ± 0.062	$1.71 \times 10^{-11} \pm 0.06 \times 10^{-11}$

Table 6-6: Parameter A_s, b_s and C_s of curve-fitting on first 300 s data for F00 and F60 epoxy samples dried in nitrogen gas for 24 h at 95 % confidence bounds

As for F60 sample, which has a surface with small water contact angle, more moisture can be absorbed within the surface layer. So, the moisture loss in nitrogen-dried F60 mostly comes from the surface and, therefore, results in the drop in current reading at the end of

the 60 min measurement time. Unlike nitrogen-dried F00 sample, the final current measurement at day 1 of nitrogen-dried F60 didn't increase to the same level as day 0 because more moisture was lost on the surface of nitrogen-dried F60, as compared to the nitrogen-dried F00, and it will take more than 3600 s for the current measurement to return to its original value in day 0. In fact, it is believed that, both nitrogen-dried and vacuum-oven-dried sample, if exposed long enough to ambient moisture, may become saturated and may show the surface current measurement as in day 0. From the curve-fitting parameters in Table 6-6, similar pattern is observed as in Table 6-2, but to a lesser extent. The dried samples in day 1 possess common exponential b_s values when compared to un-dried samples in day 0 (0.362 and 0.351 for F00, 0.370 and 0.357 for F60), while the value for parameters A_s show clear reduction. The common value of exponential $\boldsymbol{b_s}$ suggests that the polarisation mechanism during transient current phase remain the same, before and after the drying process. Nonetheless, the removal of absorbed moisture from the surface would surely reduce the moisture-assisted charge injection [176] and, hence explained the reduced value for parameters A_s after nitrogen-drying for both F00 and F60 samples.

From Figure 6-4, as in the case for the vacuum-dried samples, the surface current plot for day 0 and day 1 samples are observed to be in quasi-equilibrium with ambient humidity after 1000 s. By using the proportion approach, the proportion of reduction of current due to moisture loss from nitrogen-drying can be determined and compared against the reduction of current due to moisture loss from vacuum-oven-drying. At quasi-equilibrium point of 2000 s, the proportion of loss current due to nitrogen-drying in F60 is:

$$\frac{'F60\ Day\ 0' - 'F60\ Day\ 1'}{'F00\ Day\ 0'} = 0.29$$

Likewise, from Figure 6-2, at quasi-equilibrium point of 2000 s, the proportion of loss current due to vacuum-oven-drying in F60 is 0.51. The comparably huge proportion of current loss in vacuum-oven-dried sample, again, indicates a big loss of absorbed surface moisture due to vaporisation in vacuum-oven at high temperature, as compared to the moisture loss due to diffusion in nitrogen-dried gas at room temperature.

With regard to the surface potential decay measurements, Table 6-7 shows the weight of the samples before and after the nitrogen-drying process. Figure 6-5 shows plots of surface potential decay rate for non-fluorinated sample (F00), and 60-min-fluorinated sample (F60). For the non-fluorinated sample (F00), the weight loss due to the drying process is 0.10 % and is reflected in the surface potential decay measurement. There is a minimal reduction in surface potential after the 24-hours-drying-process with the final potential reading at 2.61 kV, up from 2.45 kV the day before. For the 60-min-surface-fluorinated sample (F60), the weight loss is slightly higher at 0.20 %, similarly due to the larger moisture content on the surface and, thus, shows a significant reduction in surface potential decay rate after the drying treatment. The final surface potential reading before drying is 0.47 kV and the potential rises to 0.84 kV after, unlike the slow decay rate for the oven-dried sample. From the fitting parameters in Table 6-8, the un-dried sample of F60 at day 0 has T_r of 0.348 h (20.1 min) while the dried F60 sample at day 1 has T_r of 0.684 h (41.0 min).

	Weight before drying	**Weight after drying**	**Percentage weight loss**
F00	0.4235 $\pm$ 0.0046 g	0.4231 $\pm$ 0.0051 g	0.10 %
F60	0.4439 $\pm$ 0.0014 g	0.4430 $\pm$ 0.0011 g	0.20 %

Table 6-7: Samples weight before and after nitrogen-drying for potential decay test. The moisture weight loss from nitrogen-drying is less than the weight loss from vacuum-oven-drying.

When comparing the parameters in Table 6-8 with the parameters in Table 6-4, the parameters for F00 samples are broadly similar. A notable difference can be seen in the parameters of F60 day 1. For the nitrogen-dried F60 sample, the ratio of pre-exponential value $\boldsymbol{A_m}$ is remarkably higher than the vacuum-oven-dried sample, indicating an increase in the number of mobile charge due to the remaining absorbed moisture on the surface. Likewise, the ratio of pre-exponential value $\boldsymbol{A_t}$ is lower in nitrogen-dried sample due to the decrease in number of trapped charges. Both time constants $\boldsymbol{B_m}$ and $\boldsymbol{B_t}$ are higher in nitrogen-dried sample, which ultimately result in faster relaxation time, $\boldsymbol{T_r}$, of 0.684 h as

opposed to 20.1 h for vacuum-oven-dried sample. The increase in time constant value of nitrogen-dried sample at day 1 does not signify that the average trapping level is deeper since there is no alteration to the physicochemical state of the sample. The remaining physically-bound absorbed moisture on the surface does increase the mobility of water molecules and, hence, faster decay.

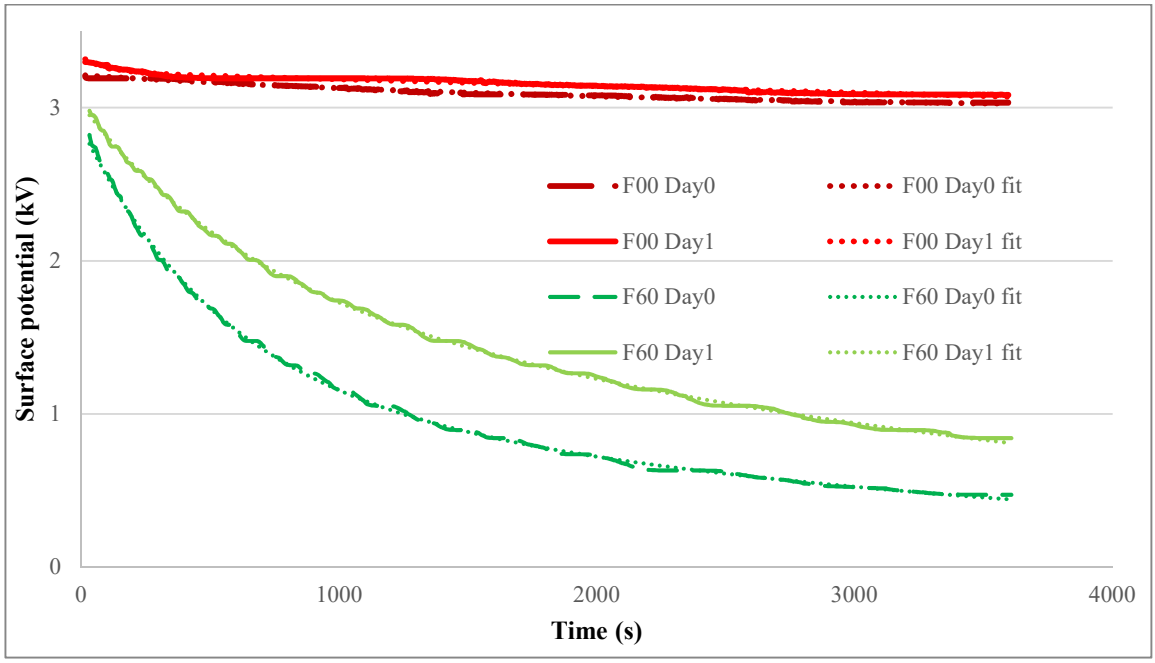

Figure 6-5: Potential decay rate for nitrogen-dried non-fluorinated (F00) and 60-min-surface-fluorinated (F60) epoxy sample. After 1 day of drying, F60 shows slower decay performance, but not to the level of F00.

By comparing the results of the nitrogen-dried sample and oven-dried sample, it is obvious that the nitrogen-dried sample shows different dielectric properties evidenced through the DC surface current and potential decay test. It is believed that most of the physically-bound moisture on the surface of the oven-dried sample were vaporised when dried at 105 °C for 24 hours. It is interesting to note from Table 6-1, Table 6-3, Table 6-5, and Table 6-7, the loss of mass due to water vaporisation are larger in the fluorinated samples, indicating good wettability value and small water contact angle on the surface of fluorinated epoxy samples [110]. It is well known that the contact angle of a water droplet on the surface of a solid

indicates the degree of wetting of the solid. If the contact angle, Ψ > 90°, the solid is non-hydrophilic, while if Ψ < 90°, the solid is easily wetted and the attraction of the water molecule by the solid surface is very strong. The wettability of a material is determined by the chemical structure on the surface, as well as the surface roughness [117]. An increase in surface roughness will make the contact angle of a water droplet reduced for a hydrophilic surface and increased for a hydrophobic surface. As evident from the SEM morphology images in Chapter 4, the surface-fluorination treatment does increase the surface roughness of the treated samples, and, therefore, reduced the water contact angle on the surface. The small water contact angle for fluorinated epoxy samples is also attributed to the introduction of polar groups of -CHF-, as well as the chain scission process that introduced a highly polar group inside the fluorinated layer [114].

Sample	A_m	$\frac{A_m}{(A_m + A_t)}$	A_t	$\frac{A_t}{(A_m + A_t)}$	B_m	B_t	T_r
F00 Day0	0.102 ± 0.009	0.03 ± 0.01	3.20 ± 0.10	0.97 ± 0.06	476 ± 86	91700 ± 2000	26.4 h
F00 Day1	0.116 ± 0.011	0.04 ± 0.01	3.13 ± 0.09	0.96 ± 0.06	498 ± 90	102000 ± 2000	27.7 h
F60 Day0	1.19 ± 0.11	0.40 ± 0.05	1.79 ± 0.07	0.60 ± 0.06	188 ± 30	2550 ± 60	0.348 h
F60 Day1	0.894 ± 0.081	0.28 ± 0.04	2.33 ± 0.08	0.72 ± 0.06	214 ± 34	3270 ± 80	0.684 h

Table 6-8: Parameter A_m, A_t, ratios, B_m, B_t and T_r of curve-fitting result for F00 and F60 epoxy samples dried in nitrogen gas for 24 h at 95 % confidence bounds

The absorbed water on the surface does contribute to a higher surface current value due to the mobility of hydrogen and hydroxyl ions [177]. Accordingly, the loss of moisture on the surface hugely affects the DC current value and the corresponding decay rates. As can be seen in Figure 6-3, the decay rate of the oven-dried F60 sample is as low as the decay rate of the non-fluorinated sample. Without the influence of absorbed moisture on the surface,

the deposited charges will remain on the surface for an extended period. Therefore, the oven-dried 60-min-fluorinated sample is only as good as the original sample in decay rate performance. The results obtained in this study is consistent with the report from Kawasaki that stated the surface current increases with the number of absorbed water molecule on the surface [178].

When the samples were dried in a mild environment inside dry nitrogen gas at room temperature, only a small fraction of the absorbed surface moisture is lost, unlike the extreme case of drying at 105 °C inside vacuum-oven. Objectively, one day of drying inside an encapsulated case is still very far away from the working condition of a real GIS, in which the epoxy spacer would be exposed to dry SF_6 gas for a full four year of a typical maintenance cycle. Nevertheless, for a short drying period of 1 day, the difference in the effect of absorbed surface moisture is clear from the surface potential decay measurement in Figure 6-3 and Figure 6-5. When only a fraction of the absorbed moisture is gone from the surface, the nitrogen-dried F60 sample can still retain its decay shape and decays just a bit slower from the previous day, with T_r of 20.1 min at day 0 and 41.0 min at day 1. Again, it has been made evident that the role of absorbed moisture has far outweighed the role of physicochemical change as a direct result from the fluorination treatment. The presence of absorbed water is considered to be the limiting factor towards the improvement of the dielectric properties in the treated material.

6.4 DECAY WITH EXTENDED DRYING TIME

So far, the moisture effect was only tested on the non-fluorinated (F00) and 60-min-surface fluorinated (F60) epoxy resin sample with the drying time duration of 24 hours. Subsequently, the 120-min-surface-fluorinated (F120) and 180-min-surface-fluorinated (F180) epoxy resin samples were used under the drying duration of up to 7 days. The same set of procedures was repeated as before. The plots in Figure 6-6 and Figure 6-7 show the surface potential decay for F120 and F180 samples dried in nitrogen gas at room temperature while Table 6-9 and Table 6-10 show the fitted parameters including the

relaxation time, T_r for both set of samples. With mild drying condition, before the drying started, both the F120 and F180 samples exhibit fast decay rate, faster than the F60 sample in previous test. After 24 hours of drying inside nitrogen gas, the decay rate started to slow down due to the loss of surface moisture as explained earlier. The decay rate becomes slower with the drying days, but still decays to 1/*e* of initial potential well before 7 min for F120, as can be seen on day 2 and day 3. After seven days of drying in nitrogen gas, the F120 sample can still decay to 1/*e* of initial surface potential but will take nearly 14 min to do so. Meanwhile for F180 sample, the sample decay to 1/*e* of initial surface potential before 2 min for day 0, day 1, day 2, and day 3 while, on day 7, the sample takes about 4 min to reach relaxation. As for the decay time constants of $\boldsymbol{B_m}$ and $\boldsymbol{B_t}$ from Table 6-9 and Table 6-10, an overall increase of these values with drying time implies slower decays for both F120 and F180 samples due to daily removal of absorbed moisture. Again, the increase of time constant values with drying time does not imply that the average trapping level is becoming deeper. Removal of absorbed moisture from the surface does not modify the physicochemical state of the samples. This action simply reduces the mobility of water molecules and, hence, slow decay. The ratio for parameter $\boldsymbol{A_m}$ for F120 and F180 samples can be seen gradually decreasing with the drying days while the ratio for parameter $\boldsymbol{A_t}$ is gradually increasing. This changes implies that the number of mobile charges is decreasing as the surface lose surface moisture while the number of trapped charges increases due to reduction in moisture assisted movement. For comparison, nitrogen-dried F60 sample from Table 6-8 also exhibit the same changes for the pre-exponential ratios within one day of drying, with a lower value of ratio for parameter $\boldsymbol{A_m}$ of 0.40 at day 0.

In short, F120 and F180 decay in a relatively short period even in the mild drying condition of seven days indicating that the value of surface current that controls the decay rate can still be retained in such condition as long as the surface moisture is still present. It is evident that the improvement in the dielectric properties of the fluorinated epoxy samples do not directly come from fluorination surface per se, but the improvement is largely due to the absorbtion of moisture onto the flourinated surface.

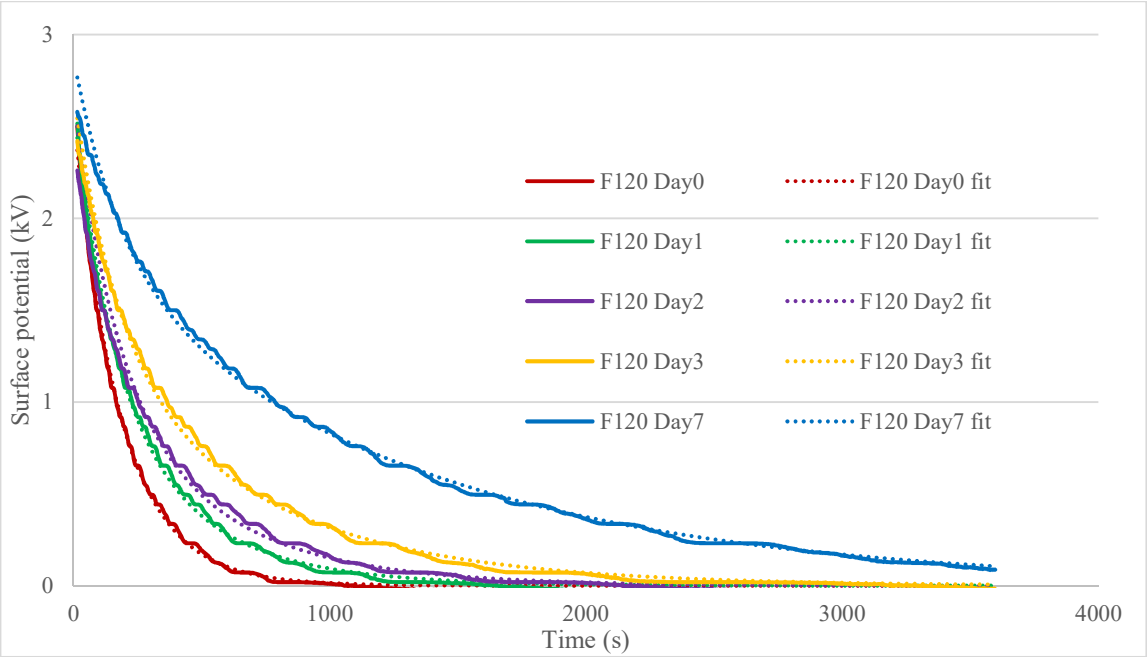

Figure 6-6: Potential decay rate for nitrogen-dried 120-min-surface-fluorinated (F120) epoxy sample and the corresponding fitted lines. F120 exhibits slower decay as the drying day increases.

Sample	A_m	$\frac{A_m}{(A_m + A_t)}$	A_t	$\frac{A_t}{(A_m + A_t)}$	B_m	B_t	T_r
F120 Day0	1.63 ± 0.15	0.63 ± 0.10	0.967 ± 0.033	0.37 ± 0.04	155 ± 4	229 ± 6	0.0517 h
F120 Day1	1.54 ± 0.14	0.59 ± 0.09	1.08 ± 0.03	0.41 ± 0.04	160 ± 4	403 ± 10	0.0680 h
F120 Day2	1.46 ± 0.13	0.54 ± 0.08	1.22 ± 0.03	0.46 ± 0.04	164 ± 3	476 ± 10	0.0886 h
F120 Day3	1.31 ± 0.12	0.48 ± 0.07	1.40 ± 0.05	0.52 ± 0.05	166 ± 4	671 ± 18	0.110 h
F120 Day7	1.06 ± 0.10	0.37 ± 0.05	1.82 ± 0.05	0.63 ± 0.05	180 ± 5	1260 ± 30	0.231 h

Table 6-9: Parameter A_m, A_t, ratios, B_m, B_t and T_r of curve-fitting result for F120 epoxy sample dried in nitrogen gas for 7 days at 95 % confidence bounds

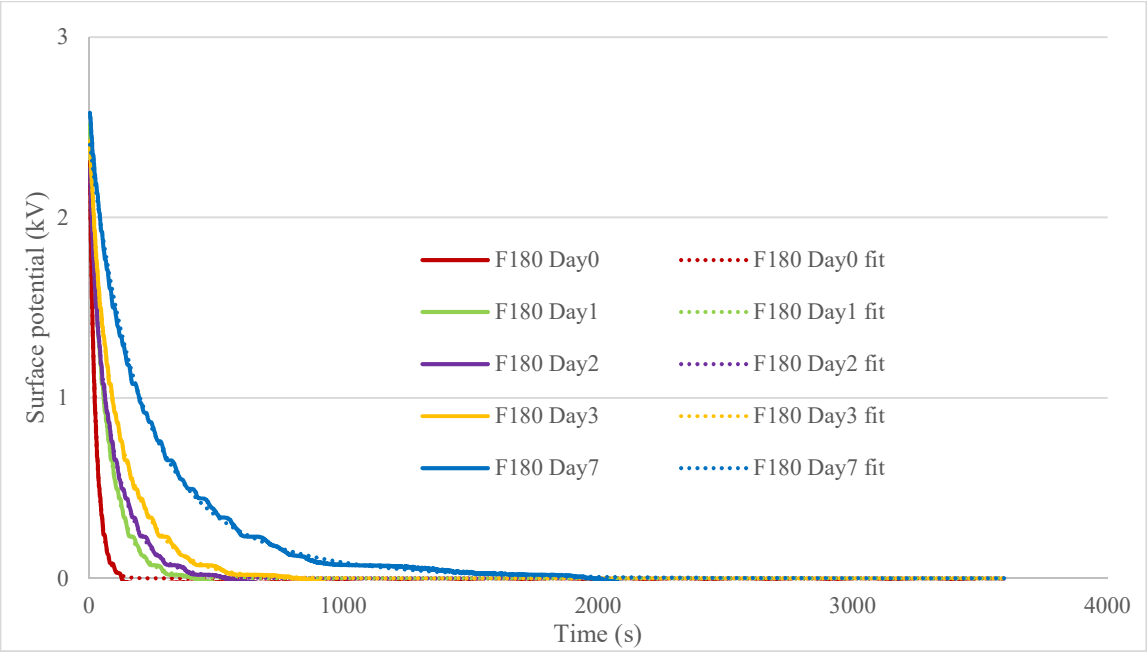

Figure 6-7: Potential decay rate for nitrogen-dried 180-min-surface-fluorinated (F180) epoxy sample and the corresponding fitted lines. F180 exhibits slower decay as the drying day increases.

Sample	A_m	$\frac{A_m}{(A_m + A_t)}$	A_t	$\frac{A_t}{(A_m + A_t)}$	B_m	B_t	T_r
F180 Day0	2.24 ± 0.08	0.95 ± 0.07	0.118 ± 0.004	0.05 ± 0.01	36.1 ± 0.9	111 ± 3	0.0107 h
F180 Day1	2.17 ± 0.05	0.83 ± 0.04	0.436 ± 0.011	0.17 ± 0.01	74.6 ± 1.8	113 ± 3	0.0229 h
F180 Day2	1.85 ± 0.05	0.81 ± 0.04	0.420 ± 0.012	0.19 ± 0.01	101 ± 2	146 ± 3	0.0302 h
F180 Day3	1.83 ± 0.07	0.76 ± 0.06	0.578 ± 0.021	0.24 ± 0.02	122 ± 3	197 ± 5	0.0375 h
F180 Day7	1.53 ± 0.04	0.62 ± 0.03	0.919 ± 0.022	0.38 ± 0.02	158 ± 3	420 ± 6	0.0594 h

Table 6-10: Parameter A_m, A_t, ratios, B_m, B_t and T_r of curve-fitting result for F180 epoxy sample dried in nitrogen gas for 7 days at 95 % confidence bounds

From Figure 6-6 and Figure 6-7, the decay plots show slower decay as the drying day increases. Judging from the plot trends, the decay would have exhibit performance similar to non-fluorinated sample if the drying days is made even longer. By taking the ratios of $\boldsymbol{A_m}$ to $\boldsymbol{A_t}$ for F120 and F180 over the 7 days of drying, the values of $\boldsymbol{A_m}' = \frac{\boldsymbol{A_m}}{(\boldsymbol{A_m}+\boldsymbol{A_t})}$ against drying days are plotted in Figure 6-8. The pre-exponential value of $\boldsymbol{A_m}$ is related to the faster decay process and is highly dependent on the degree of drying. It is observed that the value of $\boldsymbol{A_m}$ decreases as the samples loose absorbed moisture during the drying period.

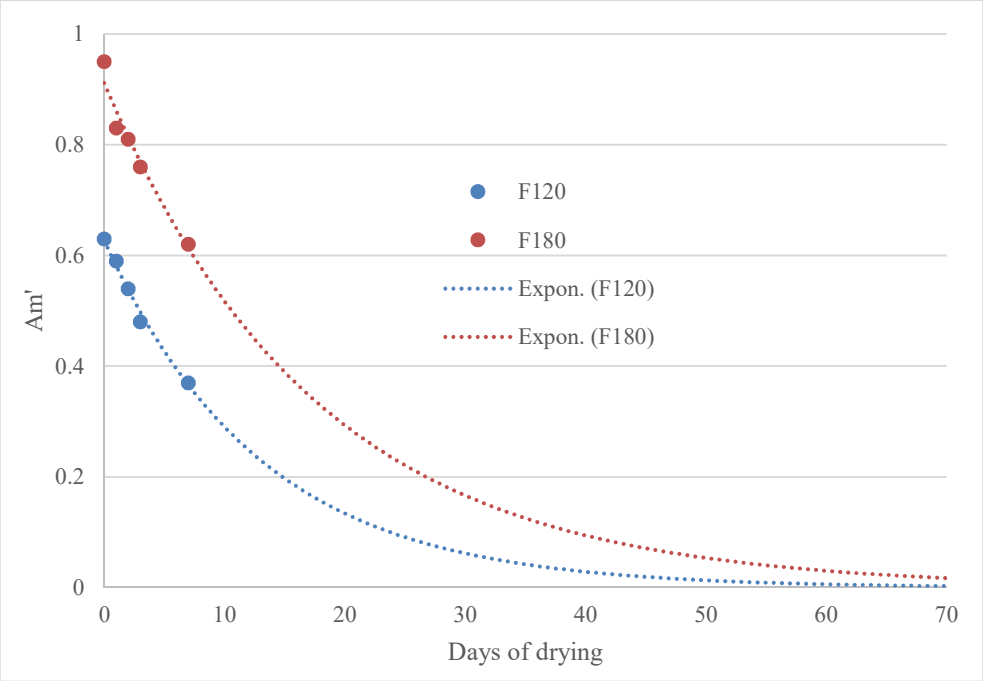

Figure 6-8: The plots of mobile charges ratio against drying days for F120 and F180 samples. Exponential curves were fitted and extrapolated to determine the time taken for pre-exponential parameter $\boldsymbol{A_m}'$ to reach value associated with F00 (~0.04).

Exponential lines were fitted to the data with the assumptions that $A_M{}'$ follows a linear relationship with concentration of water, C_{water} in the surface layer:

$$A_M{}' = \alpha C_{water}$$

and the rate of change of water concentration depends solely on the water concentration:

$$\frac{dC_{water}}{dt} = -\beta C_{water}$$

Thus:

$$C_{water} = C_0 \exp(-\beta t)$$

The water concentration is found to follow an exponential decline. By extrapolating the fitted curve, it can be seen that the ratios $A_M{}'$ under dry nitrogen will reach values associated with a non-fluorinated sample ($A_M{}' \cong 0.04$) in a period of ~40 days for F120 sample and ~60 days for F180 sample. Therefore, it is important to note that these period are alarmingly short considering the fact that fluorinated samples will lose most of its decay properties when the surface has lost its moisture, as evident from vacuum-oven test. Although it is demonstrated that these fluorinated samples still exhibit fast decay performances in extended drying time inside dry nitrogen gas, more work need to be done in order to access the fluorination effect for drying time beyond seven days in dry gas.

Meanwhile, the plots for F240 sample exhibit some degree of decrease in surface potential decay rate as seen in Figure 6-9. Similar observation was also obtained from the work done by Lie et al. [179]. Such observation indicates that the extension of fluorination time is not always favourable to increase the surface current of the epoxy resin insulator, especially for fluorination time beyond a threshold value. As discussed in detailed in Chapter 4, the measured current value on the surface of the fluorinated epoxy samples is governed by the contest in the number of compositional changes and the structural changes i.e. the chemical defects and the physical defects in the fluorinated surface layer [116]. It is believed that for a fluorination time beyond a threshold limit as in the case of F240 sample, the reduction of surface current value, which results in the slow surface potential decay rate, may have been caused by the increase in the number of chemical defects or compositional changes over physical/structural defects. Further modification in physicochemical state on the surface would also lead to alteration in the surface's interaction with water. Nevertheless, the

extension of fluorination time would very likely improve other properties of the epoxy resin insulator surface layer, such as ageing properties, which need to be investigated in the future work. After the mild drying process inside nitrogen gas, the F240 sample exhibits slower decay rate from day 1 to day 7, but at a small margin as compared to the decay rate of day 0, as evident from the decay constants and relaxation times from Table 6-11. From the fitted parameters, the ratio for pre-exponential $\boldsymbol{A_m}$ is slowly decreasing with the drying days indicating reduced number of mobile charges as the sample lose more absorbed moisture from the surface. When compared to nitrogen-dried F120 and F180 samples, the pre-exponential $\boldsymbol{A_m}$ value of nitrogen-dried F240 sample is very small, almost identical to F00 sample. The decline in $\boldsymbol{A_m}$ value with the drying days is also at a smaller margin, suggesting a small number of mobile charges initially due to small moisture absorption capacity of F240 sample. As for the time constants of F240 sample, both parameters $\boldsymbol{B_m}$ and $\boldsymbol{B_t}$ show gradual increase with drying days due to daily removal of absorbed moisture. The increase of time constant values does not suggest that the average trapping level is increasing. The lost of absorbed moisture from the surface does not change the physicochemical state of the samples. It does, however, reduce the mobility of water molecules and, hence, slower decay. When compared against Table 6-9 and Table 6-10, the exponential values of $\boldsymbol{B_m}$ and $\boldsymbol{B_t}$ for F240 sample are relatively bigger, signifying longer decay time for mobile and trapped charges due to the change in average shallow and deep trapping level. As discussed earlier, this physicochemical change may come from the increase in the number of compositional changes over structural defects, which indirectly may alter the surface's interaction with water. Indeed, more work needs to be done to evidently support this claim as there is a very dramatic change in the behaviour of the surface potential decay for F240 sample.

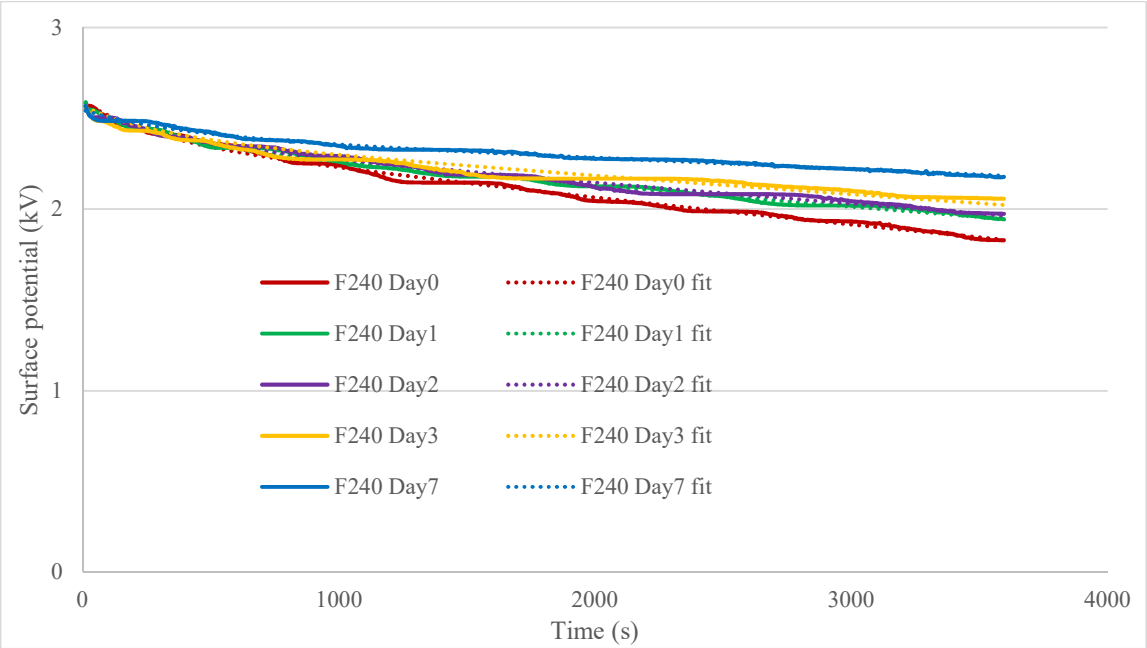

Figure 6-9: Potential decay rate for nitrogen-dried 240-min-surface-fluorinated (F240) epoxy sample and the corresponding fitted lines. F240 exhibits a very dramatic change in decay performance, unlike F120 and F180.

Sample	A_m	$\frac{A_m}{(A_m + A_t)}$	A_t	$\frac{A_t}{(A_m + A_t)}$	B_m	B_t	T_r
F240 Day0	0.194 ± 0.018	0.07 ± 0.01	2.40 ± 0.08	0.93 ± 0.07	282 ± 51	13400 ± 300	3.45 h
F240 Day1	0.190 ± 0.018	0.07 ± 0.01	2.39 ± 0.07	0.93 ± 0.06	294 ± 47	17700 ± 400	4.51 h
F240 Day2	0.164 ± 0.015	0.06 ± 0.01	2.40 ± 0.07	0.94 ± 0.06	299 ± 54	18100 ± 400	4.68 h
F240 Day3	0.160 ± 0.015	0.06 ± 0.01	2.41 ± 0.09	0.94 ± 0.07	316 ± 51	20700 ± 500	5.38 h
F240 Day7	0.134 ± 0.012	0.05 ± 0.01	2.41 ± 0.08	0.95 ± 0.07	377 ± 68	26200 ± 600	9.44 h

Table 6-11: Parameter A_m, A_t, ratios, B_m, B_t and T_r of curve-fitting result for F240 epoxy sample dried in nitrogen gas for 7 days at 95 % confidence bounds

In the case of an extreme drying condition i.e. drying in vacuum-oven, the F120 and F180 samples exhibit decay rates similar to the decay of vacuum-oven-dried F60 sample, while the F240 sample shows a slow decay rate. Figure 6-10 and Figure 6-11 show plots of surface potential decay for F120 and F180 samples dried in vacuum-oven for 7 days at 105 °C and the corresponding curve-fitting parameters are shown in Table 6-12 and Table 6-13. In this extreme drying condition, the F120 and F180 sample can only retain its fast decay rate in day 0 i.e. before the drying process. From day 1 onwards, the surface potential decay rates for F120 and F180 were as flat as the non-fluorinated sample F00 with T_r values above 15 h. Such observation indicates the total loss of surface moisture, that is, in its presence, helps to dissipate the surface charges during the decay process. The result for vacuum-oven-dried F120 and F180 sample is similar to the previous result of the oven-dried F60 sample. In both cases, most of the physically-bound water has dried after 24 hours of drying at 105 °C inside vacuum-oven that result in the slow potential decay. Similar observation can be seen for F240 plot in Figure 6-12 from day 1 onwards, in which the surface potential decay rates were flat, implying the total loss of surface moisture. The the fitting parameters in Table 6-12 to Table 6-14 numerically translates the behaviour of the fluorinated samples respectively as seen from the plots. In each table, only the vacuum-oven-dried parameter values of day 0 are broadly similar to the corresponding values in nitrogen-dried samples. After 1 day of drying in vacuum-oven and onwards, the fluorinated samples exhibit pre-exponential and exponential values broadly similar to those of F00 sample. The increase of exponential values with drying time does not imply that the average trapping level is becoming deeper. Removal of physically-bound absorbed moisture from the surface does not change the physicochemical state of the samples. It does, however, reduce the mobility of water molecules and, hence, slower decay.

For surface-fluorinated epoxy resin, water can readily be absorbed onto the surface layer due to the low water contact angle of the fluorinated surface. The contact angle is lower as the fluorination duration increases (as discussed earlier) which, in turn, introduce more water molecules onto the surface of the epoxy resin. These water molecules are tightly bound to the surface, presumably, through hydrogen bonding with hydroxyl groups in the epoxy structure. With increasing water absorption, more water molecules may reside on the

surface layer. As the surface is sufficiently covered with water molecules (i.e. before drying), the water molecules are mobile and, therefore, increase the surface conductivity. The number of ions as well as their average mobility will increase with the amount of absorbed water, hence the fast decay rate for F120 and F180 epoxy samples before the drying process. After drying, the surface is no longer sufficiently covered with water molecules and, therefore, the mobility of the charges is severely restricted. Hence the slow decay rate similar to non-fluorinated sample. Once again, the direct influence of absorbed moisture is far greater than the influence of physicochemical change on fluorinated samples, which act as the limiting factor towards the improvement of the dielectric properties in the treated material.

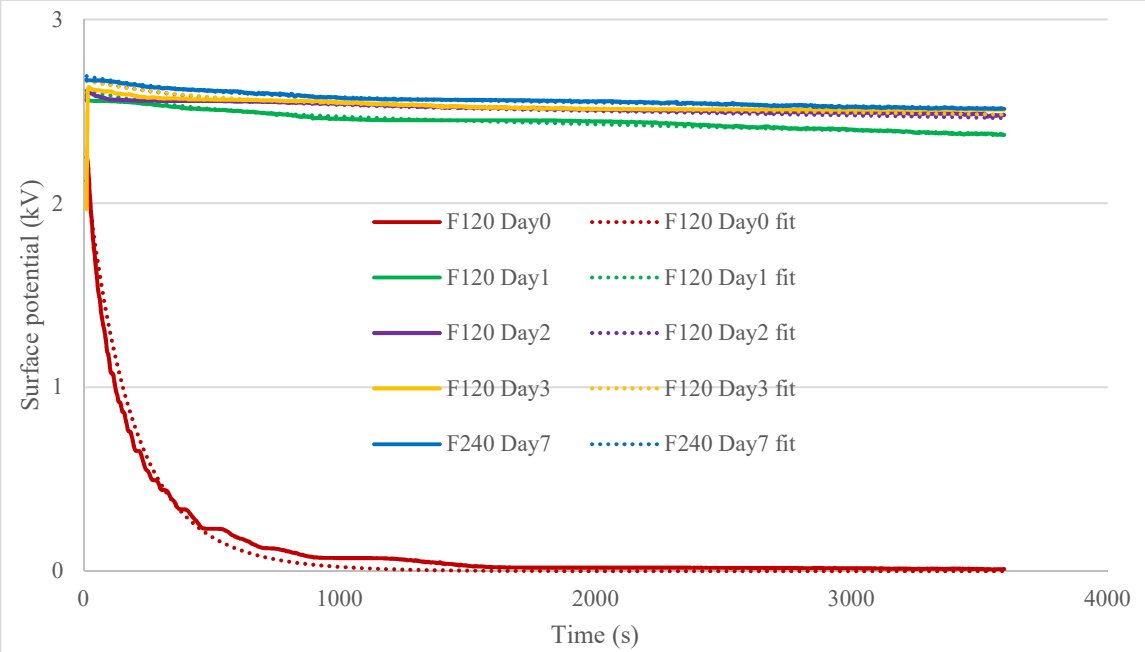

Figure 6-10: Potential decay rate for oven-dried 120-min-surface-fluorinated (F120) epoxy sample and the corresponding fitted lines. F120 exhibits decay performance similar to F00 after 1 day of drying.

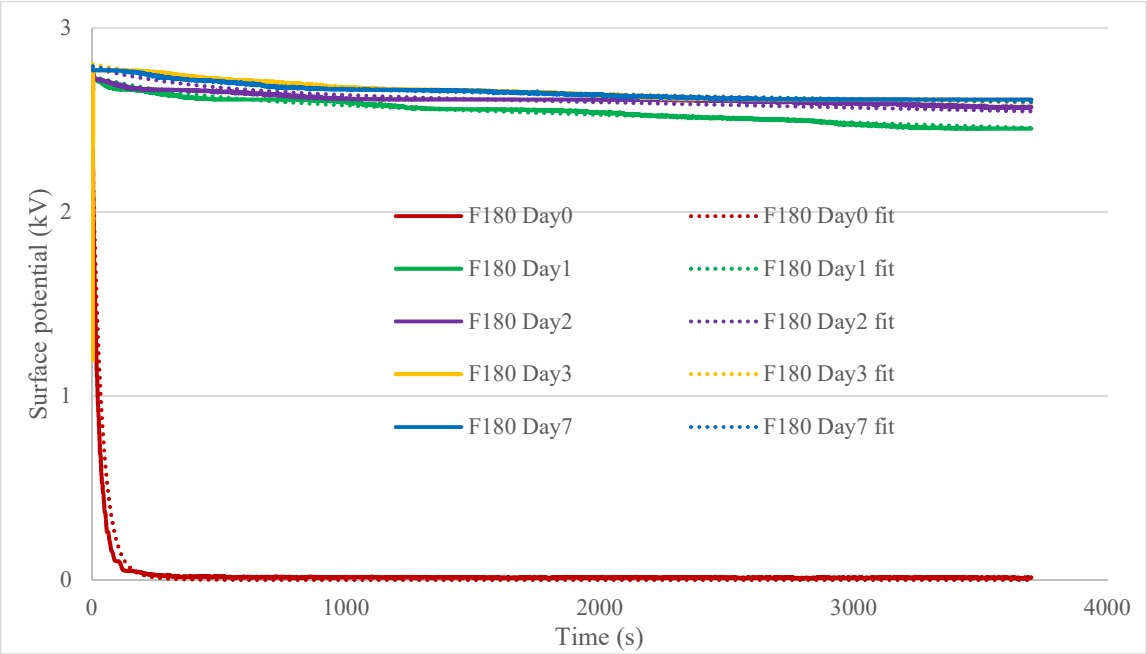

Figure 6-11: Potential decay rate for oven-dried 180-min-surface-fluorinated (F180) epoxy sample and the corresponding fitted lines. F180 exhibits decay performance similar to F00 after 1 day of drying.

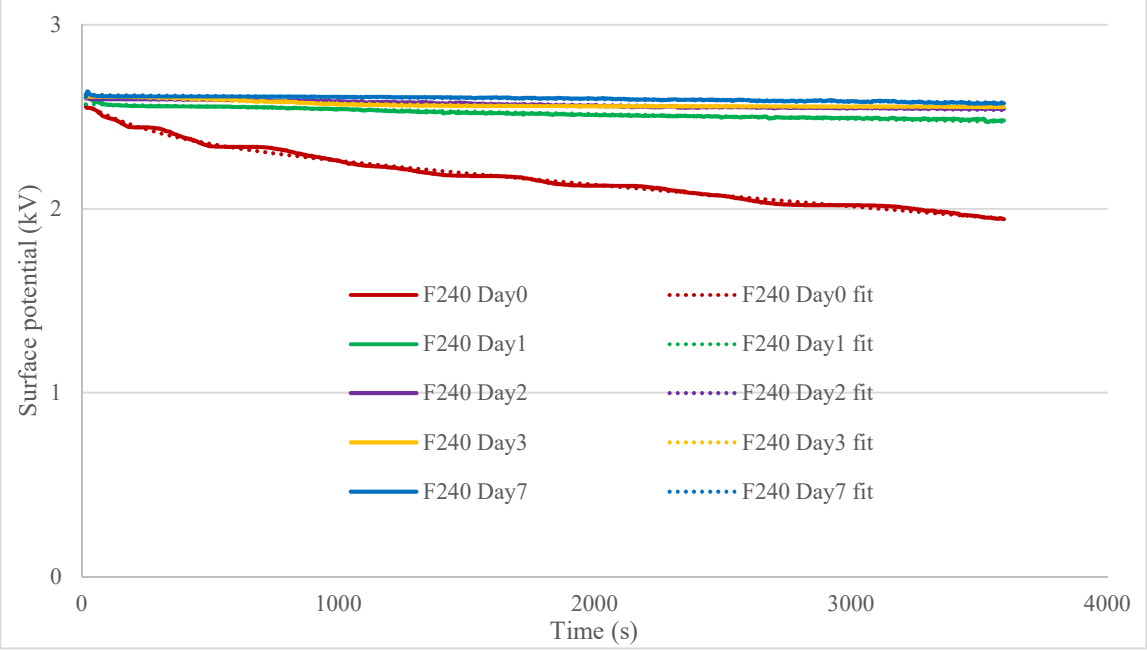

Figure 6-12: Potential decay rate for oven-dried 240-min-surface-fluorinated (F240) epoxy sample and the corresponding fitted lines. F240 exhibits decay performance similar to F00 after 1 day of drying.

Sample	A_m	$\frac{A_m}{(A_m + A_t)}$	A_t	$\frac{A_t}{(A_m + A_t)}$	B_m	B_t	T_r
F120 Day0	1.54 ± 0.14	0.68 ± 0.11	0.726 ± 0.025	0.32 ± 0.03	156 ± 25	284 ± 7	0.0529 h
F120 Day1	0.121 ± 0.014	0.05 ± 0.01	2.50 ± 0.09	0.95 ± 0.07	394 ± 71	73500 ± 2000	19.7 h
F120 Day2	0.128 ± 0.012	0.05 ± 0.01	2.55 ± 0.08	0.95 ± 0.06	402 ± 64	106000 ± 3000	28.8 h
F120 Day3	0.114 ± 0.013	0.04 ± 0.01	2.56 ± 0.07	0.96 ± 0.06	408 ± 74	125000 ± 3000	33.9 h
F120 Day7	0.108 ± 0.010	0.04 ± 0.01	2.59 ± 0.10	0.96 ± 0.08	408 ± 65	130000 ± 3000	34.3 h

Table 6-12: Parameter A_m, A_t, ratios, B_m, B_t and T_r of curve-fitting result for F120 epoxy sample dried in vacuum-oven for 7 days at 95 % confidence bounds

Sample	A_m	$\frac{A_m}{(A_m + A_t)}$	A_t	$\frac{A_t}{(A_m + A_t)}$	B_m	B_t	T_r
F180 Day0	2.32 ± 0.21	0.96 ± 0.17	0.109 ± 0.004	0.04 ± 0.01	36.9 ± 6.7	107 ± 2	0.0110 h
F180 Day1	0.124 ± 0.011	0.05 ± 0.01	2.61 ± 0.10	0.95 ± 0.07	382 ± 69	59900 ± 1000	15.9 h
F180 Day2	0.130 ± 0.012	0.05 ± 0.01	2.65 ± 0.07	0.95 ± 0.05	395 ± 71	88500 ± 2000	23.7 h
F180 Day3	0.107 ± 0.010	0.04 ± 0.01	2.70 ± 0.08	0.96 ± 0.06	403 ± 64	93500 ± 2000	25.2 h
F180 Day7	0.112 ± 0.010	0.04 ± 0.01	2.68 ± 0.09	0.96 ± 0.07	410 ± 67	118000 ± 3000	31.7 h

Table 6-13: Parameter A_m, A_t, ratios, B_m, B_t and T_r of curve-fitting result for F180 epoxy sample dried in vacuum-oven for 7 days at 95 % confidence bounds

Sample	A_m	$\frac{A_m}{(A_m + A_t)}$	A_t	$\frac{A_t}{(A_m + A_t)}$	B_m	B_t	T_r
F240 Day0	0.189 ± 0.017	0.07 ± 0.01	2.39 ± 0.09	0.93 ± 0.07	287 ± 46	17600 ± 400	4.56 h
F240 Day1	0.116 ± 0.011	0.04 ± 0.01	2.55 ± 0.09	0.96 ± 0.07	417 ± 67	107000 ± 2000	29.6 h
F240 Day2	0.106 ± 0.010	0.04 ± 0.01	2.59 ± 0.07	0.96 ± 0.05	452 ± 72	125000 ± 3000	34.4 h
F240 Day3	0.109 ± 0.010	0.04 ± 0.01	2.59 ± 0.09	0.96 ± 0.07	478 ± 87	126000 ± 3000	34.6 h
F240 Day7	0.0962 ± 0.0087	0.04 ± 0.01	2.62 ± 0.08	0.96 ± 0.06	505 ± 91	124000 ± 3000	34.2 h

Table 6-14: Parameter A_m, A_t, ratios, B_m, B_t and T_r of curve-fitting result for F240 epoxy sample dried in vacuum-oven for 7 days at 95 % confidence bounds

When compared against nitrogen-dried sample from Table 6-9 and Table 6-10, the decay time constants of B_m and B_t for F120 and F180 samples in Table 6-12 and Table 6-13 show significant jumps from the values before drying to the values after drying, implying a huge surface moisture loss in the process. Again, it is evident that samples dried inside vacuum-oven at 105 °C experienced massive moisture lost and act similar to F00 sample just within one day of drying. It is worth noting that F120 and F180 samples dried in nitrogen gas would take an estimated ~40 and ~60 days of drying time respectively to possess ratios of A_m similar to F00. From this estimation, the fluorinated samples are projected to lose its added benefits within 40 to 60 days. So, more works need to be done on the application of surface-fluorinated epoxies inside dry gas for extended period.

6.5 CHAPTER SUMMARY

This chapter was designed to look into the effect of surface water absorption on fluorinated epoxy resin samples towards the dielectric properties of the insulating material. The oven-

dried samples show a significance reduction in samples' mass due to vaporisation of surface moisture. The loss of surface moisture on fluorinated samples, which mainly contributes towards the conductivity value, translates into a reduced current reading and a slow surface potential decay rate similar to the decay rates of the original sample.

As for the nitrogen-dried samples, much smaller weight loss was recorded as only a small quantity of surface moisture was diffused into the dry environment of nitrogen gas at room temperature. Due to this fact, the fluorinated sample still shows a reduced DC current reading, but not as significant as the reduction of the oven-dried sample. The same trend is observed for the surface potential decay test. A slower decay rate is recorded after the drying process, but not to the point of the original sample's rate.

It is known that surface fluorination treatment does indeed improve the dielectric properties of the epoxy samples being treated. The surface potential decay rate is significantly faster for the treated sample as its surface conductivity is increased. The incorporation of fluorine element per se through direct-fluorination treatment into the surface layer has had minor influence towards the surface current measurement and the subsequent surface decay performance. The increase in the surface current measurement mostly comes from the fluorinated layer capacity to absorb moisture on the surface. An increase in surface roughness as a consequence from the direct-fluorination treatment reduced the water contact angle and, thus, increased the surface wettability value. As such, in an extreme environment where the absorbed surface moisture is vaporised, the fluorinated samples show current value and decay rate similar to those of original sample. However, in a mild condition, as in insulation gas at room temperature, the fluorinated samples still possess the dielectric improvement supposedly come from the chemical treatment; increased in surface DC current and faster surface potential decay rate. The role of absorbed moisture has far outweighed the role of physicochemical change as a direct result from the fluorination treatment. Indeed, the presence of absorbed water is the limiting factor towards the improvement of the dielectric properties in the treated material. It is also evident that samples dried inside vacuum-oven at 105 °C experienced massive moisture lost and act

similar to F00 sample just within one day of drying. It is worth noting that F120 and F180 samples in nitrogen gas would take an estimated ~40 and ~60 days of drying time respectively to possess ratios of $\boldsymbol{A_m}$ and $\boldsymbol{A_t}$ similar to F00. Although it is evident that these fluorinated samples still exhibit fast decay performances in extended drying time inside dry nitrogen gas, more experimental work need to be done in order to access the fluorination effect for time beyond seven days. As it stands, direct-fluorination treatment on spacers will only improve the performance of GIS operating with dry gas for a short period, as long as the surface moisture can be retained.

CHAPTER SEVEN: DC FLASHOVER

The results from surface decay and PEA measurement clearly show the dielectric improvement in term of dissipating the accumulated charges along the surface of an insulating material. This improvement should lead to an increase in the surface flashover strength as the accumulation of surface charge is one of the critical parameters that influence the surface flashover performance [7]. In general, the surface flashover strength is defined as the limiting voltage stress beyond which the insulation surface can no longer maintain its integrity. In other words, it is the measure of the insulation surface to resist decomposition under voltage stress. The applied voltage causes the top insulation to fail through a surface discharge and rupture the surface insulation. This chapter describes the DC flashover experiment carried out in the high voltage laboratory, from the design issue, simulation work, as well as experimental results and discussions.

7.1 FLASHOVER SYSTEM DESIGN

There are two types of testing methods commonly used in a laboratory work; (i) the constant stress test, in which the time to breakdown is measured at a constant electric field, and (ii) the ramp stress test, in which the electrical field magnitude at the breakdown is measured as the applied electric stress increases as a function of time. In this research, the ramp stress test is preferable because the disparity of results is less than the one in a constant stress test [180]. Additionally, over an extended time in the constant stress test, critical control of the electric field is necessary as small differences in the field can result in a difference in time to breakdown. Although constant stress test is more realistic, the ramp stress test is a better choice in this research as all samples can be forced to fail within a reasonably short time.

In term of electrode geometry, based on ASTM Standard D149-97a, a typical electrode system for surface dielectric testing consists of opposing circular plates of 150 mm

diameter and 10 mm thick with edges rounded to 3 to 5 mm radius (as illustrated in Figure 7-1). The insulating materials for this electrode arrangement are of the cylindrical shape of which the voltage gradient is parallel to the side surface. There are some concerns with regards to the implementation of this electrode arrangement. First of all, there is no control on the position of flashover as the flashover can occur anywhere on the entire side surface of the sample. On top of that, it is a challenge to produce a similar set of samples with the same finish all over the surface of the sample. For these reasons, an alternative flashover system is constructed in a typical surface breakdown arrangement as used by various authors [181-183] in which the breakdown is likely to occur along the sample surface and in between the triple junctions of electrode-epoxy-air as pictured in Figure 7-2. The tips of the electrodes are shaped like a finger with sharp edges as to generate corona effect in order to make sure that the flashover does occur at the tip of the electrodes. With this flashover arrangement, it is easier to produce batches of epoxy samples with consistent surface finish throughout the research. The actual test apparatus is shown in Figure 7-3.

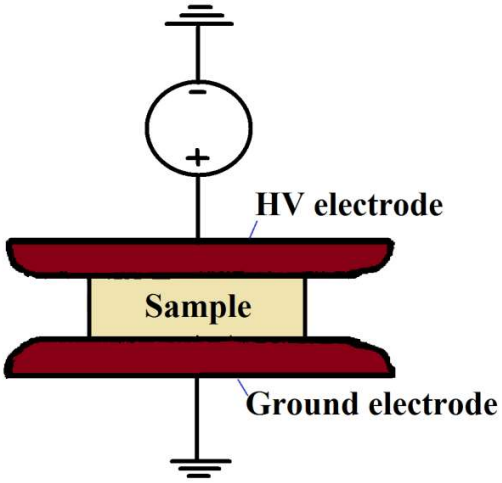

Figure 7-1: Electrode geometry from ASTM standard D149-97a consists of opposing circular plates of 150 mm diameter and 10 mm thick with edges rounded to 3 to 5 mm radius.

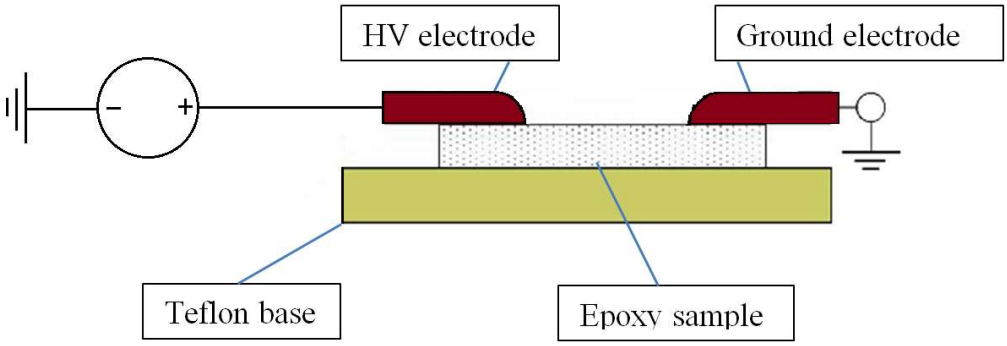

Figure 7-2: A Surface DC flashover kit schematic diagram. The samples were subjected to a linearly increased voltage of 100 V s^{-1} until they underwent flashover.

For a start, the electrodes were made from stainless steel with the edge of the electrodes were rounded to 4.5 mm radius while sockets for banana plug were made at the rear of the electrodes. The body of this system was made from clear Perspex, and the sample base is made from Teflon. The gap between the electrodes is adjustable, but for this experiment, the gap was set to 8 mm. 300 µm thick epoxy resin samples were used, and they were placed between the electrode pair and the Teflon base. A preliminary breakdown test was conducted using this electrode arrangement at atmospheric condition. In this preliminary test, the samples were subjected to a linearly increased voltage of 100 V s^{-1} until they underwent flashover, of which the flashover voltage was recorded. The test was repeated using different epoxy samples for each fluorination conditions. It has been noted that, after a number of flashover occurrences, pitting signs could be seen on the edge of the stainless steel electrodes. Therefore, the electrodes were re-polished after every five flashovers to clear the pitting signs and, hence, give more consistent results. It is worth to note that, the samples used in this breakdown test were left in ambient atmosphere until they were in equilibrium with ambient moisture. During the breakdown test, fresh sample was subjected up to four flashovers, each at different location on both side, in order to eliminate any condition on the sample which could modify the breakdown strength of the samples.

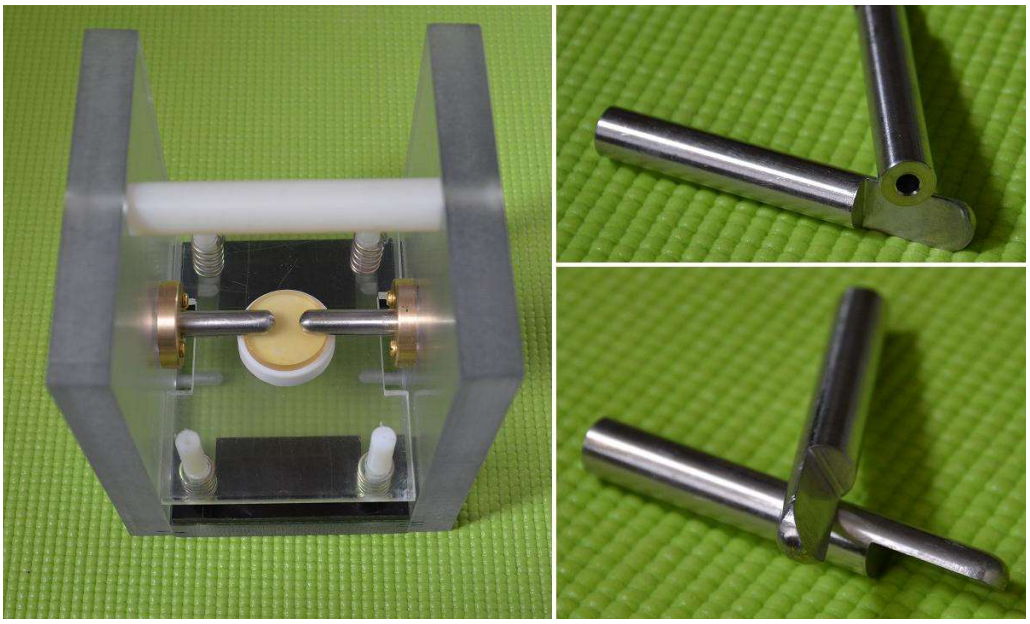

Figure 7-3: Electrode system for surface flashover with 8 mm gap. The steel electrodes were re-polished after every five flashovers to clear the pitting signs and, hence, give more consistent results

7.2 COMSOL MODEL OF ELECTRODES

To get a better understanding on the electrode arrangement, a simulation model using a finite element method was designed to study the potential scale and the corresponding current density distribution. A surface flashover model with finger-like electrodes was developed using COMSOL Multiphysics 3.5. Electrostatics module was selected for this purpose as this module can simulate electrical components and devices that depend on electrostatics, magnetostatics, and electromagnetic quasi-statics applications.

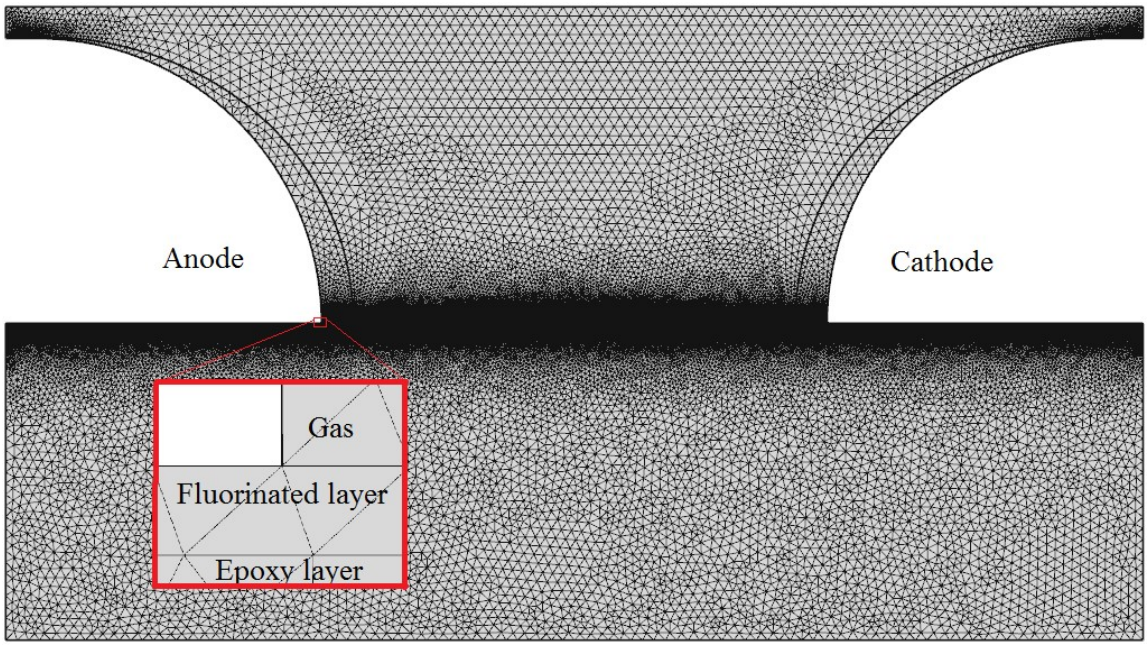

Figure 7-4: An analysis model for surface flashover of fluorinated epoxy using finger electrodes and extremely fine meshes

Figure 7-4 shows the sample with the electrode arrangement geometry and the region for analysis. The distance between the two electrodes was set at 8 mm, as in the actual setup. The settings for boundary mode and subdomain mode are listed in Table 7-1 and Table 7-2. The settings in these tables are designed for fluorination layer of 5 μm thickness. To get the simulation results of different thickness, the thickness, d for the fluorinated layer in subdomain mode is changed accordingly, as well as the thickness of the fluorinated layer in the drawn model. The simulation on the maximum potential on the surface and in the bulk of epoxy samples was performed for each fluorinating conditions. Identifying the influence of each fluorinated surface thickness on the potential distribution and current density will help determine the influence of this surface modification on the dielectric properties of the epoxy resin.

	Equation	Boundary condition	Value
Epoxy resin	n.J = 0	Electric insulation	
Fluorinated layer	n.J = 0	Electric insulation	
Gas (Air)	n.J = 0	Electric insulation	
HV electrode	$V2 = V_0$	Electric potential	50 x 10^3 V
Ground electrode	V2 = 0	Ground	

Table 7-1: Settings for boundary mode. The electric potential of anode is set at 50 kV

	Equation	Thickness, *d*	Conductivity, σ
Epoxy resin	$-\nabla.d(\sigma\nabla V2 - J^e) = dQj$	0.005 m	1 x 10^{-16} S m^{-1}
Fluorinated layer	$-\nabla.d(\sigma\nabla V2 - J^e) = dQj$	5 x 10^{-6} m	1 x 10^{-14} S m^{-1}
Gas (Air)	$-\nabla.d(\sigma\nabla V2 - J^e) = dQj$	1 m	3 x 10^{-17} S m^{-1}

Table 7-2: Settings for subdomain mode. The bulk epoxy, surface fluorinated layer, and surrounding air have different value of conductivity.

7.3 SIMULATION RESULT

To accurately determine the potential scale and current density, an extra fine mesh area was drawn at the edge of both anode and cathode, as well as on the layer of the direct-fluorinated surface. The simulation analysis is done for fluorination thickness of 0 µm, 5 µm and 10 µm. Figure 7-5 to Figure 7-7 show the simulation results for each fluorinated surface thickness of epoxy resin.

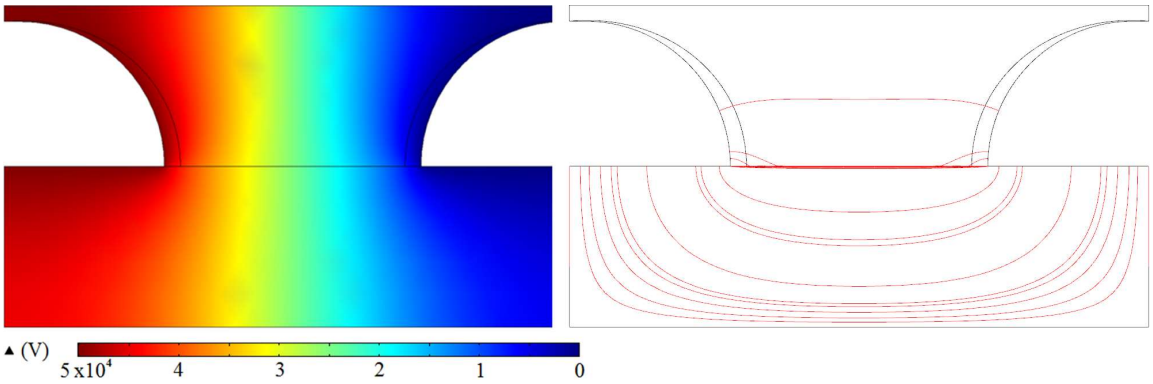

Figure 7-5: Potential scale and current density for 0µm fluorinated thickness. Potential reading at the tip of anode is 49399 V. Concentration of current can be seen evenly distributed.

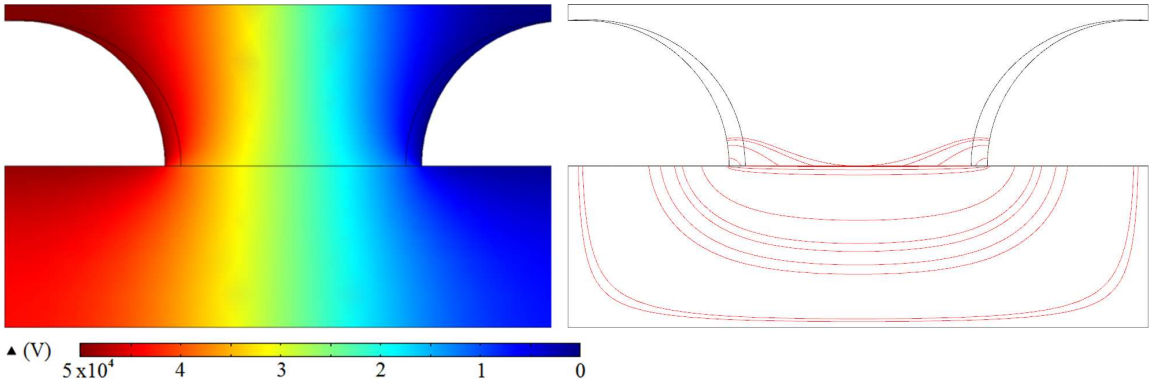

Figure 7-6: Potential scale and current density for 5µm fluorinated thickness. Potential reading at the tip of anode is 44388 V. More concentration of current can be seen on the surface.

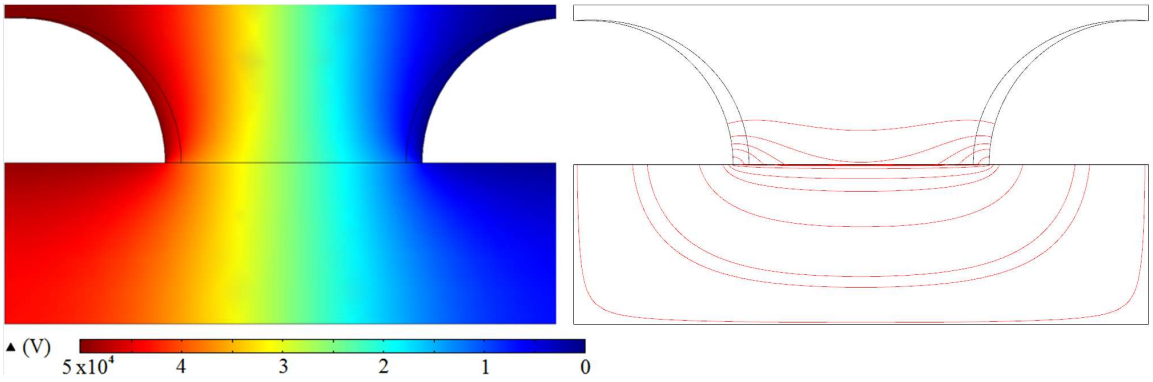

Figure 7-7: Potential scale and current density for 10 µm fluorinated thickness. Potential reading at the tip of anode is 44324 V. Even more concentration of current can be seen on the surface.

From the simulation, the obtained results clearly show the impact of the fluorinated surface layer in defining the outcome of the potential and current density distribution. From the model, at coordinate 0.00598, 0.00198, the position just beneath the tip of anode, the potential readings for 0 μm, 5 μm, and 10 μm fluorinated layer model are 49399 V, 44388 V, and 44324 V respectively. The results clearly indicate a slight reduction in the electric potential inside the bulk of epoxy resin with the fluorinated surface layer as opposed to the non-fluorinated epoxy resin. Likewise, high concentration of current density can be seen on the surface of fluorinated epoxy with the increase in thickness of fluorinated layer due to the fluorinated surface layer possesses higher conductivity than the bulk.

There is, however, one minor issue with this simulation model. The fluorinated surface thickness of 5 and 10 μm used in this simulation is, in fact, thicker than the thickness of the fluorinated layer on an actual sample, which is around a 0.5 μm. This constraint is due to the meshing size limitation of the simulation software. Nevertheless, this constraint however is not significant as this simulation is used for comparison purposes only and this model proves that the surface fluorination treatment did have a big impact on the reduction of potential and on the distribution of current density.

7.4 FLASHOVER IN NITROGEN GAS

In order to mimic the real working GIS, the flashover experiment was repeated inside a chamber filled with insulating gas. Instead of using ambient air as the insulating medium as in the preliminary test, the insulating medium used in this test is dry nitrogen gas at atmospheric pressure. Nitrogen gas is chosen as the insulating gas because it is a low-cost alternative to SF_6. The relative spark breakdown strength of atmospheric air, N_2 and SF_6 are 1.0, 1.15 and 3.0 respectively [184], hence higher flashover voltage of nitrogen gas over atmospheric air. The schematic diagram of this test is shown in Figure 7-8. The previous electrode setup as used in the preliminary test was put inside a glass chamber that was connected to a vacuum pump and nitrogen gas tank. The glass chamber was designed to provide maximum accessibility and visibility for image capturing. A high-speed camera

with the capability of capturing images at maximum 3000 fps was positioned in front of the viewing window of the glass chamber. The camera was focused on the 8 mm gap space between the electrodes. For this experiment, pure tungsten electrodes were used instead of stainless steel since pure tungsten possess the highest melting point (3422 °C), lowest vapour pressure (at temperatures above 1650 °C) and the highest tensile strength [185]. The need to change the electrode frequently because of the pitting formation was not necessary with the use of tungsten electrodes.

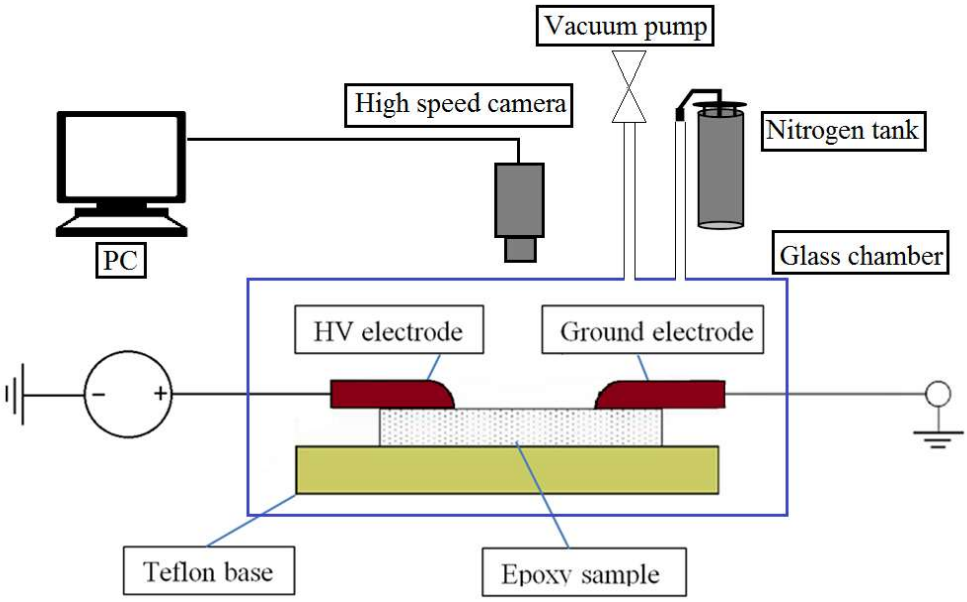

Figure 7-8: A schematic diagram of surface DC flashover kit in nitrogen gas at atmospheric condition. The chamber was vacuumed and nitrogen gas was then pumped in through a desiccant filter to dry out the nitrogen and to minimise the humidity content inside the chamber.

To start the flashover test, the chamber was vacuumed to 10^{-1} mbar to remove the remaining moisture inside the chamber. Nitrogen gas was then pumped in through a desiccant filter to dry out the nitrogen and to minimise the humidity content inside the chamber.

7.5 EXPERIMENTAL RESULTS AND DISCUSSIONS

Surface charge accumulation, which leads to surface flashover, is believed to be triggered by the field emission that occurs at the sharp edges of the electrodes under DC stress [140]. The charge carriers within the field emitted electrons from protrusions on the rough finish electrodes drift in the direction of the electric field to reach the epoxy resin surface. As explained in Chapter 2, there are three possible mechanisms for surface flashover; (i) a micro-discharge at an imperfect contact at the sample-electrode interface, (ii) a micro-discharge at an imperfection in the epoxy resin sample surface, or (iii) a particle on or near the spacer surface [67]. These effectively act as high-field spots and cause rapid electron emission and ionisation. The generated charges are trapped on the insulator surface and further distort the local electric field and initiate further ionisation processes. These micro-discharges could well develop the flashover path that leads to breakdown along the surface of the epoxy resin.

From the preliminary flashover test, the results of flashover voltages for each fluorination time were plotted using Weibull distribution as shown in Figure 7-9. ReliaSoft Weibull 7++ software was used for this analysis. The maximum likelihood estimation (MLE) was used as the parameter estimator for the breakdown data. The result, in general, shows an increasing trend in DC surface breakdown strength with the introduction of the fluorinated surface layer.

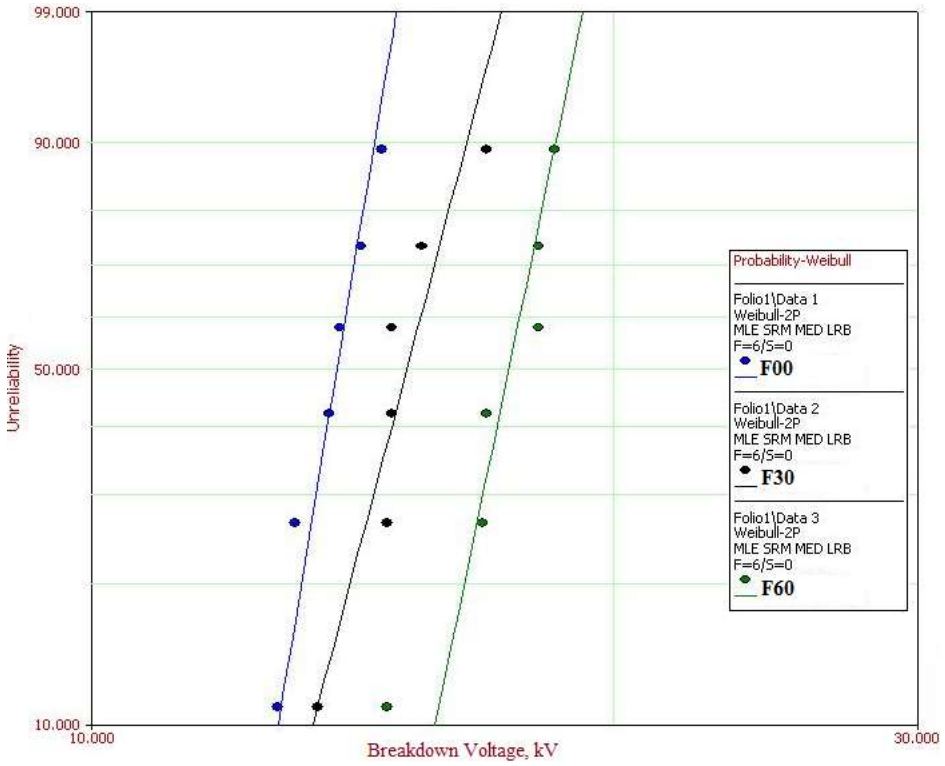

Figure 7-9: Two-parameter Weibull distribution for 300 μm surface-fluorinated epoxy resin samples of different fluorination duration undergoing surface flashover test in ambient air

Sample	Scale parameter (kV), α	Shape parameter, β
F00	14.1 ± 0.5	24.0 ± 11.1
F30	15.6 ± 0.9	15.1 ± 6.7
F60	17.7 ± 0.8	19.2 ± 9.5

Table 7-3: Weibull parameters α and β for 300 μm surface-fluorinated epoxy resin samples of different fluorination duration undergoing surface flashover test in ambient air

For non-fluorinated epoxy resin sample, low surface breakdown strength with a high shape parameter is observed. The direct-fluorinated samples show a clear improvement in surface breakdown strength with lower shape parameter. The increasing trend of surface breakdown strength as the fluorination duration increases can be explained by the introduction of the fluorinated layer. With the introduction of fluorinated substituent onto

the surface of the epoxy resin sample, the conductivity along the dielectric surface increases, as measured in DC surface current test. This increment is getting more significant with prolonged time of fluorination treatment. Interestingly, the improvement in surface conductivity enables trapped charges on the surface to leak away faster and, therefore, limits the surface charge accumulation from distorting the local electric field [186]. This observation explains the increasing trend in DC surface flashover voltage with fluorination time. As can be seen from PEA measurement in Chapter 5, fluorination treatment is also believed to introduce more traps on the surface layer. The charges that are trapped may block or shield further charge injection [43]. When further charge injection from the electrode is blocked, it will limit the number of charges accumulated along the surface and, hence, reduces their effect in enhancing the local electric field of the epoxy resin. The longer fluorination treatments of 30 and 60 min may result in more charge injection being blocked by the fluorinated layer. Consequently, it will reduce charge transport into the surface layer and, therefore, suppress space charge accumulation along the surface of epoxy resin under prolonged DC stress.

Since a minimum voltage is anticipated below which breakdown is expected not to occur, a three-parameter Weibull estimate is carried out using the same ReliaSoft Weibull 7++ software. This software uses MLE method to calculate the value of the three Weibull parameters. However, this approach is problematic in three-parameter estimation for a few reasons. Weibull distribution itself does not satisfy the regulatory conditions for MLE method to be efficient [187]. This is because the domain for random variables depends on the value of shift parameter, γ. As revealed in [188], when $\beta \leq 1$, MLE method is regarded as not consistent as there may be more than one solution. When $1 \leq \beta \leq 2$, the distribution of the estimates does not follow a normal distribution. Only when $\beta \geq 2$, the weak regularity conditions are met, and the MLE method is deem effective. It is also known that the MLE approach is biased and strongly depends on the shape parameter β and sample size n [189]. A review of some bias correction procedures are found to be based on two-parameter Weibull only and do not generalise to three-parameter Weibull distribution [190].

Due to the limitation in MLE method, this software only returns realistic estimations for breakdown distributions of F00 and F30. In the case of F60, however, the estimation for the Weibull parameter is unrealistic due the reasons stated earlier. One way to overcome this problem is by adapting a hybrid approach [191]; using the Least Squares method [192] to estimate the shift parameter, γ. Then, for consistency reason, MLE method was used to estimate the scale and shape parameters. Furthermore, MLE uses more of the information in the data, especially when there are only a few failures and the estimates are generally more precise [193, 194]. To implement this hybrid approach, a custom Weibull fitting function in MATLAB was adopted. The estimates for three-parameters Weibull for the preliminary breakdown test distribution were listed in Table 7-4.

Sample	Scale parameter (kV), α	Shape parameter, β	Shift parameter (kV), γ
F00	2.0 ± 0.3	3.0 ± 1.0	12.0
F30	3.1 ± 0.5	3.0 ± 0.9	12.3
F60	6.6 ± 0.4	6.5 ± 2.3	11.1

Table 7-4: Weibull parameters α, β, and γ for 300 μm surface-fluorinated epoxy resin samples of different fluorination duration undergoing surface flashover test in ambient air, estimated using hybrid approach; LSE and MLE with 95 % confidence bounds.

From the Weibull estimation using the hybrid approach in Table 7-4, the scale parameter, α, can be seen increasing with fluorination level. This observation implies that the surface breakdown strength increases with fluorination time. These α values of three-parameter Weibull estimation are comparably small when compared against the α values from the two-parameter estimates. Similarly, the values for shape parameter, β, of three-parameter Weibull estimation are relatively small. Such observation is due to the introduction of a new shift parameter, γ, in the Weibull distribution equation, which literally shift the probability density function (PDF) of the data by γ amount. While F60 sample shows the lowest value of shift parameter γ, it does not simply imply that the breakdown strength of F60 is the lowest. Rather, this is due to the way the F60 breakdown data is distributed. It is also noted that F60 sample has the highest value of parameter α and β.

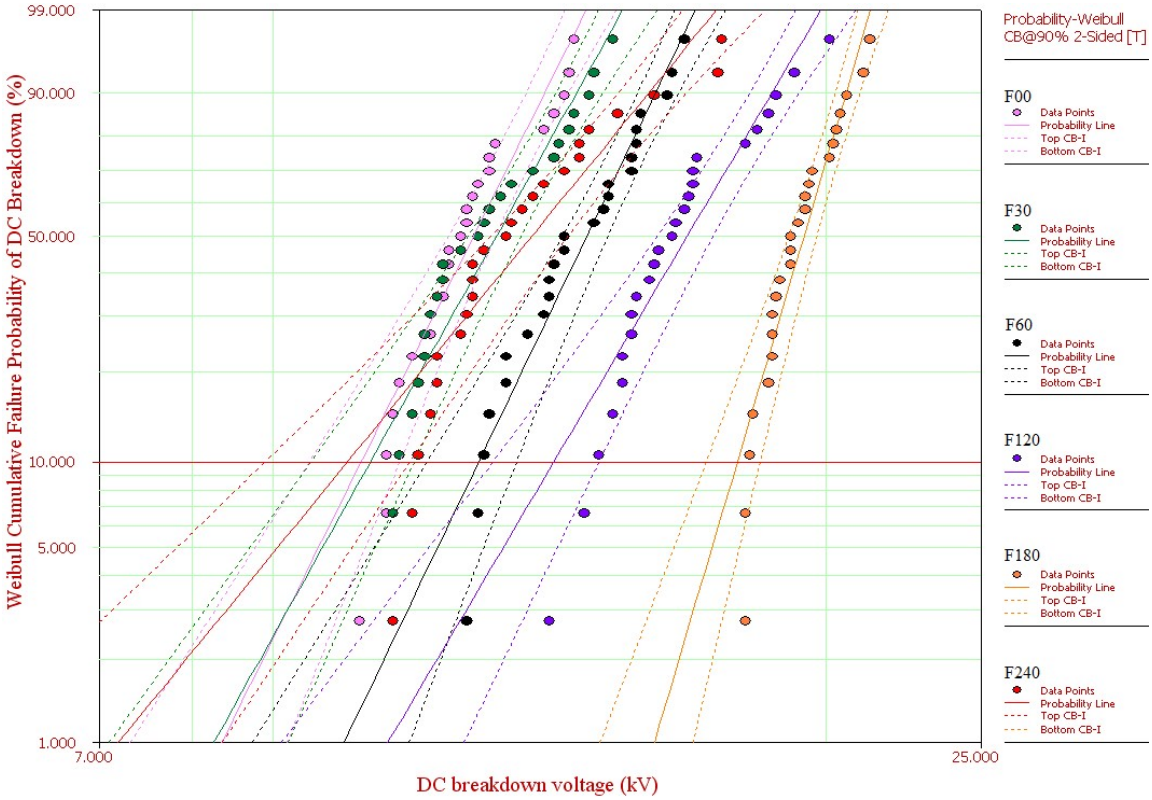

Figure 7-10: Weibull distribution with two-sided 90 % confidence bounds for 300 µm epoxy resin samples of different fluorination time undergoing surface flashover test in nitrogen gas.

Sample	Scale parameter (kV), α	Shape parameter, β
F00	12.4 ± 0.4	11.6 ± 2.9
F30	12.9 ± 0.5	10.4 ± 2.7
F60	14.6 ± 0.5	12.1 ± 3.2
F120	17.0 ± 0.7	9.8 ± 2.4
F180	19.7 ± 0.4	19.6 ± 4.9
F240	13.8 ± 0.8	7.09 ± 1.7

Table 7-5: Weibull parameters α and β for 300 µm epoxy resin samples of different fluorination time undergoing surface flashover test in nitrogen gas.

In the case of flashover in dried nitrogen gas, the flashover performance of the epoxy resin samples can also be described using Weibull distribution analysis. Assuming that the

random breakdown process follows the Weibull distribution, the graph of failure probability was plotted against the breakdown voltage, where failure probability indicates the likelihood of the breakdown occurrence in an applied field. The two-parameter Weibull distribution and parameters are shown in Figure 7-10 and Table 7-5. Since a minimum breakdown voltage is expected, a three-parameter Weibull estimation was also performed using the hybrid approach and the result is shown in Table 7-6. In a simple term, the scale parameter, α, represents the breakdown strength and the shape parameter, β, represents a measure of the spread and skewness of the breakdown data. The shift parameter, γ, represents the minimum voltage below which breakdown cannot occur. In general, both two-parameter and three-parameter estimates show an increasing trend in DC surface breakdown strength with the introduction of the fluorinated surface layer. The shift parameter, γ, is increasing with the increase in fluorination level except in the case of sample F240. However, there is no obvious trend seen for scale and shape parameters from the three-parameter Weibull estimates.

Sample	Scale parameter (kV), α	Shape parameter, β	Shift parameter (kV), γ
F00	2.3 $\pm$ 0.2	2.1 $\pm$ 0.3	9.9
F30	1.8 $\pm$ 0.3	1.3 $\pm$ 0.2	10.6
F60	2.7 $\pm$ 0.3	1.9 $\pm$ 0.3	11.6
F120	3.9 $\pm$ 0.4	2.3 $\pm$ 0.4	12.7
F180	2.0 $\pm$ 0.2	1.8 $\pm$ 0.3	17.5
F240	2.7 $\pm$ 0.4	1.4 $\pm$ 0.2	10.5

Table 7-6 Weibull parameters α, β and γ for 300 μm surface-fluorinated epoxy resin samples of different fluorination duration undergoing surface flashover test in nitrogen gas estimated using hybrid approach; LSE and MLE.

From the two-parameter estimates in Table 7-5, surface breakdown strength of a scale parameter 12.40 kV is observed for F00. The DC surface breakdown voltage increases as the fluorination time increases. The increase in breakdown voltage is marginal for F30 sample. The highest scale parameter value (from two-parameter Weibull estimates) is

recorded for F180 sample with value as high as 19.72 kV with shape parameter of 19.60. From the three-parameter estimates in Table 7-6, F180 sample also recorded the highest shift parameter estimates of 17.5 kV. However, for F240 sample, a drop in scale parameter from two-parameter estimates, and shift parameter from three-parameter estimates is observed. This observation correlates to the relaxation time, T_r (time to reach 1/e of initial potential) from the curve fitting results of surface potential decay in Chapters 5 and 6. The relaxation time for each breakdown samples are plotted in Table 7-7. Figure 7-11 shows a plot of scale parameter from two-parameter Weibull estimates against the time constant for each fluorinated samples in order to establish the nature of this correlation.

Sample	Relaxation time, T_r
F00	26.8 $\pm$ 0.4 h
F30	1.05 $\pm$ 0.13 h
F60	0.311 $\pm$ 0.065 h
F120	0.0523 $\pm$ 0.0006 h
F180	0.0109 $\pm$ 0.0002 h
F240	4.02 $\pm$ 0.56 h

Table 7-7: The relaxation time for each breakdown samples from curve fitting results of surface potential decay in Chapter 5 and 6.

From the plot, in general, as the relaxation time decreases with the degree of fluorination, the surface breakdown strength increases. The fastest relaxation time can be observed for the F180 sample with a value of 0.0109 h, i.e. it took F180 sample just 39 s to dissipate the accumulated surface charges to 1/e of its initial surface potential. During the voltage ramping in surface breakdown test, with the ramping rate of 100 V s^{-1}, the breakdown will happen within 2 to 3 min of ramping based on the scale parameter in Table 7-5. In the case of F180 sample, with a relaxation time of only 39 s, such fast relaxation time did have a significant impact on the flashover performance. F180 sample recorded the highest scale parameter of 19.72 kV within the ramping time of 2 to 3 min, hence, the highest surface flashover strength. For the F120 sample, with relaxation time of 3 min, it may take longer

time to dissipate the accumulated surface charges and, hence, its surface flashover strength is just below that of F180.

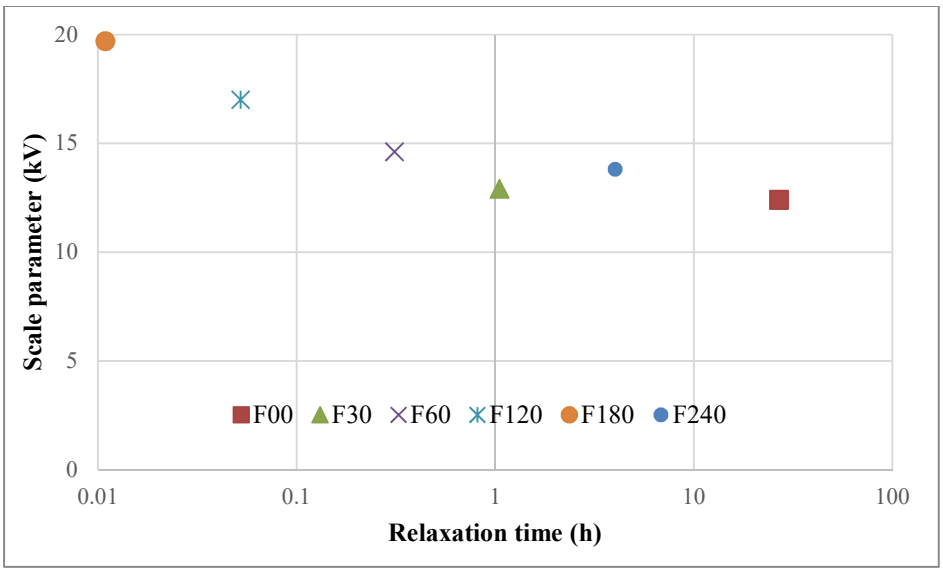

Figure 7-11: The plot of breakdown voltage against the relaxation time for each fluorinated samples in order to establish the nature of this correlation.

With the incorporation of fluorinated substituent onto the surface of epoxy resin samples as confirmed by surface current measurement in Chapter 4, the current reading along the dielectric surface increases with fluorination time [195]. The measured current is higher with longer time duration of fluorination treatment until it reaches a threshold point. Interestingly, the increase in surface conductivity enables trapped surface charges to move away faster and, as a result, suppresses the surface charge accumulation from distorting the local electric field [186]. Hence, the increasing trend in DC surface flashover strength over fluorination time with the highest surface breakdown strength is observed for sample F180. At 180 min of fluorination time, the surface layer is at optimum conductivity value which enables the generated surface charges to move away faster from traps. The increase in surface breakdown strength, which principally comes from the increase in surface conductivity, is largely attributed towards the ability of fluorinated surface to absorb surface moisture due to the increase in surface roughness [176] as explained thoroughly in

Chapter 6. The increase in surface conductivity is also attributed, to a lesser extent, to the increase in physical defects and/or structural changes from the fluorination treatment. These changes consequently introduce shallow traps on the surface which help to make the surface charges to decay faster. The increase in conductivity on the surface facilitates the ionisation process along the surface. The ensuing free surface charges are then accelerated by a high electric field and results in electrical conduction along the surface via avalanche multiplication from ionisation of molecules by ion impact.

However, there is a limit to the increase in the degree of fluorination for which the surface breakdown strength can be enhanced. As evident in sample F240, in which at this point, the insulating surface has become less conductive (as discussed in Chapter 6) presumably from the decrease in wettability ability, as well as the introduction of deep traps on the surface layer. The presence of deep traps on the surface may aid in the accumulation of surface charges and consequently distort the localised electric field. In other words, the fluorination layer on sample F240 contributes towards the formation of breakdown path on the surface layer and effectively lowers the surface breakdown strength of the insulating material, as evidenced by the flashover data.

By comparing the flashover data in nitrogen gas (Figure 7-10) with the preliminary flashover data in ambient air (Figure 7-9), it is important to note the general decrease in the surface breakdown strength of the samples in nitrogen gas. Ironically, the insulating nitrogen gas should, in fact, increase the surface breakdown strength of the samples since nitrogen gas, as an insulating medium, possess higher breakdown strength as discussed earlier. One possible explanation for such behaviour is due to the fact that the nitrogen chamber was vacuumed to 10^{-1} mbar in order to remove the remaining moisture inside the chamber. This action certainly may have caused some of the surface moisture on the sample to be removed as well, and, as a result, lower the surface conductivity values on the samples inside nitrogen gas chamber. This explains the overall high surface breakdown strength of the preliminary flashover data as compared to the flashover inside nitrogen gas. Alternatively, this observation can also be explained by the usage of stainless steel

electrodes in the preliminary flashover test while pure tungsten electrodes were used in the flashover inside nitrogen gas. It is known that pure tungsten has a work function value of 4.55 eV while stainless steel has a higher work function value of 5.05 eV. The work function is the indication of the minimum energy needed to remove an electron from a solid to a point in the vacuum immediately outside the solid surface. Szklarczyk et al. [196] have shown that under DC condition, the breakdown strength increases as the work function of the metal electrode increases. As the electrode's material work function increases, the magnitude of the current density injected onto the surface through high-field electron emission decreases. It is also believed that a greater degree of cathode shielding occurs when larger amounts of charge are injected into the gap as a result of high field emission.

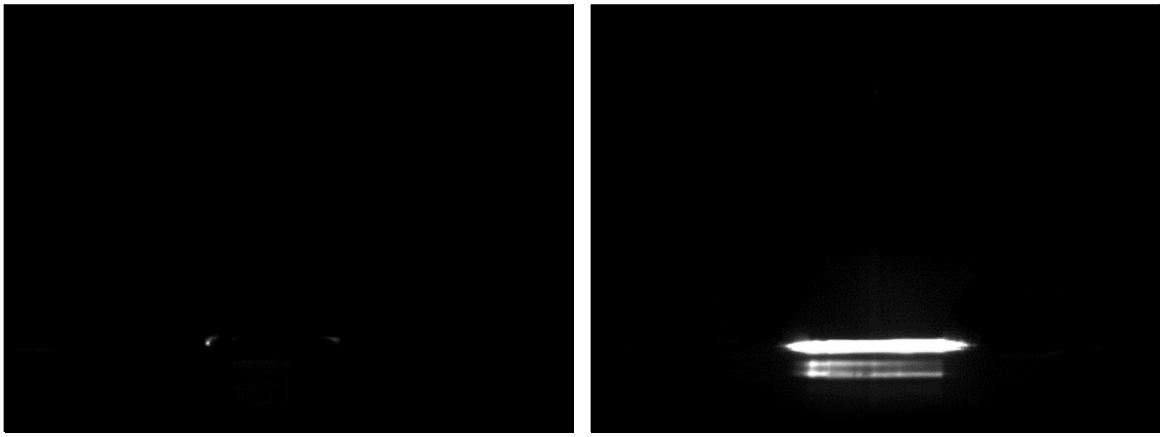

Figure 7-12: Images of surface breakdown for F00. the flashover discharges were initiated at the edge of the electrodes, where the electric field is at the highest point.

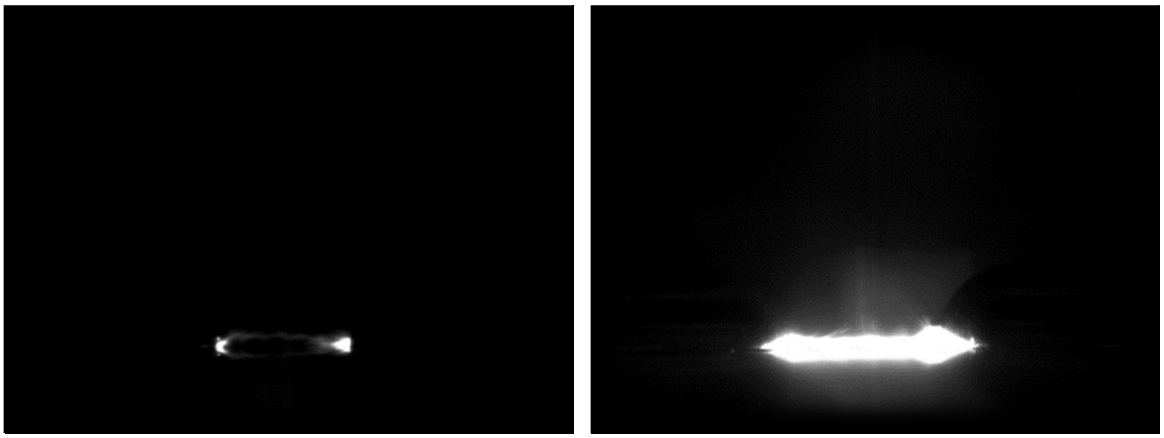

Figure 7-13: Images of surface breakdown for F180. The fact that the flashover for F180 happened at a higher breakdown voltage and, therefore, possesses a higher energy level, the flashover arc for the F180 is evidently bigger and brighter.

Figure 7-12 and Figure 7-13 are the images captured by a high-speed camera during surface flashover occurrences for non-fluorinated epoxy (F00) and 180-min-surface-fluorinated epoxy (F180) respectively. In both cases, the flashover discharges were initiated at the edge of the electrodes, where the electric field is at its highest point. A discharge path was developed between the electrodes which lead to the surface breakdown process. The fact that the flashover for F180 happened at a higher breakdown voltage and, therefore, possesses a higher energy level, the flashover arc for the F180 is evidently bigger and brighter as in the images.

7.6 CHAPTER SUMMARY

Simulation of the potential and current density distribution of surface fluorinated epoxy resin had been carried out using COMSOL Multiphysics 3.5. The results obtained denote the influence of fluorinated surface layer in the outcome of the electric potential and current density distribution. The simulation analysis clearly indicates a slight reduction in the potential distribution inside the bulk of epoxy resin with the incorporation of the fluorinated surface layer. The extra concentration of current density can be seen on the surface of the fluorinated epoxy as the thickness of fluorinated layer increases. This is due

to the fact that the fluorinated surface layer has higher conductivity as compared to the bulk.

Finally, from the DC flashover test, there is an obvious trend of increasing surface breakdown strength with the increase in the time duration of fluorination treatment. This is because the incorporation of the direct-fluorinated surface layer on epoxy resin slightly improves the conductivity along the surface. This improvement is largely attributed towards the ability of fluorinated surface to absorb surface moisture due to the increase in surface roughness as explained thoroughly in Chapter 6. The increase in surface conductivity is also attributed, to a lesser extent, to the change in physicochemical state of the fluorinated samples. Consequently, this improvement enables any trapped charges on the surface to leak away faster and, for this reason, suppresses the charges accumulation and minimises distortion of the local electric field on the epoxy resin surface. The highest value for surface breakdown strength is recorded from the 180-min-fluorinated sample that turns out to be the optimum duration for the direct-fluorination treatment. The results of this study demonstrate that the direct-fluorination treatment on epoxy resin appears to play a significant role in improving the dielectric properties of the epoxy resin.

CHAPTER EIGHT: PLASMA TREATMENT STUDY

This chapter discusses the use of plasma treatment as an alternative method to direct-fluorination for surface treatment. As discussed in Chapter 6 regarding moisture effect, we do know the increase in surface conductivity of fluorinated samples mostly comes from the absorption of surrounding moisture onto the epoxy surface. Albeit the added benefits of faster surface decay rate and higher surface breakdown strength, the usage of direct-fluorinated treatment is debatable inside a very harsh condition (low humidity and high temperature). Hence, an alternative surface treatment method by utilising radiofrequency (RF) plasma is investigated for this purpose.

8.1 THE CONCEPT OF PLASMA-ENHANCED FLUORINATION

Radiofrequency plasma technologies using fluorination gas are widely used in etching industries, or polymerisation processes in microelectronics, and in material sciences. Similar to direct-fluorination, the plasma-enhanced fluorination (PEF) treatment can be conveniently carried out at room temperature since it has a low-temperature reaction. At low-temperature, the treatment will avoid the thermal degradation of the treated material. On top of that, the chemical modification is limited to the surface only by a few tens nanometres, whereas the direct-fluorination treatment may affect the top surface by a few tens micrometres. There is also a possibility for non-equilibrium reactions. Similar to direct-fluorination, the plasma-enhanced fluorination method allows the modifications of the surface properties without altering the bulk characteristics of the original material. This treatment can be carried out with different fluorination gases such as CIF_3, CF_4, CHF_3, C-C_4F_8, C_3F_8, C_4F_8, NF_3, SF_6, F_2, and NF_3 [197]. Subject to the starting materials and adopted techniques, the improved characteristics may include mechanical behaviour, wettability, adhesion, grafting, chemical stability, biocompatibility, permeation, electrical conductivity, etc. Although fluorination treatment of polymeric materials by fluorine gas has been studied at length [198, 199], only a handful were focused on the outermost surface via PEF routes.

The attributes of C–F bonds that are formed during the reaction between the fluorine atoms and polymeric materials depend on several factors. The main factor being the PEF treatment conditions i.e. nature of the fluorinated gas, parameters of the low-pressure plasmas, etc. Another important factor that controls the nature of the C-F bonds is the physicochemical characteristics of the treated material i.e. graphitisation level, morphology of the material, nature and amount of impurities, the coherence length of the domains, etc. For instance, Tressaud et al. stated in their PEF work on polymers [47] that the C–F bonds that are formed on the surface can be attributed to CHF–CHF groups. Only 5–10 % of fluorine atoms are found on the surface. They further stated that the major components are 'ionic' fluorides, in which fluorine is bound to inorganic elements that were presented during the fabrication process of the polymers. In PEF treatments at room temperature, a gentle fluorination occurs, and only a small amount of polymer surface is affected. Interestingly, PEF treatments at an elevated temperature yield more fluorination on the surface which leads to the formation of perfluorinated ($–CF_2–$) groups and even terminal – CF_3 groups. In the latter conditions, the permeation properties are subsequently decreased.

It is also important to note that, similar to direct-fluorination treatment, PEF treatment on polymeric materials does change the way the materials interact with surrounding moisture. The degree of the contact angle for treated polymers depends on the nature of the gas phase and plasma treatment conditions. For example, the treatment in an air, oxygen, nitrogen, or ammonia discharge leads to the transformation of polyethylene surface from hydrophobic to hydrophilic [200-202]. Meanwhile, the treatment in an SF_6, C_2F_6, or C_2F_4 plasma lets the hydrophobicity of polystyrene surface to be hugely increased [203]. An increase in treatment time, discharge current, and gas pressure, for instance, in the air plasma treatment of polypropylene [204] or polyimide [205] films results in a decrease in water contact angle Ψ. Additionally, the key changes in Ψ largely happen during a short treatment time (first 15–120 s), which is also a distinctive feature of the treatment. It is important to note that PEF treatment does provide stable hydrophilicity that can be retained for a long time for practical use.

8.2 SAMPLE PREPARATION

The same set of epoxy resin (Araldite LY556, Aradur 917, and DY070) was used to make the samples. Once cured, the samples were sent to Laboratory of Plasma Physics and Materials, Beijing to undergo plasma-enhanced fluorination treatment. The reaction gas was ignited by a RF source at 30 KHz. The reactor consisted of two aluminium barrel electrodes that were coated with alumina. The inner electrode, on which the sample was positioned, was connected to the RF source while the outer one was grounded. A vacuum pump was used with a liquid nitrogen condenser that trapped any residual gases. The chamber was thermostatically controlled and maintained at room temperature during the process. Several parameters could be tuned, especially, inlet precursor composition, e.g. the possible presence of a second gas with the fluorinated reagent. Table 8-1 describes the parameters used for the PEF treatment in the laboratory. For this project, CF_4 gas was used as the fluorinated reagent with a mixture of H_2 as the second gas. The plasma treatment was done at each discharge voltage of 60 V, 80 V and 100 V with different exposure time in the range of 10 to 20 min. For ease of identification, in the following text, the epoxy samples treated at the discharge voltage of *V* for the time of *T* minutes will be referred to as sample P*V*v*T*m (e.g. P60v10m stands for PEF sample with a discharge voltage of 60 V at an exposure time of 10 min).

Sample	CF_4 flow: 15 sccm Working pressure: 20 Pa	
P60v10m	H_2	7 sccm
	Exposure time	10 min
	Discharge voltage Current	60 V 0.23 A
P80v10m	H_2	7 sccm
	Exposure time	10 min
	Discharge voltage Current	80 V 0.24 A
P100v10m	H_2	6 sccm
	Exposure time	10 min

	Discharge voltage Current	100 V 0.26 A
P60v15m	H_2	7 sccm
	Exposure time	15 min
	Discharge voltage Current	60 V 0.24 A
P80v15m	H_2	8 sccm
	Exposure time	15 min
	Discharge voltage Current	80 V 0.24 A
P100v15m	H_2	7 sccm
	Exposure time	15 min
	Discharge voltage Current	100 V 0.26 A
P60v20m	H_2	7 sccm
	Exposure time	20 min
	Discharge voltage Current	60 V 0.24 A
P80v20m	H_2	7 sccm
	Exposure time	20 min
	Discharge voltage Current	80 V 0.25 A
P100v20m	H_2	7 sccm
	Exposure time	20 min
	Discharge voltage Current	100 V 0.26 A

Table 8-1: Parameters for plasma-enhanced fluorination treatment. The unit sccm stands for standard cubic centimetres per minute, a flow measurement term.

The fluorinated reagent of CF_4 plasma is comprised of fluorine atoms and CF_x (x = 1–3) bonds. The addition of a second gas (reducing agent), such as H_2, should increase both CF and CF_2 bonds and decrease the number of fluorine atoms, by combining with them to form HF groups [206, 207]. Airoudj stated in his study [208] that from XPS measurements on plasma-treated epoxies in such conditions showed the presence of the three CF, CF_2 and CF_3 bonds whose proportions depend on plasma treatment duration and RF power. By using pure CF_4, the incorporation of fluorinated groups increases with elongated treatment

time, but decreases with increasing RF power. On the contrary, by using CF_4 / H_2 plasma treatment, the incorporation of the fluorinated groups increases continuously even for long treatment duration (higher than 110 s). He also stressed that CF and CF_2 groups are preponderant whatever treatment time and RF power are.

8.3 DC SURFACE CURRENT

The freshly treated PEF samples were first subjected to electrical characterisation test in the form of DC surface current measurement. Once the epoxy sample was removed from the sealed bag, it was placed on top of the electrode setup similar to the previous DC surface current measurement in Chapter 4. The samples' surface current value against time was plotted. Figure 8-1 shows plot of the time dependence of measured current for various plasma-enhanced fluorinated samples at a constant applied DC voltage of 5 kV across an 8 mm gap. For comparison, the surface current of non-fluorinated sample (F00) from Chapter 6 is included in the plot. The curve-fitting parameters for $\boldsymbol{A_s}$ and $\boldsymbol{b_s}$ based on the power law equation (Equation 4-3) are shown in Table 8-2. For consistency purpose, only the first 300 s of the surface current measurement data is fitted. The measurement was performed for 60 min at room temperature. It is noted that, for all the samples, the value of the resulting current drops significantly in the first minute (transient phase), and only settles down after about five minutes. However, the P100v samples show significant increment of surface current with time presumably due to moisture effect. It is important to note that the PEF treatment was performed onto the samples in Laboratory of Plasma Physics and Materials, Beijing, China. Once the treatment was done, the samples were placed in a sealed plastic bag for transportation. The transportation bag was not vacuumed, nor filled with dry gas, so a limited amount of ambient moisture was expected within the sealed plastic bag. Therefore, when the samples were taken out for measurements, the samples' surfaces were still not in equilibrium with ambient moisture; i.e. the surface would absorb surrounding moisture. The increase in water absorption level on the surface with the prolonged fluorination time introduces more hydrogen and hydroxyl ions onto the surface and, thus, yields higher surface conductivity value. More detailed explanation on moisture effect on surface-fluorinated epoxy resin samples is given in Chapter 6.

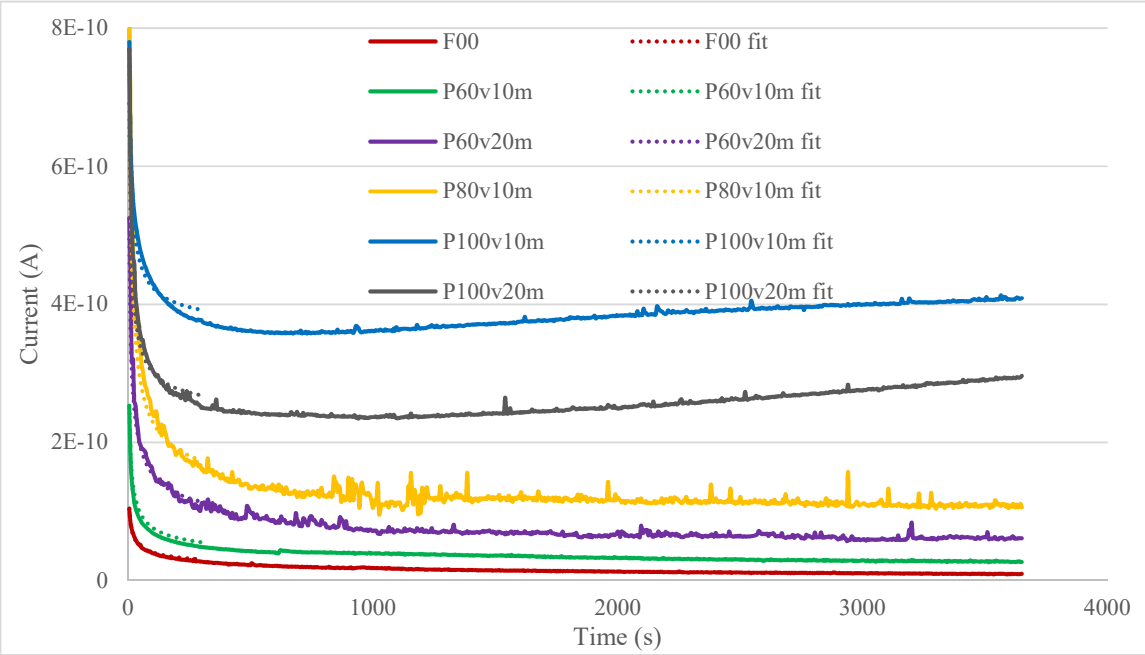

Figure 8-1: Plots of time dependence of measured current for the original and plasma-enhanced fluorinated samples at a constant applied DC voltage of 5 kV across an 8 mm gap over 60 min at room temperature.

Sample	A_s	b_s	C_s
F00	$1.96 \times 10^{-10} \pm 0.36 \times 10^{-10}$	0.363 ± 0.044	$9.32 \times 10^{-12} \pm 2.38 \times 10^{-12}$
P60v10m	$5.13 \times 10^{-10} \pm 0.25 \times 10^{-10}$	0.509 ± 0.033	$2.72 \times 10^{-11} \pm 0.04 \times 10^{-11}$
P60v20m	$9.95 \times 10^{-10} \pm 0.86 \times 10^{-10}$	0.517 ± 0.045	$6.17 \times 10^{-11} \pm 0.08 \times 10^{-11}$
P80v10m	$1.73 \times 10^{-9} \pm 0.14 \times 10^{-9}$	0.529 ± 0.033	$1.10 \times 10^{-10} \pm 0.01 \times 10^{-10}$
P100v10m	$1.44 \times 10^{-9} \pm 0.13 \times 10^{-9}$	0.578 ± 0.046	$4.08 \times 10^{-10} \pm 0.03 \times 10^{-10}$
P100v20m	$1.28 \times 10^{-9} \pm 0.32 \times 10^{-9}$	0.581 ± 0.046	$2.93 \times 10^{-10} \pm 0.01 \times 10^{-10}$

Table 8-2: Parameter A_s, b_s and C_s of curve-fitting on first 300 s data for the original and plasma-enhanced fluorinated samples at 95 % confidence bounds.

At the end of the 60 min period, the current measurement of the original sample F00 was the lowest at 9.40 x 10^{-12} A, followed by P60v10m, P60v20m and P80v10m at 2.72 x 10^{-11}

A, 6.17 x 10^{-11} A and 1.10 x 10^{-10} A respectively, showing a general increase with the treatment voltage and time. Treatment voltage does have a bigger impact on the surface current value. This trend confirms that the PEF treatment is an effective method to increase surface current on the polymeric surface. A comparable increase in electrical conduction was also discovered by H. Hayashi et al. [209] on the plasma surface-modification done on polyethylene samples. When compared against the fitting parameters of direct-fluorination samples, the steady state current observed in P60v10m sample is broadly similar to the saturated sample of F60 from Chapter 6. However, this P60v10m sample does possess higher transient current.

From Table 8-2, the exponential $\boldsymbol{b_s}$ values for PEF samples, can be seen in a higher band as compared to value of F00 sample. Inside this band, value of exponential $\boldsymbol{b_s}$ for PEF samples increases with fluorination level due to the low polarisation ability of the C-F bond [47, 109], where it is more difficult to re-orientate the bond, hence the general increase in the transient current. However, such observation is not seen in direct-fluorinated samples which possess exponential $\boldsymbol{b_s}$ values similar to F00 sample. A possible explanation for this observation is due to the decrease in charge injection barrier [210, 211] as explained later in PEA results of the PEF samples. The reduction in charge injection barrier would likely see an increase in the number of injected charges as well as the number of trapped charges in the system, which presumably give rise to the transient current [170]. In a polymer chain, segments or side groups are mobile, to some extent. A trapped charge in a polymer chain may be marginally displaced by applied field due to the displacement of the polymer segment itself [212]. Displacement of the charge may be due to flexure of polymer chain segments, or by rotation of side chains as illustrated in Figure 8-2.

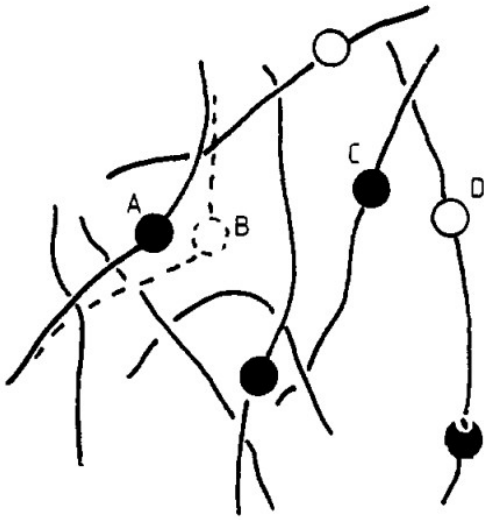

Figure 8-2 An illustration of trapped charges (black nodes A, C..) and empty sites (white nodes B, D..) in polymer chains [212]. Displacement of the charge may be due to flexure of polymer chain segments, as well as by rotation of side chains, which give rise to transient current.

From Figure 8-1, the highest measured surface current comes from P100v10m sample with a measurement of 4.13 x 10^{-10} A while, surprisingly, the P100v20m sample measured lower at 2.91 x 10^{-10} A after the hour mark. It is believed that the lower current reading for P100v20m sample, as compared to P100v10m sample, can be attributed to the degradation of the fluorinated layer by ion bombardment coming from the plasma. This observation indicates that the extension of fluorination time is not always favourable to increase the surface conductivity of the epoxy resin insulator, especially at plasma treatment above 100 V. As discussed in Chapter 4, the conductivity values on the surface of the fluorinated epoxy samples are governed by the contest in the number of compositional changes and the structural changes i.e. the chemical defects and the physical defects in the fluorinated surface layer [116]. The integration of fluorine atoms in the fluorination treatment of polymeric materials is typically followed by physical and structural changes on the surface. The chain scission process, in particular, should produce substantial physical and structural modifications, as well as the disorder at the molecular level. Moreover, the introduction of structural changes on the surface of the treated material should incorporate physical defects on the surface layer, which are known to have trap depth shallower than the trap produced by chemical defects. Hence, it is believed that for a

fluorination time beyond a certain threshold limit as in the case of P100v samples, the drop in surface current value is caused largely by the increase in the number of chemical defects or compositional changes over physical/structural defects.

8.4 MOISTURE EFFECT ON SURFACE CURRENT MEASUREMENT

Plasma-enhanced fluorination treatment has been proven to be an effective tool to enhance the dielectric properties [63, 138, 213]. As seen from previous result, this treatment improves the surface current value and may enhance the surface potential decay rate, which helps to prevent the accumulation of surface charge and consequently improve the surface breakdown strength of epoxy samples. However, the author suspects the introduction of the fluorinated layer on epoxies through PEF treatment may have the capacity to absorb moisture from the environment, similar to the case of direct-fluorination treatment. The dielectric improvements from the fluorination treatment may not only come from the fluorine layer itself, but also from the absorbed moisture on the surface layer. In such instance, the loss of moisture from the surface may lead to a loss in dielectric performance of the treated materials.

It is a well-known fact that plasma treatment, in general, is widely used to increase the printability of a surface by increasing the wettability factor. The increase in wettability gives rise to a huge amount of surface moisture being absorbed on the surface. In order to test the surface moisture effect, two sets of plasma-treated samples were left at ambient surrounding until the weight of each sample is stable i.e. the samples were in equilibrium with surrounding moisture and, therefore, didn't absorb more water. The surface moisture from the first set is forcefully dried using vacuum-oven at high temperature. For this reason, the samples were put in a vacuum-oven at 105 °C for a duration of 48 hours. Another set of samples was dried inside nitrogen gas chamber for the same period. The samples were weighed, and readings for surface DC current were taken before, during, and after the drying process. To represent the measured surface current, the same power law fitting was used as in Equation 4-3.

	Weight before drying	Weight after drying	Percentage weight loss
Day1	0.45005 ± 0.0037 g	0.44537 ± 0.0031 g	1.04%
Day2	0.45005 ± 0.0037 g	0.44530 ± 0.0022 g	1.06%

Table 8-3 Sample P100v10m weight before and after oven-drying for DC current test. The high percentage of moisture weight loss indicates a high amount of surface moisture on the sample

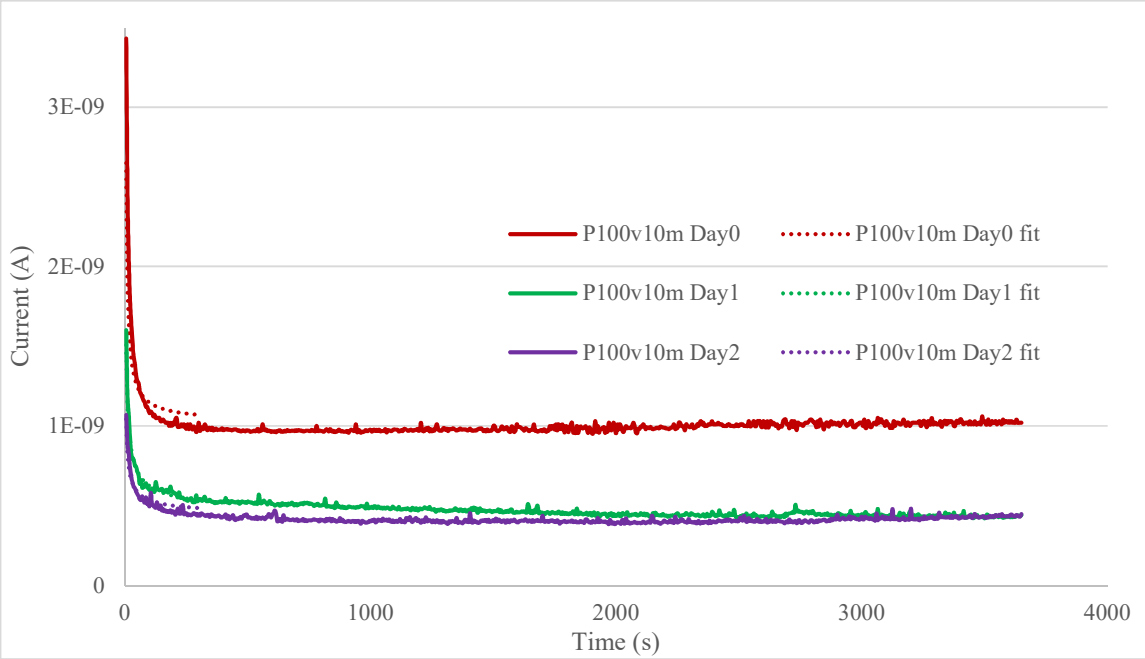

Figure 8-3: Plots of time dependence of resulting current for P100v10m dried in vacuum-oven for 2 days and the fitted lined. P100v10m shows reduced current reading as the drying day increases.

For the P100v10m sample dried in vacuum-oven, the weight loss due to the drying process is 1.04 % after 24 hours (as in Table 8-3) and is reflected in the surface current measurement in Figure 8-3. There is a huge reduction in surface current after the 24-hour-drying-process with the current reading at 4.33 x 10^{-1} A, down from 1.02 x 10^{-9} A initially i.e. a drop of 56.4 %. When the data of day 0 is compared against the data for the sample P100v10m in Figure 8-1, it can be seen that there is an increase in steady state

surface current value from of 4.13 x 10^{-10} A to 1.02 x 10^{-9} A after 60 min. This is due to the fact that the sample at day 0 is in equilibrium with surrounding moisture and, thus, possesses higher charge mobility as discussed in Chapter 6. On day 2, the weight loss is slightly higher at 1.06 % since most of the moisture had been dried away in day 1. The current measurement started lower for day 2 but ended up with the same value as day 1 after 60 min since the surface was absorbing moisture as the measurement took place. When compared to the direct-fluorinated sample of F60 under the same vacuum-oven treatment, the P100v10m sample possesses higher surface current reading (F60 sample has a surface current value of 1.03 x 10^{-11} A) after 24 hours of drying. In terms of moisture loss, P100v10m sample suffers more weight loss as compared to F60 sample (1.04% against 0.71 % weight loss) indicating a high amount of surface moisture in plasma treated samples.

P100v10m	A_s	b_s	C_s
Day0	6.43 x 10^{-9} $\pm$ 1.62 x 10^{-9}	0.603 $\pm$ 0.071	1.02 x 10^{-9} $\pm$ 0.26 x 10^{-9}
Day1	2.72 x 10^{-9} $\pm$ 0.18 x 10^{-9}	0.578 $\pm$ 0.020	4.33 x 10^{-10} $\pm$ 1.10 x 10^{-9}
Day2	1.59 x 10^{-9} $\pm$ 0.28 x 10^{-9}	0.568 $\pm$ 0.051	4.33 x 10^{-10} $\pm$ 1.10 x 10^{-9}

Table 8-4: Parameter A_s and b_s of curve-fitting on first 300 s data for P100v10m dried in vacuum-oven for 2 days at 95 % confidence bounds.

As for the curve-fitting parameters in Table 8-4, the exponential b_s values can be regarded as common within the two days of drying, similar to the observation in dried direct-fluorinated samples. This observation indicates that the polarisation mechanism during transient current phase remain the same before and after the drying process. A notable difference during the oven-drying process can be seen in the reduction of parameter A_s with drying time due to the reduction in moisture-assisted charge injection. When compared against dried direct-fluorinated samples, the values of parameter A_s for PEF sample are higher by 10 order. Again, this can be attributed to the increase in charge

injection as a result from reduction in injection barrier for PEF samples as explained earlier.

It is noteworthy that drying the sample in a vacuum-oven at a temperature of 105 °C for more than 24 hours is an extreme measure to remove the moisture from the surface. A significant weight loss up to 1.04 % was recorded within 24 hours of drying, even higher than the value of the recorded weight loss for direct-fluorination sample in Chapter 6. Accordingly, the samples were dried in insulating gas at room temperature instead. The insulation gas that was used for this test is dry nitrogen gas. To test the moisture effect for samples dried in nitrogen gas, the same set of procedure was repeated as before. Instead of using the vacuum-oven at 105 °C, this time, the samples were dried in a nitrogen gas chamber at room temperature for 48 hours. The nitrogen-dried samples were weighed, and measurements of DC current were taken before, during, and after the drying process.

	Weight before drying	**Weight after drying**	**Percentage weight loss**
Day1	0.4613 + 0.0024 g	0.4598 + 0.0014 g	0.32%
Day2	0.4613 + 0.0024 g	0.4593 + 0.0011 g	0.43%

Table 8-5 Sample P60v20m weight before and after nitrogen-drying for DC current test. The weight loss for PEF samples are comparably higher than the loss in direct-fluorinated samples.

After 24 hours of drying in nitrogen gas, the weight loss for sample P60v20m is 0.32 % as in Table 8-5. This small weight loss is reflected in the surface current measurement in Figure 8-4. Before drying, the steady state current reading after 60 min is 5.81 x 10^{-10} A (Day 0). The current measurement shows a small reduction in surface current reading after the nitrogen-drying treatment. The current measurement after one day of drying is 4.17 x 10^{-10} A (i.e. a drop of 28.2 %) and the current value drops to 3.41 x 10^{-10} A after the second day (i.e. a drop of 41.3 %). The drops in current value are much lower as compared to the drops of the oven-dried sample. Again, the exponential b_s values in Table 8-6 at day 0, day 1, and day 2 can be regarded as common after the drying in nitrogen gas, similar to

the samples dried in vacuum-oven in Table 8-4. The removal of absorbed moisture through drying would not change the physicochemical state of the system, hence the common value of exponential $\boldsymbol{b_s}$. Nevertheless, the removal of absorbed moisture from the surface would reduce the moisture-assisted charge injection and, therefore, the decrease in parameter A_s.

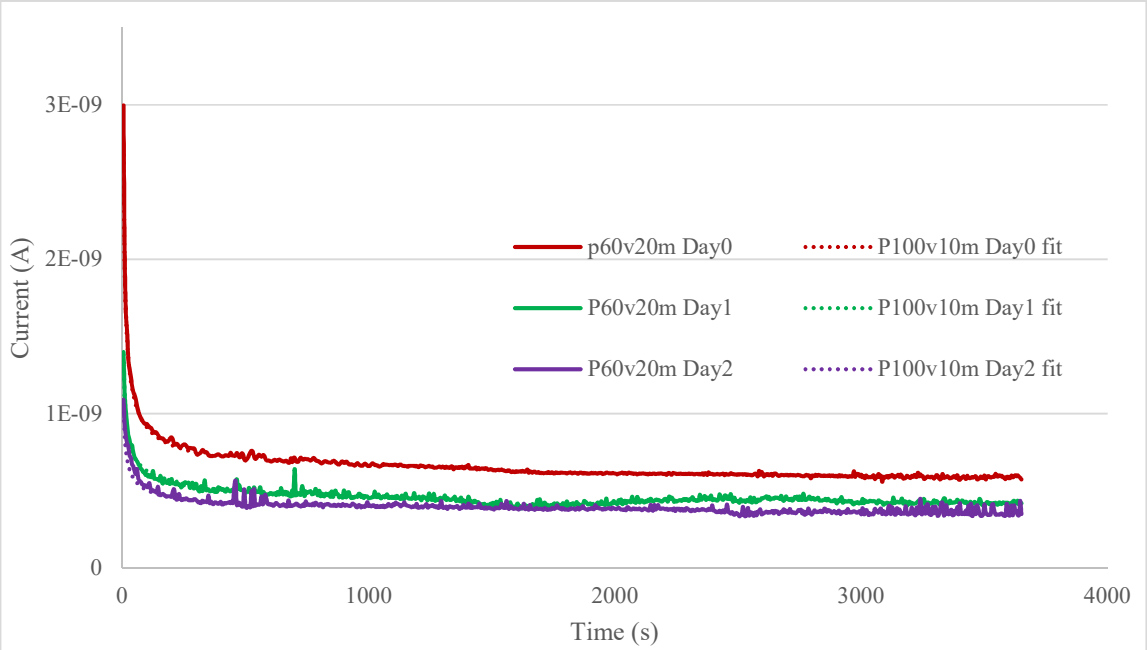

Figure 8-4: Plots of time dependence of resulting current for P60v20m dried in nitrogen gas for 2 days and the fitted lined. P60v20m shows reduced current reading as the drying day increases.

P60v20m	A_s	b_s	C_s
Day0	$5.65 \times 10^{-9} \pm 0.43 \times 10^{-9}$	0.516 ± 0.019	$5.81 \times 10^{-10} \pm 1.48 \times 10^{-10}$
Day1	$2.16 \times 10^{-9} \pm 0.16 \times 10^{-9}$	0.502 ± 0.020	$4.17 \times 10^{-10} \pm 1.06 \times 10^{-10}$
Day2	$1.59 \times 10^{-9} \pm 0.20 \times 10^{-9}$	0.492 ± 0.035	$3.41 \times 10^{-10} \pm 0.41 \times 10^{-10}$

Table 8-6: Parameter $\boldsymbol{A_s}$, $\boldsymbol{b_s}$ and $\boldsymbol{C_s}$ of curve-fitting on first 300 s data for P60v20m dried in nitrogen gas for 2 days at 95 % confidence bounds

From the moisture effect results, it is evident that the nitrogen-dried sample shows better dielectric properties in term of DC surface current values. Most of the moisture on the surface of the oven-dried sample were vaporised when dried at 105 °C for 24 hours. It is interesting to note from Table 8-3 and Table 8-5, the loss of mass due to water vaporisation and diffusion are larger for PEF samples when compared to direct-fluorination samples, indicating good wettability value and small water contact angle on the surface of PEF samples. The findings are in line to the work done by Wu [214] which confirms that the PEF treatment of polymer surfaces in air, oxygen, inert gases, or their mixtures leads to a change in the water contact angles. In another work done by Gil'man [213], he has shown that the generation of charge states have a significant contribution towards the hydrophilisation of the surface. For polymeric materials treated in the DC or AC glow-discharge cathode fall, it was discovered that a negative charge from localisation of injected plasma electrons in different traps is formed on the film surface facing the electrode and in the near-surface layer. He concludes that charge induced on the polymer surface is the main cause of variation in the contact angles on polymers and an increase in their surface energy in some cases. A similar study by Y. Ma et al. [215] confirms that plasma treatment on polymer surface shows that as the treatment time increases, the contact angle decreases and the surface energy increases. Both the surface roughness and the oxygen-containing groups increase after the treatment. As discussed in Chapter 6, the small water contact angle for fluorinated epoxy samples is attributed to the introduction of polar groups of -C-H-F-, as well as the chain scission process that introduced a highly polar group inside the fluorinated layer. The absorbed water on the surface does possess higher conductivity value due to the higher mobility of hydrogen and hydroxyl ions. The loss of moisture on the surface hugely affects the DC current values and the corresponding decay rates. However, as can be seen in Figure 8-3, the steady state current value of the oven-dried P100v10m sample (4.33 x 10^{-1} A) is lower than its initial value in day 0 (1.02 x 10^{-9} A), but much higher than the steady state current value of non-fluorinated epoxy sample (9.40 x 10^{-12} A). This implies that, even after the surface moisture had been dried away, the fluorinated layer still possesses a relatively high intrinsic value of surface current. Such observation is none existence in direct-fluorination sample of F60. This observation is comparable to the work done by Liu et al. [179] in which they observed an intrinsically high surface conductivity

value for the fluorinated sample as compared to the original sample surface at low relative humidity (RH).

8.5 Potential Decay Measurement

Similar to previous surface potential decay measurement setup in Chapter 5, the PEF sample was placed on top of a rotatable earthed electrode plate, just underneath the high-voltage needle electrode and the wire mesh grid electrode. In this experimental setup, the distance between the needle and the grid was 4.5 cm while the distance between the grid and the ground plate was 1.5 cm. The grid had a surface area of 150 cm², wide enough to provide uniform distribution of corona charge on the sample surface of 16 cm² (4 cm x 4 cm). The PEF epoxy samples were negatively charged by corona effect on their free surface for one minute. The needle and grid voltage were -16 kV and -5 kV respectively. Immediately after charging, the sample was quickly moved using the rotating system towards a compact JCI 140 static monitor to measure the surface potential decay and the decay's time characteristic was plotted.

Different rates of surface potential decay for epoxy resin samples of different plasma voltage and time can clearly be observed, as shown in Figure 8-5 and Figure 8-6. At a constant plasma treatment time of 10 min, the increase in treatment voltage translates into an increase in potential surface decay rate. The fastest decay rate is observed for P100v10m sample followed by P80v10m sample and P60v10m sample with values of relaxation time, T_r, 18.7 min, 18.2 min, and 9.9 min (from Table 8-7) respectively. Against direct-fluorination samples, the decays of these plasma-fluorinated samples are comparable to those between F30 and F60 samples. Similarly, the increase in decay rate mainly occurs because the increase in treatment voltage may have increased the surface current value of epoxy samples as proven earlier. Consequently, this improvement may enable any trapped charges on the surface to move away faster as reflected from the resulting plot. From the pre-exponential ratios in Table 8-7, it can be deduced that the number of mobile charges (shallow traps) is increasing with plasma voltage while the number of trapped charges in deep traps is decreasing, indicating the conductivity is increasing with the degree of

fluorination. From the exponential parameters, the values for time constant $\boldsymbol{B_m}$ are broadly similar, suggesting that the average shallow trapping level is constant with the plasma treatment. The value for time constant $\boldsymbol{B_t}$, on the other hand, shows a significant decrease as the plasma voltage increases, implying a decrease in the average deep trapping value, hence faster decay. The faster decay can also be attributed to the increase in moisture assisted charge movement as the absorbed surface moisture increases with the degree of fluorination, as seen in direct-fluorinated samples in Chapter 6.

When compared against the fitting parameters of direct-fluorinated samples, the time constant values of $\boldsymbol{B_m}$ and $\boldsymbol{B_t}$ for P100v10m sample in Table 8-7 are broadly similar to F60 sample from preliminary surface decay measurement in Table 5-1. P100v10m sample also exhibit higher ratio for $\boldsymbol{A_m}$which result in faster relaxation time $\boldsymbol{T_r}$. In the case of P80v10m samples, the exponential parameters $\boldsymbol{B_m}$ and $\boldsymbol{B_t}$ are largely similar to the saturated F60 day 0 sample from Table 6-4. For P60v10m sample, the values of the time constant parameters fall in between the values for F30 and F60 from the preliminary surface current measurement while the values for pre-exponential $\boldsymbol{A_m}$ of P60v10m is relatively higher. Although PEF samples possess comparably high surface current value, as well as higher intrinsic surface current value when the surface moisture was dried, as evident from surface current measurement, the decay properties of PEF samples are only equivalent to direct-fluorinated F30 and F60 samples. The same observation can be seen from Table 8-8, with the time constant values of $\boldsymbol{B_m}$ and $\boldsymbol{B_t}$ for the P60v15m sample are broadly similar to the time constants of saturated F60 day 0 sample, while the time constant values of $\boldsymbol{B_m}$ and $\boldsymbol{B_t}$ for the P60v20m sample are broadly similar to the time constants of F60 sample from preliminary surface decay measurement. Again, the PEF samples from Table 8-8 also exhibit higher ratio for pre-exponential $\boldsymbol{A_m}$ presumably due to higher surface moisture content and, hence, more charges become mobile from moisture assisted charge movement.

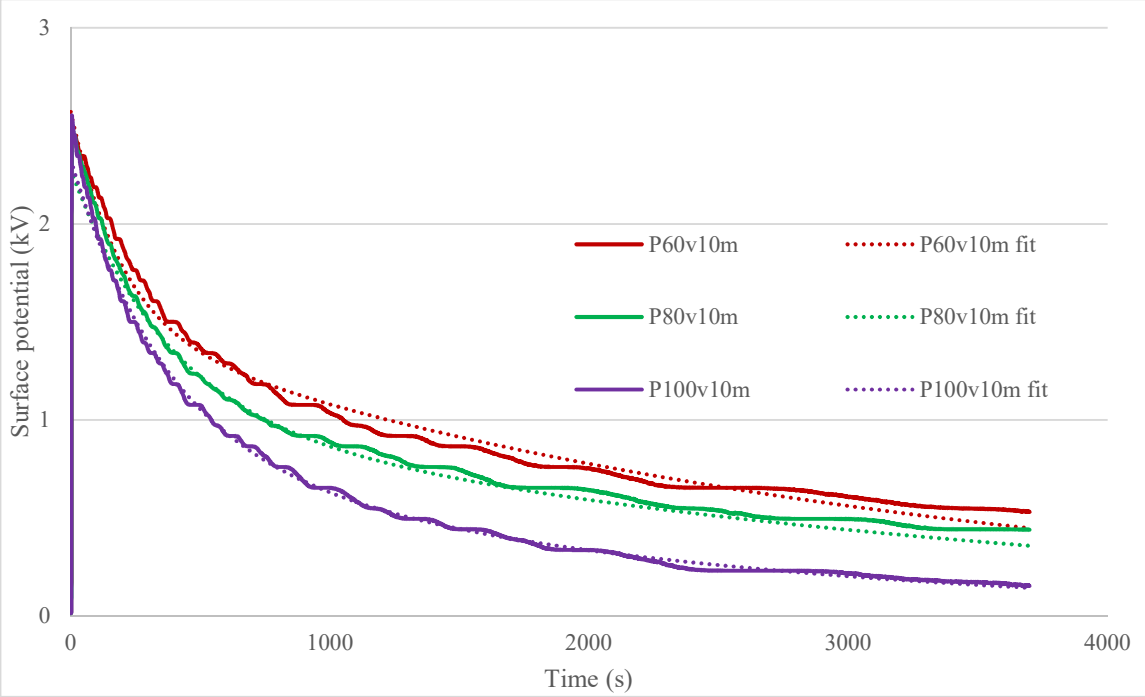

Figure 8-5: Potential decay for plasma-enhanced fluorinated epoxy resin samples with varying treatment voltage and the fitted lines. The plot exhibits faster decay rate as the plasma treatment voltage increases.

Sample	A_m	$\frac{A_m}{(A_m + A_t)}$	A_t	$\frac{A_t}{(A_m + A_t)}$	B_m	B_t	T_r
P60v10m	1.09 ± 0.02	0.42 ± 0.02	1.48 ± 0.03	0.58 ± 0.02	195 ± 6	3130 ± 120	0.413 h
P80v10m	1.05 ± 0.02	0.46 ± 0.02	1.23 ± 0.04	0.54 ± 0.03	194 ± 6	2810 ± 110	0.303 h
P100v10m	1.21 ± 0.03	0.48 ± 0.03	1.33 ± 0.06	0.52 ± 0.04	192 ± 7	1450 ± 50	0.165 h

Table 8-7: Parameters A_m, A_t, ratios, B_m, B_t and T_r of curve-fitting result for plasma-enhanced fluorinated epoxy resin samples with varying treatment voltage at 95 % confidence bounds

When the treatment voltage is kept constant and the treatment time is varied, the increase in decay rate (which is determined by the surface conductivity value) is even more significant with a prolong time of plasma treatment, as can be seen in Figure 8-6. The fastest decay rate is observed for P60v20m sample, followed by P60v15m sample and finally P60v10m sample with values of relaxation time, T_r, 18.7 min, 20.0 min, and 24.8 min (from Table 8-8) respectively. This trend signifies that, in general, the increase in treatment time would also increase the surface conductivity as well as the decay rate of the treated surface. However, there is an exception to this trend, as can be seen earlier from the current measurement where the increase in treatment time for the plasma-enhanced fluorinated samples treated at 100 V results in a decrease in the current reading and the decay rate as well (the decay rate for P100v samples is not shown here). The changes in decay rate is in agreement with the increase in surface current as measured earlier, which implies that the surface current value determines the resulting potential decay rate. From the pre-exponential ratios in Table 8-8, the ratios of $\boldsymbol{A_m}$ and $\boldsymbol{A_t}$ are broadly similar, suggesting that the number of mobile charges (shallow traps) and the number of trapped charges in deep traps remain the same as the degree of fluorination increases. From the exponential parameters, the values for time constant $\boldsymbol{B_m}$ are also broadly similar, suggesting that the average shallow trapping level is constant with the plasma treatment. The value for time constant $\boldsymbol{B_t}$, on the other hand, shows a significant decrease as the plasma duration increases, implying a decrease in the average deep trapping value, hence faster decay.

In this study, however, there is no data available regarding the moisture effect on surface potential decay performances of PEF samples. More work need to be done in investigating the dependability of PEF samples on absorbed moisture in the improvement of dielectric performances. This is crucial as it is evident in direct-fluorinated samples, the improvement in dielectric properties of direct-fluorinated samples largely comes from the capacity of the treated surface to absorb moisture. The physicochemical change in the direct-fluorinated samples only play a minor role in the dielectric improvement.

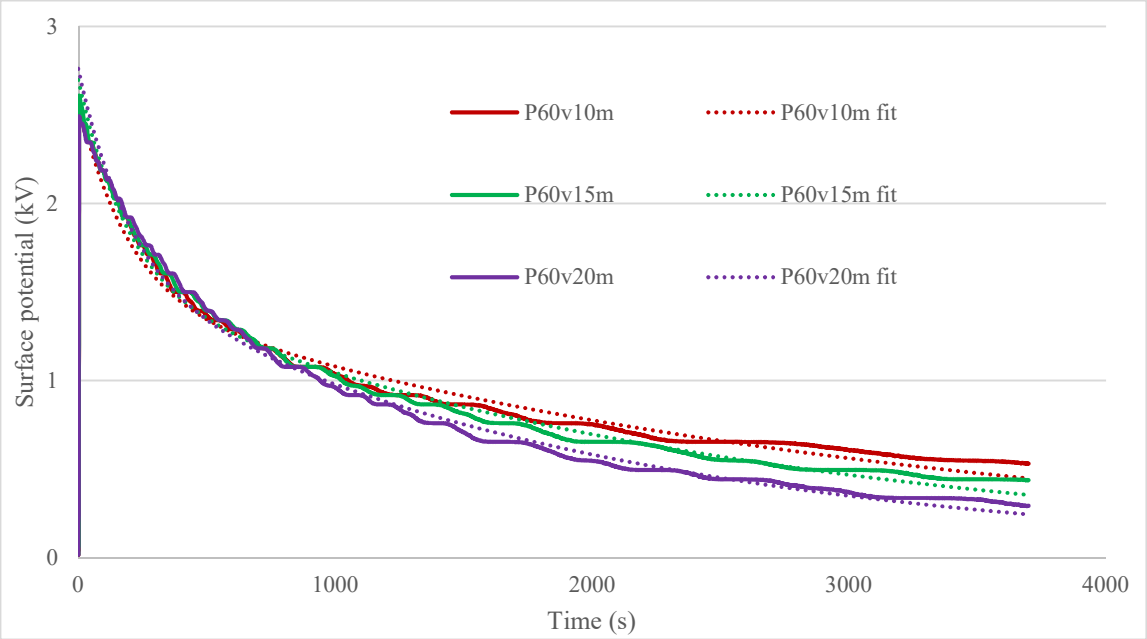

Figure 8-6: Potential decay for plasma-enhanced fluorinated epoxy resin samples with varying treatment time and the fitted lines. The plot exhibits faster decay rate as the plasma treatment time increases.

Sample	A_m	$\frac{A_m}{(A_m + A_t)}$	A_t	$\frac{A_t}{(A_m + A_t)}$	B_m	B_t	T_r
P60v10m	1.09 ± 0.02	0.42 ± 0.02	1.48 ± 0.03	0.58 ± 0.02	195 ± 6	3130 ± 120	0.413 h
P60v15m	1.15 ± 0.03	0.43 ± 0.02	1.55 ± 0.04	0.57 ± 0.03	193 ± 6	2510 ± 100	0.334 h
P60v20m	1.14 ± 0.02	0.41 ± 0.01	1.62 ± 0.03	0.59 ± 0.02	195 ± 7	1950 ± 80	0.312 h

Table 8-8: Parameters A_m, A_t, ratios, B_m, B_t and T_r of curve-fitting result for plasma-enhanced fluorinated epoxy resin samples with varying treatment time at 95 % confidence bounds

8.6 SPACE CHARGE MEASUREMENT

To further examine the charge dynamics in the PEF samples, the charge measurement in the bulk may provide supporting evidence. The PEA method was used to observe the space charge behaviour inside the fluorinated epoxy sample. A voltage of 7 kV was applied to samples of approximately 300 µm in thickness (23.33 V mm^{-1}) at room temperature for 120 min. At each time interval (0 min, 1 min, 3 min, 5 min, 60 min, and 120 min), a pulse of 600 V was applied to generate acoustic pulses from the stored charges within the dielectrics for measurement purposes. After 120 min, the voltage supply was turned off, and the decay measurement was taken at every time interval for 1 hour. Unlike previous samples of direct-fluorination, these PEF samples were treated on one surface only. For a start, the treated surface was placed at the cathode where the accumulation of charges was bound to happen based on the previous result of original epoxy sample F00.

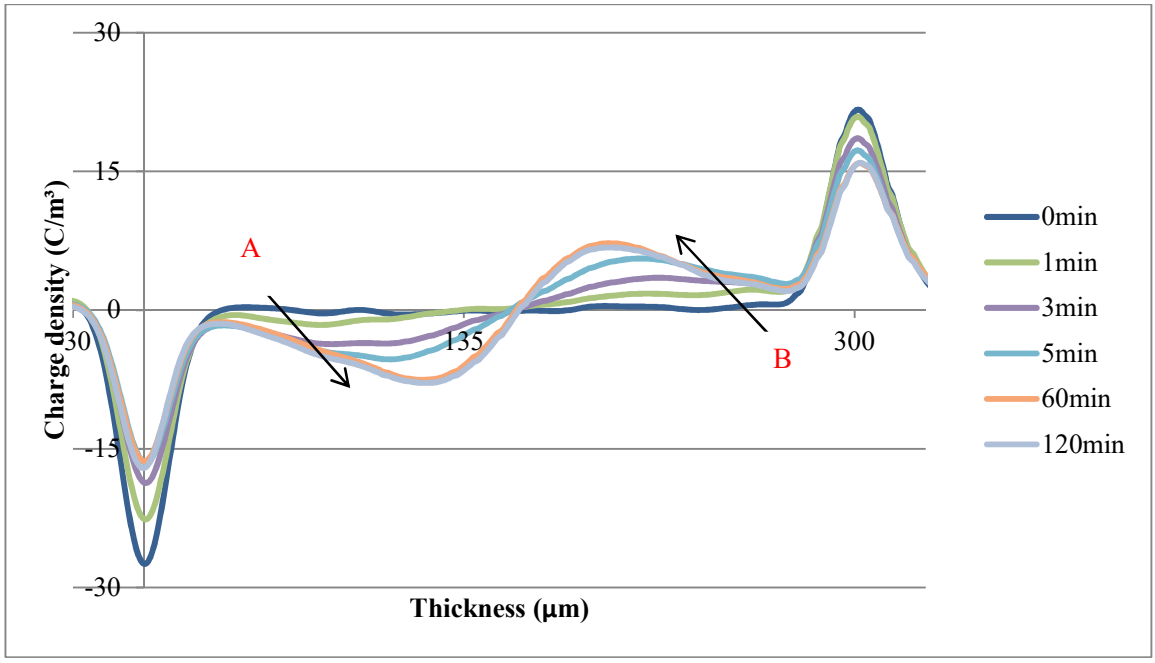

Figure 8-7: Charge build-up in P60v10m at 7 kV (23.33 V mm^{-1}) for 120 min. Arrow A and B show the charge accumulation position

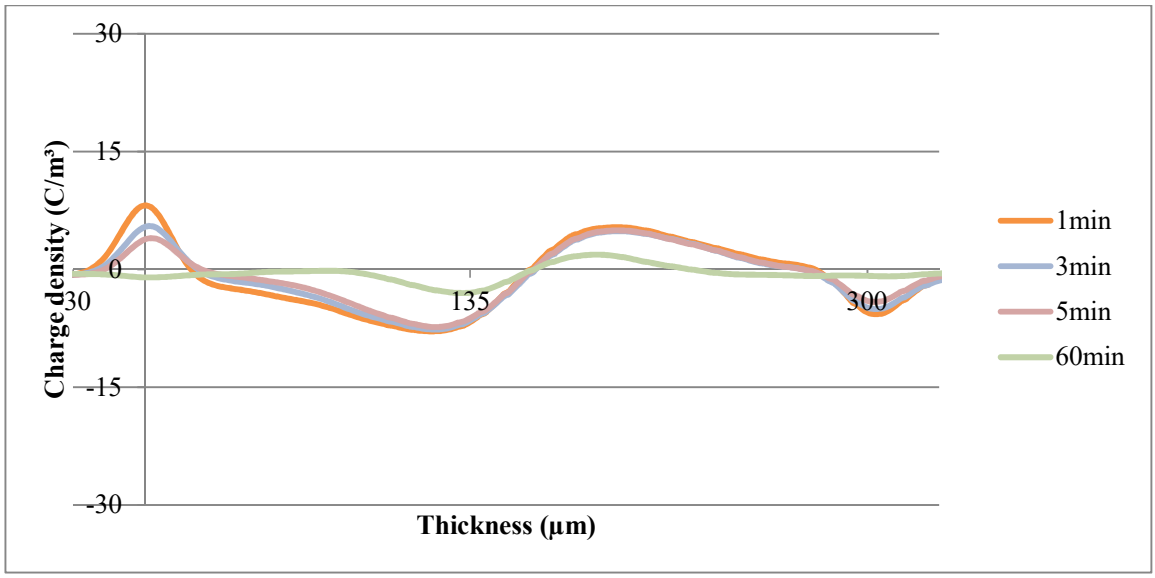

Figure 8-8: Charge decay in P60v10m for 60 min when the voltage source is removed

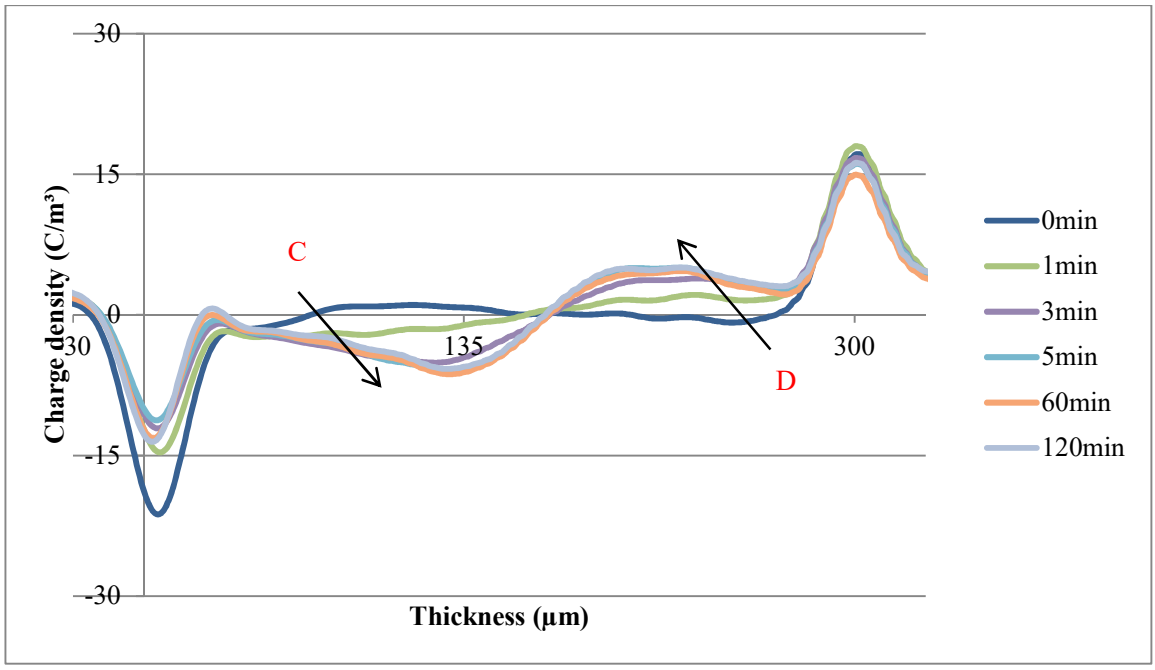

Figure 8-9: Charge build-up in P80v10m at 7 kV (23.33 V mm^{-1}) for 120 min. Arrow C and D show the charge accumulation position.

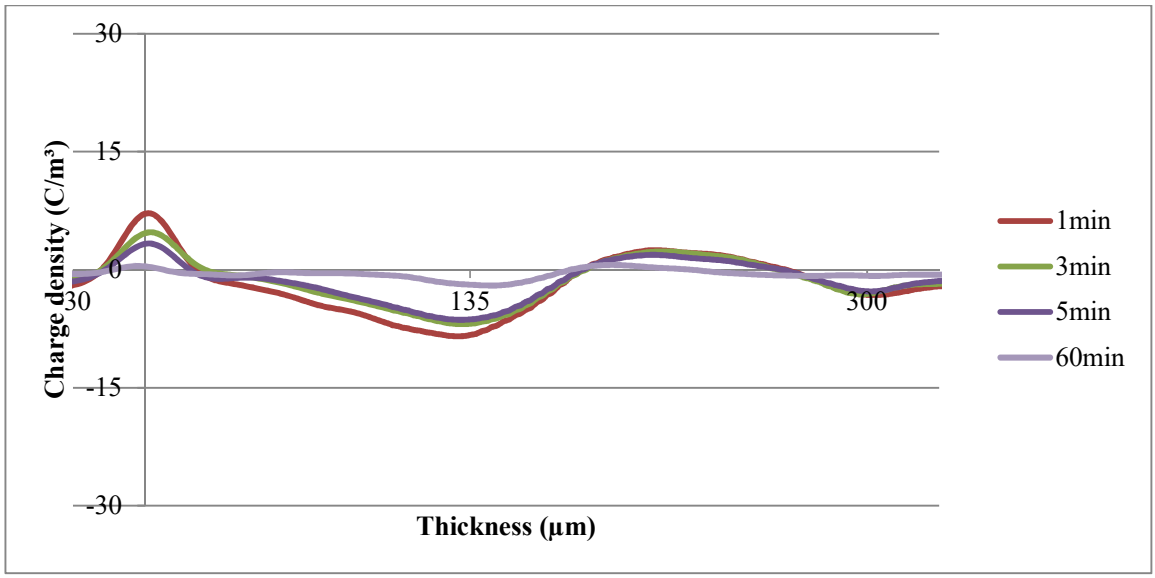

Figure 8-10: Charge decay in P80v10m for 60 min when the voltage source is removed.

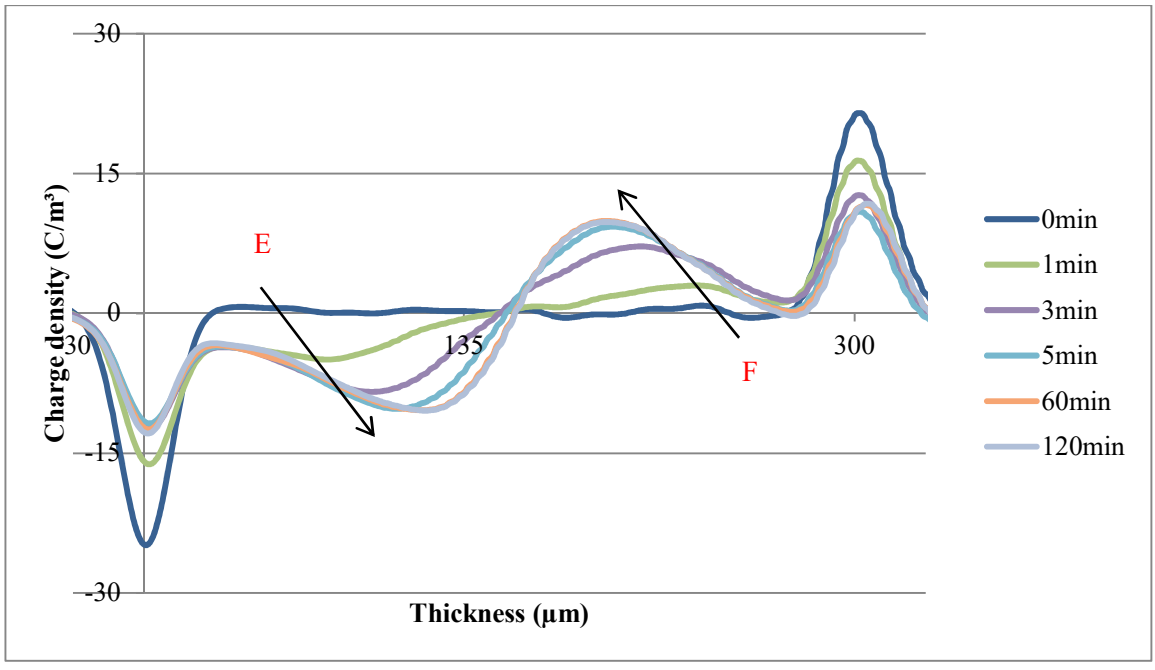

Figure 8-11: Charge build-up in P100v10m at 7 kV (23.33 V mm^{-1}) for 120 min. Arrow E and F show the charge accumulation position

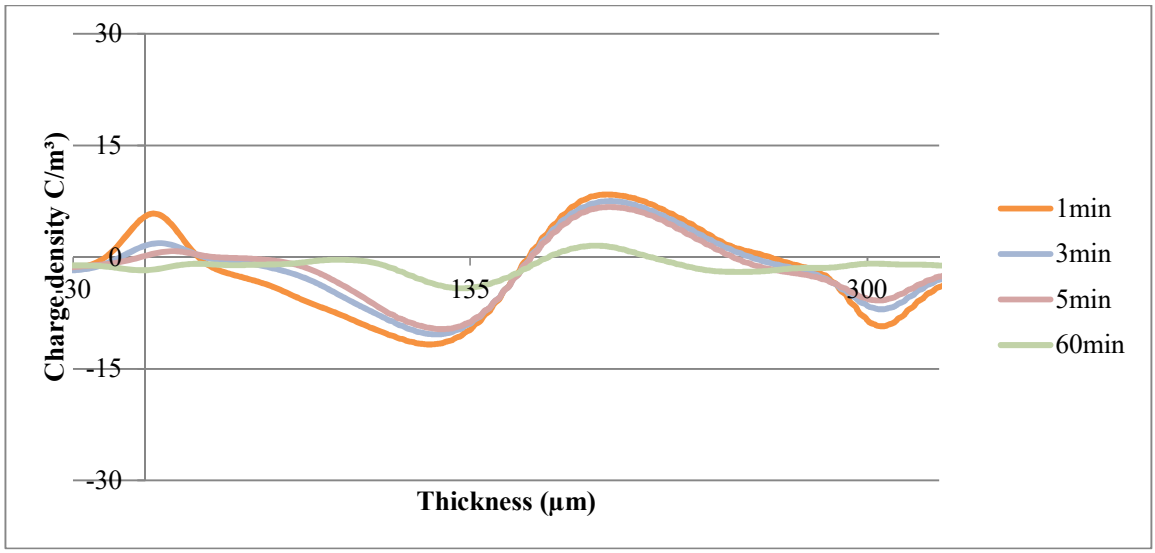

Figure 8-12: Charge decay in P100v10m for 60 min when the voltage source is removed.

The PEA charge profile in Figure 8-7 shows that, for P60v10m sample, a homocharge formation (arrow A and B) is observed in the vicinity of both electrodes. The amount of charge increases with the time of applied voltage and moves towards the bulk. The formation of homocharges inside epoxy resin sample is due to charge injection from adjacent electrodes. At higher treatment voltage as in P100v10m (as seen in Figure 8-11), charge accumulation in the bulk appears to be greatly enhanced (arrow E and F). From previous PEA measurement on direct-fluorinated samples, the fluorinated layer acts as a shield to block further charge injection from the electrodes. However, this is not the case for plasma-enhanced fluorination as homocharges appears to be injected from the electrodes, through the treated layer and into the bulk. The fluorination layer no longer blocks charge injection as in direct-fluorination samples. It is also noteworthy that, from previous PEA measurement on original epoxy sample F00, there is no visible charge formation at the anode (Figure 5-10). In this plasma-enhanced fluorination sample, however, the formation of homocharges is obvious in the vicinity of anode. The surface that is in contact with the anode is untreated and, in theory, should possess charge dynamics properties similar to those of original epoxy sample. It is believed that the accumulation of injected homocharges from cathode (PEF treated side) will enhance the electric field at the opposite end, resulting in further charge injection from anode. From the

decay waveform in Figure 8-8, Figure 8-10 and Figure 8-12, the fast dissipation of injected charges, near the electrodes, after voltage removal, implies that there is a fast de-trapping process going on near the surface, and the charges were then extracted at the neighbouring electrode, similar to the case of direct-fluorination sample. However, in the bulk, the decay of the accumulated homocharges is relatively slower due to the slow bulk conduction in epoxy. It is important to note that all the samples under investigation possess high glass transition temperature T_g (128 °C from DSC measurement) while the PEA measurements were performed at room temperature. While the PEF samples were deep in their glassy state, when the voltage was turned off, the movement of accumulated charges from the bulk would be restricted. Small portion of homocharges can still be seen in the bulk at the end of the decay measurement. Therefore, plasma-enhanced fluorination treatment is believed to provide fast decay on the surface and at the same time allows charge accumulation into the bulk in the presence of a high electric field.

In order to see the charge dynamics of the plasma-enhanced fluorinated layer at anode, the PEA measurement was repeated with the sample being flipped over (the sample is turned upside-down) i.e. the treated surface facing anode. Figure 8-13 and Figure 8-15 show the charge formation inside sample P60v10m and P80v10m that were flipped over so that the high voltage electrode is in contact with the treated surface. A similar pattern of charge formation can be seen, but, to a lesser degree than the previous measurement. The plasma-enhanced fluorinated surface still allows charge accumulation in the bulk (arrow G and I) and a same magnitude but opposite polarity charge is seen at the opposite end (arrow H and J).

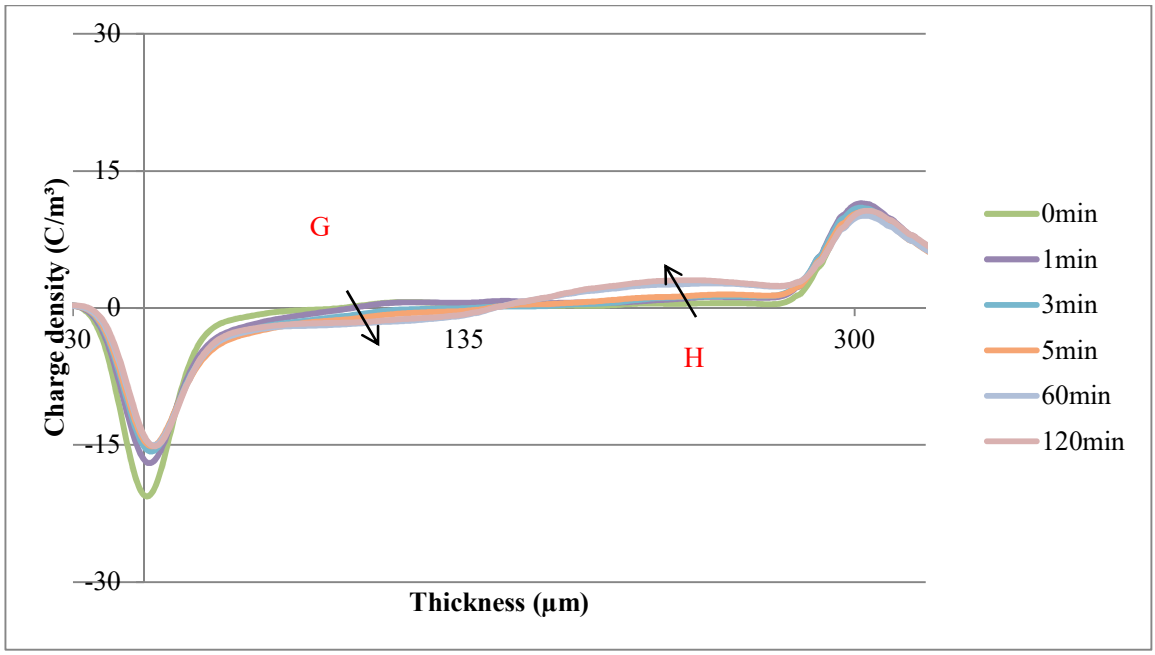

Figure 8-13: Charge build-up in flipped (the sample is turned upside-down) P60v10m at 7 kV (23.33 V mm^{-1}) for 120 min. Arrow G and H show the charge accumulation position

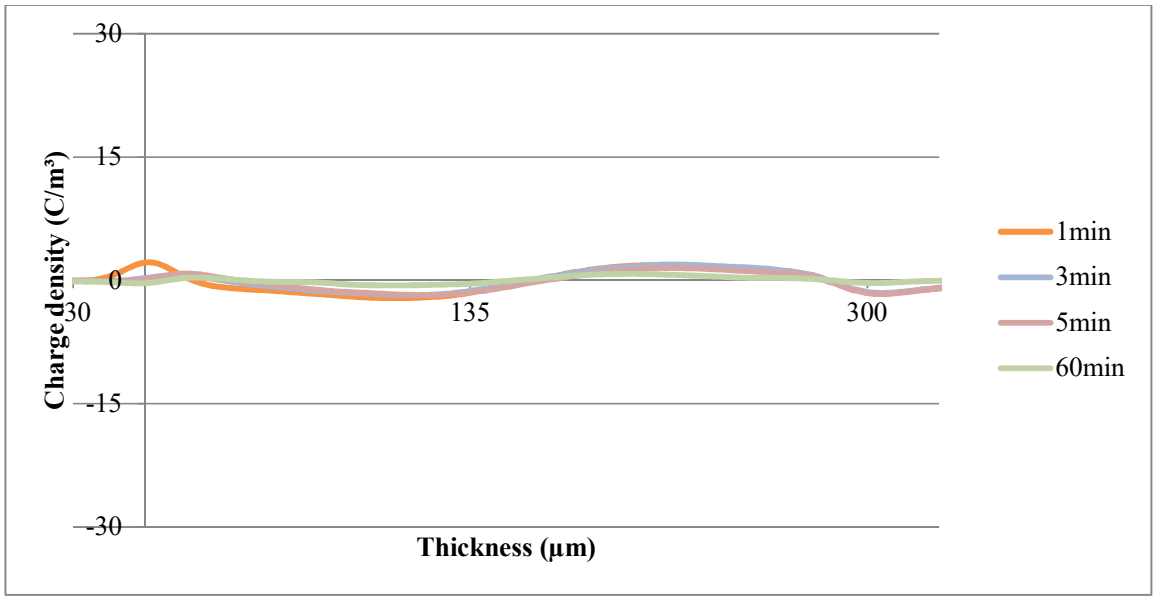

Figure 8-14: Charge decay in in flipped (the sample is turned upside-down) P60v10m for 60 min when the voltage source is removed.

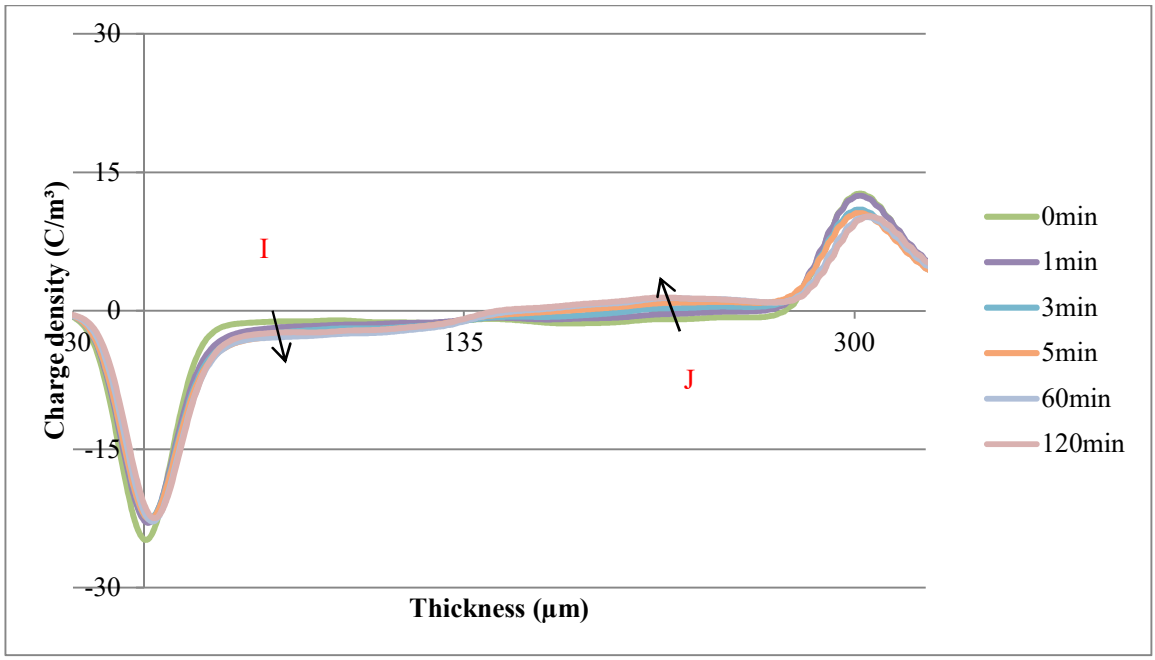

Figure 8-15: Charge build-up in flipped (the sample is turned upside-down) P80v10m at 7 kV (23.33 V mm^{-1}) for 120 min. Arrow I and J show the charge accumulation position

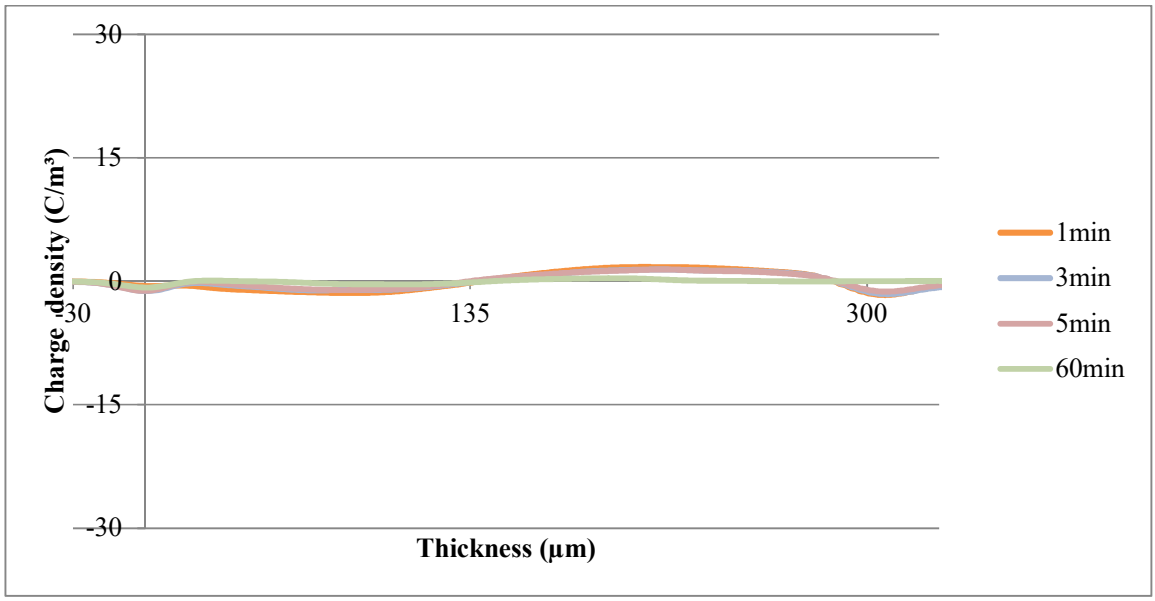

Figure 8-16: Charge decay in in flipped (the sample is turned upside-down) P60v10m for 60 min when the voltage source is removed.

The movement of charges into the bulk for both cases of PEA measurement (flipped and non-flipped) for PEF samples implies that the treatment does modify the surface and possibly the bulk characteristics of the treated materials to a certain extent. Such observations are not without precedent. The plasma treatment on the epoxy sample is believed to have caused a reduction in charge injection barrier, which makes it easier for charges to be injected into the sample. The reduction in charge injection barrier becomes more severe as the intensity of the plasma treatment increased, as observed in the PEA data. For this reason, the formation of homocharges inside the bulk is clearly evident, which is not visible in the direct-fluorinated samples, as well as the original sample. A comparable reduction in barrier height (0.4 – 0.5 eV) was also discovered by Paskeleva et al. [210] on the plasma treated material resulting from the plasma-generated charges breaking of strained bonds. Another study conducted by T. Y. Chang et al. [211] on CF_4 plasma pre-treatment revealed that the plasma-fluorinated material possesses lower barrier height when compared to the original sample.

Another possible theory to explain the formation of homocharges is through the bulk modification. Although plasma treatment is known to modify only the surface of the treated material, there are instances in which the treatment had led to substantial changes to the structure, comprising the whole volume, as well as the polymer surface [216-219]. In direct-fluorination sample, no charge movement is observed in the bulk of epoxy because the materials were deep in their glassy state and, therefore, the polarisation and movement of any internal impurities present in the materials will be restricted. However, this is not the case for plasma-treated samples as charge formation can clearly be observed in the bulk. Ironically, it is important to note that until recently, the plasma treatment of polymers was regarded to be a treatment limited to modification to the surface properties only. Structural and chemical changes happened only on the surface and did not affect the bulk properties of polymeric materials. In fact, the plasma UV radiation may breach into the bulk of a polymeric material and may change its bulk properties. The penetration depth and absorption of the UV radiation depend on the properties and structure of the modified material. In a similar case, by adopting differential scanning calorimetry (DSC), IR spectroscopy, and X-ray diffraction techniques on plasma treated “quenched”

polypropylene, Yoshimura et al. [216] revealed the transformations from the amorphous to the smectic phase, as well as from the smectic to the α-crystalline phase.

8.7 DC FLASHOVER

From the previous results of DC current, surface decay and PEA measurement, one can clearly see the change in electrical properties of plasma-enhanced fluorinated epoxy resin in term of dissipating the accumulated charge along the surface of the insulating material. Furthermore, this trait should lead to an increase in surface flashover strength as the dissipation of the accumulated surface charge is one of the key factors that influence the surface flashover performance. The surface flashover strength is defined as a measure of insulation surface to resist decomposition under voltage stress. The applied voltage causes the top insulation to fail through a surface discharge and ruptures the surface insulation. In this test, each fresh samples were subjected to 2 flashovers at different location on the treated surface. A two-parameter Weibull distribution with 90 % confidence bounds was plotted in Figure 8-17, with the estimated parameters listed in Table 8-9. Since minimum flashover voltage is expected, the three-parameter Weibull distribution was also carried out. Again, fitting method using hybrid approach was adopted in order to get the best fitting result. The three-parameter Weibull estimated parameters are listed in Table 8-10.

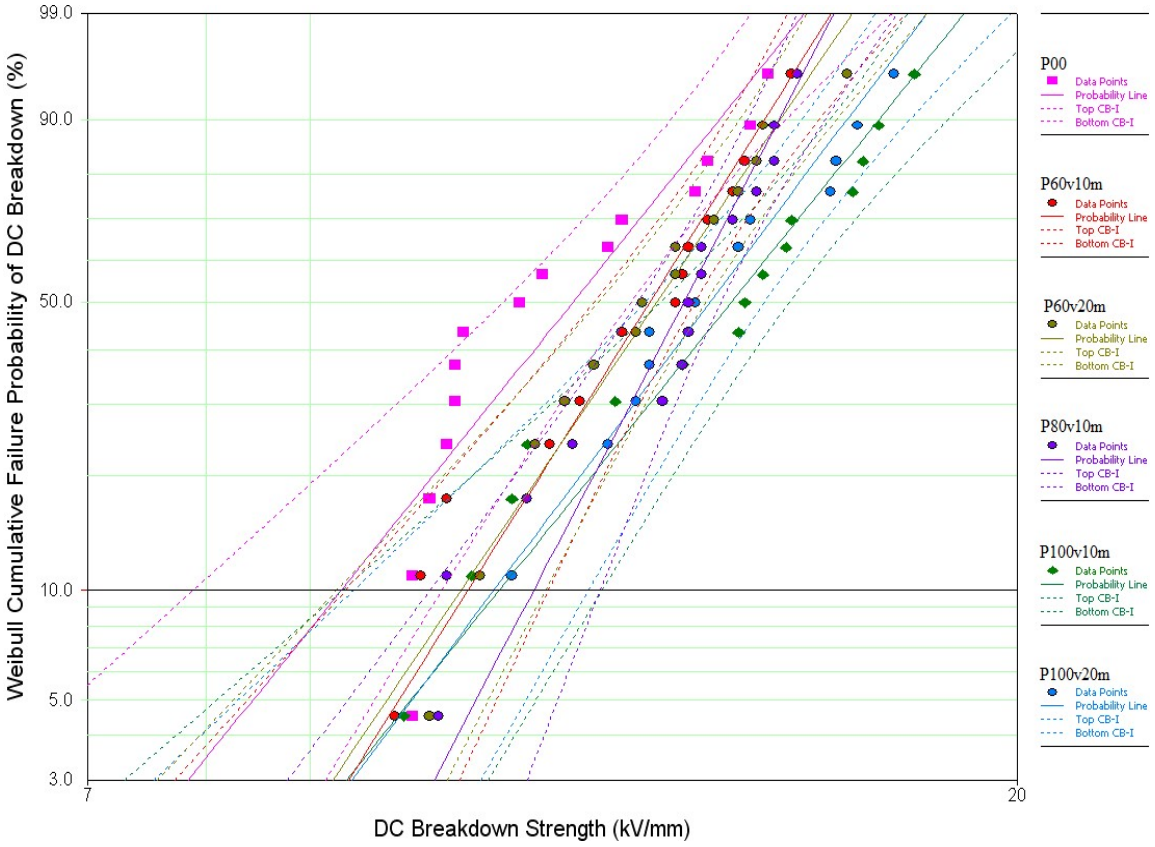

Figure 8-17: Two-parameter Weibull distribution with two-sided 90 % confidence bounds for PEF epoxy resin samples of different plasma voltage and time

Sample	Scale parameter (kV), α	Shape parameter, β
P00	12.7 ± 0.9	7.2 ± 2.3
P60v10m	13.7 ± 0.8	9.2 ± 3.1
P60v20m	13.9 ± 0.8	9.2 ± 2.7
P80v10m	14.2 ± 0.7	11.1 ± 3.8
P100v10m	15.2 ± 1.1	7.2 ± 2.4
P100v20m	14.8 ± 1.0	7.7 ± 2.5

Table 8-9: Weibull parameters α and β for PEF epoxy resin samples of different plasma voltage and time

Sample	Scale parameter (kV), α	Shape parameter, β	Shift parameter (kV), γ
P00	1.9 ± 0.5	0.9 ± 0.2	10.0
P60v10m	6.2 ± 0.4	3.8 ± 0.8	7.4
P60v20m	4.5 ± 0.5	2.6 ± 0.5	9.2
P80v10m	6.3 ± 0.4	4.5 ± 1.0	7.8
P100v10m	7.1 ± 0.6	3.0 ± 0.7	7.9
P100v20m	5.9 ± 0.6	2.9 ± 0.6	8.7

Table 8-10: Weibull parameters α, β and γ for 300 µm surface-fluorinated epoxy resin samples of different fluorination duration undergoing surface flashover test in nitrogen gas estimated using hybrid approach; MLE and LSE.

The result in Figure 8-17 shows an increasing trend in DC surface breakdown strength with the introduction of the fluorinated surface layer. For non-fluorinated epoxy resin sample (P00), lower surface breakdown strength with a low shape parameter is observed. Whereas, the treated samples, in general, show a clear improvement in surface breakdown strength as the treatment voltage and time increases. The highest surface breakdown voltage was observed in sample P100v10m, while sample P100v20m experiences a small drop in surface breakdown voltage due to a lower surface conductivity value. A comparable increase in the bulk breakdown voltage was also discovered by M. Binder et al. [220] in the work done on the CF_4 plasma-treated polymer films. They recorded a 14 % increase in the bulk breakdown voltage. The outcome of the three-parameters Weibull estimates in Table 8-10 doesn't show any clear trends in the three estimated parameters with the increase in degree of fluorination. Sample P100v10m, for example, is estimated to have a minimum breakdown voltage of only 7.9 kV from the three-parameter Weibull estimation, where at the same time, from the two-parameter Weibull estimation, P100v10m possesses the highest scale parameter of 15.2 kV. Likewise, the original P00 sample is estimated to have the highest minimum voltage of 10.0 kV. Such unclear trend can be attributed to the close distribution of the breakdown data. In addition, the data points do not fall on a concave up or down curve, but on a straight line, which is more suited for two-parameter Weibull distribution. The small number of breakdown samples also contributes towards a bias estimation which ultimately return unsatisfactory results.

Nevertheless, the two-parameter Weibull distribution, in general, show a clear improvement in surface breakdown strength as the treatment voltage and time increases. This observation correlates to the relaxation time, T_r (time to reach 1/e of initial potential) from the curve fitting results of surface potential decay in Table 8-7 and Table 8-8. However, there is no relaxation time data available for sample P100v20m. The available relaxation times are plotted against the scale parameter from two-parameter Weibull distribution in Figure 8-18, to further demonstrate the nature of this correlation. In general, as the relaxation time decreases with the fluorination level, the surface breakdown strength increases. The fastest relaxation time can be observed for the P100v10m sample with a value of 0.165 h, i.e. it took P100v10m sample just 594 s to dissipate the accumulated surface charges to 1/e of its initial surface potential. During the voltage ramping in surface breakdown test, with the ramping rate of 100 V s^{-1}, the breakdown would occur in take 2 to 3 min based on the scale parameter. In the case of P100v10m sample, with a relaxation time of 594 s, the decay rate did have a significant impact on the flashover performance (with the highest scale parameter of 15.2 kV) within the ramping time of 2 to 3 min, hence the highest surface flashover strength.

When compared against the breakdown data of direct-fluorinated samples in Table 7-5, The surface flashover performances of PEF samples are comparable to the performances of F30 and F60 samples. The scale parameter from Table 8-9 for all the PEF samples are largely similar to the scale parameter of F30 and F60 samples. This observation is consistent with the surface decay performances of PEF samples, which show broad similarity with the decay of performances of direct-fluorinated samples of F30 and F60.

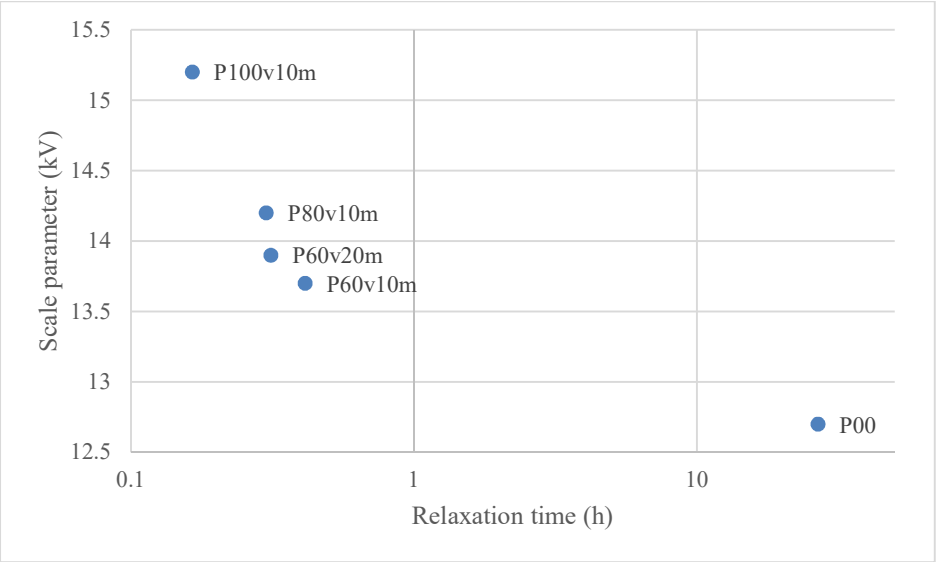

Figure 8-18: The plot of scale parameter against the relaxation time for each PEF samples. As the relaxation time decreases with the fluorination level, the surface breakdown strength increases.

With the introduction of fluorinated substituent onto the surface of epoxy resin sample, the conductivity along the dielectric surface is increased, as proven in DC surface current test. This increment is getting more significant with higher treatment voltage and longer exposure time. Interestingly, improvement in surface conductivity enables trapped charges on the surface to move away faster and, therefore, limits surface charge accumulation from distorting the local electric field. Hence, the increasing trend in DC surface flashover strength over fluorination time. Equally, the increase in breakdown strength is mainly attributed to the increase in the conductivity and decay rate on the surface. When surface charge is easily dispersed, it may limit the number of charge accumulation along the surface and, therefore, reduced their effect in enhancing the localised electric field on epoxy resin. As evidenced by the Weibull distribution for PEF samples, the higher treatment voltage and longer treatment time may result in more charge being dispersed from the surface. Consequently, it will reduce charge transport onto the surface layer and, therefore, suppress space charge accumulation along the surface of epoxy resin under prolonged DC stress.

8.8 CHAPTER SUMMARY

This chapter was designed to determine the effect of the plasma-enhanced fluorination treatment on epoxy resin structure as an alternative to improving the dielectric properties of the material for the use in high voltage DC applications. The PEF treated epoxy resins had been electrically characterised and investigated to give a better understanding of its insulating performance. The results of this study show that the PEF treatment on epoxy resin appears to be a suitable alternative in improving the dielectric properties of cast epoxy resins.

The result from DC surface current test shows a general increase in surface current with respect to the treatment voltage and time. The PEF samples do absorb a substantial amount of surface moisture that enhances its surface conductivity value, but can still retain the intrinsic surface conductivity value when the surface moisture is lost. Also, the fluorinated epoxy resins were subjected to surface potential decay test with negative corona discharge, as well as PEA analysis to determine the charge dynamics in this insulation materials. With an increase in fluorination time, substantial increase in the decay rate of the surface potential is seen due to higher surface current value, similar to the effect in the direct-fluorinated samples of F30 and F60. From the PEA data, a large amount of homocharges is observed inside the bulk, which is not visible inside the direct-fluorinated sample. This is because the introduction of plasma-fluorinated surface layer does not have the same suppression effect as in the direct-fluorination treatment.

Finally, from the two-parameter Weibull estimates of DC flashover data, there is a clear trend of increasing surface breakdown strength as the treatment voltage and time increases, since the incorporation of a fluorinated surface layer on epoxy resin increases the conductivity along the surface. This treatment enables any trapped charges on the surface to move away faster and, therefore, reduces the effect of distortion of the local electric field on the epoxy resin surface. These plasma-treated samples are comparable to F30 and F60 samples from direct-fluorination treatment in terms of surface potential decay rate, and

surface flashover performance. From space charge dynamics study, injected charges can easily accumulate in the bulk of the PEF material as the surface treatment is believed to have reduced the injection barrier, as opposed to direct-fluorination treatment that blocks charge injection into the bulk. Regarding the moisture effect, the PEF treated samples have higher intrinsic surface conductivity value once the surface moisture was dried, which makes it more suitable to be used in a low humidity condition. Indeed, the PEF treatment appears to be a suitable alternative to improving the dielectric properties of the epoxy resin.

CHAPTER NINE: CONCLUSION & FUTURE WORK

This chapter sets out to recap the main conclusions drawn throughout this project and to propose potential future works in order to expand the research further. These conclusions purposely answer the objectives set out at the beginning of this thesis.

9.1 CONCLUSIONS

This whole thesis was designed to determine the effect of the fluorination treatment on epoxy resin structure in enhancing the dielectric properties of the material for the use in high voltage DC applications. There were two routes towards fluorination treatment that were applied in this research; the first one being the direct-fluorination i.e. the materials were treated with fluorine or fluorine-inert gas inside a chamber, while the second alternative is through the use of plasma. A commercial set of Bisphenol-A type epoxy resin (Araldite LY556) together with anhydride hardener (Aradur 917) and imidazole accelerator (DY070) from Huntsman Advanced Materials (with weight ratio 100:90:2) were used throughout this study. The fluorinated epoxy resins had been characterised and electrically investigated to give a better understanding of its insulating performance. The results of this test indicate that the introduction of the fluorinated layer on epoxy resin appears to be a key factor in improving the dielectric properties of epoxy resin.

For characterisation purposes on direct-fluorination treatment, morphological analysis was performed through the use of SEM as reported in Chapter 4. The microscopy images show a clear formation of a layer, getting thicker as the fluorination treatment time increases. By using the confocal mode in Raman spectroscopy analysis, it is clear that the spectrum shows a decrease in C–F absorption and an increase in C–H absorption as the focus goes from the surface fluorinated layer and into the bulk of epoxy resin. From Raman subtraction, a broad Raman peak can be seen in the central section of the subtraction spectrum, and can be attributed to the destruction and disorder in the epoxy structure due to

the fluorination treatment. DC surface current measurement was also carried out to determine the extent of dielectric improvement that the fluorination treatment has had on the epoxy resin samples. The space charge accumulation is closely linked to the characteristics of the fluorinated layer and, therefore, this treatment plays an important role in dielectric performance.

In chapter 5, the direct-fluorinated epoxy resins were subjected to surface potential decay test with negative corona discharge, as well as PEA analysis in order to determine the electrical properties of this insulation materials. With the increase in fluorination time, substantial increase in the decay rate of the surface potential is observed due to the slight improvement in surface current. From the PEA waveform of the fluorinated epoxy sample, a large amount of heterocharges is observed near the vicinity of both electrodes, which is not visible inside the untreated sample. This is because the introduction of the fluorinated surface layer is believed to have a suppression effect, which effectively blocks further charge injection from the electrodes into the epoxy resin sample. The mechanism that governs the decay process is believed to be conduction along the surface as the introduction of fluorinated layer suppresses charge injection into the bulk.

In addition to PEA analysis, the DC flashover test was also performed on the direct-fluorinated epoxy resin samples. For untreated epoxy resin sample, lower surface breakdown strength with a high shape parameter is observed. However, the direct-fluorinated samples show a clear improvement in surface breakdown strength with lower shape parameter. There is a clear trend of increasing surface breakdown strength as the fluorination time increases, since the incorporation of the fluorinated surface layer on epoxy resin increases the conductivity along the surface. This enables any trapped charges on the surface to leak away faster and, therefore, reduces the effect of distortion of local electric field on the epoxy resin surface. Direct-fluorination treatment is also believed to deepen the traps in the surface layer and the charges trapped in the deep traps may block or shield further charge injection. The results of this study indicate that the introduction of the

fluorinated layer on epoxy resin appears to be a key factor in improving the dielectric properties of the epoxy resin.

The improvement in the surface current value for the direct-fluorination samples largely comes from the treated surface capacity to absorb moisture onto the surface. In an extreme environment where the absorbed surface moisture is dried away, the fluorinated samples show surface conductivity value and decay rate similar to those of original untreated sample. But in a mild condition, as in the insulating gas of nitrogen at room temperature, the fluorinated samples still possess the dielectric improvement supposedly come from the chemical treatment; increased surface DC current and faster surface potential decay rate. The role of absorbed moisture has far outweighed the role of physicochemical change as a direct result from the fluorination treatment. Indeed, the presence of absorbed water is considered to be the limiting factor towards the improvement of the dielectric properties in the treated material. It is also noteworthy that fluorinated samples in nitrogen gas would take an estimated ~40 to ~60 days of drying time to possess ratios of $\boldsymbol{A_m}$ similar to F00. As it stands, direct-fluorination treatment on spacers will only improve the performance of GIS operating with dry gas for a short period, as long as the surface moisture can be retained.

As an alternative to direct-fluorination, another batch of epoxy resin samples was treated using the plasma enhanced fluorination treatment. The result from DC surface current test shows a general increase in surface current with respect to the treatment voltage and time. The PEF sample does absorb a substantial amount of surface moisture that enhances its surface current value, but can still retain the intrinsic surface conductivity value once the surface moisture is lost. With the increase in treatment voltage and time, substantial increases in the decay rate of surface potential can be observed due to the increase in its surface current value, comparable to the effect in direct-fluorinated samples of F30 and F60. From the PEA waveform, a large amount of homocharges is observed inside the bulk, which is not visible for the direct-fluorinated samples. This is because the introduction of plasma-fluorinated surface layer does not possess the same suppression effect as in direct-

fluorination treatment. Finally, from the DC flashover test, there is a clear trend of increasing surface breakdown strength as the treatment voltage and time increases.

In a nutshell, the results of this research show that the introduction of the fluorinated layer on epoxy resin, either through direct-fluorination or plasma-enhanced fluorination treatment, appears to be a key factor in improving the dielectric properties of the epoxy resin. The presence of absorbed water is considered to be the limiting factor towards the improvement of the dielectric properties in the treated material. More work is needed before this treatment can be applied on the insulation in high voltage DC equipment as direct-fluorination treatment on spacers will only improve the performance of GIS operating with dry gas for a short period, as long as the surface moisture can be retained.

9.2 FUTURE WORK

There are several areas of this research present potential for further study. For one, the DC flashover test and surface decay measurement are performed under normal atmospheric pressure that subject to changing environmental conditions such as pressure, humidity and gas present in the volume surrounding the polymeric insulator. The author suggests that before surface fluorinated epoxy resin goes ahead into the design for insulation spacer in high voltage DC GIS systems, a study similar to this one should be carried out inside pressurised SF_6-filled chamber to mimic the actual working environment of a GIS system. In doing so, the results obtained will be more practical and similar to the real working system.

As far as the simulation work is concerned, modelling the trapped charges on the surface of insulation layer would give a better interpretation on the distribution of electric field and the charge density lines. The current simulation only shows the initial stage of charge density distribution for different thickness of fluorination layer without giving any information on the influence of the accumulated surface charges. It would also be

interesting to simulate the surface potential decay of epoxy sample with a surface layer of differing conductivity in order to see clearly the movement of charges from the surface.

It would also be interesting to assess the effects of other types of plasma treatment gas such as CHF_3, C_3F_8, C_4F_8, NF_3, SF_6, F_2, NF_3, and ClF_3 onto the surface of epoxy resin and its influence on the dielectric properties. Plasma treatment does not yield dangerous by product, unlike the case with direct-fluorination treatment.

Finally, the current work using the sample of 4 cm x 4 cm size demonstrates that the fluorination treatment does have a major impact on enhancing its dielectric properties, as long as the surface moisture can be retained. Therefore, the use of a full-scale cast epoxy resin sample as an insulating spacer inside a working GIS compartment for a long period (beyond 7 days) is worth exploring with a view to producing the best spacer design for HVDC GIS.

REFERENCES

[1] H. Koch, *Gas-Insulated Transmission Lines (GIL)*: John Wiley & Sons, Ltd, 2012.

[2] B. H. E. Limited, *Handbook of Switchgears*: The McGraw-Hill Companies, 2007.

[3] E. Volpov, "Dielectric strength coordination and generalized spacer design rules for HVAC/DC SF6 gas insulated systems," *Dielectrics and Electrical Insulation, IEEE Transactions on,* vol. 11, pp. 949-963, 2004.

[4] E. Volpov, "Electric field modeling and field formation mechanism in HVDC SF₆ gas insulated systems," *Dielectrics and Electrical Insulation, IEEE Transactions on,* vol. 10, pp. 204-215, 2003.

[5] K. D. Srivastava and M. M. Morcos, "A review of some critical aspects of insulation design of GIS/GIL systems," in *Transmission and Distribution Conference and Exposition, 2001 IEEE/PES*, pp. 787-792 vol.2, 2001.

[6] D. D. Chowdary and J. Amarnath, "Electric field analysis at the triple junction of a optimum profile disc type spacer in SF6 gas insulated system with abnormalities under DC voltages," in *Electrical Insulation and Dielectric Phenomena (CEIDP), 2011 Annual Report Conference on*, pp. 215-218, 2011.

[7] H. Fujinami, T. Takuma, M. Yashima, and T. Kawamoto, "Mechanism and effect of DC charge accumulation on SF6 gas insulated spacers," *Power Delivery, IEEE Transactions on,* vol. 4, pp. 1765-1772, 1989.

[8] H. Hama, T. Hikosaka, S. Okabe, and H. Okubo, "Cross-equipment study on charging phenomena of solid insulators in high voltage equipment," *Dielectrics and Electrical Insulation, IEEE Transactions on,* vol. 14, pp. 508-519, 2007.

[9] K. Nakanishi, A. Yoshioka, Y. Arahata, and Y. Shibuya, "Surface Charging On Epoxy Spacer At Dc Stress In Compressed SF6 GAS," *Power Apparatus and Systems, IEEE Transactions on,* vol. PAS-102, pp. 3919-3927, 1983.

[10] S. Okabe, "Phenomena and mechanism of electric charges on spacers in gas insulated switchgears," *Dielectrics and Electrical Insulation, IEEE Transactions on,* vol. 14, pp. 46-52, 2007.

[11] S. O. Kaneko, Shigemitsu; Kobayashi, Takayuki; Nojima, Kenichi; Takei, Masafumi; Miyamoto, Taketoshi, " Insulation Resistance under DC Stress and Electrification Characteristics of GIS Epoxy Insulator," *IEEJ Transactions on Power and Energy,* vol. 127, pp. 1009-1015, 2007.

[12] J. H.-J. K. K.-C. C. Seung-Kil, "Optimal Design of a Permittivity Graded Spacer Configuration in a Gas Insulated Switchgear," *Journal of the Korean Physical Society,* vol. 55, pp. 1803-1807, 2009.

[13] M. Kurimoto, K. Kato, M. Hanai, Y. Hoshina, M. Takei, and H. Okubo, "Application of functionally graded material for reducing electric field on electrode and spacer interface," *Dielectrics and Electrical Insulation, IEEE Transactions on,* vol. 17, pp. 256-263, 2010.

[14] S. Li, T. Zhang, Q. Huang, W. Li, F. Ni, and J. Li, "Improvement of Surface Flashover Performance of Al 2 O 3 Ceramics in Vacuum by Adopting A-B-A Insulation System," *Plasma Science and Technology,* vol. 13, p. 235, 2011.

[15] T. Nitta and K. Nakanishi, "Charge accumulation on insulating spacers for HVDC GIS," *Electrical Insulation, IEEE Transactions on,* vol. 26, pp. 418-427, 1991.

[16] F. Messerer, M. Finkel, and W. Boeck, "Surface charge accumulation on HVDC-GIS-spacer," in *Electrical Insulation, 2002. Conference Record of the 2002 IEEE International Symposium on*, pp. 421-425, 2002.

[17] F. Messerer and W. Boeck, "High resistance surface coating of solid insulating components for HVDC metal enclosed equipment," in *High Voltage Engineering, 1999. Eleventh International Symposium on (Conf. Publ. No. 467)*, pp. 63-66 vol.4, 1999.

[18] F. Messerer and W. Boeck, "Gas insulated substation (GIS) for HVDC," in *Electrical Insulation and Dielectric Phenomena, 2000 Annual Report Conference on*, pp. 698-702 vol.2, 2000.

[19] J. Zhijie, Z. Bin, T. Xiaoya, and Z. Qiaogen, "Flashover Characteristics along the Insulator in SF6 Gas under DC Voltage," in *Power and Energy Engineering Conference, 2009. APPEEC 2009. Asia-Pacific*, pp. 1-4, 2009.

[20] A. P. Kharitonov, "Direct fluorination of polymers—From fundamental research to industrial applications," *Progress in Organic Coatings,* vol. 61, pp. 192-204, 2008.

[21] A. Tressaud, E. Durand, C. Labrugère, A. P. Kharitonov, and L. N. Kharitonova, "Modification of surface properties of carbon-based and polymeric materials through fluorination routes: From fundamental research to industrial applications," *Journal of Fluorine Chemistry,* vol. 128, pp. 378-391, 2007.

[22] L. W. McKeen, *Fluorinated Coatings and Finishes Handbook*: William Andrew Publishing, 2006.

[23] J. Yue, A. Zhenlian, L. Chenxia, Z. Feihu, and Z. Yewen, "Influence of oxyfluorination time on space charge behavior in polyethylene," *Dielectrics and Electrical Insulation, IEEE Transactions on,* vol. 17, pp. 1814-1823, 2010.

[24] Z. An, Q. Yang, C. Xie, Y. Jiang, F. Zheng, and Y. Zhang, "Suppression of charge injection to linear low density polyethylene by surface fluorination modification," in *Electrical Insulating Materials, 2008. (ISEIM 2008). International Symposium on*, pp. 368-371, 2008.

[25] R. J. J. W. Jean-Pierre Pascault, *Epoxy Polymers: New Materials and Innovatio*: Wiley-VCH Verlag GmbH & Co. KGaA, Weinheim, 2010.

[26] S. Kaneko, S. Okabe, T. Kobayashi, K. Nojima, M. Takei, and T. Miyamoto, "Insulation resistance under DC stress and electrification characteristics of GIS epoxy insulator," *Electrical Engineering in Japan,* vol. 168, pp. 6-13, 2009.

[27] Q. Wang, "The Effect of Nano Size Fillers on Electrical Performance of Epoxy Resin" PhD thesis," PhD, ECS, University of Southampton, UK, 2012.

[28] Y. Tanaka and H. Kakiuchi, "Study of epoxy compounds. Part I. Curing reactions of epoxy resin and acid anhydride with amine and alcohol as catalyst," *Journal of Applied Polymer Science,* vol. 7, pp. 1063-1081, 1963.

[29] M. F. G.-L. a. P. M. D Harran, "Avancement de la réaction chimique au point de gel d'une résine epoxyde: Systèmes (diglycidyl ether du bisphénol A-diamino diphényl méthane et diglycidyl ether du bisphénol A-diamino diphényl sulfone)," *European Polymer Journal,* vol. 24, p. 225, 1988.

[30] P. J. Flory, *Principles of Polymer Chemistry*. New York: Cornell University, 1988.

[31] H. H. Winter, *Techniques in Rheological Measurement (A.A. Ed)*. London: Chapman & Hall, 1997.

[32] D. J. O'Brien, P. T. Mather, and S. R. White, "Viscoelastic Properties of an Epoxy Resin during Cure," *Journal of Composite Materials,* vol. 35, pp. 883-904, May 15, 2001 2001.

[33] J. K. G. a. J. B. Enns, "On the cure and properties of thermosetting polymers using Torsional Braid Analysis," *Trends in Polymer Science,* vol. 2, p. 406, 1994.

[34] a. J. K. G. G Wisanrakki, "The Glass Transition Temperature (Tg) as an Index of Chemical Conversion for a High-Tg Amine/Epoxy System: Chemical and Diffusion Controlled Reaction Kinetics," *Journal of Coatings Technology,* vol. 62, p. 35, 1990.

[35] M. Aronhime and J. Gillham, "Time-temperature-transformation (TTT) cure diagram of thermosetting polymeric systems," in *Epoxy Resins and Composites III*. vol. 78, K. Dušek, Ed., ed: Springer Berlin Heidelberg, pp. 83-113, 1986.

[36] J. M. H Stutz, and K Nuebeche, "Kinetics of thermoset cure and polymerization in the glass transition region," *Journal of Polymer Science Part A: Polymer Chemistry,* vol. 31, p. 1879, 1993.

[37] G. V. Assche, A. V. Hemelrijck, H. Rahier, and B. V. Mele, "Modulated differential scanning calorimetry: isothermal cure and vitrification of thermosetting systems," *Thermochimica Acta,* vol. 268, pp. 121-142, 1995.

[38] R. B. Prime, *Thermal Characterization of Polymeric Materials*. San Diego: Academic Press, 1997.

[39] I. Hamerton, *Recent Developments in Epoxy Resins*: Rapra Technology Limited, 1997.

[40] C. A. May, *Epoxy Resins: Chemistry and Technology*: Marcel Dekker Inc, 1988.

[41] H. G. Tsuyoshi Nakajima, *Fluorinated Materials for Energy Conversion*: Elsevier Ltd, 2005.

[42] E. Kissa, *Fluorinated Surfactants and Repellents* vol. 97: Marcel Dekker, Inc., 2001.

[43] Z. An, Q. Yang, C. Xie, Y. Jiang, F. Zheng, and Y. Zhang, "Suppression effect of surface fluorination on charge injection into linear low density polyethylene," *Journal of Applied Physics,* vol. 105, p. 064102, 2009.

[44] A. P. Kharitonov, "Practical applications of the direct fluorination of polymers," *Journal of Fluorine Chemistry,* vol. 103, pp. 123-127, 2000.

[45] A. P. Kharitonov, R. Taege, G. Ferrier, V. V. Teplyakov, D. A. Syrtsova, and G. H. Koops, "Direct fluorination—Useful tool to enhance commercial properties of polymer articles," *Journal of Fluorine Chemistry,* vol. 126, pp. 251-263, 2005.

[46] A. Zhenlian, L. Chenxia, C. Xuan, Z. Feihu, and Z. Yewen, "Correlation between space charge accumulation in polyethylene and its fluorinated surface layer characteristics," *Journal of Physics D: Applied Physics,* vol. 45, p. 035302, 2012.

[47] A. Tressaud, E. Durand, and C. Labrugère, "Surface modification of several carbon-based materials: comparison between CF4 rf plasma and direct F2-gas fluorination routes," *Journal of Fluorine Chemistry,* vol. 125, pp. 1639-1648, 2004.

[48] A. Fridman, A. Chirokov, and A. Gutsol, "Non-thermal atmospheric pressure discharges," *Journal of Physics D: Applied Physics,* vol. 38, p. R1, 2005.

[49] G. Greene, G. Yao, and R. Tannenbaum, "Deposition and Wetting Characteristics of Polyelectrolyte Multilayers on Plasma-Modified Porous Polyethylene," *Langmuir,* vol. 20, pp. 2739-2745, 2004/03/01 2004.

[50] K. M. Baumgärtner, J. Schneider, A. Schulz, J. Feichtinger, and M. Walker, "Short-time plasma pre-treatment of polytetrafluoroethylene for improved adhesion," *Surface and Coatings Technology,* vol. 142–144, pp. 501-506, 2001.

[51] A. J. H. Maas, M. M. Viitanen, and H. H. Brongersma, "Low-energy ion scattering (LEIS) study of the ageing of oxygen-plasma-treated high-density polyethylene (HDPE) surfaces," *Surface and Interface Analysis,* vol. 30, pp. 3-6, 2000.

[52] A. C. J. Michelle L. Steen, Ellen R. Fisher, "Hydrophilic modification of polymeric membranes by low temperature H2O plasma treatment," *Journal of Membrane Science,* vol. 204, pp. 341-357, 2002.

[53] H. S. Choi, V. V. Rybkin, V. A. Titov, T. G. Shikova, and T. A. Ageeva, "Comparative actions of a low pressure oxygen plasma and an atmospheric pressure glow discharge on the surface

modification of polypropylene," *Surface and Coatings Technology,* vol. 200, pp. 4479-4488, 2006.

[54] M. Moravej, X. Yang, R. Hicks, J. Penelon, and S. Babayan, "A radio-frequency nonequilibrium atmospheric pressure plasma operating with argon and oxygen," *Journal of applied physics,* vol. 99, pp. 93305-93305, 2006.

[55] M. A. Lieberman and A. J. Lichtenberg, *Principles of plasma discharges and materials processing*: John Wiley & Sons, 2005.

[56] P. Raizer Yu, "Gas discharge physics," ed: Berlin: Springer, 1991.

[57] R. Woo, "RF voltage breakdown and the Paschen curve," in *IEEE Proceedings*, 1974, p. 521.

[58] J. M. Meek and J. D. Craggs, "Electrical breakdown of gases," 1978.

[59] S. Babayan, J. Jeong, V. Tu, J. Park, G. Selwyn, and R. Hicks, "Deposition of silicon dioxide films with an atmospheric-pressure plasma jet," *Plasma Sources Science and Technology,* vol. 7, p. 286, 1998.

[60] A. Schutze, J. Y. Jeong, S. E. Babayan, J. Park, G. S. Selwyn, and R. F. Hicks, "The atmospheric-pressure plasma jet: a review and comparison to other plasma sources," *IEEE transactions on plasma science,* vol. 26, pp. 1685-1694, 1998.

[61] R. J. Zollweg and R. W. Liebermann, "Electrical conductivity of nonideal plasmas," *Journal of Applied Physics,* vol. 62, pp. 3621-3627, 1987.

[62] G. Röpke, "Quantum-statistical approach to the electrical conductivity of dense, high-temperature plasmas," *Physical Review A,* vol. 38, pp. 3001-3016, 1988.

[63] L. Kowa Thermo Technologies & Products CO. (2014). *Atmospheric Pressure Plasma Treatment System*. Available: http://www.kowaden.co.jp/plasma_e.html

[64] A. H. Cookson "Review of high-voltage gas breakdown and insulators in compressed gas" *IEE Proceedings A (Physical Science, Measurement and Instrumentation, Management and Education, Reviews) 128(4),* 303-312, 1981.

[65] J. R. Laghari, "Spacer Flashover in Compressed Gases," *Electrical Insulation, IEEE Transactions on,* vol. EI-20, pp. 83-92, 1985.

[66] T. Nitta, Y. Shibuya, Y. Fujiwara, Y. Arahata, H. Takahashi, and H. Kuwahara, "Factors Controlling Surface Flashover in SF6 Gas Insulated Systems," *Power Apparatus and Systems, IEEE Transactions on,* vol. PAS-97, pp. 959-968, 1978.

[67] A. H. Cookson "Electrical breakdown for uniform fields in compressed gases" *Proceedings of the Institution of Electrical Engineers 117(1),* 269-280, 1970.

[68] A. De Lorenzi, L. Grando, A. Pesce, P. Bettini, and R. Specogna, "Modeling of epoxy resin spacers for the 1 MV DC gas insulated line of ITER neutral beam injector system," *Dielectrics and Electrical Insulation, IEEE Transactions on,* vol. 16, pp. 77-87, 2009.

[69] E. Volpov, "HVDC gas insulated apparatus: electric field specificity and insulation design concept," *Electrical Insulation Magazine, IEEE,* vol. 18, pp. 7-36, 2002.

[70] W. Nelson, "Applied Life Data Analysis," 1982.

[71] H. Hirose, "Maximum likelihood estimation in the 3-parameter Weibull distribution. A look through the generalized extreme-value distribution," *IEEE transactions on dielectrics and electrical insulation,* vol. 3, pp. 43-55, 1996.

[72] J. C. Fothergill, "Estimating the cumulative probability of failure data points to be plotted on Weibull and other probability paper," *Electrical Insulation, IEEE Transactions on,* vol. 25, pp. 489-492, 1990.

[73] T. I. o. E. a. E. Engineers, ""IEEE Guide for the Statistical Analysis of Electrical Insulation Voltage Endurance Data," in *ANSI/IEEE Std. 930* ed. New York: The Institute of Electrical and Electronics Engineers, 1987.

[74] W. E. Collection. *The Generalized Gamma Distribution*. Available: http://reliawiki.org/index.php/The Generalized_Gamma_Distribution

[75] Z. Xu, "comparing graphical method and a modified method to fit weibull distribution," 2012.

[76] P. Morshuis and M. Jeroense, "Space charge measurements on impregnated paper: a review of the PEA method and a discussion of results," *Electrical Insulation Magazine, IEEE,* vol. 13, pp. 26-35, 1997.

[77] A. Cherifi, M. A. Dakka, and A. Toureille, "The validation of the thermal step method," *Electrical Insulation, IEEE Transactions on,* vol. 27, pp. 1152-1158, 1992.

[78] R. Gerhard-Multhaupt, "Analysis of pressure-wave methods for the nondestructive determination of spatial charge or field distributions in dielectrics," *Physical Review B,* vol. 27, pp. 2494-2503, 1983.

[79] P. Laurençeau, G. Dreyfus, and J. Lewiner, "New Principle for the Determination of Potential Distributions in Dielectrics," *Physical Review Letters,* vol. 38, pp. 46-49, 1977.

[80] Y. Li, M. Yasuda, and T. Takada, "Pulsed electroacoustic method for measurement of charge accumulation in solid dielectrics," *Dielectrics and Electrical Insulation, IEEE Transactions on,* vol. 1, pp. 188-195, 1994.

[81] M. A. T. Hirai, "Relationship between electrode polarization and electrical actuation of dielectric PVC gel actuators," *Royal Society of Chemistry,* vol. 8, pp. 3694-3699, 2012.

[82] A. Smekal, " The quantum theory of dispersion," *Naturwissenschaften,* vol. 11, p. 873, 1923.

[83] C. V. R. K. S. Krishnan, " The optical analog of the Compton effect," *Nature,* vol. 121, p. 711, 1928.

[84] J. Laserna "An Introduction to Raman Spectroscopy" 2009.

[85] andor.com. *An introduction to Raman Spectroscopy* Available: http://www.andor.com/learning-academy/raman-spectroscopy-an-introduction-to-raman-spectroscopy

[86] R. Tabaksblat, R. J. Meier, and B. J. Kip, "Confocal Raman Microspectroscopy: Theory and Application to Thin Polymer Samples," *Applied Spectroscopy,* vol. 46, pp. 60-68, 1992.

[87] P. D. Zoon. *Single Molecule Spectroscopy with Confocal Microscopy*. Available: http://staff.science.uva.nl/~zoon/sms/SMS.html

[88] M. Knoll, "Aufladepotentiel und sekundäremission elektronenbestrahlter körper," *Zeitschrift für technische Physik,* vol. 16, p. 467, 1935.

[89] I. L. Hosier, "Morphology and Electrical Properties of Polyethylene Blends," PhD, University of Southampton, UK, 1996.

[90] *Microprobe-SEM: Instrumentation*. Available: http://www4.nau.edu/microanalysis/Microprobe-SEM/Instrumentation.html

[91] R. Hessel and B. Gross, "Escape depth of secondary electrons from electron-irradiated polymers," *Electrical Insulation, IEEE Transactions on,* vol. 27, pp. 831-834, 1992.

[92] S. Laboratories. *How SEM-EDS Works*. Available: http://www.seallabs.com/how-sem-eds-works.html

[93] J. Paterson, J. Chapman, W. Nicholson, and J. Titchmarsh, "Characteristic X-ray production cross-sections for standardless elemental analysis in EDX," *Journal of Microscopy,* vol. 154, pp. 1-17, 1989.

[94] S. J. B. Reed, *Electron microprobe analysis and scanning electron microscopy in geology*: Cambridge University Press, 2005.

[95] W. Van Borm and F. Adams, "Recent advances in electron-probe x-ray microanalysis," *Analytica chimica acta,* vol. 218, pp. 185-215, 1989.

[96] J. C. Russ, *Fundamentals of Energy Dispersive X-Ray Analysis: Butterworths Monographs in Materials*: Butterworth-Heinemann, 2013.

[97] B. K. Agarwal, *X-ray spectroscopy: an introduction* vol. 15: Springer, 2013.

[98] M. I. G. S. I. Shinohara, "A decay process of surface electric charges across polyethylene film," *Journal of Applied Physics,* vol. 6, pp. 793-794, 1967.

[99] P. Molinié, "Charge injection in corona-charged polymeric films: potential decay and current measurements," *Journal of Electrostatics,* vol. 45, pp. 265-273, 1999.

[100] M. A. Noras, "Non-contact surface charge/voltage measurements: Capacitive probe-principle of operation," *Trek Application Note,* 2002.

[101] M. K. DA Hill, *The Measurement Instrumentation and Sensor Handbook*: CRC Press LLC, 1999.

[102] P. Llovera, P. Molinié, A. Soria, and A. Quijano, "Measurements of electrostatic potentials and electric fields in some industrial applications: Basic principles," *Journal of Electrostatics,* vol. 67, pp. 457-461, 2009.

[103] M. Instruments. *Electric Field Mill operation*. Available: http://www.missioninstruments.com/pages/learning/about_fm2.html

[104] Huntsman. *Hot Curing Epoxy Matrix System*. Available: http://www.mouldlife.net/ekmps/shops/mouldlife/resources/Other/ly-556-917-dy-070.pdf

[105] X. Gong, H. Kang, Y. Liu, and S. Wu, "Decomposition mechanisms and kinetics of amine/anhydride-cured DGEBA epoxy resin in near-critical water," *RSC Advances,* vol. 5, pp. 40269-40282, 2015.

[106] V. T. Nguyen, "Nanodielectrics for Machine Insulation," PhD, University of Southampton, UK, 2013.

[107] J. J. Reisinger and M. A. Hillmyer, "Synthesis of fluorinated polymers by chemical modification," *Progress in Polymer Science,* vol. 27, pp. 971-1005, 2002.

[108] A. P. Kharitonov and L. N. Kharitonova, "Surface modification of polymers by direct fluorination: a convenient approach to improve commercial properties of polymeric articles," *Pure and Applied Chemistry,* vol. 81, pp. 451-471, 2009.

[109] D. F. Persico and R. J. Lagow, "Synthesis of branched perfluoro ethers by direct fluorination, copolymers based on hexafluoroacetone," *Macromolecules,* vol. 18, pp. 1383-1387, 1985.

[110] L. Yaqiang, A. Zhenlian, C. Jun, Z. Yewen, and Z. Feihu, "Significant suppression of surface charge accumulation on epoxy resin by direct fluorination," *Dielectrics and Electrical Insulation, IEEE Transactions on,* vol. 19, pp. 1143-1150, 2012.

[111] H. Seiler, "Secondary electron emission in the scanning electron microscope," *Journal of Applied Physics,* vol. 54, pp. R1-R18, 1983.

[112] G. d. S. Padilha, V. Mansanares, and J. R. Bartoli, "Effect of plasma fluorination variables on the deposition and growth of partially fluorinated polymer over PMMA films," *Polímeros,* vol. 23, pp. 585-589, 2013.

[113] Y. Liu, Z. An, Q. Yin, F. Zheng, and Y. Zhang, "Effective modulation of surface conductivity of epoxy resin insulators by direct fluorination," in *Solid Dielectrics (ICSD), 2013 IEEE International Conference on*, pp. 1072-1075, 2013.

[114] L. Yaqiang, A. Zhenlian, Y. Qianqian, Z. Feihu, L. Qingquan, and Z. Yewen, "Characteristics and electrical properties of epoxy resin surface layers fluorinated at different temperatures," *Dielectrics and Electrical Insulation, IEEE Transactions on,* vol. 20, pp. 1859-1868, 2013.

[115] M. Meunier, N. Quirke, and A. Aslanides, "Molecular modeling of electron traps in polymer insulators: Chemical defects and impurities," *The Journal of Chemical Physics,* vol. 115, pp. 2876-2881, 2001.

[116] A. Zhenlian, Y. Qianqian, L. Yaqiang, Z. Feihu, L. Qingquan, and Z. Yewen, "Modulation of surface electrical properties of epoxy resin insulator by changing fluorination temperature and time," *Dielectrics and Electrical Insulation, IEEE Transactions on,* vol. 22, pp. 526-534, 2015.

[117] B. J. Ryan and K. M. Poduska, "Roughness effects on contact angle measurements," *American Journal of Physics,* vol. 76, pp. 1074-1077, 2008.

[118] U. o. C. Riverside, "Introduction to Energy Dispersive X-ray Spectrometry (EDS)," *Central Facility for Advanced Microscopy and Microanalysis,* p. 1.

[119] F. J. du Toit and R. D. Sanderson, "Surface fluorination of polypropylene: 1. Characterisation of surface properties," *Journal of Fluorine Chemistry,* vol. 98, pp. 107-114, 1999.

[120] A. Mohamad, G. Chen, Y. Zhang, and Z. An, "Surface fluorinated epoxy resin for high voltage DC application," *Dielectrics and Electrical Insulation, IEEE Transactions on,* vol. 22, pp. 101-108, 2015.

[121] R. J. Lagow and J. L. Margrave, "Direct Fluorination: A “New” Approach to Fluorine Chemistry," in *Progress in Inorganic Chemistry*, ed: John Wiley & Sons, Inc., pp. 161-210, 2007

[122] V. Nazarov, "Surface Modification of Polymers," *Moscow, MSUPA,* 2008.

[123] N. Hara, H. Fukumoto, and M. Watanabe, "In-situ Kinetic Studies on Direct Fluorination of Thin Polyethylene Films with QCM," *Bulletin of the Chemical Society of Japan,* vol. 68, pp. 1232-1238, 1995.

[124] Y.-H. Lin, K.-H. Liao, C.-K. Huang, N.-K. Chou, S.-S. Wang, S.-H. Chu*, et al.*, "Superhydrophobic films of UV-curable fluorinated epoxy acrylate resins," *Polymer International,* vol. 59, pp. 1205-1211, 2010.

[125] Y. HongJun, Z. Wei, L. HaoDong, L. ZiGeng, Z. GuiMing, and Y. Yong, "Synthesis and characterization of fluorinated carbon nanotubes for lithium primary batteries with high power density," *Nanotechnology,* vol. 24, p. 424003, 2013.

[126] H. V. V. Křesálek, "Quasi real-time monitoring of epoxy resin crosslinking via Raman microscopy," *International journal of mathematical models and methods in applied science,* vol. 5, pp. 1197-1204, 2011.

[127] L. C. Boogh, R. J. Meier, H. H. Kausch, and B. J. Kip, "A Raman microscopy study of stress transfer in high-performance epoxy composites reinforced with polyethylene fibers," *Journal of Polymer Science Part B: Polymer Physics,* vol. 30, pp. 325-333, 1992.

[128] M. Bernard, S. Duval, S. Joiret, M. Keddam, F. Ropital, and H. Takenouti, "Analysis of corrosion products beneath an epoxy-amine varnish film," *Progress in organic coatings,* vol. 45, pp. 399-404, 2002.

[129] R. Wang and T. Xie, "Macroscopic evidence of strong cation–π interactions in a synthetic polymer system," *Chemical Communications,* vol. 46, pp. 1341-1343, 2010.

[130] G. Legeay, A. Coudreuse, J.-M. Legeais, L. Werner, A. Bulou, J.-Y. Buzaré*, et al.*, "AF fluoropolymer for optical use: spectroscopic and surface energystudies; comparison with other fluoropolymers," *European polymer journal,* vol. 34, pp. 1457-1465, 1998.

[131] E. Mickelson, C. Huffman, A. Rinzler, R. Smalley, R. Hauge, and J. Margrave, "Fluorination of single-wall carbon nanotubes," *Chemical physics letters,* vol. 296, pp. 188-194, 1998.

[132] K. Takai, H. Sato, T. Enoki, N. Yoshida, F. Okino, H. Touhara*, et al.*, "Effect of Fluorination on Nano-Sized π-Electron Systems," *Journal of the Physical Society of Japan,* vol. 70, pp. 175-185, 2001.

[133] J. S. Im, E. Jeong, S. J. In, and Y.-S. Lee, "The impact of fluorinated MWCNT additives on the enhanced dynamic mechanical properties of e-beam-cured epoxy," *Composites Science and Technology,* vol. 70, pp. 763-768, 2010.

[134] Keithley, "Volume and Surface Resistivity Measurements of Insulating Materials Using the Model 6517A Electrometer/High Resistance Meter," in *Keithley Application Note Series*, ed, pp. 1-4.

[135] V. Adamec and J. Calderwood, "Electrical conduction and polarisation phenomena in polymeric dielectrics at low fields," *Journal of Physics D: Applied Physics,* vol. 11, p. 781, 1978.

[136] V. Adamec and J. H. Calderwood, "Electrical conduction and polarisation phenomena in polymeric dielectrics at low fields," *Journal of Physics D: Applied Physics,* vol. 11, p. 781, 1978.

[137] A. R. Blythe and D. Bloor, *Electrical properties of polymers*: Cambridge University Press, 2005.

[138] A. P. Kharitonov, G. V. Simbirtseva, A. Tressaud, E. Durand, C. Labrugère, and M. Dubois, "Comparison of the surface modifications of polymers induced by direct fluorination and rf-plasma using fluorinated gases," *Journal of Fluorine Chemistry,* vol. 165, pp. 49-60, 2014.

[139] A. Crisci, B. Gosse, J. Gosse, and V. Ollier-Duréault, "Surface-potential decay due to surface conduction," *The European Physical Journal Applied Physics,* vol. 4, pp. 107-116, 1998.

[140] A. Mohamad, G. Chen, Y. Zhang, and Z. An, "Influence of fluorination time on surface flashover of polymeric insulation," in *Electrical Insulation and Dielectric Phenomena (CEIDP), 2013 IEEE Conference on*, pp. 482-485, 2013

[141] K. Y. Lau, "Structure and Electrical Properties of Silica-based Polyethylene Nanocomposites," PhD, FACULTY OF PHYSICAL SCIENCES AND ENGINEERING, UNIVERSITY OF SOUTHAMPTON, 2013.

[142] H. Wintle, "Conduction processes in polymers," *Engineering dielectrics. Vol IIA, Electrical properties of solid insulating materials: molecular structure and electrical behaviour. ASTM Special Technical Publication,* vol. 783, pp. 239-354, 1983.

[143] W. S. Z. E. Kuffel, J. Kuffel, *High Voltage Engineering: Fundamentals*: Pergamon Press, 2000.

[144] Y. Zhuang, "Charge Transport Mechanisms in Corona Charged Polymeric Materials," PhD, University of Southampton, UK, 2013.

[145] P. Molinie, M. Goldman, and J. Gatellet, "Surface potential decay on corona-charged epoxy samples due to polarization processes," *Journal of Physics D: Applied Physics,* vol. 28, p. 1601, 1995.

[146] J. Lambert, G. de Loubens, C. Guthmann, M. Saint-Jean, and T. Mélin, "Dispersive charge transport along the surface of an insulating layer observed by electrostatic force microscopy," *Physical Review B,* vol. 71, p. 155418, 2005.

[147] G. Chen and J. Zhao, "Observation of negative differential mobility and charge packet in polyethylene," *Journal of Physics D: Applied Physics,* vol. 44, p. 212001, 2011.

[148] R. Scott, L. McLean, and P. Parker, "Stimulus artefact in somatosensory evoked potential measurement," *Medical and Biological Engineering and Computing,* vol. 35, pp. 211-215, 1997.

[149] F. Gao, R. K. Leach, J. Petzing, and J. M. Coupland, "Surface measurement errors using commercial scanning white light interferometers," *Measurement Science and Technology,* vol. 19, p. 015303, 2007.

[150] E. Baum, T. Lewis, and R. Toomer, "Decay of electrical charge on polyethylene films," *Journal of Physics D: Applied Physics,* vol. 10, p. 487, 1977.

[151] S. Alam, Y. V. Serdyuk, and S. M. Gubanski, "Potential decay on silicone rubber surfaces affected by bulk and surface conductivities," *Dielectrics and Electrical Insulation, IEEE Transactions on,* vol. 22, pp. 970-978, 2015.

[152] J. Kindersberger and C. Lederle, "Surface charge decay on insulators in air and sulfurhexafluorid-Part II: Measurements," *Dielectrics and Electrical Insulation, IEEE Transactions on,* vol. 15, pp. 949-957, 2008.

[153] C. L. Josef Kindersberger, "Surface Charge Decay on Insulators in Air and Sulfurhexafluoride – Part II: Measurements," *IEEE Transactions on Dielectrics and Electrical Insulation,* vol. 15, pp. 949-957, 2008.

[154] Z. Ziari, S. Sahli, and A. Bellel, "Surface potential decay of low density polyethylene (LDPE) films under different corona discharge conditions," *MJ Condensed Matter,* vol. 12, pp. 218-222, 2010.

[155] T. Iizuka, H. Takai, K. Fukunaga, and T. Maeno, "Measurement of space charge distribution in epoxy resin after water absorption treatment," in *Electrical Insulation and Dielectric Phenomena, 1997. IEEE 1997 Annual Report., Conference on*, pp. 41-44 vol.1, 1997.

[156] K. Fukunaga, T. Maeno, and V. Griseri, "Space charge observation of a filler free epoxy resin," in *Electrical Insulation and Dielectric Phenomena, 2000 Annual Report Conference on*, pp. 125-127 vol.1, 2000.

[157] L. A. Dissado, V. Griseri, W. Peasgood, E. S. Cooper, K. Fukunaga, and J. C. Fothergill, "Decay of space charge in a glassy epoxy resin following voltage removal," *Dielectrics and Electrical Insulation, IEEE Transactions on,* vol. 13, pp. 903-916, 2006.

[158] S. Das and N. Gupta, "Space charge accumulation in epoxy resin and polyethylene," in *Properties and Applications of Dielectric Materials (ICPADM), 2012 IEEE 10th International Conference on the*, pp. 1-4, 2012

[159] C. Guillermin, P. Rain, A. Sylvestre, and S. Rowe, "Space charge measurements in epoxy resin under DC voltage," *2002 Annual Report Conference on Electrical Insulation and Dielectric Phenomena (Cat. No.02CH37372),* pp. 606-609, 2002 2002.

[160] E. Kissa, *Handbook of Fiber Science and Technology* vol. Vol. II. New York: Marcel Dekker Inc, 1984.

[161] R. F. Brady, Jr., *Encyclopaedia of Polymer Science and Technology*. Chichester, U.K.: John Wiley & Sons, 1986.

[162] Y.-b. Chong and H. Ohara, "Modification of carbon fiber surfaces by direct fluorination," *Journal of Fluorine Chemistry,* vol. 57, pp. 169-175, 1992.

[163] S. A. Lee, S. H. Oh, and W. Lee, "The effect of direct fluorination of polydimethylsiloxane films on their surface properties," *Journal of colloid and interface science,* vol. 332, pp. 461-466, 2009.

[164] J. Y. Wang and H. J. Ploehn, "Dynamic mechanical analysis of the effect of water on glass bead epoxy composites," *Journal of Applied Polymer Science,* vol. 59, pp. 345-357, Jan 1996.

[165] M. C. Lee and N. A. Peppas, "Water Transport In Epoxy-Resins," *Progress in Polymer Science,* vol. 18, pp. 947-961, 1993.

[166] K. Doukkali and Y. Segui, "Effect Of Moisture Sorption On AC Properties Of Glass-Epoxy Composites," *Journal of Applied Polymer Science,* vol. 41, pp. 1533-1547, 1990.

[167] S. Popineau, C. Rondeau-Mouro, C. Sulpice-Gaillet, and M. E. R. Shanahan, "Free/bound water absorption in an epoxy adhesive," *Polymer,* vol. 46, pp. 10733-10740, 2005.

[168] S. Yangyang, Z. Zhuqing, and C. P. Wong, "Fundamental research on surface modification of nano-size silica for underfill applications," in *Electronic Components and Technology Conference, 2004. Proceedings. 54th*, pp. 754-760 Vol.1, 2004.

[169] O. H. Lin, H. M. Akil, and Z. A. Mohd Ishak, "Surface-activated nanosilica treated with silane coupling agents/polypropylene composites: Mechanical, morphological, and thermal studies," *Polymer Composites,* vol. 32, pp. 1568-1583, 2011.

[170] D. D. Gupta and K. Joyner, "On the nature of absorption currents in polyethyleneterephthalate (PET)," *Journal of Physics D: Applied Physics,* vol. 9, p. 829, 1976.

[171] M. Liu, P. Wu, Y. Ding, and S. Li, "Study on diffusion behavior of water in epoxy resins cured by active ester," *Physical Chemistry Chemical Physics,* vol. 5, pp. 1848-1852, 2003.

[172] C. Zou, J. C. Fothergill, and S. W. Rowe, "The effect of water absorption on the dielectric properties of epoxy nanocomposites," *IEEE Transactions on Dielectrics and Electrical Insulation,* vol. 15, pp. 106-117, 2008.

[173] J. T. Law and E. E. Francois, "The Adsorption Of Gases And Vapors On Germanium," *Annals of the New York Academy of Sciences,* vol. 58, pp. 925-936, 1954.

[174] T. J. Blasing, "Recent Greenhouse Gas Concentrations," Office of Science, US Department of Energy2016.

[175] V. Ollier-Durbault and B. Gosse, "Photo-oxidation and electrical aging of anhydride-cured epoxy resins," *Dielectrics and Electrical Insulation, IEEE Transactions on,* vol. 5, pp. 935-943, 1998.

[176] A. Mohamad, G. Chen, Y. Zhang, and Z. An, "Moisture effect on surface fluorinated epoxy resin for high-voltage DC applications," *IEEE Transactions on Dielectrics and Electrical Insulation,* vol. 23, pp. 1148-1155, 2016.

[177] T. S. Light, S. Licht, A. C. Bevilacqua, and K. R. Morash, "The Fundamental Conductivity and Resistivity of Water," *Electrochemical and Solid-State Letters,* vol. 8, pp. E16-E19, 2005.

[178] K. Kawasaki, "On the variation of surface coduction current of solid by adsorption of water vapour and its phase transition of absorbed layer," *Bull. Electrotech. Lab. Tokyo,* vol. 19, pp. 825-832, 1955.

[179] Y. Liu, Z. An, Q. Yin, F. Zheng, Y. Zhang, and Q. Lei, "Rapid potential decay on surface fluorinated epoxy resin samples," *Journal of Applied Physics,* vol. 113, p. 164105, 2013.

[180] L. A. Dissado, J. C. Fothergill, S. V. Wolfe, and R. M. Hill, "Weibull Statistics in Dielectric Breakdown; Theoretical Basis, Applications and Implications," *Electrical Insulation, IEEE Transactions on,* vol. EI-19, pp. 227-233, 1984.

[181] L. Cheng Rong, D. Li Jian, L. Jin Zhuang, T. You Ping, and C. YangChun, "The relation of trap distribution of alumina with surface flashover performance in vacuum," *Dielectrics and Electrical Insulation, IEEE Transactions on,* vol. 13, pp. 79-84, 2006.

[182] M. Serkan, H. Kirkici, and K. Koppisetty, "Surface Flashover Characteristics of Nano Particle Cast EPOXY Resin," in *Pulsed Power Conference, 2005 IEEE*, pp. 950-953, 2005

[183] J. T. Krile, A. Neuber, J. C. Dickens, and H. G. Krompholz, "DC and Pulsed Dielectric Surface Flashover at Atmospheric Pressure," *Plasma Science, IEEE Transactions on,* vol. 33, pp. 1149-1154, 2005.

[184] Cobine, *Conduction of Electricity through Gases* vol. 2: Cambridge University Press, 1958.

[185] C. Hammond, "The elements," *Handbook of chemistry and physics,* vol. 81, 2000.

[186] A. Mohamad, G. Chen, Y. Zhang, and Z. An, "Surface potential decay measurements on fluorinated polymeric insulation for high voltage DC applications," in *Electrical Insulation and Dielectric Phenomena (CEIDP), 2013 IEEE Conference on*, pp. 1132-1135, 2013.

[187] N. M. Kiefer. (2007). *Maximum likelihood estimation (MLE)*. Available: http://instruct1.cit.cornell.edu/courses/econ620/reviewm5.pdf

[188] R. L. Smith, "Maximum likelihood estimation in a class of nonregular cases," *Biometrika,* vol. 72, pp. 67-90, 1985.

[189] D. Cousineau, S. Brown, and A. Heathcote, "Fitting distributions using maximum likelihood: Methods and packages," *Behavior Research Methods, Instruments, & Computers,* vol. 36, pp. 742-756, 2004.

[190] M. Cacciari, G. Mazzanti, and G. Montanari, "Comparison of maximum likelihood unbiasing methods for the estimation of the Weibull parameters," *IEEE Transactions on Dielectrics and Electrical Insulation,* vol. 3, pp. 18-27, 1996.

[191] R. Corporation. (2013). *Discussion of Maximum Likelihood Estimation for the 3-Parameter Weibull Distribution*. Available: http://www.weibull.com/hotwire/issue148/hottopics148.htm

[192] J. L. Horowitz, "The bootstrap," *Handbook of econometrics,* vol. 5, pp. 3159-3228, 2001.

[193] U. Genschel and W. Q. Meeker, "A comparison of maximum likelihood and median-rank regression for Weibull estimation," *Quality Engineering,* vol. 22, pp. 236-255, 2010.

[194] F. N. Nwobi and C. A. Ugomma, "A Comparison of Methods for the Estimation of Weibull Distribution Parameters," *Metodološki Zvezki,* vol. 11, pp. 65-78, 2014.

[195] A. Mohamad, G. Chen, Y. Zhang, and Z. An, "Mechanisms for surface potential decay on fluorinated epoxy in high voltage DC applications," in *Electrical Insulation and Dielectric Phenomena (CEIDP), 2014 IEEE Conference on*, 2014, pp. 863-866.

[196] M. Szklarczyk, R. C. Kainthla, and J. O. M. Bockris, "On the dielectric breakdown of water: an electrochemical approach," *Journal of The Electrochemical Society,* vol. 136, pp. 2512-2521, 1989.

[197] C. Cardinaud, A. Tressaud, T. Nakajima, A. Tressaud, and B. Žemva, "Advanced Inorganic Materials," ed: Elsevier, 2000.

[198] N. Watanabe, T. Nakajima, and H. Touhara, "Graphite fluorides" ed: Elsevier, Amsterdam, 1988.

[199] T. Nakajima and N. Watanabe, *Graphite fluorides and carbon-fluorine compounds*: CRC, 1991.

[200] R. Foerch, N. McIntyre, and D. Hunter, "Modification of polymer surfaces by two-step plasma sensitized reactions," *Journal of Polymer Science Part A: Polymer Chemistry,* vol. 28, pp. 803-809, 1990.

[201] T. G. Vargo, J. A. Gardella, A. E. Meyer, and R. E. Baier, "Hydrogen/liquid vapor radio frequency glow discharge plasma oxidation/hydrolysis of expanded poly (tetrafluoroethylene)(ePTFE) and poly (vinylidene fluoride)(PVDF) surfaces," *Journal of Polymer Science Part A: Polymer Chemistry,* vol. 29, pp. 555-570, 1991.

[202] Z.-F. Li, A. Netravali, and W. Sachse, "Ammonia plasma treatment of ultra-high strength polyethylene fibres for improved adhesion to epoxy resin," *Journal of materials science,* vol. 27, pp. 4625-4632, 1992.

[203] M. Strobel, P. A. Thomas, and C. S. Lyons, "Plasma fluorination of polystyrene," *Journal of Polymer Science Part A: Polymer Chemistry,* vol. 25, pp. 3343-3348, 1987.

[204] A. Gil'man, L. Rishina, A. Drachev, and L. Shibryaeva, "Polypropylene Films in a Direct-Current Discharge," *High Energy Chemistry,* vol. 35, pp. 128-133, 2001.

[205] A. Gil'Man, A. Drachev, A. Kuznetsov, and V. Potapov, "Effect of Positive and Negative Components of a Direct-Current Glow Discharge on Properties of Polyimide Films," *High energy chemistry,* vol. 32, pp. 46-49, 1998.

[206] R. d'Agostino, F. Cramarossa, V. Colaprico, and R. d'Ettole, "Mechanisms of etching and polymerization in radiofrequency discharges of CF4–H2, CF4–C2F4, C2F6–H2, C3F8–H2," *Journal of Applied Physics,* vol. 54, pp. 1284-1288, 1983.

[207] E. Truesdale and G. Smolinsky, "The effect of added hydrogen on the rf discharge chemistry of CF4, CF3H, and C2F6," *Journal of Applied Physics,* vol. 50, pp. 6594-6599, 1979.

[208] A. Airoudj, D. Debarnot, B. Bêche, B. Boulard, and F. Poncin-Epaillard, "Improvement of the optical transmission of polymer planar waveguides by plasma treatment," *Plasma processes and polymers,* vol. 5, pp. 275-288, 2008.

[209] H. Hayashi, T. Nakano, K. Ishii, and Y. Ohki, "Effect of plasma surface-modification on the electrical conduction in high-density polyethylene," in *Electrical Insulation and Dielectric Phenomena, 1990. Annual Report., Conference on*, pp. 190-195, 1990.

[210] A. Paskaleva and E. Atanassova, "Fowler-Nordheim tunnelling injection in the Si-SiO2 system treated with argon plasma," *Semiconductor science and technology,* vol. 8, p. 1566, 1993.

[211] T. Y. Chang, J. W. Lee, T. F. Lei, C.-L. Lee, and H. C. Wen, "Growing High-Performance Tunneling Oxide by CF 4 Plasma Pretreatment," *Journal of The Electrochemical Society,* vol. 150, pp. G33-G38, 2003.

[212] J. Lowell, "Absorption and conduction currents in polymers: a unified model," *Journal of Physics D: Applied Physics,* vol. 23, p. 205, 1990.

[213] A. B. Gil'man, "Low-Temperature Plasma Treatment as an Effective Method for Surface Modification of Polymeric Materials," *High Energy Chemistry,* vol. 37, pp. 17-23, 2003.

[214] S. Wu, *Polymer interface and adhesion*: M. Dekker, 1982.

[215] Y. Ma, C. Zhang, R. Wang, and T. Shao, "Surface modification of LDPE film by nanosecond-pulse dielectric barrier discharge at atmospheric pressure," in *Plasma Sciences (ICOPS), 2015 IEEE International Conference on*, pp. 1-1, 2015

[216] R. Yoshimura, M. Hikita, S. Tomaru, and S. Imamura, "Low-loss polymeric optical waveguides fabricated with deuterated polyfluoromethacrylate," *Lightwave Technology, Journal of,* vol. 16, pp. 1030-1037, 1998.

[217] B. Bêche, P. Papet, D. Debarnot, E. Gaviot, J. Zyss, and F. Poncin-Epaillard, "Fluorine plasma treatment on SU-8 polymer for integrated optics," *Optics communications,* vol. 246, pp. 25-28, 2005.

[218] F. Poncin-Epaillard, J. Brosse, and T. Falher, "Cold plasma treatment: Surface or bulk modification of polymer films?," *Macromolecules,* vol. 30, pp. 4415-4420, 1997.

[219] J. Fresnais, J. Chapel, and F. Poncin-Epaillard, "Synthesis of transparent superhydrophobic polyethylene surfaces," *Surface and Coatings Technology,* vol. 200, pp. 5296-5305, 2006.

[220] M. Binder, W. L. Wade Jr, P. Cygan, T. R. Jow, and R. J. Mammone, "Breakdown voltages of commercial polymer films following exposure to various gas plasmas," *Electrical Insulation, IEEE Transactions on,* vol. 27, pp. 399-401, 1992.

APPENDIX – MATLAB CODE FOR 3-PARAMETER WEIBULL

```
x = data;
n = length(x);
p = ((1:n)-0.5)' ./ n;
r2 = @(x,y) 1 - norm(y - polyval(polyfit(x,y,1),x)).^2 / norm(y - mean(y)).^2;
threshObj = @(c) -r2(log(-log(1-p)),log(x-c));
cHat = fminbnd(threshObj,.75*min(x), .9999*min(x));
poly = polyfit(log(-log(1-p)),log(x-cHat),1);
paramHat = [exp(poly(2)) 1/poly(1) cHat]
```

.